



<https://theses.gla.ac.uk/>

Theses Digitisation:

<https://www.gla.ac.uk/myglasgow/research/enlighten/theses/digitisation/>

This is a digitised version of the original print thesis.

Copyright and moral rights for this work are retained by the author

A copy can be downloaded for personal non-commercial research or study,
without prior permission or charge

This work cannot be reproduced or quoted extensively from without first
obtaining permission in writing from the author

The content must not be changed in any way or sold commercially in any
format or medium without the formal permission of the author

When referring to this work, full bibliographic details including the author,
title, awarding institution and date of the thesis must be given

Enlighten: Theses

<https://theses.gla.ac.uk/>
research-enlighten@glasgow.ac.uk

Individual Channel Analysis and Design
and its Application to
Helicopter Flight Control

A DISSERTATION SUBMITTED TO
THE DEPARTMENT OF ELECTRONICS AND ELECTRICAL ENGINEERING
OF THE UNIVERSITY OF GLASGOW
FOR THE DEGREE
OF DOCTOR OF PHILOSOPHY

Graham John William Dudgeon

October 1996

© Copyright 1996 by Graham John William Dudgeon

All Rights Reserved

ProQuest Number: 10992040

All rights reserved

INFORMATION TO ALL USERS

The quality of this reproduction is dependent upon the quality of the copy submitted.

In the unlikely event that the author did not send a complete manuscript and there are missing pages, these will be noted. Also, if material had to be removed, a note will indicate the deletion.



ProQuest 10992040

Published by ProQuest LLC (2018). Copyright of the Dissertation is held by the Author.

All rights reserved.

This work is protected against unauthorized copying under Title 17, United States Code
Microform Edition © ProQuest LLC.

ProQuest LLC.
789 East Eisenhower Parkway
P.O. Box 1346
Ann Arbor, MI 48106 – 1346

THESIS 10950
copy 1



To my Family

Abstract

The publication in 1989 of the Aeronautical Design Standard (ADS)-33C (which, in 1994, was upgraded to ADS-33D) has provided a focus for helicopter flight control research, by both industrial and academic engineers. Helicopters are highly coupled, open-loop unstable systems with complex dynamics, mainly due to the main rotor, and as a consequence available mathematical models have a high degree of uncertainty. Because of these reasons, the design of control laws to enable ADS-33 Level 1 Handling Qualities requirements to be met has been thought to preclude the use of classical one-loop-at-a-time control system design techniques (the helicopter will exhibit Level 1 Handling Qualities if minimal pilot compensation is required during a flying task). The need for control laws which are robust to model uncertainty and demonstrate good decoupling has caused recent attention to be focused on so called 'modern' techniques which synthesis controllers by closing all loops simultaneously and can cater, to some degree, for performance and robustness issues. However, it can be argued that much of the physical insight that classical techniques allow is lost when using modern techniques. A recent development in classical control theory known as *Individual Channel Analysis and Design* (ICAD) is unique in that it explicitly captures multivariable metrics as part of the single-input single-output (SISO) analysis and design process. These multivariable metrics are known as *multivariable structure functions* (MSFs) and have three important uses. First they provide a robustness diagnostic which indicates when classical SISO gain and phase margins can be reliably interpreted as robustness measures of a multivariable system. Second, they are used to establish sequential (one-loop-at-a-time) design procedures which will guarantee closed-loop stability and third, they indicate attainable performance of the control system. This thesis develops the theory of ICAD to a level where it can effectively and efficiently be applied to the design of helicopter flight control laws and which will cater for meeting the requirements of ADS-33 in the design process. The development includes the extension of ICAD to cater for non-square systems and a technique to

express the MSFs in state space form, thus enabling numerically reliable state space algorithms to be used for computation. The development is generic in nature and therefore can be applied to a wide range of control problems. The analysis and design of four different helicopter flight control laws is described in detail. The control laws are of low order and after extensive linear and non-linear simulation are found to satisfy Level 1 requirements over a wide flight envelope. ICAD is found to be a highly effective technique for the analysis and design of helicopter flight control laws which will meet ADS-33 Level 1 requirements.

Table of Contents

| | |
|---|-----|
| <i>List of Figures</i> | vi |
| <i>List of Tables</i> | xii |
| <i>Acknowledgements</i> | xv |
| Chapter 1 Overview | 1 |
| 1.1. Introduction | 1 |
| 1.2. Aim of Thesis | 2 |
| 1.3. Outline of Thesis | 2 |
| 1.4. Original Contribution of Research | 3 |
| Chapter 2 Helicopter Dynamics, Handling Qualities and Flight Control | 5 |
| 2.1. Introduction | 5 |
| 2.2. Helicopter Dynamics | 6 |
| 2.2.1. Rigid Body Dynamics | 6 |
| 2.2.2. Rotor Dynamics | 9 |
| 2.2.2.1. Flapping | 9 |
| 2.2.2.2. Pitch to Roll Coupling | 15 |
| 2.2.2.3. Yaw due to Height Rate Coupling | 16 |
| 2.2.2.4. Feathering | 18 |
| 2.2.2.5. Pilot Control | 19 |
| 2.2.3. The Simulation Model | 21 |
| 2.3. Helicopter Handling Qualities | 23 |
| 2.3.1. ADS-33 Terminology | 24 |
| 2.3.2. Small Amplitude Requirements | 26 |
| 2.3.2.1. Short-Term Response to Control Inputs (Bandwidth) | 26 |
| 2.3.2.2. Mid-Term Response to Control Inputs | 29 |
| 2.3.3. Moderate Amplitude Requirement (Attitude Quickness) | 33 |
| 2.3.4. Interaxis Coupling | 34 |
| 2.3.4.1. Yaw due to Collective | 34 |

| | |
|---|-----------|
| 2.3.4.2. Pitch to Roll and Roll to Pitch..... | 35 |
| 2.3.4.3. Collective to Attitude Coupling..... | 36 |
| 2.3.5. Height Response Characteristics..... | 37 |
| 2.4. A Review of Helicopter Control Research..... | 38 |
| 2.4.1. The Characteristic Locus Method..... | 39 |
| 2.4.2. Nyquist Array Methods..... | 40 |
| 2.4.3. Quantitative Feedback Theory..... | 40 |
| 2.4.4. Linear Quadratic Methods..... | 42 |
| 2.4.5. Eigenstructure Assignment..... | 44 |
| 2.4.6. H-Infinity..... | 46 |
| 2.5. The Potential for Individual Channel Analysis and Design..... | 47 |
| 2.6. Summary..... | 49 |
| Chapter 3 Individual Channel Analysis of Square Systems..... | 50 |
| 3.1. Introduction..... | 50 |
| 3.2. Decomposition of a m-input m-output System into Individual Channels..... | 52 |
| 3.3. The Channel MSF as a Sensitivity Measure..... | 58 |
| 3.4. How Close can an MSF be to the (1,0) Point Before Robustness Problems Occur?..... | 61 |
| 3.5. Channel Gain and Phase Margins as Robustness Measures..... | 63 |
| 3.6. Individual Channel Analysis of Systems with Non-Diagonal Controllers..... | 65 |
| 3.7. Summary..... | 68 |
| Chapter 4 Individual Channel Analysis of Non-Square Systems..... | 69 |
| 4.1. Introduction..... | 69 |
| 4.2. Non-Square Systems with Two Sets of Feedback Loops..... | 70 |
| 4.3. Derivation of Transfer Function Elements Outwith the Inner Feedback System..... | 71 |
| 4.4. Sensitivity of the Outer Open-Loop Transfer Function Elements..... | 76 |
| 4.5. Analysis Before the Inner Loop Has been Designed..... | 81 |
| 4.6. Summary..... | 82 |

| | | |
|------------------|---|-----|
| Chapter 5 | <i>Individual Channel Analysis of State Space Systems</i> | 84 |
| 5.1. | Introduction | 84 |
| 5.2. | A Review of Applicable State Space Theory | 85 |
| 5.3. | Calculation of Plant Transmission Zeros | 87 |
| 5.4. | The Approximate Multivariable Structure Function | 88 |
| 5.4.1. | Calculation of the Approximate MSF using the Transfer Function Matrix | 89 |
| 5.4.2. | Calculation of the Approximate MSF using the State Space Model | 91 |
| 5.5. | The Actual Multivariable Structure Function | 94 |
| 5.5.1. | Calculation of the Actual MSF using the Transfer Function Matrix | 97 |
| 5.5.2. | Calculation of the Actual MSF using the State Space Model | 98 |
| 5.6. | Determination of the Zeros of the Channels and the Plant from the Appropriate MSFs | 99 |
| 5.7. | Applied Example of Computation of Approximate MSFs | 100 |
| 5.8. | Summary | 102 |
| Chapter 6 | <i>Controller Design Using Individual Channel Analysis</i> | 104 |
| 6.1. | Introduction | 104 |
| 6.2. | Design Philosophy | 105 |
| 6.3. | Prerequisites for Developing a Design Procedure to Guarantee Closed-Loop Stability | 107 |
| 6.4. | Design using Nested Channels | 110 |
| 6.5. | Conditions Sufficient for Closed-Loop Stability of a Minimum Phase Plant | 113 |
| 6.5.1. | MSF High Frequency Limit less than One | 114 |
| 6.5.1.1. | Designing to Meet the Sufficient Conditions | 116 |
| 6.5.1.1.1. | <i>Design of Controller k_4</i> | 116 |
| 6.5.1.1.2. | <i>Design of Controller k_3</i> | 117 |
| 6.5.1.1.3. | <i>Design of Controller k_2</i> | 118 |
| 6.5.1.1.4. | <i>Design of Controller k_1</i> | 119 |
| 6.5.2. | MSF High Frequency Limits Greater Than One | 120 |
| 6.6. | Example of Designing for Closed-Loop Stability of a Non-Minimum Phase Plant | 126 |

| | |
|---|-----|
| 6.7. Performance Considerations when Designing using Nested Channels..... | 133 |
| 6.8. Robustness Issues Arising from the Use of Nested Channels..... | 136 |
| 6.9. A Look at ICAD Feedforward..... | 139 |
| 6.9.1. Applied Example..... | 141 |
| 6.10. Summary..... | 146 |
| Chapter 7 <i>Attitude Command Attitude Hold</i> | 147 |
| 7.1. Introduction..... | 147 |
| 7.2. Design Considerations..... | 148 |
| 7.3. Approximate Sensitivity Analysis..... | 156 |
| 7.4. Stabilisation and Potential Performance of the ACAH System..... | 159 |
| 7.5. Feedback Controller Design..... | 164 |
| 7.6. Individual Channel Analysis..... | 173 |
| 7.7. Pre-Compensation..... | 181 |
| 7.8. Handling Qualities Assessment..... | 186 |
| 7.8.1. Attitude Hold..... | 186 |
| 7.8.2. Small Amplitude Attitude Changes..... | 187 |
| 7.8.3. Mid-Term Response..... | 191 |
| 7.8.4. Interaxis Coupling..... | 192 |
| 7.8.5. Response to Collective..... | 194 |
| 7.9. Summary..... | 195 |
| Chapter 8 <i>Rate Command</i> | 196 |
| 8.1. Introduction..... | 196 |
| 8.2. Design Considerations..... | 197 |
| 8.3. Approximate Sensitivity Analysis..... | 198 |
| 8.4. System Behaviour at Zero Frequency..... | 201 |
| 8.5. Stabilisation and Potential Performance of the Rate System..... | 206 |
| 8.6. Control Law..... | 211 |
| 8.7. Individual Channel Analysis..... | 213 |
| 8.8. Handling Qualities Assessment..... | 220 |
| 8.8.1. Small Amplitude Attitude Changes..... | 220 |

| | |
|---|-----|
| 8.8.2. Moderate Amplitude Attitude Changes..... | 223 |
| 8.8.3. Mid-Term Response..... | 225 |
| 8.8.4. Interaxis Coupling..... | 227 |
| 8.8.5. Response to Collective..... | 229 |
| 8.9. Summary..... | 230 |
| Chapter 9 <i>Translational Rate Command</i> | 231 |
| 9.1. Introduction..... | 231 |
| 9.2. Design Considerations..... | 232 |
| 9.3. Individual Channel Analysis of Inner Attitude System..... | 236 |
| 9.4. TRC System..... | 237 |
| 9.4.1. Analysis of the Loose Transfer Functions..... | 239 |
| 9.4.2. Stabilisation and Potential Performance of the TRC System..... | 243 |
| 9.4.3. Controller Design..... | 244 |
| 9.4.4. Individual Channel Analysis..... | 249 |
| 9.5. Handling Qualities Assessment..... | 250 |
| 9.6. Elliptical Turn Robustness Test..... | 251 |
| 9.7. Summary..... | 258 |
| Chapter 10 <i>Conclusions and Future Work</i> | 259 |
| 10.1. Conclusions..... | 259 |
| 10.2. Future Work..... | 261 |
| Bibliography | 264 |
| Appendix I <i>Helicopter Configuration Data</i> | 273 |
| Appendix II <i>Hover State Space Model</i> | 274 |
| Appendix III <i>30 Knots Forward Flight State Space Model</i> | 277 |
| Appendix IV <i>80 Knots Forward Flight State Space Model</i> | 281 |
| Appendix V <i>Non-Minimum Phase State Space Model</i> | 283 |
| Appendix VI <i>Matlab[®] Code of MSF Calculations</i> | 284 |

List of Figures

| | | |
|--------------|---|----|
| Figure 2.1. | Rigid body degrees of freedom..... | 6 |
| Figure 2.2. | Definition of Euler Angles..... | 7 |
| Figure 2.3. | Rotor blade velocity distribution in hover..... | 10 |
| Figure 2.4. | Blade segment in airstream..... | 10 |
| Figure 2.5. | Rotor blade velocity distribution in forward flight..... | 11 |
| Figure 2.6. | Change in angle of attack due to induced velocity..... | 13 |
| Figure 2.7. | (a) Longitudinal flapping and coning, (b) Lateral flapping and coning | 14 |
| Figure 2.8. | (a) Teetering rotor, (b) Rotor with hinge offset..... | 15 |
| Figure 2.9. | Helicopter trimmed in forward flight..... | 16 |
| Figure 2.10. | Balance of main rotor torque with tail rotor thrust..... | 17 |
| Figure 2.11. | (a) Flapping rotor blade, (b) Feathering rotor blade..... | 19 |
| Figure 2.12. | (a) Swashplate, (b) Tilted swashplate to induce feathering..... | 20 |
| Figure 2.13. | Definitions of bandwidths and phase delay..... | 27 |
| Figure 2.14. | (a) Handling Qualities requirements for small amplitude pitch response. (b) Handling Qualities requirements for small amplitude roll response. | 29 |
| Figure 2.15. | Example of second order impulse response..... | 30 |
| Figure 2.16. | Second order on-axis response and indeterminate off-axis response.... | 31 |
| Figure 2.17. | Limits on pitch (roll) oscillations for hover and low speed..... | 32 |
| Figure 2.18. | Lateral-directional oscillatory requirements in forward flight..... | 33 |
| Figure 2.19. | Agility boundaries for (a) Pitch attitude changes, (b) Roll attitude changes..... | 34 |

| | | |
|--------------|--|-----|
| Figure 2.20. | Collective-to-yaw coupling requirements..... | 35 |
| Figure 2.21. | Pitch to roll coupling assessment..... | 36 |
| Figure 3.1. | Block diagram for determination of Channel 1..... | 53 |
| Figure 3.2. | m-input m-output ICAD decomposition..... | 56 |
| Figure 3.3. | Phase sensitivity of $(1 - \gamma_i(\omega_x))$ | 60 |
| Figure 4.1. | Block diagram of non-square system..... | 71 |
| Figure 4.2. | Block diagram of conceptual example..... | 79 |
| Figure 6.1. | Nyquist plot of γ | 121 |
| Figure 6.2. | Bode plot of $k_2 g_{22}$ | 123 |
| Figure 6.3. | Nyquist plot of γ (solid) and $\gamma_{\mathcal{H}_2}$ (dashed)..... | 123 |
| Figure 6.4. | Bode plot of Channel 2..... | 125 |
| Figure 6.5. | Nyquist plot of (a) Γ_1 , (b) Γ_2 , (c) Γ_3 , (c ₁) expansion of (1,0) region of (c)..... | 128 |
| Figure 6.6. | (a) Nyquist plot of Γ_3 (solid) and γ_{123} (dashed), (b) expansion of (1,0) region..... | 130 |
| Figure 6.7. | Nyquist plot of Γ_2 (solid) and γ_{12} (dashed)..... | 131 |
| Figure 6.8. | Nyquist plot of Γ_1 (solid) and γ_1 (dashed)..... | 132 |
| Figure 6.9. | Block diagram of feedforward configuration..... | 140 |
| Figure 6.10. | Nyquist plot of approximate MSF of longitudinal subsystem..... | 142 |
| Figure 6.11. | Bode plot of g_{12} | 142 |
| Figure 6.12. | Nyquist plot of γ (solid) and γ_f (dashed)..... | 144 |
| Figure 6.13. | Response of system with and without feedforward to commanded step input in pitch Channel..... | 145 |
| Figure 7.1. | Nyquist plots of MSFs of $\theta/\delta_{\text{long}}$ (solid) and q/δ_{long} (dashed)..... | 150 |

| | | |
|--------------|--|-----|
| Figure 7.2. | Bode plot of q/θ_{1s} | 151 |
| Figure 7.3. | Bode plots of $\dot{\theta} \cos \Phi_0/\theta_{1s}$ (solid) and $\dot{\psi} \cos \Theta_0 \sin \Phi_0/\theta_{1s}$ (dashed)..... | 151 |
| Figure 7.4. | Approximate closed-loop phase of roll attitude response..... | 154 |
| Figure 7.5. | Nyquist plots of (a) $\hat{\Gamma}_1$, (b) $\hat{\Gamma}_2$, (b ₁) Expansion of (1,0) region of (b), (c) $\hat{\Gamma}_3$, (c ₁) Expansion of (1,0) region of (c), (d) $\hat{\Gamma}_4$, (d ₁) Expansion of (1,0) region of (d)..... | 158 |
| Figure 7.6. | Nyquist plot of (a) Γ_1 , (b) Γ_2 , (b ₁) Expansion of (1,0) region of (b), (c) Γ_3 , (c ₁) Expansion of (1,0) region of Γ_3 | 162 |
| Figure 7.7. | Bode plot of g_{44} (dashed) and $k_4 g_{44}$ (solid)..... | 166 |
| Figure 7.8. | (a) Nyquist plot of Γ_3 (solid) and γ_{123} (dashed), (b) Expansion of (1,0) region..... | 167 |
| Figure 7.9. | Bode plot of C'_3 without controller (dashed) and C'_3 with controller (solid)..... | 168 |
| Figure 7.10. | (a) Nyquist plot of Γ_2 (solid) and γ_{12} (dashed), (b) Expansion of (1,0) region..... | 169 |
| Figure 7.11. | Bode plot of C'_2 without controller (dashed) and C'_2 with controller (solid)..... | 170 |
| Figure 7.12. | (a) Nyquist plot of Γ_1 (solid) and γ_1 (dashed)..... | 172 |
| Figure 7.13. | Bode plot of (a) C_1 (solid) and C'_1 (dashed), (b) C_2 (solid) and C'_2 (dashed), (c) C_3 (solid) and C'_3 (dashed), (d) C_4 (solid) and C'_4 (dashed)..... | 175 |
| Figure 7.14. | Nyquist plot of (a) γ_1 , (b) γ_2 , (c) γ_3 , (d) γ_4 | 178 |
| Figure 7.15. | Comparison of linear time responses of stable and unstable system due to commanded step inputs in: (a) Pitch Channel, (b) Roll Channel.... | 180 |

| | | |
|--------------|--|-----|
| Figure 7.16. | Bode plot of p_{41} (solid) and $(-t_{41}/t_{44})$ (dashed)..... | 182 |
| Figure 7.17. | Linear response of \dot{h} (solid) and r (dashed) due to a commanded height rate of 5 ft/s, with and without decoupling filter..... | 182 |
| Figure 7.18. | Block diagram of ACAH system..... | 183 |
| Figure 7.19. | Linear time response of ACAH system at 30 knots to (a) height rate command of 5 ft/s, (b) pitch attitude command of 5° , (c) roll attitude command of 5° , (d) yaw rate command of 5° /s..... | 185 |
| Figure 7.20. | Non-linear response of (a) pitch attitude to commanded pulse from hover to 80 knots, (b) roll attitude to commanded pulse from hover to 80 knots..... | 187 |
| Figure 7.21. | Bode plots of (a) $\theta/\delta_{\text{ong}}$, (b) ϕ/δ_{lat} , (c) $\psi/\delta_{\text{tail}}$ at 30 knots, with Handling Qualities parameters shown..... | 189 |
| Figure 7.22. | Handling Qualities bandwidth and phase delay assessment for (a) Pitch attitude, (c) Roll attitude, (c) Yaw attitude..... | 190 |
| Figure 7.23. | Mid-Term assessment of pitch and roll attitude responses. Hover and low speed..... | 191 |
| Figure 7.24. | Mid-Term assessment of roll attitude response. Forward flight..... | 192 |
| Figure 7.25. | Assessment of yaw rate due to collective..... | 192 |
| Figure 7.26. | (a) Non-linear response of commanded pitch attitude step of 30° , (b) Non-linear response of commanded roll attitude step of 30° | 193 |
| Figure 8.1. | Nyquist plots of (a) $\hat{\Gamma}_1$, (b) $\hat{\Gamma}_2$, (b ₁) Expansion of (1,0) region of (b), (c) $\hat{\Gamma}_3$, (c ₁) Expansion of (1,0) region of (c), (d) $\hat{\Gamma}_4$, (d ₁) Expansion of (1,0) region of (d)..... | 201 |
| Figure 8.2. | Nyquist plots of (a) Γ_1 , (b) Γ_2 , (c) Γ_3 | 209 |
| Figure 8.3. | Block diagram of Rate Command system..... | 212 |

| | | |
|--------------|---|-----|
| Figure 8.4. | Bode plot of (a) Channel 1, (b) Channel 2, (c) Channel 3, (d) Channel 4..... | 215 |
| Figure 8.5. | Nyquist plot of (a) γ_1 , (b) γ_2 , (c) γ_3 , (d) γ_4 | 217 |
| Figure 8.6. | Small amplitude time histories of (a) 1 ft/s height rate command, (b) 1°/s pitch rate command, (c) 1°/s roll rate command, (d) 1°/s yaw rate command..... | 219 |
| Figure 8.7. | Bode plots of (a) $\theta/\delta_{\text{long}}$, (b) ϕ/δ_{lat} , (c) $\psi/\delta_{\text{tail}}$ at 30 knots, with Handling Qualities parameters shown..... | 221 |
| Figure 8.8. | Handling Qualities bandwidth and phase delay assessment for (a) Pitch attitude, (b) Roll attitude, (c) Yaw attitude..... | 222 |
| Figure 8.9. | Non-linear Moderate Amplitude assessment for hover and low speed of (a) Pitch attitude, (b) Roll attitude, (c) Yaw attitude..... | 224 |
| Figure 8.10. | Non-linear Moderate Amplitude assessment of roll attitude for forward flight..... | 225 |
| Figure 8.11. | Mid-Term assessment of pitch rate and roll rate responses. Hover and low speed..... | 226 |
| Figure 8.12. | Mid-Term assessment of roll rate response. Forward flight..... | 226 |
| Figure 8.13. | Assessment of yaw rate due to collective..... | 227 |
| Figure 8.14. | (a) Response of commanded pitch attitude of 30°, (b) Response of commanded roll attitude of 30° | 228 |
| Figure 9.1. | Helicopter moving from one position to another..... | 233 |
| Figure 9.2. | Block diagram of proposed TRC feedback system..... | 234 |
| Figure 9.3. | Nyquist plot of γ_2 of the inner attitude system..... | 236 |
| Figure 9.4. | Nyquist plot of $\bar{\gamma}$ up to 2 rad/s..... | 239 |
| Figure 9.5. | Nyquist plot of (a) $\bar{\gamma}_{52}$, (b) $\bar{\gamma}_{63}$ | 241 |
| Figure 9.6. | Magnitude Bode plot of $\text{abs}(1-\bar{\gamma}_{52})$ | 242 |

| | | |
|--------------|---|-----|
| Figure 9.7. | Nyquist plot of $\bar{\gamma}$ | 243 |
| Figure 9.8. | Bode plot of $p_2\bar{q}_{63}$ (solid) and \bar{q}_{63} (dashed)..... | 245 |
| Figure 9.9. | (a) Nyquist plot of $\bar{\gamma}$ (solid) and $\bar{\gamma} h_{63}$ (dashed - refer to (b)), (b) Expansion of (0,0) region of (a)..... | 246 |
| Figure 9.10. | Bode plot of $p_1\bar{q}_{52}(1 - \bar{\gamma}.h_{63})$ (solid) and $\bar{q}_{52}(1 - \bar{\gamma}.h_{63})$ (dashed)..... | 247 |
| Figure 9.11. | Block diagram of TRC system..... | 248 |
| Figure 9.12. | Nyquist plot of $\bar{\gamma}h_{63}$ (solid) and $\bar{\gamma}h_{52}$ (dashed)..... | 249 |
| Figure 9.13. | (a) Non-linear response due to commanded forward velocity of 30 ft/s, (b) Non-linear response due to commanded side velocity of 30 ft/s... | 251 |
| Figure 9.14. | Elliptical turn..... | 252 |
| Figure 9.15. | Non-linear yaw rate response due to a commanded yaw rate of 5°/s with no shaping filter..... | 253 |
| Figure 9.16. | Non-linear yaw rate response due to a commanded yaw rate of 5°/s with shaping filter..... | 254 |
| Figure 9.17. | Earth referenced forward and side velocities..... | 255 |
| Figure 9.18. | Flight path of helicopter during elliptical turn test..... | 256 |
| Figure 9.19. | Responses of (a) u_h , (b) v_h | 257 |

List of Tables

| | | |
|-------------|---|-----|
| Table 2.1. | Maximum values for pitch-roll and roll-pitch coupling..... | 36 |
| Table 2.2. | Maximum values for height rate response due to collective step input..... | 37 |
| Table 5.1. | Structure of Γ_1 calculated from transfer function technique..... | 101 |
| Table 5.2. | Structure of Γ_1 and $(1-\Gamma_1)$ calculated from state space technique..... | 102 |
| Table 6.1. | Relationship of nested MSFs..... | 111 |
| Table 6.2. | Relationship of nested Channels..... | 111 |
| Table 6.3. | Structure of parameters of Eqn (6.26)..... | 121 |
| Table 6.4. | Zero structure of $k_2 g_{22}$ and $(1 + k_2 g_{22})$ | 122 |
| Table 6.5. | Zero structure of $(1-\gamma)$ and $(1-\gamma h_2)$ | 124 |
| Table 6.6. | Zero structure of C_1 and $(1+C_1)$ | 124 |
| Table 6.7. | Structure of parameters of Eqn (6.14)..... | 128 |
| Table 6.8. | Zero structure of g_{44} and $(1 + k_4 g_{44})$ | 130 |
| Table 6.9. | Zero structure of C'_3 and $(1+C'_3)$ | 131 |
| Table 6.10. | Zero structure of C'_2 and $(1+C'_2)$ | 132 |
| Table 6.11. | Zero structure of C'_1 and $(1+C'_1)$ | 133 |
| Table 6.12. | Channel gain and phase margins..... | 144 |
| Table 7.1. | Approximate open-loop Channel specifications..... | 155 |
| Table 7.2. | Structure of G | 156 |
| Table 7.3. | Structure of parameters of Eqn (7.7)..... | 163 |

| | | |
|-------------|--|-----|
| Table 7.4. | Comparison of C'_4 metrics with C_4 approximate specifications..... | 166 |
| Table 7.5. | Zero structure of C'_4 and $(1+C'_4)$ | 166 |
| Table 7.6. | Comparison of C'_3 metrics with C_3 approximate specifications..... | 168 |
| Table 7.7. | Zero structure of C'_3 and $(1+C'_3)$ | 169 |
| Table 7.8. | Comparison of C'_2 metrics with C_2 approximate specifications..... | 171 |
| Table 7.9. | Zero structure of C'_2 and $(1+C'_2)$ | 171 |
| Table 7.10. | Comparison of C'_1 metrics with C_1 approximate specifications..... | 173 |
| Table 7.11. | Zero structure of C'_1 and $(1+C'_1)$ | 173 |
| Table 7.12. | Comparison of metrics of actual Channels and nested Channels..... | 176 |
| Table 7.13. | Structure of perturbed closed-loop Channels..... | 179 |
| Table 7.14. | Values of $\left \theta_{\text{peak}} / n_{z_{\text{peak}}} \right $ for commanded height rate step of 30 ft/s..... | 194 |
| Table 7.15. | Height rate response parameters from hover to 40 knots..... | 195 |
| Table 8.1. | Approximate open-loop Channel specifications..... | 197 |
| Table 8.2. | Structure of G | 198 |
| Table 8.3. | Structure of parameters of Eqn (8.17)..... | 210 |
| Table 8.4. | Channel parameters of final design..... | 215 |
| Table 8.5. | Values of $\left \theta_{\text{peak}} / n_{z_{\text{peak}}} \right $ for commanded height rate step of 30 ft/s..... | 229 |
| Table 8.6. | Height rate response parameters from hover to 40 knots..... | 229 |
| Table 9.1. | Gain and phase margins of Channels of inner attitude system..... | 237 |
| Table 9.2. | Structure of \bar{Q} | 238 |
| Table 9.3. | Structure of parameters of Eqn (9.17)..... | 244 |
| Table 9.4. | Zero structure of \bar{q}_{63} and $(1+p_2\bar{q}_{63})$ | 245 |

Table 9.5. Zero structure of $p_1\bar{q}_{52}(1-\bar{\gamma}.h_{63})$ and $(1+p_1\bar{q}_{52}(1-\bar{\gamma}.h_{63}))$ 247

Table 9.6. Gain and phase margins of TRC Channels..... 249

Acknowledgements

First and foremost I would like to thank my supervisor, Dr Jeremy Gribble, for his guidance and criticism of the work of this thesis, and for putting up with me for three years. Thanks are also due to Professor John O'Reilly of the University of Glasgow and Dr William Leithead of the University of Strathclyde for their useful comments concerning Individual Channel Analysis and Design.

I am grateful to DRA (Bedford) for supplying the HELISIM and HELISTAB software packages, for offering informal support during my research period and for giving me the opportunity to spend a week at DRA (Bedford).

I am indebted to the EPSRC for funding my research and to the Department of Electronics and Electrical Engineering for partially funding my attendance to the 21st European Rotorcraft Forum, for funding my attendance to the UKACC International Conference on Control'96 and for funding my visit to DRA (Bedford).

Finally, I would like to thank my family and friends for their encouragement and support during the last three years.

1.1. Introduction

The publication in 1989 of the Aeronautical Design Standard (ADS)-33C (which has since been upgraded to ADS-33D [3]) has provided a focus for helicopter flight control research, by both industrial and academic engineers. ADS-33 was the first attempt to capture mission-related criteria within a design standard which arose through the development of the Comanche RAH-66, and has since become the standard for assessing helicopter Handling Qualities. The stringent requirements contained within ADS-33 have arisen through a continuing drive for increased operational effectiveness, i.e. 24 hours a day, all weather, and the requirements have consequently become the technology driver for increased stability and control augmentation. For high gain/bandwidth feedback within the automatic flight control system (AFCS) to be effective on the actual helicopter requires robustness, both in stability and performance, to uncertainty in the design model. This need for good multivariable robustness, combined with inter-axis decoupling, has been thought to preclude classical 'one-loop-at-a-time' control design techniques and has therefore created interest in modern multivariable control design techniques. Such techniques synthesise controllers by closing all feedback loops simultaneously and tolerance to uncertainty is measured by appropriate singular value measures; see for example Gribble [15], Innocenti and Stanziola [30], Manness and Murray-Smith [46] and Walker and Postlethwaite [78]. However, it can be argued that much of the physical insight that classical single-input single-output (SISO) control design techniques allow, is lost when using such techniques. Individual Channel Analysis and Design is a recent theory which quantifies

the multivariable nature of a system in such a way that enables classical SISO techniques to explicitly be applied to the analysis and design of multivariable control laws. It quantifies the multivariable nature of systems through the use of *multivariable structure functions* (MSFs). These MSFs have three important uses. First, they provide a robustness diagnostic which indicates when classical SISO gain and phase margins can be reliably interpreted as robustness measures of a multivariable system. Second, they are used to establish sequential (one-loop-at-a-time) design procedures which will guarantee closed-loop stability and third, they indicate attainable performance of the control system. This thesis is concerned with Individual Channel Analysis and Design and its application to helicopter flight control.

1.2. Aim of Thesis

This thesis has three aims. The first is to identify shortcomings in current control system design techniques applied to helicopter flight control and to propose ICAD as a technique which, potentially, will not suffer from these shortcomings. Second, ICAD will be developed to a level where it can be efficiently applied to the design of helicopter flight control laws. This development will be generic in nature and can be applied to other multivariable problems apart from helicopter flight control. Third, the application of ICAD to helicopter flight control, with particular emphasis on meeting Handling Qualities requirements, will be assessed.

1.3. Outline of Thesis

The outline of this thesis is as follows. Chapter 2 gives an introduction to helicopter dynamics and a description of helicopter Handling Qualities with particular reference to the criteria which will be assessed in this thesis. In addition, a review of current research of various control law design techniques which have been applied to helicopter

flight control is given and potential inadequacies are identified. ICAD is identified as a technique capable of providing a more transparent procedure. Chapter 3 describes the aspects of Individual Channel Analysis which are relevant for the work of this thesis. Chapter 4 describes a method of analysing non-square systems within the context of Individual Channel Analysis. Chapter 5 describes a method in which state space algorithms can be used to calculate multivariable structure functions. Chapter 6 describes procedures for designing control laws for systems which have more than 2-inputs and 2-outputs. Both minimum-phase and non-minimum phase systems are considered. Chapters 7 through 9 describe the analysis and design of various helicopter flight control laws using ICAD. Chapter 10 concludes the work of the thesis and describes possible future work.

1.4. Original Contribution of Research

The original contributions of research in this thesis are as follows:

The development of ICAD for the analysis of non-square systems. This is covered in Chapter 4. This work has resulted in the submission of a paper entitled 'Analysis and Design of Non-Square Systems using Individual Channel Analysis and Design' to the International Journal of Control.

The development of state space methods to calculate multivariable structure functions. This is covered in Chapter 5. This work has resulted in the submission of a paper entitled 'Computation of Multivariable Structure Functions' to the International Journal of Control.

The description of a design procedure for systems with more than 2-inputs and 2-outputs. This is covered in Chapter 6.

The design of a helicopter Attitude Command Attitude Hold system using ICAD and the linear and non-linear assessment of its Handling Qualities. This work has resulted in two conference papers entitled 'The use of Individual Channel Analysis and Design to Meet Helicopter Handling

Qualities Requirements' [9] and 'Individual Channel Analysis and Helicopter Flight Control in Moderate and Large Amplitude Manoeuvres' [10]. This work has also resulted in the submission of a paper entitled 'Helicopter Attitude Command Attitude Hold using Individual Channel Analysis and Design' to the Journal of Guidance, Control and Dynamics and a paper entitled 'Individual Channel Analysis and Helicopter Flight Control in Moderate and Large Amplitude manoeuvres' to Control Engineering Practice.

The technique to approximately determine closed-loop Handling Qualities bandwidths from open-loop data before the feedback control law has been designed, thus allowing explicit consideration of Handling Qualities bandwidths in the feedback design process. This technique is first covered in Chapter 7, Section 7.2.

The design of a helicopter Rate Command system using ICAD and the linear and non-linear assessment of its Handling Qualities. This is covered in Chapter 8.

The design of a helicopter Translational Rate Command system using ICAD and the linear and non-linear assessment of its Handling Qualities. This is covered in Chapter 9. This work has resulted in a conference paper entitled 'Helicopter Translational Rate Command using Individual Channel Analysis and Design' [11].

Helicopter Dynamics, Handling Qualities and Control

2.1. Introduction

The design of a successful control law can be attributed to three factors (four, if you include luck - a factor a control engineer should never rely on). The first is a good understanding of the dynamics of the system that is to be controlled. The second is an understanding of why the specifications that the design is to meet are defined as they are. The third factor is the ability to choose a control system design technique which exhibits 'visibility', in that the designer knows that the design procedures will enable the specifications to be met. This Chapter bears the above factors in mind and so contains three main Sections. In Section 2.2 the reader will be given an introduction to helicopter dynamics to a sufficient level to understand the behaviour of a helicopter in flight, the sources of cross-coupling unique to the helicopter and how 'desired' motion can be effected by the pilot. In addition, there will be some discussion on the simulation model used in the work of this thesis. Section 2.3 will describe helicopter Handling Qualities specifications in some detail. Handling Qualities are a level of the ease and precision with which a pilot can perform a task and 'good' Handling Qualities are essential for enhanced operational effectiveness and safety. Section 2.4 will present a review of linear control system design techniques which have been applied to helicopter flight control in recent years in order to weigh the potential benefits and pitfalls of the techniques. Section 2.5 summarises the findings of Section 2.4 and highlights the need for consideration of Individual Channel Analysis and Design to the analysis and design of helicopter flight control laws.

2.2. Helicopter Dynamics

This Section gives the reader an introduction to the dynamics of helicopter flight to a level relevant to the understanding of the work of this thesis. For a more thorough description of helicopter dynamics the reader is referred to Padfield [60] and Prouty [63,64].

2.2.1 Rigid Body Dynamics

The rigid body dynamics of a helicopter relate to the dynamical characteristics of the centre of gravity of the fuselage when subject to aerodynamical, gravitational, and inertial forces and moments. The fuselage has 6 degrees of freedom; 3 translational degrees of freedom and 3 rotational degrees of freedom. Figure 2.1 shows these degrees of freedom.

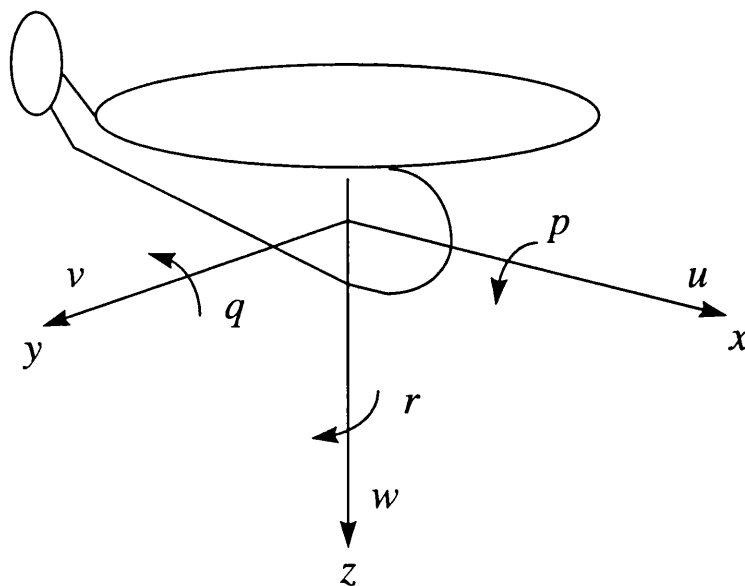


Figure 2.1. Rigid body degrees of freedom.

The x -, y - and z -axes are known as the body referenced axes as they remain fixed to the fuselage of the helicopter, regardless of its orientation relative to the earth. u , v and w are the body referenced forward, side and heave velocities respectively. u is positive forwards, v is positive to starboard (to the right) and w is positive downwards. p , q and r are the body referenced roll, pitch and yaw rates respectively. p is positive clockwise if looking out the nose of the helicopter, q is positive in the nose-up direction and r is positive clockwise if looking down on the helicopter.

The orientation of the fuselage with respect to the earth is described by the so called Euler angles, θ , ϕ and ψ , the pitch, roll and yaw attitudes respectively. Figure 2.2 shows the Euler angles in graphical form. It is seen that the pitch and roll attitudes are referenced to the surface of the earth and the yaw attitude is referenced to some heading, in the case of Figure 2.2(c) the reference heading is north, which is standard.

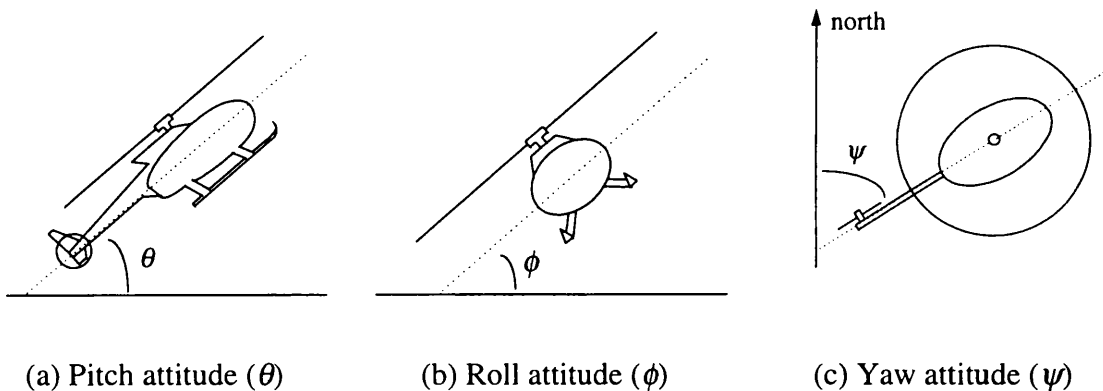


Figure 2.2. Definition of Euler angles.

The motions and Euler angles can be divided into longitudinal and lateral states. Longitudinal dynamics act within the x - z plane and so includes u , w , q and θ . Lateral dynamics act within the x - y and y - z planes and so includes v , p , ϕ , r and ψ .

There are 3 sets of equations which are used to describe the rigid body dynamics. These sets of equations are the force, moment and kinematic equations.

The force equations relate to the translational motion and are given by,

$$\dot{u} = -(wq - vr) + \frac{X}{M_h} - g \sin \theta \quad (2.1)$$

$$\dot{v} = -(ur - wp) + \frac{Y}{M_h} - g \cos \theta \sin \phi \quad (2.2)$$

$$\dot{w} = -(vp - uq) + \frac{Z}{M_h} - g \cos \theta \cos \phi \quad (2.3)$$

where g is the gravitational constant (9.81 ms^{-1}), M_h is the mass of the helicopter and X , Y and Z are the components of force in the x -, y - and z -body axes. It is seen from Eqns (2.1) - (2.3) that there is coupling between the translational accelerations and the rotational rates.

The moment equations relate to the rotational rates of motion and are given by,

$$I_{xx} \dot{p} = (I_{yy} - I_{zz})qr + I_{xz}(\dot{r} + pq) + L \quad (2.4)$$

$$I_{yy} \dot{q} = (I_{zz} - I_{xx})pr + I_{xz}(r^2 - p^2) + M \quad (2.5)$$

$$I_{zz} \dot{r} = (I_{xx} - I_{yy})pq + I_{xz}(\dot{p} - qr) + N \quad (2.6)$$

where I_{xx} , I_{yy} and I_{zz} are the moments of inertia and I_{xz} is the product of inertia. L , M and N are the components of moment in the x -, y - and z -body axes.

The rotational motion of the fuselage is referenced to the earth-fixed axis system through the use of the kinematic equations which are given as,

$$\dot{\phi} = p + q \sin \phi \tan \theta + r \cos \phi \tan \theta \quad (2.7)$$

$$\dot{\theta} = q \cos \phi - r \sin \phi \quad (2.8)$$

$$\dot{\psi} = (q \sin \phi + r \cos \phi) \sec \theta \quad (2.9)$$

The forces and moments acting on the fuselage can be written as the sum of the contributions from the various helicopter components (Padfield [60]). For example, the total X force acting on the fuselage can be written in component form as,

$$X = X_R + X_{TR} + X_f + X_{fp} + X_{fn} \quad (2.10)$$

where the subscript R refers to the main rotor, TR to the tail rotor, f to the fuselage, tp to the horizontal tail plane and fn to the vertical fin.

The main rotor is fundamental to the operation of a helicopter and its dynamics impinge greatly upon the fuselage dynamics. The following Section describes the dynamics of the main rotor both qualitatively and in basic mathematical terms. Some sources of cross-coupling unique to the helicopter (i.e. dynamics which fixed-wing aircraft do not exhibit) will be described, and the way in which a pilot can effect desired motion will be explained.

2.2.2 Rotor Dynamics

2.2.2.1. Flapping

To explain the concept of flapping, some preliminaries of rotor aerodynamics must first be dealt with. Consider first the helicopter trimmed in hover (an aircraft is regarded as being trimmed if the sum of the forces and the sum of the moments are zero, i.e. it is in a steady flight condition). In hover, the velocity distribution on the main rotor blades is equal, regardless of azimuthal position. Figure 2.3 shows a top view of a main rotor which is spinning anti-clockwise when viewed from above. Shown on Figure 2.3 is the definition of azimuthal position ψ (note that azimuthal position has the same symbol as yaw attitude, but the distinction will be clear from the context).

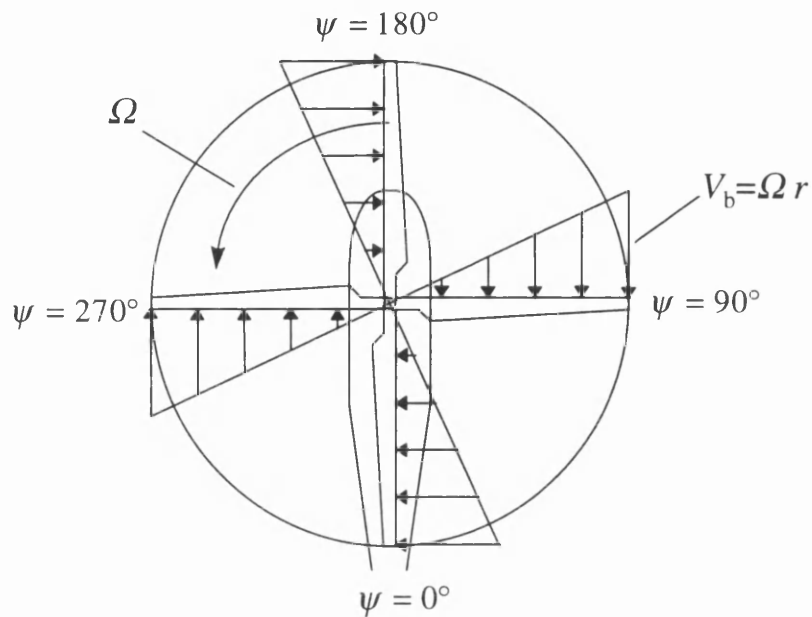


Figure 2.3. Rotor blade velocity distribution in hover.

The rotor spins with an angular velocity of Ω rad/s and so the velocity that a segment of blade will see at radius r , for any azimuthal position, will be,

$$V_b = \Omega r \quad (2.11)$$

It is seen from Eqn (2.11) and Figure 2.3 that the velocity the blade sees is greater at the tip than at the root. Figure 2.4 shows a cross-section of a blade segment and shows the lift vector resulting from the blade being placed in an air stream (drag is neglected here for clarity).

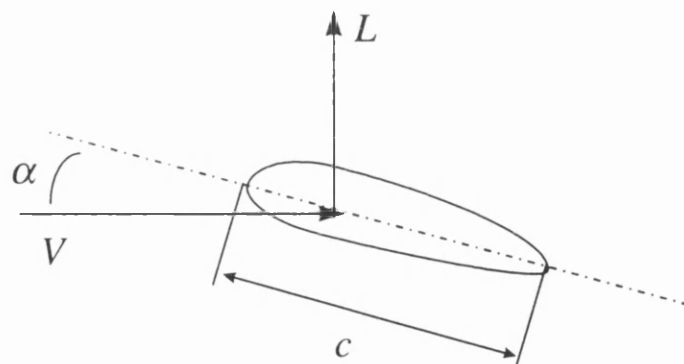


Figure 2.4. Blade segment in airstream.

A simple expression for the lift is given as,

$$L = \frac{1}{2} \rho V^2 c a_0 \alpha \quad (2.12)$$

where ρ is the air density, c is the blade chord, a_0 is the lift coefficient and α is the angle of attack. It is seen from Eqn (2.12) that the lift increases as the airspeed increases. If the blades have a uniform angle of attack from root to tip then the lift would be greater at the tip, with the result that the blade would suffer greater loads at the tip. To make the lift more evenly distributed over the blade, the blade can be twisted such that the effective angle of attack decreases as the distance from the blade root increases.

If each rotor blade is set to have the same angle of attack distribution then the lift distribution over the rotor disc will be uniform when in hover. In forward flight however, the lift distribution is not uniform over all the rotor blades. Figure 2.5 shows a top view of a helicopter with some forward velocity V .

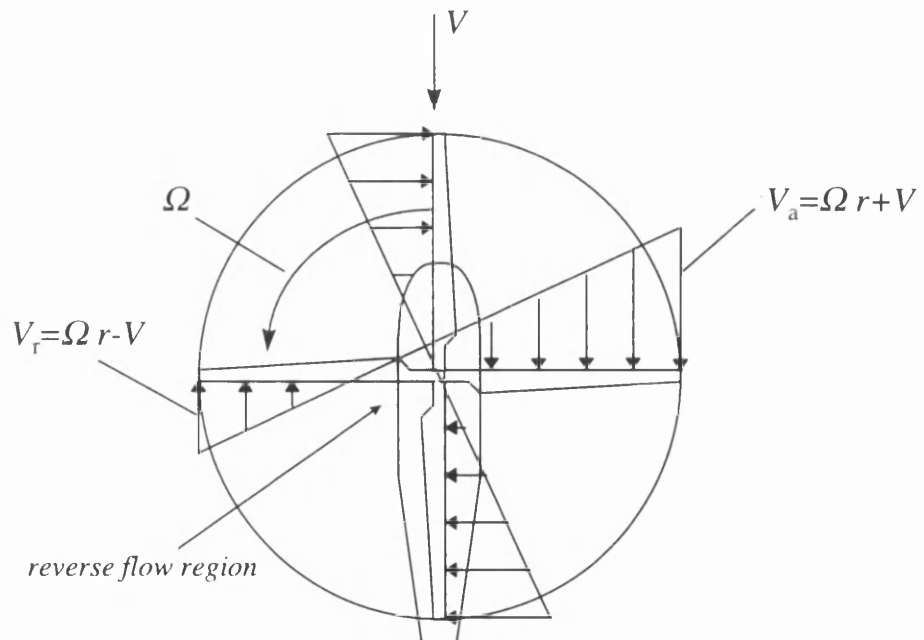


Figure 2.5. Rotor blade velocity distribution in forward flight.

From Figure 2.5 it is seen that the lift that a blade segment will see is given as,

$$V_b = \Omega r + V \sin \psi \quad (2.13)$$

It is noted that the blade passing through $\psi = 90^\circ$ is known as the advancing blade and the blade passing through $\psi = 270^\circ$ is known as the retreating blade, hence the subscripts on the velocities shown in Figure 2.5. There is a region near the rotor hub where the retreating blade is seeing reverse flow. This region is aptly named the *reverse flow region* and becomes larger as the forward velocity increases. If the rotors were rigid, then this discontinuity in flow would create more lift on the advancing side and less lift on the retreating side, hence causing a clockwise rolling moment which increases in magnitude as forward speed increases, which is highly undesirable. In order to make the lift distribution more even over the rotor disc in forward flight, the blades are hinged, thus enabling them to *flap*.

Before describing the concept of blade flapping, consider an arbitrary blade segment. If the speed of the air passing over the blade were to increase, the lift would increase causing it to begin accelerating upwards. Aerodynamic damping would then occur, neutralising the acceleration, and the blade will have a resultant upward velocity. This has the effect of reducing the effective angle of attack of the blade and, from Eqn (2.12), reducing the lift. The effective decrease in angle of attack is seen graphically in Figure 2.6(a), where V is the freestream velocity, V_i is the induced velocity, V_r is the resultant velocity and α is the angle of attack. Likewise, if the speed of the air passing over the blade were to decrease then the blade would accelerate downwards. Aerodynamic damping then occurs and the blade will have a resultant downward velocity. This has the effect of increasing the effective angle of attack of the blade and, from Eqn (2.12), increasing the lift. The effective increase in angle of attack is seen graphically in Figure 2.6(b).

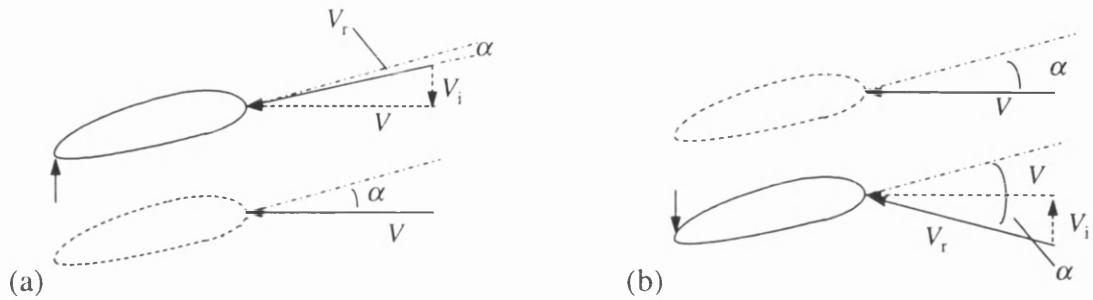


Figure 2.6. Change in angle of attack due to induced velocity.

For the rotor in forward flight to have a balanced lift distribution, the lift must be decreased on the advancing side and increased by a proportional amount on the retreating side. To achieve this, the advancing blade must be seen to have a positive rate of climb and the retreating blade must be seen to have a negative rate of climb.

As seen in Figure 2.5 the advancing blade sees a higher velocity and, as it is hinged, will begin to rise. If the rotor is hinged at the rotor shaft (this is known as a teetering rotor) then the blade will continue rising until it reaches the nose of the helicopter, where it will stop rising. As the blade retreats from the nose, the effect of the forward velocity of the helicopter will reduce the effective velocity of the blade and it will begin to drop, until it reaches the tail where the descent will stop. The blade will therefore ascend on the advancing side, and descend on the retreating side. These are the conditions required to balance the lift distribution in forward flight. Figure 2.7(a) shows this type of flapping in graphical form for some arbitrary flight condition. It is known as longitudinal flapping as it occurs in the longitudinal plane of the helicopter, and this displacement of the tip-path plane of the rotor from the plane of rotation is given the symbol β_{lc} . Also shown on Figure 2.7(a) is an additional blade angle which is given the symbol β_0 . This motion of the rotor is known as coning (as it causes the rotor to form a cone shape). Of course, flapping can occur in the lateral plane as well as the longitudinal plane and Figure 2.7(b) shows the lateral flap angle, β_{ls} , graphically.

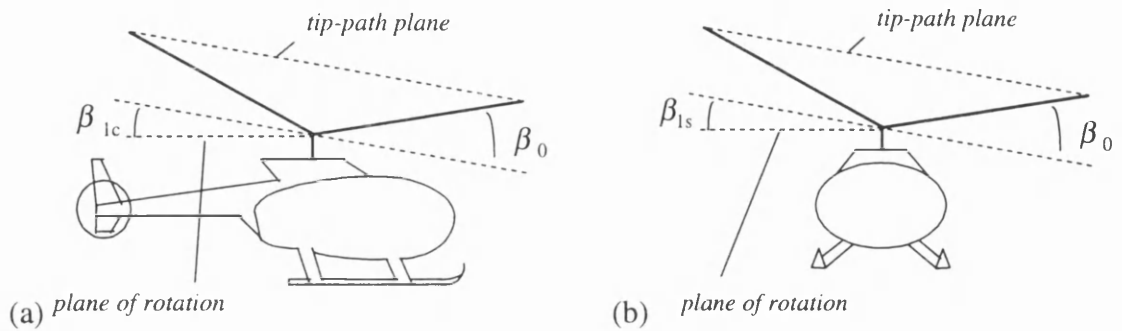


Figure 2.7. (a) Longitudinal flapping and coning, (b) Lateral flapping and coning.

From the above discussion, it is seen that a flapping teetering rotor displays the characteristics of a system in resonance. A system in resonance is a system which receives an input which is at the same frequency as the system's natural frequency. The output of a system in resonance lags its input by 90° . This lag means that there will be a time delay before the helicopter reacts to resonant stimuli. This time delay is a function of rotor speed and is calculated as,

$$\tau = \frac{1}{4} \frac{2\pi}{\Omega} = \frac{\pi}{2\Omega} \quad (2.14)$$

where τ has the unit of seconds and Ω is the main rotor angular rate and has the unit of rad/s.

If the rotor flaps out of a trim condition then two simple expressions can be used to describe how the resulting steady state flap angles affect the rigid body dynamics. They are given as (Padfield [60]),

$$M = -N_b \frac{K_\beta}{2} \beta_{1c} \quad (2.15)$$

$$L = -N_b \frac{K_\beta}{2} \beta_{1s} \quad (2.16)$$

where M and L are the rigid body pitch and roll moments, N_b is the number of rotor blades and K_β is the rotor stiffness.

The flapping dynamics can be approximated by a second order differential equation of the form,

$$\beta'' + C_{M0}\beta' + D_{M0}\beta = H_{M0}(\psi) \quad (2.17)$$

where the prime indicates differentiation with respect to rotor azimuth. C_{M0} , D_{M0} and $H_{M0}(\psi)$ are coefficient matrices and,

$$\beta = [\beta_0 \quad \beta_{1c} \quad \beta_{1s}] \quad (2.18)$$

For Eqn (2.17) the rotor is approximated as a disc rather than consisting of individual blades. The reader is referred to Padfield [60] for more details on the coefficient matrices and the approximations used.

2.2.2.2. Pitch to Roll Coupling

Two sources of coupling between pitch and roll which are unique to the helicopter will be explained here.

The first source of coupling is caused when the rotor has a hinge offset. Figure 2.8 shows the difference between a teetering rotor and a rotor with a hinge offset.

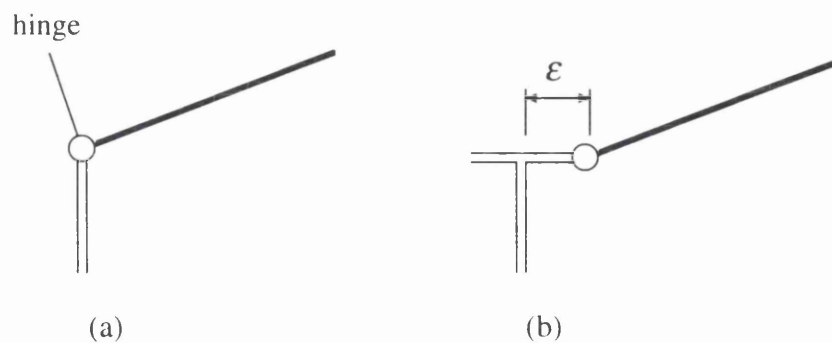


Figure 2.8. (a) Teetering rotor, (b) Rotor with hinge offset.

A rotor with a hinge offset is more manoeuvrable than a teetering rotor, as an additional hub moment is caused due to centrifugal force. However, the rotor will no longer flap in resonance due to the hinge offset, but will tend to lag an input by some angle less

than 90° . This will cause coupling between longitudinal and lateral flapping with the consequence that pitching and rolling motion of the fuselage will be coupled. For the Lynx the effective hinge offset is approximately 12.5%, which causes the rotor lag to be about 75° – 80° .

The second source of coupling arises in forward flight. Because the main rotor is coning, the free airstream will hit the underside of the rotor blade over the nose, and the top of the rotor blade over the tail. This is shown graphically in Figure 2.9.

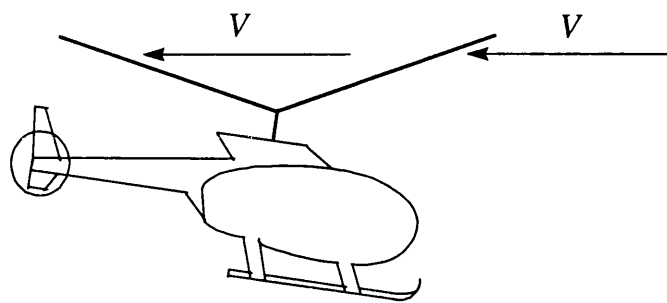


Figure 2.9. Helicopter trimmed in forward flight.

The airstream impinging upon the blade over the nose effectively increases its angle of attack and so the blade will flap up to reach a maximum at $\psi = 270^\circ$. In addition, the airstream impinging upon the blade over the tail effectively decreases its angle of attack and so the blade will flap down to reach a minimum at $\psi = 90^\circ$. This flapping in the lateral plane will cause the helicopter to roll to starboard. This rolling motion becomes more pronounced if the helicopter pitches up and so is a source of cross-coupling.

2.2.2.3. Yaw due to Height Rate Coupling

Another source of coupling unique to the helicopter is that of an induced yaw rate due to a change in the height rate of the helicopter. The reason for this is explained by

consideration of Figure 2.10. It is seen that, when trimmed, the lift produced by the tail rotor, T_t , produces a moment $l_t T_t$ which cancels the torque of the main rotor, Q , in order to stop the fuselage from spinning. i.e.,

$$Q = l_t T_t \quad (2.19)$$

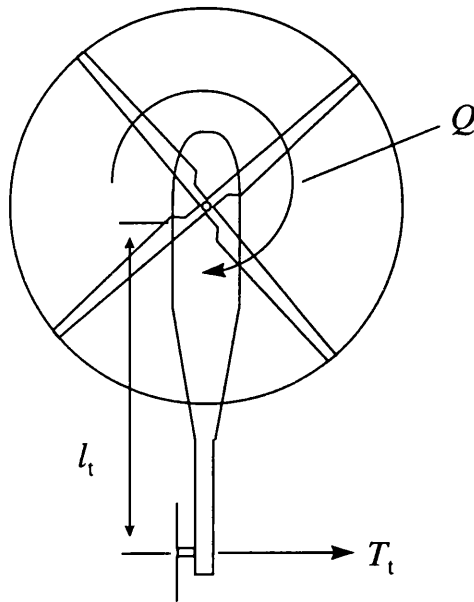
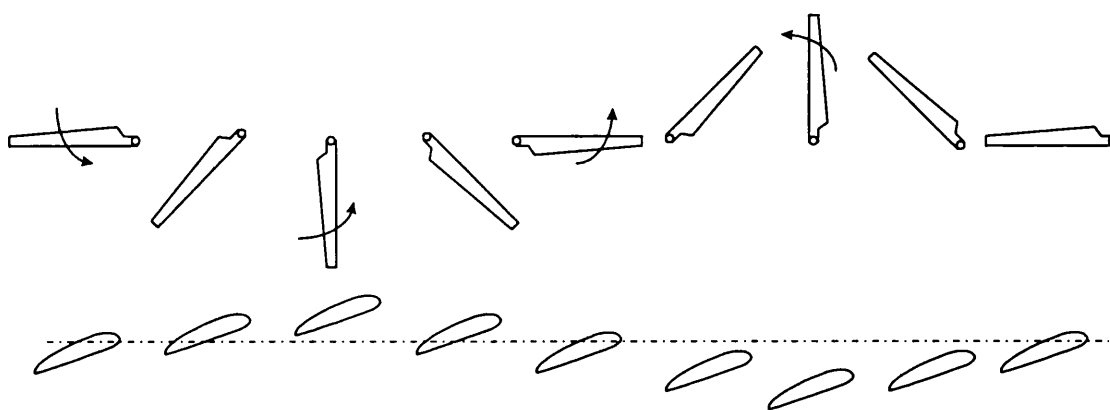


Figure 2.10. Balance of main rotor torque with tail rotor thrust

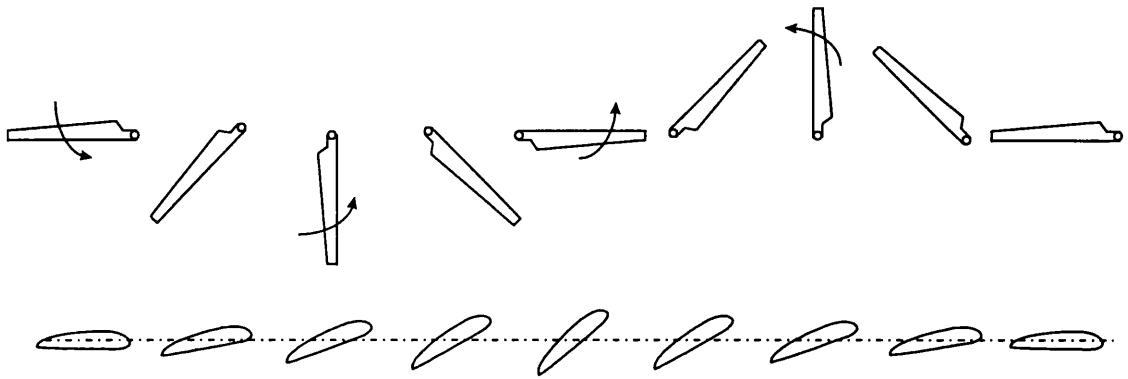
If the lift of the main rotor is increased in order to augment the height rate, the main rotor torque will increase correspondingly and hence the main rotor torque will be greater than the moment produced by the tail rotor. As a consequence the helicopter will begin yawing clockwise. Likewise, if the torque is decreased then the helicopter will yaw anti-clockwise.

2.2.2.4. Feathering

It was shown in Section 2.2.2.1 how the rotor can flap in order to balance the lift distribution when velocity conditions at the rotor disc are changed. The same effect in lift distribution can be produced if the rotor blades are rigid, but are able to feather. As far as the lift on a blade is concerned, only the local angle of attack is of importance. Recall from the discussion on flapping that on the advancing blade, the resulting upward motion of the blade caused the effective angle of attack to be decreased, and vice-versa for the retreating blade. The same effect can be produced on a blade which is unable to flap, by rotating the advancing blade nose-down to reduce the angle of attack and rotating the retreating blade nose-up to increase the angle of attack. Therefore, to produce an equivalent aerodynamic effect on rigid blades, each blade would be rotated cyclically in a nose-up and nose-down manner. The blades are able to rotate in this way via the use of a feathering hinge. Figure 2.11 shows the 'equivalence' of flapping and feathering for one revolution of a rotor blade in forward flight, where the aerodynamic effect on each rotor blade will be the same. The reader should note that rotor blades usually have the ability to both feather and flap. In this case, feathering the rotor blades out of a trim condition will tend to cause the rotor blades to flap correspondingly.



(a)



(b)

Figure 2.11. (a) Flapping rotor blade (b) Feathering rotor blade.

2.2.2.5. Pilot Control

Feathering is an effective way for a pilot to induce desired rotor behaviour. For example, if the pilot forced a cyclic feather of each blade such that the angle of attack increased on the advancing blade and decreased on the retreating blade then the blade would flap up over the nose and flap down over the tail, thus causing the helicopter to pitch up. With an effective feathering mechanism, the helicopter can be manoeuvred in any direction. One such mechanism is known as a swash plate. Figure 2.12(a) shows a schematic diagram of a swash plate and Figure 2.12(b) shows how feathering is effected by tilting the swash plate.

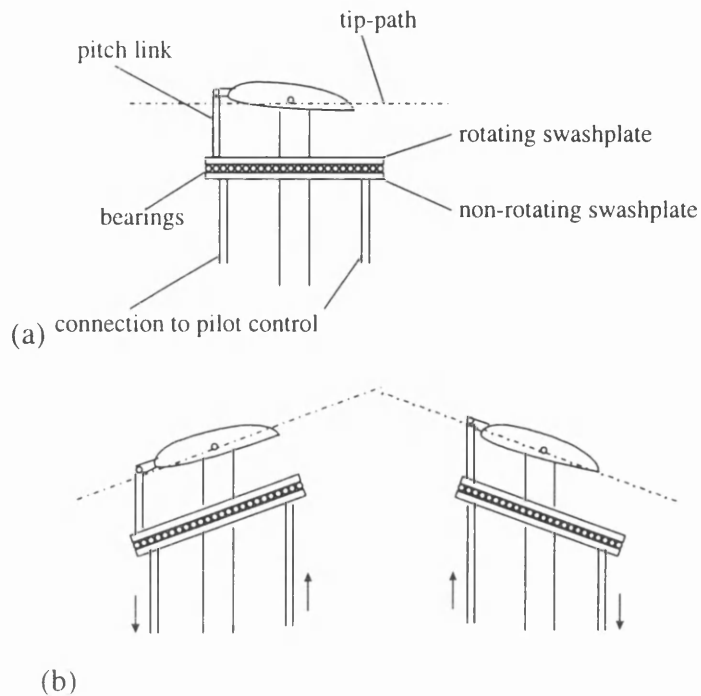


Figure 2.12. (a) Swashplate, (b) Tilted swashplate to induce feathering (blades shown are at opposite sides of swashplate)

There are three ways in which the swash plate can be used to effect changes in the main rotor.

- i) The swash plate can be moved up and down by use of the pilots collective lever. This motion will equally and simultaneously change the pitch attitude of all the rotor blades. This means that the lift on all the blades will change equally and so this motion of the swash plate is primarily used for height control. The blade angle formed by such a change of the swash plate is given the symbol θ_0 and is known as the main rotor collective blade angle.
- ii) Longitudinal tilt of the swash plate is effected by use of the longitudinal cyclic. This motion will cause the rotor blades to cyclically change their angle of attack with their maximum and minimum angles of attack at $\psi = 90^\circ$ and $\psi = 270^\circ$ respectively (aft motion - pulling the stick backwards) or maximum and minimum at $\psi = 270^\circ$ and $\psi = 90^\circ$ (fore motion - pushing the stick forwards). This will cause the rotor blades to flap in the longitudinal plane and hence the lift vector can be rotated fore and aft. The

blade angle formed by such a change of the swash plate is given the symbol θ_{1s} and is known as the longitudinal cyclic blade angle.

iii) Lateral tilt of the swash plate is effected by use of the lateral cyclic. This motion will cause the rotor blades to cyclically change their angle of attack with their maximum and minimum angles of attack at $\psi = 0^\circ$ and $\psi = 180^\circ$ respectively (port motion - pulling the stick to the left) or $\psi = 180^\circ$ and $\psi = 0^\circ$ (starboard motion - pulling the stick to the right). This will cause the rotor blades to flap in the lateral plane and hence the lift vector can be rotated port and starboard. The blade angle formed by such a change of the swash plate is given the symbol θ_{1c} and is known as the lateral cyclic blade angle.

The above three degrees of freedom of the swash plate can be used to move the helicopter in any direction. In addition to the main rotor control, the pilot also has access to the angle of attack of the tail rotor blades, through the use of pedals, and so can use this degree of freedom to point the fuselage by changing the lift of the tail rotor. The tail rotor collective blade angle is given the symbol θ_{0T} .

2.2.3. The Simulation Model

As the Sections above indicate, the helicopter is an extremely complex dynamical system, and the development of simulation models which describe these dynamics accurately is the topic of a great deal of on-going research (see for example, Fu and Kaletka [12], Harding [18], Houston [26] and Padfield [60]). The main source of uncertainty in the simulation models, to date, is the dynamics of the main rotor. This uncertainty arises from both unmodelled dynamics and uncertainty in model parameters and is a fundamental problem in the design of high-bandwidth, highly augmented flight control systems (Murray-Smith [52]). The problem arises from uncertain, and hence unquantifiable, signals being fed through the feedback system. A control system must therefore exhibit robustness to such uncertainty.

The simulation model used for the work of this thesis is known as the *rationalised helicopter model* (RHM) and is based on a model developed by Padfield [59]. The RHM is a generic non-linear helicopter model which includes rigid body dynamics, second order flapping dynamics, actuator dynamics, engine dynamics, actuator rate limits and blade angle limits. The rigid body dynamic equations and the flapping dynamic equations used in the RHM are of the form given in Sections 2.2.1 and 2.2.2. For the work of this thesis the RHM was configured as a Lynx-like helicopter. The configuration data for a Lynx-like helicopter, relevant to the equations of motion listed in Sections 2.2.1 and 2.2.2, is given in Appendix I.

For the purposes of control system design the RHM model (with engine dynamics neglected - as they do not impinge significantly upon the motion dynamics) is linearised to produce linear models of the form,

$$\dot{x} = Ax + Bu \quad (2.20)$$

$$y = Cx \quad (2.21)$$

where the A matrix contains the stability derivatives, the B matrix the control derivatives and the C matrix observes the appropriate outputs. Appendices II, III and IV give the linearised state space models for hover, 30 and 80 knots respectively.

The state vector x is given by ,

$$x = \left[u \quad w \quad q \quad \theta \quad v \quad p \quad \phi \quad r \quad \psi \quad \beta_0 \quad \beta_{1c} \quad \beta_{1s} \quad \dot{\beta}_0 \quad \dot{\beta}_{1c} \quad \dot{\beta}_{1s} \quad \theta_{0act} \quad \theta_{1sact} \quad \theta_{1cact} \quad \theta_{0Tact} \right] \quad (2.22)$$

where the rigid body states and rotor states are previously defined but are now the perturbations of the states from some trim condition. θ_{0act} , θ_{1sact} , θ_{1cact} and θ_{0Tact} are actuator states for each of the four helicopter inputs. The actuators are modelled as first order lags of the form,

$$\frac{\theta_x}{\delta_x} = \frac{1}{1 + sT_x} \quad (2.23)$$

where T_x is the time constant of the actuator. The actuator time constants for the Lynx-like helicopter are given in Appendix I.

The control input u is given as,

$$u = [\theta_0 \quad \theta_{ls} \quad \theta_{lc} \quad \theta_{or}] \quad (2.24)$$

where the inputs are previously defined.

In this thesis, the earth referenced height rate is chosen as a controlled output. For straight and level flight, height rate is given in linear form as,

$$\begin{aligned} \dot{h} = & \sin \Theta_0 u - \cos \Theta_0 \cos \Phi_0 w + (U_0 \cos \Theta_0 + W_0 \sin \Theta_0 \cos \Phi_0) \theta \dots \\ & \dots - \cos \Theta_0 \sin \Phi_0 v + W_0 \cos \Theta_0 \sin \Phi_0 \phi \end{aligned} \quad (2.25)$$

where Θ_0 is the trimmed pitch attitude, Φ_0 is the trimmed roll attitude, U_0 is the trimmed forward velocity and W_0 is the trimmed heave velocity.

2.3. Helicopter Handling Qualities

If an aircraft, whether it be of fixed or rotary wing form, is capable of being flown safely and effectively by the pilot throughout its flight envelope then it is regarded as having 'good' Handling Qualities. Ultimately, the question of whether a particular aircraft can be safely and effectively flown can only be answered by the pilots who will fly it. However, experience has shown that dynamical characteristics of an aircraft which a pilot will find undesirable can be quantified and hence can be subject to numerical assessment. This allows Handling Qualities considerations to be included in the design process from the onset and it is important that flight control engineers use the quantitative criteria to guide the development of flight control systems. In the rotorcraft community, the United States Army has led the development of a Handling Qualities specification known as the Aeronautical Design Standard (ADS-33). ADS-33 is continually going through revision due to the always expanding database on which it is based, the latest update being ADS-33D [3] which was published in 1994.

ADS-33D contains both quantitative and qualitative criteria. The quantitative criteria are criteria that are relevant for control system design and it is these criteria which will

be reviewed in this Chapter. Qualitative criteria relate to pilot opinion and is outwith the scope of the work in this thesis.

Before moving on to the discussion of the requirements which will be used to assess the designs in this thesis, this is an appropriate point to define various ADS-33 terminology which will be used not only in this Chapter, but also in Chapters 7 through 9 which deal with the design of specific control laws.

2.3.1. ADS-33 Terminology

Levels - A rating of the Handling Qualities of the helicopter based on the Cooper-Harper Pilot Rating Scale (Cooper and Harper [8]). Level 1 is when the helicopter handles satisfactorily without improvement. Level 2 has deficiencies which warrant improvement and Level 3 has deficiencies which require improvement. Level 1 is desired. Level 2 is acceptable with a tolerable pilot workload, but only adequate performance will be achievable. Level 3 is unacceptable.

Mission Task Element (MTE) - An element of a mission that can be treated as a Handling Qualities task. MTEs are defined such that they have pre-defined and measurable start and end points, that allow the Handling Qualities to be assessed in a repeatable and quantifiable manner. Examples of MTEs are Target Acquisition and Tracking, Precision Hover and Rapid Hovering Turn.

Response-Type - A characterisation of the rotorcraft response to a control input in terms of well recognised stability augmentation systems. Response types under consideration in this thesis are listed below.

Attitude Command Attitude Hold (ACAH)- A deflection in the pilot's cyclic control (joystick) will result in a proportional pitch or roll attitude (Attitude Command), e.g. if the pilot pulls the stick towards him/herself then the helicopter will pitch up by a proportional amount. In addition, if no input is commanded by the pilot the helicopter will maintain its initial pitch and roll orientation (Attitude Hold).

Rate Command (RC) - A deflection in the pilot's cyclic control will result in a proportional pitch rate or roll rate.

Translational Rate Command (TRC) - A deflection in the pilots cyclic control will result in a proportional longitudinal or lateral velocity, e.g. if the pilot pushes the stick forward then the longitudinal velocity of the helicopter will increase.

Hover - Hovering flight is defined as all operations occurring at ground speeds less than 15 knots (7.7 m/s).

Low Speed - Low speed flight is defined as all operations occurring at ground speeds between 15 and 45 knots (7.7 and 23 m/s).

Forward Flight - Forward flight is defined as all operations with a ground speed greater than 45 knots (23 m/s).

Useable Cue Environment (UCE) - A rating determining the ability of the pilot to use outside visual cues and artificial vision aids to control the attitude and velocity of the helicopter. A good visual environment will be UCE=1 and a severely degraded visual environment, such as heavy fog, will be UCE=3.

2.3.2. Small Amplitude Requirements

This Section deals with the small amplitude quantitative criteria. These criteria are assessed in both the frequency domain and the time domain. The frequency domain criterion determines the Handling Qualities bandwidths and the time domain criterion, or Mid-Term Response criterion, assesses the oscillatory modes. The bandwidth criterion predicts closed-loop tracking capability by the pilot whereas the Mid-Term assessment predicts the ability of the helicopter to remain trimmed if momentarily left unattended (Hoh [22]).

2.3.2.1. Short-Term Response to Control Inputs (Bandwidth)

This criterion assesses Handling Qualities bandwidths which are measured from the frequency response that the pilot ‘sees’. In the case of a helicopter which has an automatic control system implemented, the responses the pilot sees will be the frequency responses of the closed-loop system. Two bandwidths are defined, the phase limited bandwidth, $\omega_{BW_{phase}}$, and the gain limited bandwidth, $\omega_{BW_{gain}}$. $\omega_{BW_{phase}}$ is the frequency at which the phase of the response is -135° and $\omega_{BW_{gain}}$ is the frequency at which the gain is 6dB more than the gain at the -180° crossover frequency, ω_{-180° . These parameters are shown in graphical form in Figure 2.13.

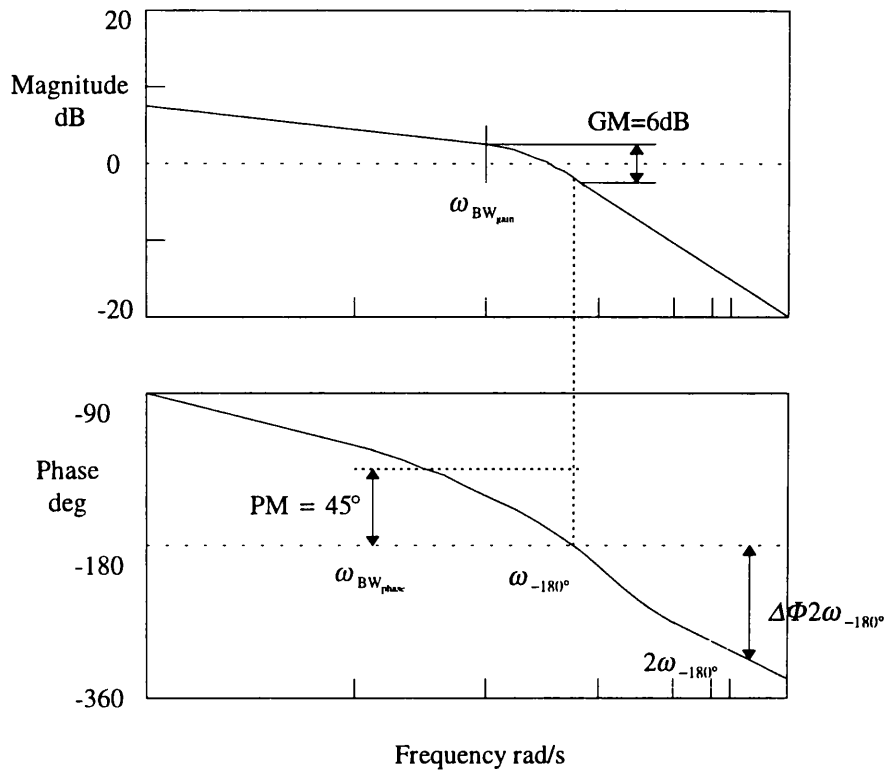


Figure 2.13. Definitions of Bandwidth and Phase Delay.

If $\omega_{BW_{phase}}$ is less than $\omega_{BW_{gain}}$ then the helicopter is referred to as having a *phase limited* bandwidth, and vice versa.

Conceptually, $\omega_{BW_{phase}}$ is the highest frequency a pilot can operate at without threatening the stability of the helicopter. If a pilot were to operate above this frequency, then small changes in the phase characteristics of the helicopter could render the system unstable, i.e. the pilot could suddenly find him/herself operating at above ω_{-180° which is particularly hazardous if the pilot is unprepared. To stabilise the helicopter in such a situation would require the pilot introducing additional phase lead. Although pilots are capable of operating at such frequencies, additional workload is required which can result in degraded Handling Qualities. The situation where the pilot operates at such frequencies is known as pilot equalisation (Ockier and Pausder [54]). Also, pilot induced oscillations (PIOs) may occur if the phase bandwidth of the aircraft is low and the task bandwidth is high (Padfield *et al* [62]).

$\omega_{BW_{gain}}$ is the highest frequency that the pilot can operate at without threatening stability if he/she is acting as a pure gain controller. It relates particularly to situations where aggressive or precision manoeuvring will be required. It is recognised that ACAH systems are more likely to be gain limited because the gain response is inherently flat at low frequency. However, for ACAH systems, PIOs are not threatening to helicopter safety because the pilot can always release the controls and be confident that the aircraft will return to trimmed flight, which would not be the case for a Rate Command system. If $\omega_{BW_{phase}}$ is less than $\omega_{BW_{gain}}$ then a gain margin of at least 6dB is available to the pilot which will reduce the risk of PIOs.

Shown on Figure 2.13 is an additional parameter, $\Delta\Phi_{2\omega_{-180^\circ}}$. This is used to calculate the phase delay of the response. the phase delay is calculated as,

$$\tau_p = \frac{\Delta\Phi_{2\omega_{-180^\circ}}}{57.3(2\omega_{-180^\circ})} \quad (2.26)$$

Phase delay characterises the phase roll-off in the region of the -180° crossover frequency. A high phase roll-off is indicative of PIO tendencies. Pilots are very sensitive to this phase delay, particularly in the roll axis for precision tasks and this is reflected in the Handling Qualities requirements. Figure 2.14(a) shows the boundaries for the pitch attitude for Target Acquisition and Tracking in hover and low speed and Air Combat in forward flight, the most stringent requirements which share the same boundaries. Figure 2.14(b) shows the boundaries for the roll attitude for Target Acquisition and Tracking in hover and low speed and Air Combat in forward flight, the most stringent requirements which also share the same boundaries. It is seen that the roll response has an upper bound on the required phase delay for Level 1 and Level 2 whereas the pitch response does not.

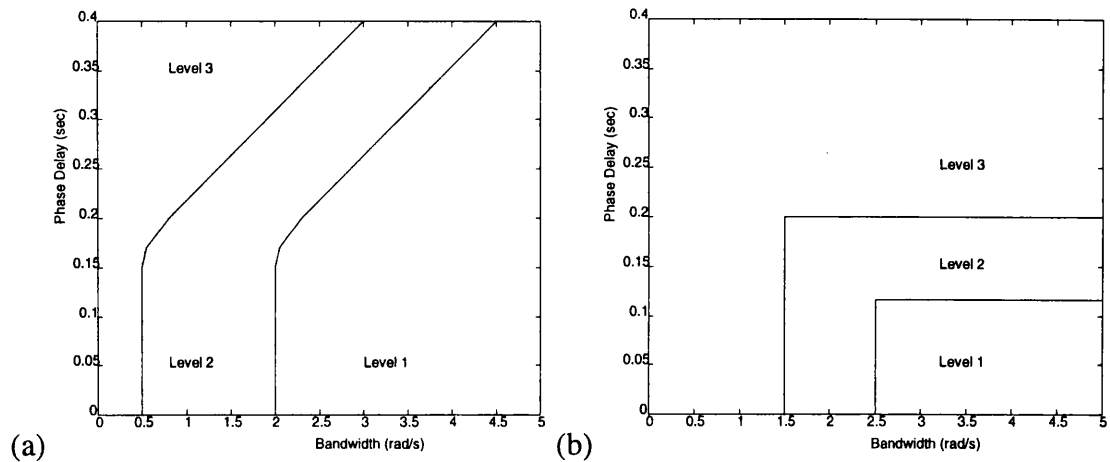


Figure 2.14. (a) Handling Qualities requirements for small amplitude pitch response.
(b) Handling Qualities requirements for small amplitude roll response

2.3.2.2. Mid-Term Response to Control Inputs

The Mid-Term response characteristics apply at frequencies below the Handling Qualities bandwidths and relates to pitch and roll changes. It is assessed by inserting a pulse input into the appropriate inceptor and measuring the effective damping ratio of the resulting oscillatory modes. The Mid-Term response is a measure of the ability of the helicopter to remain trimmed if pilot attention is diverted momentarily. Often an Attitude Hold (AH) function is sufficient to meet this requirement and so Mid-Term response assessment particularly relates to systems which do not possess AH.

ADS-33D does not explicitly state how the effective damping ratio is defined. In the fixed wing community, the damping ratio of a response is taken from an equivalent second order response (Adams *et al* [1]). It seems very likely that the rotorcraft community adopt this procedure also. The helicopter Handling Qualities toolbox produced by DRA (Bedford) (Howitt [27]) adopts a slightly different, but essentially similar, technique to the second order curve fit. It involves measuring neighbouring maxima and minima and calculating the effective damping ratio. Figure 2.15 shows an example of a response with the relevant parameters highlighted.

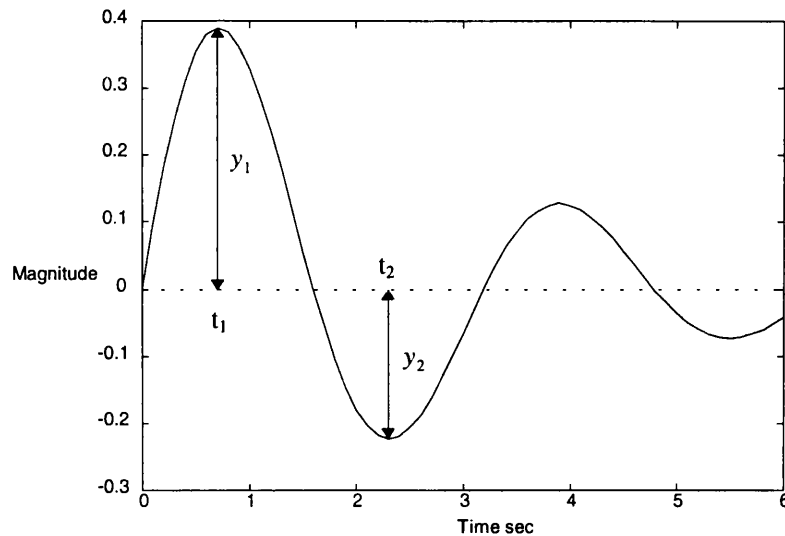


Figure 2.15. Example of second order impulse response.

The damping ratio is related to y_1 and y_2 by the following equation,

$$\frac{|y_2|}{|y_1|} = e^{-\pi\zeta/\sqrt{1-\zeta^2}} \quad (2.27)$$

rearranging Eqn (2.26) gives,

$$\zeta = \sqrt{\frac{K^2}{1 + K^2}} \quad (2.28)$$

where $K = -\ln(|y_2|/|y_1|)/\pi$.

The damped natural frequency of the response is given as,

$$\omega_d = \frac{\pi}{|t_1 - t_2|} \quad (2.29)$$

and the undamped natural frequency of the response, ω_n is calculated as,

$$\omega_n = \frac{\omega_d}{\sqrt{1 - \zeta^2}} \quad (2.30)$$

One may argue that if the response is not qualitative second order then this technique is not applicable. However, if the response is not qualitative second order it will not be possible to fit an appropriate second order response to it and so this is a meaningless

argument. In addition, if an on-axis attitude time response is not qualitative second order then the control system has definite room for improvement. A problem arises with this technique in the assessment of off-axis oscillations, e.g. roll oscillations due to a pulse input in the pitch inceptor. Off-axis responses, particularly for systems of high order, do not fit well into the category of having second order characteristics. The author has noted, for example, off-axis responses which oscillate with very little damping for only a short period of time and then suddenly die out. The effective damping of responses such as these is very difficult to quantify. The view taken in this thesis is that only the effective damping factor of the on-axis responses will be assessed, e.g. pitch due to pitch input, as this will be a relatively simple task. The resulting effective damping factor will be taken as representative of all the oscillatory modes as long as the off-axis oscillatory modes have sufficiently decayed by the time the on-axis oscillation has decayed. Figure 2.16 shows an example of an on-axis response of damping factor 0.6 and an off-axis response whose damping factor is indeterminate, but which has sufficiently decayed by the time that the on-axis response has decayed to an acceptable magnitude.

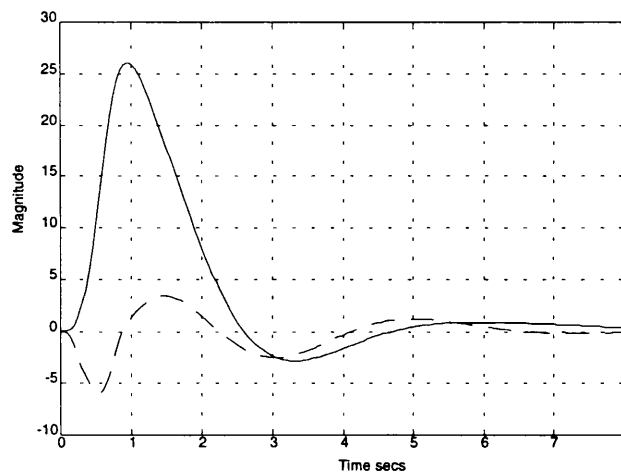


Figure 2.16. Second order on-axis response and indeterminate off-axis response.

Figure 2.17 shows the Handling Qualities boundaries for the Mid-Term response in hover and low speed. It is seen that an unstable response is allowable without degrading the handling from Level 1 only if the pilot is *fully attentive* to the control of the rotorcraft.

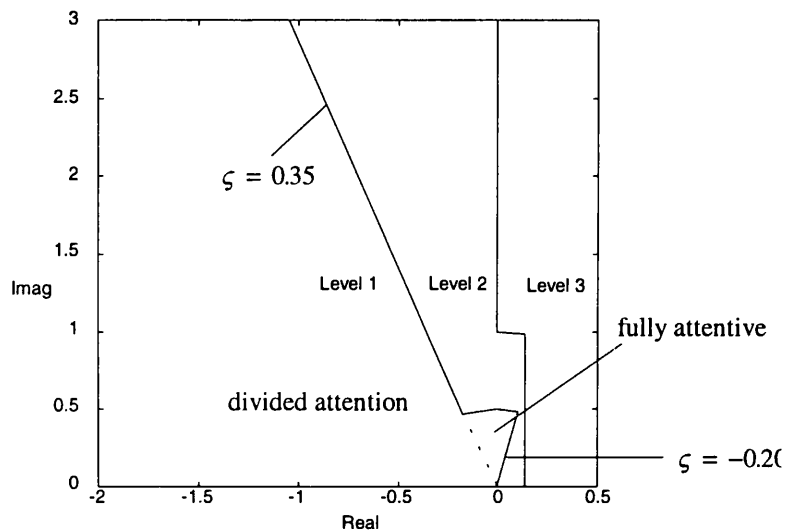


Figure 2.17. Limits on pitch (roll) oscillations for hover and low speed.

In forward flight, any oscillatory modes following a pulse controller input in the lateral axis (roll) shall meet the requirements shown in Figure 2.18.

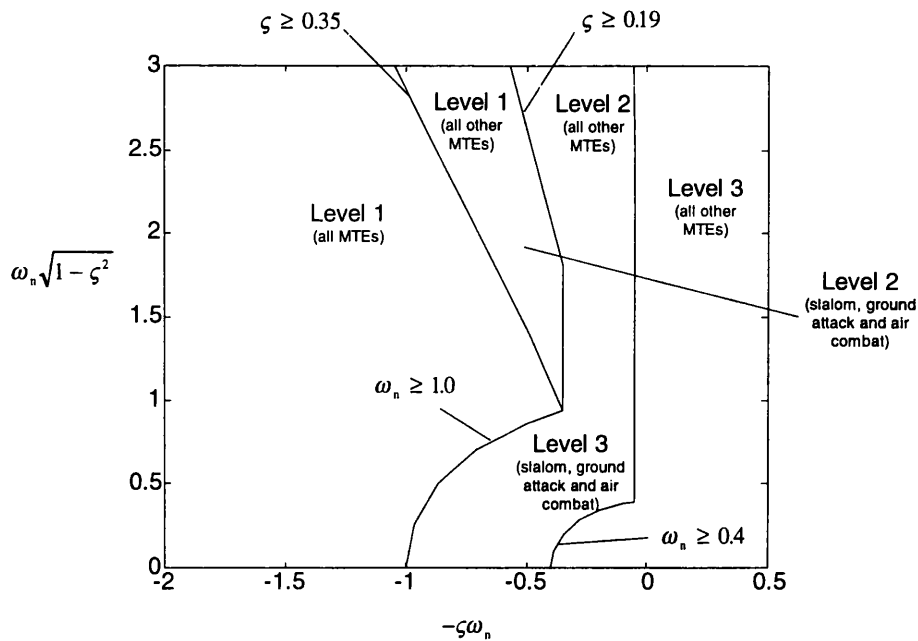


Figure 2.18. Lateral-directional oscillatory requirements in forward flight.

2.3.3. Moderate Amplitude Requirement (Attitude Quickness)

The moderate amplitude assessment is a measure of the helicopter's agility. The quicker a helicopter can change its attitudes then the more agile it is and this type of manoeuvring is the basis for the assessment.

Quickness is inherently related to both attitude bandwidth and attitude control power and makes the link between the two (Padfield [60]). Quickness is bounded by bandwidth as the attitude change tends to zero and bounded by control power as the attitude change becomes very large. It is principally a metric for Rate Command systems and need not be applied to ACAH, since this is principally a low speed, precision mode and not a high agility 'acrobatic' mode.

The agility of a helicopter is determined by a variety of factors including inertia, aerodynamic characteristics, actuator rate limits and rotor blade angle limits. Padfield [60] states that for helicopters with Rate Command augmentation the quickness is dependent on pulse amplitude and pulse width. The quicker the pulse and the larger the

amplitude, then the quicker the helicopter will change attitude. Sharp enough inputs must be used in this instance to establish the quickness bounds.

Figure 2.19 shows the quickness bound for pitch and roll attitude changes respectively. Note that the larger the required attitude change, the less ‘quick’ the helicopter needs to be to meet Level 1. This reflects the fact that large attitude changes take a longer time to achieve as the helicopter cannot move faster than the inertia, actuator rate limits etcetera, will allow.

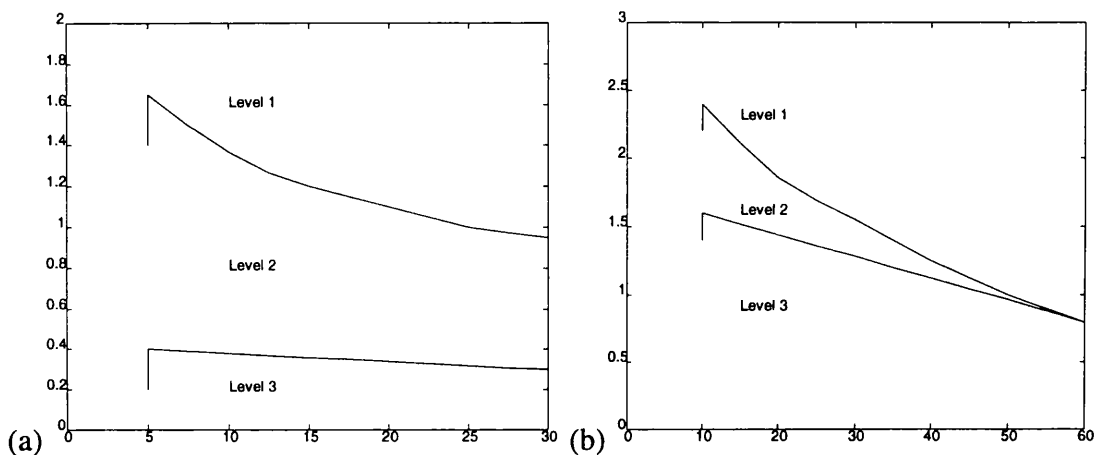


Figure 2.19. Agility boundaries for (a) Pitch attitude changes
(b) Roll attitude changes.

2.3.4. Interaxis Coupling

2.3.4.1. Yaw due to Collective

For abrupt collective inputs in hover and low speed flight there is a requirement on the allowable yaw rate. Three parameters are required for this assessment. These are; the value of the height rate measured at 3 seconds, $\dot{h}(3)$, and also two parameters r_1 and r_3 where,

r_1 = the first peak of the yaw rate (before 3 seconds) or, if no peak occurs before 3 seconds, the value of the yaw rate at 1 second, $r(1)$.

$r_3 = r(3) - r_1$ for $r_1 > 0$, or $r_3 = r_1 - r(3)$ for $r_1 < 0$. $r(3)$ is the yaw rate measured at 3 seconds.

Figure 2.20 shows the requirements in graphical form.

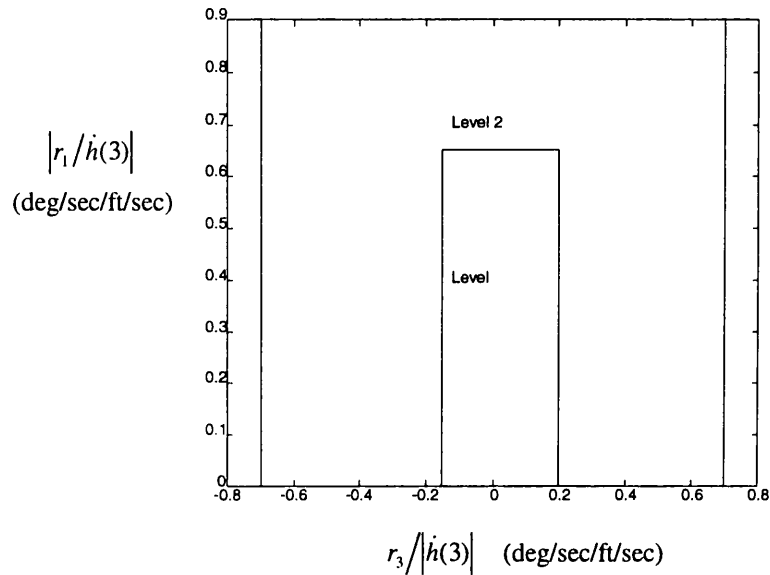


Figure 2.20. Collective-to-yaw coupling requirements.

2.3.4.2. Pitch to Roll and Roll to Pitch

During aggressive manoeuvring the ratio of the peak off-axis attitude response from trim *within* 4 seconds to the on-axis attitude from response *at* 4 seconds, $\Delta\theta_{pk}/\Delta\phi_4$ ($\Delta\phi_{pk}/\Delta\theta_4$), should not exceed the limits of Table 2.1.

Table 2.1. Maximum values for pitch-roll and roll-pitch coupling.

| | Level 1 | Level 2 |
|--|------------|------------|
| $(\Delta\theta_{pk} / \Delta\phi_4) \delta_{long}$ | ± 0.25 | ± 0.60 |
| $(\Delta\phi_{pk} / \Delta\theta_4) \delta_{lat}$ | ± 0.25 | ± 0.60 |

Figure 2.21 shows the necessary parameters for an example pitch attitude command.

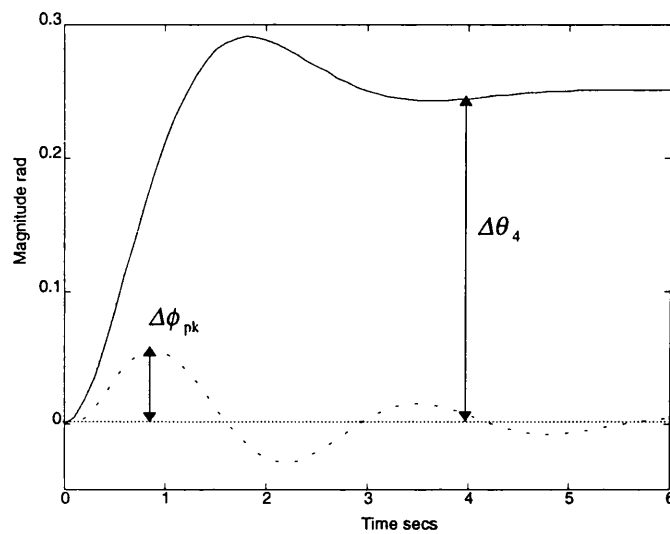


Figure 2.21. Pitch to roll coupling assessment.

2.3.4.3. Collective to Attitude Coupling

In forward flight the coupling of the pitch attitude, θ , and normal acceleration, n_z , of the helicopter due to collective step inputs is to be assessed. It is a requirement that the peak pitch attitude, θ_{peak} , occurring within the first three seconds following a 'large' step change in collective shall be such that the ratio $|\theta_{peak} / n_{z_{peak}}|$, where $n_{z_{peak}}$ is the peak normal acceleration, is less than 0.5 deg/ft/sec^2 in the up direction.

2.3.5. Height Response Characteristics

The height rate response due to a step collective input is to have a qualitative first order appearance for at least 5 seconds. The response is fitted to the following equivalent first order transfer function,

$$\frac{\dot{h}}{\delta_{\text{coll}}} = \frac{Ke^{-\tau_{\dot{h}_{\text{cuj}}} s}}{T_{\dot{h}_{\text{cuj}}} s + 1} \quad (2.31)$$

$\tau_{\dot{h}_{\text{cuj}}}$ is an equivalent time delay and $T_{\dot{h}_{\text{cuj}}}$ is an equivalent rise time. Table 2.2 shows the limits of the parameters in order to meet Level 1 and Level 2.

Table 2.2. Maximum values for height rate response due to collective step input.

| | $T_{\dot{h}_{\text{cuj}}}$ (sec) | $\tau_{\dot{h}_{\text{cuj}}}$ (sec) |
|---------|----------------------------------|-------------------------------------|
| Level 1 | 5.0 | 0.20 |
| Level 2 | ∞ | 0.30 |

The way in which the response is fitted to Eqn (2.30) is now described.

Height rate response data is collected at intervals no greater than 0.05 seconds from 0 to 5 seconds. This gives at least 101 data points.

A three variable non-linear least squares algorithm is then used to obtain a best fit for the data using the following time domain representation of Eqn (2.30).

$$\dot{h}_{\text{est}}(t) = K \left[1 - \exp \left\{ -(t - \tau_{\dot{h}_{\text{cuj}}}) / T_{\dot{h}_{\text{cuj}}} \right\} \right] \quad (2.32)$$

The function to be minimised in the least squares algorithm is the sum of squares of the error, ϵ , defined as,

$$\epsilon = \sum_{i=1}^n \left[\dot{h}(t = t_i) - \dot{h}_{\text{est}}(t = t_i) \right]^2 \quad (2.33)$$

where t_i is the time in seconds at the i -th data point and n is the number of data points.

The goodness of fit of the estimated curve is determined by the coefficient of determination, r^2 , which is defined as,

$$r^2 = \frac{\sum_{i=1}^n [\dot{h}_{\text{est}}(t = t_i) - \bar{\dot{h}}]^2}{\sum_{i=1}^n [\dot{h}(t = t_i) - \bar{\dot{h}}]^2} \quad (2.34)$$

where $\bar{\dot{h}}$ is the mean of the observed \dot{h} and is given by,

$$\bar{\dot{h}} = \frac{\sum_{i=1}^n \dot{h}(t = t_i)}{n} \quad (2.35)$$

r^2 is required to be greater than 0.97 and less than 1.03.

2.4. A Review of Current Research

This Section will focus on six linear control system design techniques which have been applied in recent years to helicopter flight control. It is not the purpose of this Section to give a tutorial of the techniques, the reader will be referred to appropriate literature in this instance, rather it is to review the findings of the various researchers who have substantial experience on the application of the techniques to helicopter flight control. An assessment of the cumulative findings will then be made. The techniques which will be reviewed in this Section are the Characteristic Locus Method, Nyquist Array methods, Quantitative Feedback Theory, Linear Quadratic techniques, Eigenstructure Assignment and H^∞ .

2.4.1. The Characteristic Locus Method

The Characteristic Locus Method is a neo-classical technique which attempts to reduce an m -input m -output (MIMO) multivariable design problem into m single-input single-output (SISO) design problems by manipulating the m frequency dependent eigenvalues (characteristic gains) in such a way that the closed-loop system will meet stability and performance requirements. A dynamic compensator is used to shape the loci of the characteristic gains, and the generalised Nyquist criterion (Maciejowski [43]) can be applied to make a statement regarding the stability of the closed-loop system. A problem can arise due to the fact that the control law is designed on the characteristic gains and not the actual responses, and so performance and robustness issues become unclear, particularly for highly coupled systems. To 'map' the control law onto the actual system, it is augmented by eigenvector matrices which correspond to the eigenvectors of the plant, thus forming an approximate commutative controller (MacFarlane and Kouvaratikas [42]). The eigenvectors used to augment the control law are valid at one frequency only, and so if the eigenvectors of the system vary substantially with frequency then the controller will only be effective in a narrow frequency range only, in the vicinity of the frequency at which its eigenvectors were calculated.

In applying the technique to the design of an RCAH system for a Lynx at 80 knots forward flight, Manness *et al* [45] site a difficulty in interpreting the physical significance of the characteristic loci in that the loci directions vary strongly as a function of frequency (due to the changing levels of cross coupling in the plant). This variation was most pronounced in the range 0.1-10 rad/s which includes the design point frequencies and so a satisfactory control law was not achievable.

Brinson [6] successfully applied the technique to the design of a rate feedback system for a helicopter, although high gain was not achievable due to the introduction of non-minimum phase zeros during the design procedure.

2.4.2. Nyquist Array Methods

The methods of Inverse Nyquist Array (INA) and Direct Nyquist Array (DNA) are neo-classical techniques which involve the design of an open-loop precompensator and then a stabilising diagonal feedback control law (Maciejowski [43], Manness *et al* [45]). The role of the precompensator is to make the open-loop plant diagonally dominant either along the rows (INA) or the columns (DNA). For reasons of clarity, the proceeding discussion will focus on INA although the arguments are equally applicable to DNA. In INA a system is regarded as possessing row dominance if the i -th element of the i -th row, $i=1..m$, is greater in magnitude than the sum of the magnitude of the remaining elements. This means that if a square system possesses row dominance then its diagonal elements will be dominant, and hence the design of the diagonal control law can proceed as a set of single-input single-output (SISO) design problems. The use of so-called Ostrowski bands on the diagonally dominant elements (Maciejowski [43]) give some indication that closed-loop performance and stability robustness will be within a tolerable bound.

In applying the technique to helicopter flight control, Manness *et al* [45] found that the pseudo-decoupling approach led to compensators which were either unrealisable or whose zeros cancelled resonant poles of the system. the cancellation of resonant poles is ill-advised as feedback will not change their position, with the consequence that disturbances at the input to the helicopter may excite the resonant mode. The authors stopped the design at the precompensation stage and stated that the technique required further consideration.

2.4.3. Quantitative Feedback Theory

Quantitative Feedback Theory (QFT) is a neo-classical technique which involves a two degree of freedom design procedure, i.e. the design of a feedback controller and the design of a precompensator. The design of the feedback controller is such that the variation of the closed-loop frequency response over a frequency range of interest does

not exceed pre-defined limits. The design of the pre-filter outside the loop then insures that the performance specifications on the commanded responses is satisfied. QFT guarantees robustness by ensuring that the loop transmission exhibit positive gain and phase margins for all plant uncertainty. The reader is referred to Horowitz [24] for more detail of the theory. Various QFT approaches exist and the reader is referred to Horowitz [25] for a review of these approaches.

QFT involves the design of controllers on the basis of transmittances which assume that all other loops have infinite gain control. This technique is sometimes referred to as the constrained variable method (Tischler [75]).

Hess and Gorder [19] apply QFT to the design of a controller for the longitudinal dynamics (height rate and pitch attitude) of an Apache AH-64 in hover. The model used did not include rotor or actuator dynamics. The uncertainty bounds were chosen arbitrarily as no data was available on 'real' uncertainty. The frequency range 0.3-30 rad/s is used as the frequency range of interest and six frequency points were used for the design. The authors note that because the technique is primarily concerned with designing to remain within some magnitude bound, phase is not explicitly considered. This means that the Handling Qualities phase limited bandwidth and phase delay must be assessed after the design is complete. The final design was found to provide acceptable command/response performance in the face of 'considerable uncertainty'.

Hess [20] reports the design of a QFT controller for the longitudinal dynamics of a BO-105. The design uses BO-105 models from hover to 100 knots to define the bounds that the QFT procedure uses. The models do not include actuator or rotor dynamics. The frequency range 0.3-30 rad/s is used as the frequency range of interest and seven frequency points were used for the design. The design proceeded with the closure of the height rate loop first, which was chosen arbitrarily as QFT offers no insight into which loop should be closed first. The QFT technique used is the *Basically Non-Interacting Approach* (BNIA) which involves the design of a diagonal control law. A full 4-input 4-output design would involve consideration of 16 transmissions, which has the potential to become unmanageable. Hess notes that the phase bounds of the final design, although not explicitly considered in the design process, generally follow the

desired phase bounds and so the phase limited Handling Qualities bandwidth and phase delay were found to meet Level 1. The resulting controller was of low order and was found to give excellent tracking performance across a wide range of airspeed. However, because the control law was only for the longitudinal dynamics it could not be assessed on a full non-linear model.

Catapang *et al* [7] use a QFT based approach to design crossfeeds which will decouple the pitch and roll response of the UH-60 Black Hawk in near hover, over the frequency range 2-10 rad/s. The QFT templates were formed by using a nominal model and 4 off-nominal conditions. The crossfeeds were found to provide significant improvement in the roll coupling when compared to static or fixed operating point crossfeeds.

From the above review it is seen that QFT allows a good degree of physical insight concerning the consideration of transmission gain, but does not explicitly consider phase in the design process. QFT offers no insight into which loop should be closed first and this can result in difficulties if the wrong choice is made. Also, the technique may become unmanageable for a full 4-input 4-output (longitudinal and lateral) design and is computationally extensive due to the need to generate error bounds. This is reflected by the small number of frequency points used for design (six and seven in the above papers).

2.4.4. Linear Quadratic Methods

Linear Quadratic methods involve the minimisation of a time domain cost function by solving an algebraic Riccati equation. The cost function involves two weighting matrices which weight the states of the plant and the inputs. These weighting matrices can be chosen by appropriate singular value loop shaping of the plant. The singular values of a multivariable plant are measures which are 'analogous' to the gain of a single-output single-output (SISO) system. However, singular values cannot be as easily interpreted in physical terms as SISO gains can, as singular value plots do not relate directly to input-output transmissions. This can be objectionable to many control

engineers. The reader is referred to Maciejowski [43] for more detail on singular values and Athans [5] for more detail of the application of Linear Quadratic techniques to the design of control systems.

Gribble and Murray-Smith [16] use Linear Quadratic Regulator (LQR) with explicit model following to design a controller for a Lynx-like helicopter trimmed at 80 knots forward flight. The basis of the design is a 9th order rigid body model. The actuator and rotor modes are modelled as an equivalent time delay. LQR is used to achieve the desired attitude hold capability of the system. The authors cite a problem with the LQR technique due to the lack of visibility in choosing appropriate weighting functions. The problem is partially resolved by using a numerical optimisation routine to obtain a suitable weighting matrix for the helicopter states. The weighting matrix relating to the helicopter inputs was chosen by trading off bandwidth with robustness. The design was assessed on a subset of the Handling Qualities requirements and was found to meet Level 1 for most requirements.

Ingle and Celi [28] note a lack of a systematic procedure in choosing weighting matrices, with respect to helicopter applications, to achieve desired performance using Linear Quadratic techniques. The authors also report that the resulting iterative selection procedure is not directly related to Handling Qualities specifications.

A more recent paper by Gribble [15] investigated the design of a LQG controller with Loop Transfer Recovery (LTR) for a helicopter in low speed flight. The need for LTR arose due to an awareness that the 'guaranteed' stability margins of LQR can sometimes not be 'guaranteed' at the plant inputs if a state estimator is used. In this case, the stability margins must be recovered at the plant input using LTR (Stein and Athans [71]). The design was found to meet Level 1 small signal Handling Qualities requirements from 10 to 50 knots without the need for gain scheduling. However, the overall design process did not relate strongly to achievement of Handling Qualities specifications.

From the above review it is seen that Linear Quadratic techniques do not cater well for physical insight in the design process. Also, if a state estimator is used the system may suffer from robustness problems.

2.4.5. Eigenstructure Assignment

Eigenstructure Assignment (EA) is a technique for synthesis of feedback control laws that allows the designer to place closed-loop eigenvalues in specified positions and also shape the corresponding eigenvectors. The placement of closed-loop eigenvalues is very attractive to the flight control engineer as it allows the achievement of desired modes of response which Handling Qualities requirements essentially specify. For more information on the theory of EA the reader is referred to Andry *et al* [2].

Innocenti and Stanziola [30] consider the performance-robustness trade off of EA applied to helicopter flight control and compares the technique to LQR. They state that although EA is very good for achieving desired time responses the technique lacks the ability of guaranteeing a robust system. The design procedures in the paper are not transparent, i.e. trial and error is used until an acceptable trade-off between performance and robustness is obtained. The authors conclude that EA is a viable alternative to LQR in terms of performance and robustness, but cited a need for further research.

Garrard and Liebst [13] identify that EA is well suited to the achievement of Level 1 Handling Qualities due to the ability to place closed-loop poles in specified positions and also to decouple responses. The design procedure, however does not explicitly cater for robustness and this aspect must be assessed after the design is complete. Although the design was expected to be robust, evaluation on a higher order model exhibited an unstable mode at approximately 30 rad/s due to rotor interaction. This instability was eliminated by using a notch filter and so was not dealt with using EA.

Manness and Murray-Smith [46] identify the need to have a thorough comprehension of the dynamics of the rotorcraft before any control technique can be used to its greatest effect. EA is proposed as a viable technique due to the physical insight that it allows. The resulting control laws are found to meet their objectives although several iterations were required to arrive at the final design. The ACAH system was assessed in non-

linear simulation and a gain scheduled controller (scheduled as a function of forward velocity) was required to achieve performance requirements from -5 to 45 knots.

Low and Garrard [41] use EA in order to design an inner rate system as a preliminary to designing for specified response-types . This is potentially very appealing as the inner loop essentially decouples the system and so classical SISO techniques can be used in an outer loop to achieve the required response types. Although performance of the nominal system is excellent, slight deviation from the nominal results in noticeably degraded performance, highlighting a need to gain schedule the EA control law.

Ingle and Celi [28] note that EA controllers exhibit rather poor robustness when the flight conditions or the characteristics of the helicopter are only slightly changed.

What becomes clear from the above review is that EA is potentially very well suited to achieve Handling Qualities requirements but suffers from a distinct lack of robustness due to only small dynamical changes of the helicopter, particularly forward velocity.

A hybrid methodology was developed by Apkarian [4] which uses EA for performance considerations and then optimises the robustness through structured singular value analysis. The technique was applied to the design of a controller for a DOLPHIN helicopter trimmed at 75 km/hr forward flight. Unfortunately, Apkarian did not assess the design on different flight conditions and so the ability of the technique to produce controllers which are robust to varying flight conditions is unanswered.

There has been additional research on robust EA techniques for aircraft control (Mudge and Patton [51]) but the techniques have not yet been applied to the helicopter problem.

2.4.6. H-Infinity

H-infinity (H^∞ for compactness) is one of the newer optimal synthesis techniques and involves the synthesis of control laws which minimise the infinity-norm of a multivariable system. The infinity-norm of a multivariable system is the maximum value, over frequency, of the maximum singular value. The reader is referred to McFarlane and Glover [49] for more details.

Young and Lin [79] use H^∞ to design a Translational Rate Command system (TRC). The responses of this system have room for much improvement, although this is likely to be a consequence of the authors failing to have adequate insight into the dynamics which were being controlled, and not a consequence of using H^∞ . The design procedure adopted is very mathematical and lacks physical insight. Also, the authors give no indication as to the complexity of the resulting control law.

Takahashi [72] considers the design of helicopter control laws with and without rotor state feedback. In order to meet Handling Qualities requirements the bandwidths of the feedback loops are placed at high frequencies and pre-filters are used to achieve the requirements. The H^∞ feedback design process in this case does not cater for Handling Qualities requirements.

Walker and Postlethwaite [78] report on the design and piloted simulation of an H^∞ control law designed to give ACAH response. Handling Qualities requirements are catered for in the design process by using a model following technique. The model was designed so that it had Level 1 Handling Qualities characteristics. The H^∞ control law was designed such that the closed-loop system was forced to approximate the model by reducing the infinity-norm of the error between the two. Level 1 characteristics of the closed-loop are achievable only if the error can be made small enough, and this is only achievable if the weighting functions are chosen correctly. The design procedure utilised the loop-shaping procedure of McFarlane and Glover [49] which gives some insight into achieving specifications such as disturbance rejection and stability robustness, as it allows one to relate classical metrics such as high gain at low

frequency/low gain at high frequency to the shaping of the open-loop singular values. Such insight is broad and not focused, in that it deals with the plant as a whole and not with individual responses, which is the reason for using the model following technique to achieve desired responses. The system was simulated on the Large Motion Simulator (LMS) at DRA (Bedford), but due to real-time problems rotor modes were unable to be simulated. Pilot comment was favourable and the design was found to perform well from 0-60 knots and remained functional at speeds in excess of 100 knots. How much in excess of 100 knots is not stated.

Ingle and Celi [28] conclude that H^∞ is not well tailored to the design criteria of ADS-33. Also, if higher order dynamics are required to be explicitly considered then the resulting control law tends to be of relatively high order. However, H^∞ controllers tend to exhibit greater robustness to changes in aircraft configuration and flight condition, as opposed to EA and LQG solutions.

The above review shows that although H^∞ can yield successful control laws, physical insight does not play a key role in their development. Also, the resulting control laws can be of relatively high order and so implementation problems are an issue.

2.5. The Potential For Individual Channel Analysis and Design

The previous Section can be summarised as follows:

The Characteristic Locus method involves the shaping of each of the characteristic gains of the system and so performance and robustness issues of the real system become unclear, particularly in a system which contains a large degree of coupling. The procedure often fails with such a system.

Nyquist Array Methods attempt to decouple the open-loop plant to a degree where SISO design can be performed within an acceptable tolerance. However, attempting to pseudo-decouple the plant can result in a compensator which is unrealisable or which cancels resonant poles.

QFT allows some degree of physical insight and yields robust, low order controllers, but for the full 4-input 4-output helicopter problem may result in an unmanageable design procedure. Also, there is no insight into which sequence the loops should be closed. The wrong choice can cause problems in the QFT design process.

Linear Quadratic techniques lack physical insight and may not yield robust controllers. In addition, if high order models are used for design then a high order control law will result.

EA allows for physical insight but the robustness of the controllers for the specific application to helicopter flight control tend to lack robustness.

H^∞ lacks physical insight but yields robust controllers. In addition, if high order models are used for design then a high order control law will result.

It is seen that there is a niche in the field of control law design techniques for application to helicopter flight control. This niche can be filled by a technique which caters for physical insight, can be applied to any system regardless of the degree of coupling, yields robust, low order controllers designed using single-input single-output (SISO) techniques, offers insight into the ordering of loop closure and whose application to the helicopter problem is not unmanageable. Individual Channel Analysis and Design (ICAD) has the potential to fill this niche.

Another point which should be made relates directly to the Handling Qualities requirements. The specifications in ADS-33D are measured using *classical* criteria. For instance, the Handling Qualities bandwidth measurements are phase and gain margins measured from SISO loop transmissions. It is the bandwidth requirements which are perhaps the most important to meet, as they dictate the stability robustness of the combination of the pilot and the helicopter. A method which can cater for these requirements in the design process is obviously of high value to helicopter flight control engineers. ICAD has the potential to consider a large subset of the applicable requirements of ADS-33D in the design process.

The applicability of ICAD to the design of helicopter flight control laws, which will meet Level 1 quantitative criteria, is the main motivation behind the work described in the remainder of this thesis.

2.6. Summary

This Chapter has given a tutorial of the Handling Qualities requirements which will be assessed in the design work of future Chapters. Current research of helicopter flight control has also been reviewed and it has been found that these techniques have left a niche in the field of helicopter flight control, which Individual Channel Analysis and Design can potentially fill.

Individual Channel Analysis of Square Systems

3.1. Introduction

The purpose of this Chapter is to give the reader an introduction to the technique of Individual Channel Analysis (ICA) as applied to square multivariable systems. The first paper concerning Individual Channel Analysis and Design was published in 1991 (O'Reilly and Leithead [53]). To sum up best the motivation behind the development of the theory, the abstract of this first paper is quoted.

“A new approach - individual channel design (ICD) - to an enduring problem - multivariable feedback control - is presented. The approach is applications-oriented: it starts from the engineering premise that feedback control design is interactive: it involves an interplay between customer specification, uncertain plant characteristics and the multivariable feedback design process itself. It is shown that individual signal transmission channels arise naturally from customer specification on selected plant outputs with no loss of structural (loop interaction) information. By invoking customer performance specification on different channels, highly successful single-input single-output classical (Nyquist-Bode) design is made possible. ICD is not a design method per se; rather it is a global structural framework wherein the possibilities and limitations for local-loop-shaping design (e.g. Bode or Nichols) of a particular plant are made apparent from the outset. Also, the conditions

are established whereby channel gain and phase margins are robust measures of stability. In this way, a transparent, flexible and supportive design methodology is developed which directly aims to meet the users' control requirements and is well suited to the engineering context..."

There are some points to clarify from the above abstract. When the word '*structure*' is referred to within the context of Individual Channel Analysis and Design (ICAD), what is meant is whether *right half plane poles* (RHPPs) and/or *right half plane zeros* (RHPZs) exist. For example, if one analyses a particular system using ICA and someone asks "What is the structure of the first Channel?", then the answer might be "There are two RHPPs at 5 rad/s and 1 RHPZ at 20 rad/s". The existence of RHPPs and RHPZs in a Channel plays a role in what is achievable, in terms of performance, with a feedback system. The statement made concerning the conditions whereby Channel gain and phase margins are robust measures of stability is motivated by the fact that it is known that single-input single-output (SISO) gain and phase margins applied to multivariable systems can sometimes be erroneous, due to the effects of loop interaction (O'Reilly and Leithead [53]). ICA identifies the loop interaction and quantifies it in functions known as *multivariable structure functions* (MSFs). It will be seen in this Chapter that one of the uses of these MSFs is that they indicate when Channel gain and phase margins can be reliably interpreted as robustness indicators. Chapter 6 will describe the use of MSFs for design purposes. The outline of this Chapter is as follows. Section 3.2 describes how an m-input m-output plant can be decomposed into m Individual Channels. Section 3.3 shows how the MSFs can be used as a sensitivity measure. Section 3.4 gives some discussion concerning the MSF as a sensitivity measure. Section 3.5 considers conditions under which Individual Channel gain and phase margins are valid as robustness measures for a general m-input m-output plant. Section 3.6 describes the analysis of systems with non-diagonal control laws using ICA.

3.2. Decomposition of an m-input m-output System into Individual Channels

Consider an m-input m-output plant which is described by the transfer function matrix $G(s)$ (from hereon, it is implicitly assumed that any frequency dependent terms are a function of s and so the (s) notation will be dropped. It should be clear from the context when elements are frequency dependent). G can be written as,

$$G = \begin{bmatrix} g_{11} & \cdots & g_{1m} \\ \vdots & \ddots & \vdots \\ g_{m1} & \cdots & g_{mm} \end{bmatrix} \quad (3.1)$$

In ICAD, G is preceded by an $m \times m$ controller K , which is constrained to be diagonal. K is given as,

$$K = \begin{bmatrix} k_1 & 0 & \cdots & 0 \\ 0 & \ddots & \ddots & \vdots \\ \vdots & \ddots & \ddots & 0 \\ 0 & \cdots & 0 & k_m \end{bmatrix} \quad (3.2)$$

To form Individual Channel i (Channel i for brevity), The feedback loop from output i to input i is broken, but the remaining $(m-1)$ feedback loops remain closed. Figure 3.1 shows the block diagram for determination of Channel 1 of a system.

Applying linear algebra, the SISO transfer function describing y_i/r_i , Channel i , is given by,

$$C_i = k_i g_{ii} - k_i G_{ij} (I + G_{jj} K_{jj})^{-1} G_{ji} \quad (3.3)$$

where k_i is element (i,i) of the controller, g_{ii} is element (i,i) of G , G_{ij} is row i of G with element (i,i) removed, G_{jj} is G with row i and column i removed, K_{jj} is K with row i and column i removed and G_{ji} is column i of G with element (i,i) removed.

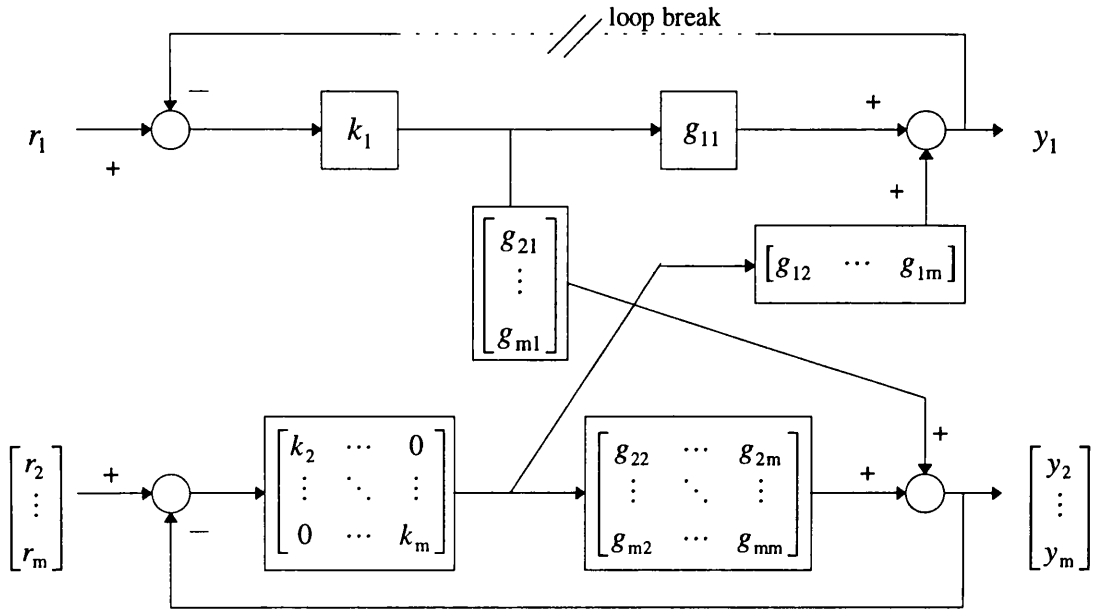


Figure 3.1. Block diagram for determination of Channel 1.

Rearranging Eqn (3.3) yields,

$$C_i = k_i g_{ii} (1 - \gamma_i) \quad (3.4)$$

where γ_i is defined as,

$$\gamma_i = g_{ii}^{-1} G_{ij} (I + G_{jj} K_{jj})^{-1} G_{ji} \quad (3.5)$$

γ_i is commonly written in determinant form in order that explicit expressions can easily be written. The determinant form also enables a state space representation of γ_i to be realised, as will be shown in Chapter 5.

In determinant form,

$$\gamma_i = \frac{-|\bar{G}_i|}{g_{ii} |\bar{G}^i|} \quad (3.6)$$

where $\bar{G} = K^{-1} + G$, \bar{G}_i is \bar{G} with element (i,i) set to zero, \bar{G}^i is \bar{G} with row i and column i removed and $|\cdot|$ is the determinant. The diagonal elements of \bar{G} are $k_i^{-1} + g_{ii}$. These diagonal elements can be alternatively written as g_{ii}/h_i , where

$h_i = k_i g_{ii} / (1 + k_i g_{ii})$. h_i is the closed loop subsystem when loop i is closed but all other loops are open. For illustration, γ_i is written in full,

$$\gamma_1 = \frac{\begin{vmatrix} 0 & g_{12} & \cdots & g_{1(m-1)} & g_{1m} \\ g_{12} & g_{22}/h_2 & g_{23} & \vdots & \vdots \\ \vdots & g_{32} & \ddots & \ddots & \vdots \\ \vdots & \vdots & \ddots & g_{(m-1)(m-1)}/h_{(m-1)} & g_{(m-1)m} \\ g_{m1} & g_{m2} & \cdots & g_{m(m-1)} & g_{mm}/h_m \end{vmatrix}}{\begin{vmatrix} g_{22}/h_2 & g_{23} & \cdots & g_{1(m-1)} & g_{1m} \\ g_{32} & \ddots & \ddots & \ddots & \vdots \\ \vdots & \ddots & \ddots & g_{(m-1)(m-1)}/h_{(m-1)} & g_{(m-1)m} \\ g_{m2} & \cdots & \cdots & g_{m(m-1)} & g_{mm}/h_m \end{vmatrix}} \quad (3.7)$$

γ_i is known as the multivariable structure function (MSF) of Channel i and ICA recognises the implications of γ_i as a sensitivity measure. This will be explained in detail in Section 3.3.

Referring to Figure 3.1, a SISO transfer function can be derived which describes the response between output i and inputs j ($j=1..m, j \neq i$). The expression, denoted d_i , is given by,

$$d_i = G_{ij} (I + K_{jj} G_{jj})^{-1} R_i \quad (3.8)$$

where G_{ij} and G_{jj} are previously defined and R_i is input vector R with input i removed. d_i can be regarded as an additive disturbance on Channel i due to non-zero inputs injected into the other Channels. In determinant form d_i is written as,

$$d_i = \frac{\begin{vmatrix} 0 & G_{ij} \\ R_i & \overline{G}^i \end{vmatrix}}{|\overline{G}^i|} \quad (3.9)$$

For illustration, d_1 is shown in full,

$$d_1 = \frac{\begin{vmatrix} 0 & g_{12} & \cdots & g_{1(m-1)} & g_{1m} \\ r_2 & g_{22}/h_2 & g_{23} & \vdots & \vdots \\ \vdots & g_{32} & \ddots & \ddots & \vdots \\ \vdots & \vdots & \ddots & g_{(m-1)(m-1)}/h_{(m-1)} & g_{(m-1)m} \\ r_m & g_{m2} & \cdots & g_{m(m-1)} & g_{mm}/h_m \end{vmatrix}}{\begin{vmatrix} g_{22}/h_2 & g_{23} & g_{1(m-1)} & g_{1m} \\ g_{32} & \ddots & \ddots & \vdots \\ \vdots & \ddots & g_{(m-1)(m-1)}/h_{(m-1)} & g_{(m-1)m} \\ g_{m2} & \cdots & g_{m(m-1)} & g_{mm}/h_m \end{vmatrix}} \quad (3.10)$$

The complete multivariable system, with diagonal control and unity negative feedback, can therefore be equivalently expressed as m Individual Channels with additive disturbances. Figure 3.2 shows the ICAD decomposition for an m -input m -output system.

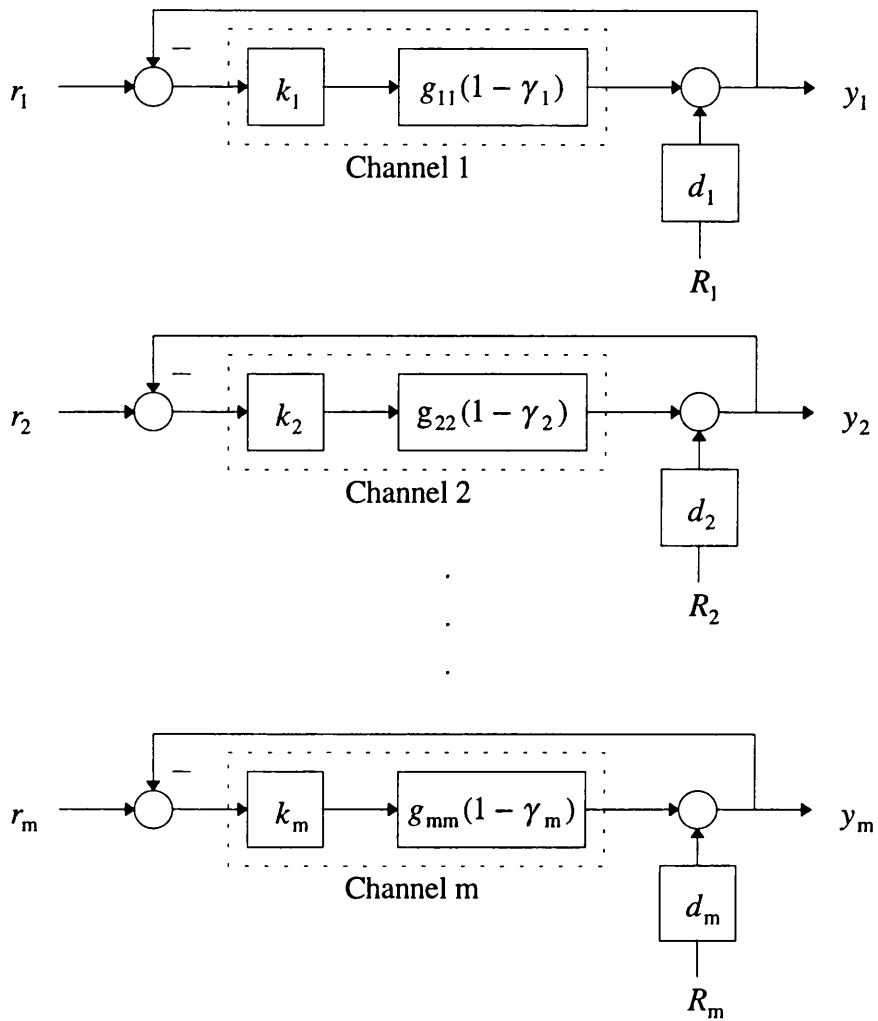


Figure 3.2. m-input m-output ICAD decomposition.

Before the controllers have been designed, approximate Channel MSFs can be defined which are independent of the controllers. The approximate Channel MSFs are defined as,

$$\hat{\Gamma}_i = \frac{-|G_i|}{g_{ii}|G^i|}, \quad i = 1..m \quad (3.11)$$

where G_i is G with element (i,i) set to zero, G^i is G with row i and column i removed and g_{ii} is element (i,i) .

For illustration $\hat{\Gamma}_1$ is written in full,

$$\hat{\Gamma}_1 = \frac{\begin{vmatrix} 0 & g_{12} & \cdots & g_{1(m-1)} & g_{1m} \\ g_{12} & g_{22} & g_{23} & \vdots & \vdots \\ \vdots & g_{32} & \ddots & \ddots & \vdots \\ \vdots & \vdots & \ddots & g_{(m-1)(m-1)} & g_{(m-1)m} \\ g_{m1} & g_{m2} & \cdots & g_{m(m-1)} & g_{mm} \end{vmatrix}}{\begin{vmatrix} g_{22} & g_{23} & g_{1(m-1)} & g_{1m} \\ g_{32} & \ddots & \ddots & \vdots \\ \vdots & \ddots & g_{(m-1)(m-1)} & g_{(m-1)m} \\ g_{m2} & \cdots & g_{m(m-1)} & g_{mm} \end{vmatrix}} \quad (3.12)$$

Comparing Eqn (3.12) with Eqn (3.7) it is seen that $\hat{\Gamma}_i$ will be close to γ at frequencies where the h_j s, $j = 1..m$, $j \neq i$, are close to one. In fact, $\hat{\Gamma}_i$ is a specialised version of γ where controllers k_j , $j = 1..m$, $j \neq i$ are assumed to have infinite gain.

$(1 - \hat{\Gamma}_i)$ is written as,

$$(1 - \hat{\Gamma}_i) = \frac{g_{ii}|G^i| + |G_i|}{g_{ii}|G^i|} = \frac{|G|}{g_{ii}|G^i|} \quad (3.13)$$

Eqn (3.13) shows that the zeros of $(1 - \hat{\Gamma}_i)$ are the zeros of $|G|$, provided no pole-zero cancellation occurs. The zeros of $|G|$ are the transmission zeros of G . The transmission zeros of G are those values of s where G drops rank (Maciejowski [43]). i.e., if G drops rank when $s = z_0$, then z_0 is a transmission zero of G . The transmission zeros of a multivariable plant are analogous to the zeros of a SISO plant in that the existence of RHP transmission zeros can limit the performance of a multivariable control system in much the same way as RHPZs can limit the performance of a SISO control system. The way in which RHP transmission zeros limit performance in multivariable systems is dealt with in more detail in Chapter 6.

The significance of the Channel MSFs within the context of a robustness analysis will be described in more detail in the next two Sections.

3.3. The Channel MSF as a Sensitivity Measure

Recall the equation for Channel i of a system,

$$C_i = k_i g_{ii} (1 - \gamma_i) \quad (3.14)$$

If γ_i approaches the $(+1,0)$ point at some frequency then a sensitivity problem may exist at that frequency. There is in fact two forms of sensitivity which can arise if γ_i is close to the $(+1,0)$ point. Those sensitivities are known as *structural sensitivity* and *phase sensitivity* (O'Reilly and Leithead [53]).

Structural sensitivity is best explained through consideration of the Nyquist Criterion. For some SISO transfer function L and return difference $(1+L)$, the Nyquist Criterion states that,

$$N = Z - P \quad (3.15)$$

where N is the net number of clockwise encirclements of the $(-1,0)$ point of the Nyquist plot of L , Z is the number of RHPZs of $1+L$ and P is the number of RHPPs of L .

Eqn (3.15) can also be applied to γ_i and $(1-\gamma_i)$, where N is the number of net clockwise encirclements of the $(+1,0)$ point of γ_i , Z is the number of RHPZs of $(1-\gamma_i)$ and P is the number of RHPPs of γ_i .

If γ_i closely approaches the $(1,0)$ point (the '+' before the 1 is now dropped) at some frequency then 'small' plant uncertainty could be sufficient to change the number of encirclements of the $(1,0)$ point of γ_i , with the consequence that the zero structure of $(1-\gamma_i)$, and hence the zero structure of C_i , would change. The reason that this is a problem is explained below.

If the Channels of the nominal plant are all minimum phase up to some frequency x rad/s say, then in theory the loop gain of the Channels can be made greater than 1 up to x rad/s without jeopardising closed loop stability. In this thesis, a controller which is designed such that its corresponding Channel has a loop gain greater than one at all frequencies below the 0dB crossover is known as a *high performance* controller. For a purely minimum phase Channel, where x is infinity, then the 0dB crossover would be

limited by such considerations as noise attenuation, high frequency phase behaviour, achievable controller gain, actuator limits *etcetera*. If a RHPZ exists in some Channel then the loop gain of that Channel must be made less than 1 at the frequency of the RHPZ in order to achieve closed-loop stability. By making the gain greater than 1 at that frequency, a pole will be attracted to the RHPZ once the loop is closed and will come to rest in the right half plane. This pole will therefore be unstable. If the zero structure of $(1-\gamma_i)$ changes from minimum phase to non-minimum phase, due to γ_i changing its number of encirclements of the (1,0) point, then the stability of the closed loop system will be compromised if C_i has loop gain greater than 1 at the frequency of the newly formed RHPZ. This type of sensitivity is therefore of concern at frequencies below the 0dB crossover frequency of C_i . It is of no concern at frequencies above the 0dB crossover frequency where the loop gain of Channel i will be less than 1.

The concept of phase sensitivity is best explained graphically. Figure 3.3 shows the position of a nominal γ_i at some frequency ω_x ($\gamma_i(\omega_x)$) with an arbitrary error bound around the nominal value. Also shown is the vector $(1-\gamma_i(\omega_x))$ which has the same error bound as $\gamma_i(\omega_x)$ except that its phase differs by 180° . The phase of $\gamma_i(\omega_x)$ is seen to vary by α degrees, and the phase of $(1-\gamma_i(\omega_x))$ is seen to vary by β degrees, where β is noticeably larger than α . This demonstrates that the closer the approach of γ_i to the (1,0) point then the more sensitive the phase of $(1-\gamma_i)$ is to variation in phase of γ_i . Notice that if the origin is included in the error bound of $(1-\gamma_i(\omega_x))$ then the phase of Channel i is *completely* uncertain. This is equivalent to Channel i exhibiting structural sensitivity.

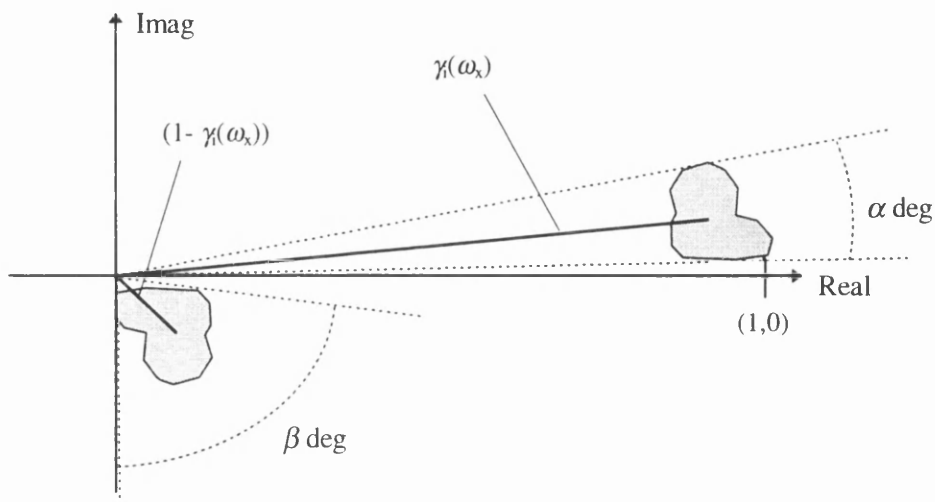


Figure 3.3. Phase sensitivity of $(1-\gamma(\omega_x))$

If $(1-\gamma)$ exhibits phase sensitivity then it is of concern at frequencies within some region of the 0dB crossover frequency of Channel i . This is because small variation in γ could be sufficient to cause Channel i to change phase by an amount larger than its corresponding phase margin, even if the phase margin has been designed to be generous by classical design criteria.

Before the controllers have been designed the approximate Channel MSFs, \hat{T}_i s, can be used to assess the potential sensitivity of the Channels. Note that from Eqn (3.13), if \hat{T}_i is close to the $(1,0)$ point then the transmission zeros of the system will be sensitive to changes in \hat{T}_i .

3.4. How Close can an MSF be to the (1,0) Point Before Robustness Problems Occur?

What arises from the previous Section is that if the MSF of a Channel is close to the (1,0) point at frequencies below the 0dB crossover frequency of the Channel, then the Channel may exhibit a high level of sensitivity due to only small changes in the plant. This means that gain and phase margins associated with the Channel may be highly optimistic and may not be valid as robustness indicators of the closed-loop Channel.

A question that arises from the above discussion is 'How close can an MSF approach the (1,0) point before robustness problems are likely to arise?'. This question cannot be answered generally due to the huge diversity of systems that exist. However, some general discussion is given below.

Industrial control engineers usually have a good level of knowledge of the general dynamical characteristics of the system that they are designing a control law for (or at least one would like to think they have). In this case ICA may highlight the potential of the system becoming non-minimum phase but the control engineer may be confident that this is very unlikely to occur in practice. In this case, a decision would be made as to whether the sensitivity will be disregarded in order to allow the design of high performance control. i.e. a risk assessment is made. This would be for the case where the frequency region of the sensitivity is well below the Channel 0dB crossover region. In the case where the sensitivity is in the region of the 0dB crossover frequency of the Channel then phase sensitivity becomes an issue. Because every system is subject to uncertainty it is highly likely that phase sensitivity will cause serious robustness problems. How close an approach of the (1,0) point of the MSF is tolerable will, again, be decided upon by the engineer's knowledge of the system. The way to avoid this sensitivity, if it is deemed hazardous, is to place the 0dB crossover frequencies sufficiently far from the sensitive frequencies, either above or below such frequencies, but only above if the possibility of structural sensitivity has been eliminated.

With respect to the dynamics of a helicopter, a wealth of literature does exist on the identification of helicopters such as the BO-105 (see for example Kaletka and

Gimonet [31], Fu and Kaletka [12]) and the Apache (see for example Harding [18], Schroeder *et al* [68]). Identification of the Puma has also been reported (Padfield and DuVal [61]) which assigns standard deviations to the estimates of the stability derivatives. However, the authors of these papers did not have ICAD in mind and so no useful information on possible error bounds for rotorcraft, in general, is available from these sources. In addition, the author could find no literature which could aid in deciding upon error bounds of the dynamics of the particular combat rotorcraft which is the topic of this thesis.

The establishment of representative error bounds around the MSFs is a topic for future work and is outwith the scope of this thesis. The view taken in this thesis is that if the Nyquist plot of a MSF is within a circle of radius 0.2 around the (1,0) point then it is regarded as being 'close'. This is a somewhat arbitrary choice due to the lack of information available concerning error bounds of the helicopter models under consideration. However, it is the author's opinion that this is a reasonable value. One may think that a radius of 0.2 is not sufficient as it corresponds to a gain margin of approximately 2dB and a phase margin of approximately 11° which in classical terms may not be regarded as being sufficient. However, the stability margins of the MSFs do not have the same relation to transient response as the Channel gain and phase margins do. Considering a SISO system, gain and phase margins of 2dB and 11° may actually be sufficient to keep the closed-loop system stable for all plant uncertainty, but the transient response of the closed-loop system to commanded inputs would be highly oscillatory and would be deemed inadequate. For a SISO system, it is typical to specify an allowable peak overshoot of the response, due to a step input, of less than 20% (Golten and Verwer [14]). This specification corresponds approximately to gain and phase margins of at least 5dB and 50° respectively [14] and so it is the transient response of the closed-loop system, and not its stability robustness, which is the driving factor for setting these gain and phase margins as 'acceptable minimums'. Considering the transient response of a Channel to a step input; regardless of how close the corresponding Channel MSF is to the (1,0) point, as long as the Channel gain and phase margins are large enough then the transient response of the nominal system will be satisfactory.

It is noted that in the presence of knowledge of the errors of the system, the robustness bounds can be characterised to reflect this knowledge.

As far as the robustness assessment of the control systems in this thesis are concerned, extensive use of non-linear simulation will be made to add weight to the findings of ICA.

3.5. Channel Gain and Phase Margins as Robustness Measures

This Section considers in more detail the applicability of Channel gain and phase margins as robustness measures.

Section 3.3 demonstrated that if the MSF of a Channel was close to the (1,0) point at some frequency below the 0dB crossover frequency of the Channel then the Channel may exhibit a high level of structural and/or phase sensitivity.

From the above considerations, sufficient conditions for a plant to possess stability robustness are given below.

Condition 3.1.

For an m -input m -output closed-loop system to possess stability robustness it is sufficient that the Channels have adequate gain and phase margins and that the MSFs of the Channels are far from the (1,0) point at frequencies below the Channel 0dB crossover frequencies.

Although these conditions are sufficient, they may not be necessary for certain systems. If the conditions are not met, further analysis should be done to determine whether the closed-loop system possesses stability robustness. Note also that if knowledge of the correlation of the variation of transfer function elements exists then the sufficient conditions can be tailored to account for the correlation and so all the criteria of

Condition 3.1 may not be required. For example, consider the approximate MSF of a 2-input 2-output system given as,

$$\gamma = \frac{g_{12}g_{21}}{g_{11}g_{22}} \quad (3.16)$$

If it is known that relative changes in g_{12} cause equal relative changes in g_{11} and that relative changes in g_{21} cause equal relative changes in g_{22} , then γ will not change due to such changes. It is worth noting that a plant having variations of this kind is not an unrealistic situation. An example of such variation would be dynamic error in sensors and this type of consideration could have implications for sensor fault tolerance. This type of error is classed as *diagonal multiplicative perturbations* (Safonov [66]) and it is noted in [66] that this type of perturbation arises ‘commonly’. The amended MSF, γ' , due to such variation is written as,

$$\gamma' = \frac{g_{12}(1 + \delta_1)g_{21}(1 + \delta_2)}{g_{11}(1 + \delta_1)g_{22}(1 + \delta_2)} = \frac{g_{12}g_{21}}{g_{11}g_{22}} \quad (3.17)$$

It is seen from Eqn (3.17) that the transmission zeros of the plant will not be structurally sensitive to changes in the transfer function elements, regardless of how close γ is to the (1,0) point. Therefore if high performance control is used and γh_1 and γh_2 are close to (1,0) well below the desired 0dB crossovers of the Channels the sensitivity can be safely ignored. However, if γh_1 and γh_2 are close to (1,0) in the vicinity of the 0dB crossovers of the Channels phase sensitivity may still be an issue if h_1 and h_2 are subject to variation in this region.

3.6. Individual Channel Analysis of Systems with Non-Diagonal Controllers

This Section gives an introduction as to how one can analyse a system containing a non-diagonal control law using Individual Channel Analysis. For further details of the issues concerning the analysis of systems with non-diagonal controllers, the reader is referred to Leithead and O'Reilly [38].

Non-diagonal controllers tend to be used to decouple (to some degree), or diagonalise, the open-loop system. It may be thought that if the system can be decoupled then the actual MSFs of the Channels will be very small and hence any sensitivity problem that the system may exhibit will disappear. This is in fact not the case and an example will now be given.

To demonstrate that decoupling the open-loop system will not decrease any sensitivity that may exist a rather extreme example is now shown. Consider a 2-input 2-output system which has been subject to a pre-filter such that the nominal open-loop system has been decoupled completely. The plant is given as,

$$G = \begin{bmatrix} g_{11} & g_{12} \\ g_{21} & g_{22} \end{bmatrix} \quad (3.18)$$

An example of a pre-filter which can potentially completely decouple the system is given as,

$$P = \begin{bmatrix} 1 & p_{12} \\ p_{21} & 1 \end{bmatrix} \quad (3.19)$$

The prefiltered system, GP , is given as,

$$GP = \begin{bmatrix} g_{11} & g_{12} \\ g_{21} & g_{22} \end{bmatrix} \begin{bmatrix} 1 & p_{12} \\ p_{21} & 1 \end{bmatrix} = \begin{bmatrix} g_{11} + p_{21}g_{12} & g_{12} + p_{12}g_{11} \\ g_{21} + p_{21}g_{22} & g_{22} + p_{12}g_{21} \end{bmatrix} \quad (3.20)$$

for GP to be completely decoupled p_{12} and p_{21} are designed to be,

$$p_{12} = -\frac{g_{12}^0}{g_{11}^0} \quad (3.21)$$

$$p_{21} = -\frac{g_{21}^0}{g_{22}^0} \quad (3.22)$$

where the superscript '0' indicates that the elements are the nominal values of the transfer function elements.

GP then becomes,

$$GP = \begin{bmatrix} g_{11} - \frac{g_{21}^0 g_{12}^0}{g_{22}^0} & 0 \\ 0 & g_{22} - \frac{g_{12}^0 g_{21}^0}{g_{11}^0} \end{bmatrix} = \begin{bmatrix} g_{11}(1 - \gamma_{11}) & 0 \\ 0 & g_{22}(1 - \gamma_{22}) \end{bmatrix} \quad (3.23)$$

where,

$$\gamma_{11} = \frac{g_{12}^0 g_{21}^0}{g_{11}^0 g_{22}^0} \quad (3.24)$$

$$\gamma_{22} = \frac{g_{12}^0 g_{21}^0}{g_{11}^0 g_{22}^0} \quad (3.25)$$

It is seen from Eqn (3.23) that if the approximate MSF of the system, γ , is close to (1,0) at some frequency then the diagonal elements of GP will exhibit increased sensitivity at this frequency. No gain in robustness has been made by decoupling the open-loop system. Perfect decoupling is unlikely to be attempted in practice but partial decoupling will also fail to increase the robustness of the system.

To analyse a system in general which has a non-diagonal control law one can define MSFs which contain an inversely proportional representation of the transfer function element under consideration (in order to remain consistent with MSF definitions). i.e. an MSF of the following form is required,

$$\hat{\gamma}_{ij} = \frac{A}{g_{ij}B} \quad (3.26)$$

where A and B are some functions of the controller and of the elements of the plant which are not g_{ij} .

To develop the required expression, consider a 2-input 2-output plant with a non-diagonal 2-input 2-output controller. The transfer function describing output 1 due to input 1 with loop 1 open will be referred to as Channel 1. Channel 1 is given by,

$$C_1 = \frac{\begin{vmatrix} g_{11}k_{11} + g_{12}k_{21} & g_{11}k_{12} + g_{12}k_{22} \\ g_{21}k_{11} + g_{22}k_{21} & 1 + g_{21}k_{12} + g_{22}k_{22} \end{vmatrix}}{1 + g_{21}k_{12} + g_{22}k_{22}} = \frac{nC_1}{dC_1} \quad (3.27)$$

The numerator of Channel 1, nC_1 , can be expanded as,

$$\begin{aligned} nC_1 = & g_{11}[k_{11}(1 + g_{21}k_{12} + g_{22}k_{22}) - k_{12}(g_{21}k_{11} + g_{22}k_{21})] - \dots \dots \\ & \dots \dots g_{12}[k_{22}(g_{21}k_{11} + g_{22}k_{21}) - k_{21}(1 + g_{21}k_{12} + g_{22}k_{22})] \end{aligned} \quad (3.28)$$

The zeros of Channel 1 are also the zeros of $(1 - \hat{\gamma}_{11})$ where $\hat{\gamma}_{11}$ is given as,

$$\hat{\gamma}_{11} = \frac{-\begin{bmatrix} 0 & 0 \\ 0 & 1 \end{bmatrix} + \begin{bmatrix} 0 & g_{12} \\ g_{21} & g_{22} \end{bmatrix} \cdot \begin{bmatrix} k_{11} & k_{12} \\ k_{21} & k_{22} \end{bmatrix}}{g_{11} \begin{bmatrix} 0 & 0 \\ 0 & 1 \end{bmatrix} + \begin{bmatrix} 1 & 0 \\ g_{21} & g_{22} \end{bmatrix} \cdot \begin{bmatrix} k_{11} & k_{12} \\ k_{21} & k_{22} \end{bmatrix}} \quad (3.29)$$

For a general m -input m -output plant, $\hat{\gamma}_{ij}$ can be written as,

$$\hat{\gamma}_{ij} = \frac{(-1)^{i+j+1} |\mathbf{I}_i + G_{ij}K|}{g_{ij} |\mathbf{I}_i + G_i^{ij}K|} \quad (3.30)$$

where G_{ij} is G with element (i,j) set to zero, G_i^{ij} is G with element (i,j) set to one and the remaining elements of row i set to zero. \mathbf{I}_i is the identity matrix with element (i,i) set to zero.

Notice that if one assumes infinite gain control, then the $\hat{\gamma}_{ij}$ s, $i = j$, are equal to the approximate Channel MSFs defined in Section 3.2.

The question arises as to whether only a subset of the $\hat{\gamma}_{ij}$ s are sufficient to gain a representative picture of the sensitivity of a system with a non-diagonal controller. This question cannot be addressed generally as one cannot generally quantify the effect that the non-diagonal controller will have on the system. To be absolutely sure that no sensitivity exists the control engineer would be required to assess *all* the $\hat{\gamma}_{ij}$ s, unless knowledge of the correlation of the transfer function elements exists. However, if the approximate MSFs of the plant do not show any potential sensitivity problems then the possibility of the non-diagonal controller introducing problems is small. As a general rule, the possibility of the closed-loop system destabilising due to loop interaction is a property of the plant and not a property of the controller. If the multivariable nature of the plant is found to be insensitive to variation, no problems are likely to arise.

3.7. Summary

This Chapter has given an introduction to the technique of Individual Channel Analysis (ICA). It was shown that an m-input m-output plant could be decomposed into m Individual Channels with no loss of information regarding loop interaction. Multivariable structure functions (MSFs) were defined which quantify the loop interaction between the Channels. These MSFs not only quantify loop interaction but can be used as sensitivity measures to determine the conditions under which Channel gain and phase margins are valid as robustness measures. Finally, MSFs were defined which can assess the sensitivity of systems with non-diagonal control laws due to changes in the individual elements of the system. It was noted that robustness problems due to loop interaction are generally a property of the plant and that if the multivariable nature of the plant was found to be insensitive to changes in the transfer function elements, then it was unlikely that non-diagonal control would introduce problems.

Individual Channel Analysis of Non-Square Systems

4.1. Introduction

This Chapter describes a method in which the robustness of a particular class of non-square system can be assessed within the framework of Individual Channel Analysis (ICA). To date, ICA has been developed for application to square systems only. The need for an extension of the theory to non-square systems is evident when one wishes to analyse and/or design a system which has an inner and an outer loop, where the number of feedback variables is greater than the number of plant inputs. A practical example of such a system is a Translational Rate Command (TRC) system for a helicopter in hover. This system has two sets of feedback loops: an inner set involving the feedback of height rate, pitch attitude, roll attitude and yaw rate to the four inputs, and an outer set which involves the feedback of forward velocity and side velocity to the inputs which primarily control forward and side velocity, which are the same inputs which primarily control pitch and roll. Although one may think that such a system can be assessed as two independent square systems, the loop interaction between the two systems needs to be quantified and its robustness implications assessed. The design of a TRC system is dealt with in Chapter 9.

This Chapter is organised as follows: Section 4.2 briefly describes a non-square system with an inner and an outer loop. The case where the system has more than two sets of feedback loops is not considered here, although the theory can be extended in a straightforward manner. Section 4.3 derives expressions for transfer function elements which are 'outside' the inner feedback loop. These transfer function elements are referred to as being 'loose'. Section 4.4 develops a method to perform an analysis of the

loose transfer function elements using ICA and proposes conditions for assessing the robustness of a non-square system.

4.2. Non-Square Systems with Two Sets of Feedback Loops

The non-square system under investigation is shown in block diagram form in Figure 4.1.

The plant G has m inputs and n outputs where n is greater than m . It is assumed that $n \leq 2m$. K is constrained to be a diagonal $m \times m$ controller and P is a diagonal $(n-m) \times (n-m)$ controller. m outputs are fed back to K and the remaining $n-m$ outputs are fed back to P .

The system within the dashed box in Figure 4.1 is the effective open-loop system for the outer loop, and will be referred to here after as \bar{Q} . The transfer function matrix of \bar{Q} is given by,

$$\bar{Q} = \begin{bmatrix} \bar{q}_{(m+1)1} & \cdots & \bar{q}_{(m+1)m} \\ \vdots & \ddots & \vdots \\ \bar{q}_{n1} & \cdots & \bar{q}_{nm} \end{bmatrix} \quad (4.1)$$

Note that \bar{Q} has the same number of inputs as G , but only the last $(n-m)$ outputs.

The numbering of the individual elements of \bar{Q} is done in such a way so as to avoid notational confusion in later Sections.

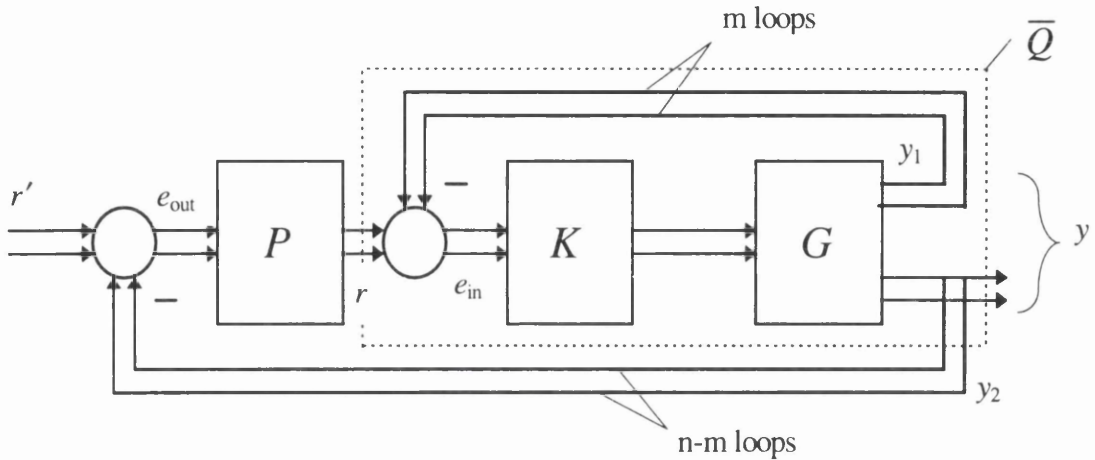


Figure 4.1. Block diagram of non-square system.

4.3. Derivation of Transfer Function Elements Outwith the Inner Feedback System

It is assumed that for an m -input n -output system that outputs $1..m$ are fed back to inputs $1..m$ and that outputs $(m+1)..n$ are loose. It is also assumed at this stage that the inner ICAD controller of dimension (m,m) is already designed. Notice that for systems whose outer system has less feedback lines than the inner system has feedback lines, the inner system will have feedback lines which are not strictly 'inner' loops of the outer system. However, because such loops will undoubtedly be designed without regard for the outer system, those loops which are not strictly 'inner' loops will nonetheless be described as inner loops and the $m \times m$ system will remain known as the inner system.

Referring to Figure 4.1, the feedback vector of the inner loop is,

$$y_1 = y(1..m) \quad (4.2)$$

The $m \times 1$ error signal into the system is given as,

$$e_{in} = r - y_1 \quad (4.3)$$

and the $n \times 1$ output vector y is given as,

$$y = GKr - GK y_1 \quad (4.4)$$

Now, as y_1 is a sub-vector of y ,

$$GK y_1 = \begin{bmatrix} GK & 0_{n,n-m} \end{bmatrix} y \quad (4.5)$$

When transfer function matrices are enclosed in brackets and have a subscript of the form a,b this means that row(s) a and column(s) b of the matrix are selected, unless otherwise stated. $0_{n,n-m}$ is a zero matrix with n rows and $(n-m)$ columns.

Substituting Eqn (4.5) into Eqn (4.4) and rearranging,

$$y = \begin{bmatrix} I_m + (GK)_{1..m,1..m} & 0_{m,n-m} \\ (GK)_{m+1..n,1..m} & I_{n-m} \end{bmatrix}^{-1} GK r \quad (4.6)$$

The SISO transfer function y_j/r_i is found by,

$$\frac{y_j}{r_i} = F_j \begin{bmatrix} I_m + (GK)_{1..m,1..m} & 0_{m,n-m} \\ (GK)_{m+1..n,1..m} & I_{n-m} \end{bmatrix}^{-1} (GK) D_i \quad (4.7)$$

where F_j is a zero vector of dimension $(1,n)$ except element j which is set to 1, D_i is a zero vector of dimension $(m,1)$ except element i which is set to 1.

$(GK) D_i = (GK)_{1..n,i}$, which is column i of GK .

Because y_j/r_i is SISO, $|y_j/r_i| = y_j/r_i$ and so by using the following determinantal identity (Leithead and O'Reilly [34]).

$$\left| -X_{12} X_{22}^{-1} X_{21} \right| = \left| \begin{array}{c|c} 0 & X_{12} \\ \hline X_{21} & X_{22} \end{array} \right| / |X_{22}| \quad (4.8)$$

and taking,

$$X_{12} = -F_j, \quad X_{22} = \begin{bmatrix} I_m + (GK)_{1..m,*} & 0_{m,n-m} \\ (GK)_{(m+1)..n,*} & I_{n-m} \end{bmatrix}, \quad X_{21} = (GK)_{1..n,i} \quad (4.9)(a,b,c)$$

(the '*' means that *all* rows/columns are selected) we have,

$$\frac{y_j}{r_i} = \frac{\begin{vmatrix} 0 & F_j \\ (GK)_{i..n,i} & \begin{bmatrix} I_m + (GK)_{l..m,*} & 0_{m,n-m} \\ (GK)_{(m+1)..n,*} & I_{n-m} \end{bmatrix} \end{vmatrix}}{\begin{vmatrix} I_m + (GK)_{l..m,*} & 0_{m,n-m} \\ (GK)_{(m+1)..n,*} & I_{n-m} \end{vmatrix}}$$

$$= \frac{\begin{vmatrix} 0 & F_j \\ (GK)_{l..n,i} & \begin{bmatrix} I_m + (GK)_{l..m,*} & 0_{m,n-m} \\ (GK)_{(m+1)..n,*} & I_{n-m} \end{bmatrix} \end{vmatrix}}{|I_m + (GK)_{l..m,*}|} \quad (4.10)$$

Two simplified expressions of interest come out of Eqn (4.10), one for the case where $j = i$ and the other for the case where $j = (m+1)..n$. To avoid cumbersome notation, define,

$$\hat{G} = I_m + (GK)_{l..m,*} \quad (4.11)$$

For the case where $j = i$.

$$\frac{y_j}{r_i} = \frac{\begin{vmatrix} \hat{G}_{*,l..(i-1)} & (GK)_{l..m,i} & \hat{G}_{*,(i+1)..m} \end{vmatrix}}{|\hat{G}|} \quad (4.12)$$

Notice that Eqn (4.12) is the expression for the closed Loop Channel i of a square system. The reason that the columns of the numerator expression are ordered as they are is to ensure that the sign of Eqn (4.12) is the same as the sign of Eqn (4.10).

To help one visualise that the ordering of the columns maintains the correct sign, consider a 3-input 4-output system where loops 1, 2 and 3 are closed and the expressions for y_2/r_2 and y_3/r_3 are to be determined. The numerator of Eqn (4.10) for y_2/r_2 will be,

$$\begin{vmatrix} 0 & 0 & 1 & 0 & 0 \\ k_2 g_{12} & 1 + k_1 g_{11} & k_2 g_{12} & k_3 g_{13} & 0 \\ -k_2 g_{22} & k_1 g_{21} & 1 + k_2 g_{22} & k_3 g_{23} & 0 \\ k_2 g_{32} & k_1 g_{31} & k_2 g_{32} & 1 + k_3 g_{33} & 0 \\ k_2 g_{42} & k_1 g_{41} & k_2 g_{42} & k_3 g_{43} & 1 \end{vmatrix} = - \begin{vmatrix} k_2 g_{12} & 1 + k_1 g_{11} & k_3 g_{13} \\ k_2 g_{22} & k_1 g_{21} & k_3 g_{23} \\ k_2 g_{32} & k_1 g_{31} & 1 + k_3 g_{33} \end{vmatrix} \quad (4.13)$$

and for y_3/r_3 ,

$$\begin{vmatrix} 0 & 0 & 0 & 1 & 0 \\ k_3 g_{13} & 1 + k_1 g_{11} & k_2 g_{12} & k_3 g_{13} & 0 \\ -k_3 g_{23} & k_1 g_{21} & 1 + k_2 g_{22} & k_3 g_{23} & 0 \\ k_3 g_{33} & k_1 g_{31} & k_2 g_{32} & 1 + k_3 g_{33} & 0 \\ k_3 g_{43} & k_1 g_{41} & k_2 g_{42} & k_3 g_{43} & 1 \end{vmatrix} = \begin{vmatrix} k_3 g_{13} & 1 + k_1 g_{11} & k_2 g_{12} \\ k_3 g_{23} & k_1 g_{21} & 1 + k_2 g_{22} \\ k_3 g_{33} & k_1 g_{31} & k_2 g_{32} \end{vmatrix} \quad (4.14)$$

By the properties of determinants, the right hand side of Eqn (4.13) can be written as,

$$- \begin{vmatrix} k_2 g_{12} & 1 + k_1 g_{11} & k_3 g_{13} \\ -k_2 g_{22} & k_1 g_{21} & k_3 g_{23} \\ k_2 g_{32} & k_1 g_{31} & 1 + k_3 g_{33} \end{vmatrix} = \begin{vmatrix} 1 + k_1 g_{11} & k_2 g_{12} & k_3 g_{13} \\ k_1 g_{21} & k_2 g_{22} & k_3 g_{23} \\ k_1 g_{31} & k_2 g_{32} & 1 + k_3 g_{33} \end{vmatrix} \quad (4.15)$$

and the right hand side of Eqn (4.14) can be written as,

$$\begin{vmatrix} k_3 g_{13} & 1 + k_1 g_{11} & k_2 g_{12} \\ k_3 g_{23} & k_1 g_{21} & k_2 g_{22} \\ k_3 g_{33} & k_1 g_{31} & 1 + k_2 g_{22} \end{vmatrix} = \begin{vmatrix} 1 + k_1 g_{11} & k_2 g_{12} & k_3 g_{13} \\ k_1 g_{21} & 1 + k_2 g_{22} & k_3 g_{23} \\ k_1 g_{31} & k_2 g_{32} & k_3 g_{33} \end{vmatrix} \quad (4.16)$$

The right hand side of Eqns (4.16) and (4.15) are equal to those calculated by Eqn (4.12). It is seen by this example that by using Eqn (4.12), not only is the sign of the determinant correctly calculated, but the elements of the numerator matrix are in their correct position.

For the case where $j = (m+1)..n$,

$$\frac{y_j}{r_i} = - \frac{\begin{vmatrix} \hat{G}_{1..(i-1),*} \\ (GK)_{j,*} \\ \hat{G}_{(i+1)..m,*} \end{vmatrix}}{|\hat{G}|} \quad (4.17)$$

It is seen that $(GK)_{j,*}$ replaces the i -th row of \hat{G} . This is done in order that the sign of Eqn (4.17) will equal the sign of Eqn (4.10).

The simplification of Eqn (4.10) to Eqn (4.17) is not very obvious from inspection of Eqn (4.10). In order to demonstrate the manner in which Eqn (4.17) is arrived at, consider a non-square system which has 2 inputs and 3 outputs. Loops 1 and 2 are closed and y_3/r_1 is to be found. The numerator of Eqn (4.10) is written as,

$$\begin{aligned} & \begin{vmatrix} 0 & 0 & 0 & 1 \\ k_1g_{11} & 1+k_1g_{11} & k_2g_{12} & 0 \\ k_1g_{21} & k_1g_{21} & 1+k_2g_{22} & 0 \\ k_1g_{31} & k_1g_{31} & k_2g_{32} & 1 \end{vmatrix} = \begin{vmatrix} k_1g_{11} & 1+k_1g_{11} & k_2g_{12} \\ k_1g_{21} & k_1g_{21} & 1+k_2g_{22} \\ k_1g_{31} & k_1g_{31} & k_2g_{32} \end{vmatrix} \\ & = k_1g_{11} \begin{vmatrix} k_1g_{21} & 1+k_2g_{22} \\ k_1g_{31} & k_2g_{32} \end{vmatrix} - k_1g_{11} \begin{vmatrix} k_1g_{21} & 1+k_2g_{22} \\ k_1g_{31} & k_2g_{32} \end{vmatrix} - \begin{vmatrix} k_1g_{21} & 1+k_2g_{22} \\ k_1g_{31} & k_2g_{32} \end{vmatrix} \end{aligned} \quad (4.18)$$

Therefore,

$$\begin{vmatrix} 0 & 0 & 0 & 1 \\ k_1g_{11} & 1+k_1g_{11} & k_2g_{12} & 0 \\ k_1g_{21} & k_1g_{21} & 1+k_2g_{22} & 0 \\ k_1g_{31} & k_1g_{31} & k_2g_{32} & 1 \end{vmatrix} = - \begin{vmatrix} k_1g_{21} & 1+k_2g_{22} \\ k_1g_{31} & k_2g_{32} \end{vmatrix} \quad (4.19)$$

From the properties of determinants the right hand side of Eqn (4.19) can be written as,

$$- \begin{vmatrix} k_1g_{21} & 1+k_2g_{22} \\ k_1g_{31} & k_2g_{32} \end{vmatrix} = \begin{vmatrix} k_1g_{31} & k_2g_{32} \\ k_1g_{21} & 1+k_2g_{22} \end{vmatrix} \quad (4.20)$$

The right hand side of Eqn (4.20) agrees with the numerator of Eqn (4.17). By using Eqn (4.17), not only is the sign of the determinant calculated correctly, but element g_{ji} will always be placed in the numerator matrix such that it is a diagonal element. This means that if one expands the determinant down a column or along a row which contains g_{ji} then the element $g_{ji}L_{ji}$ will always be of positive sign, where L_{ji} is the cofactor of g_{ji} . This is a useful property, as will become evident later.

As the controller is diagonal, Eqn (4.17) can be alternatively written as,

$$\frac{y_j}{r_i} = \frac{\begin{vmatrix} (K^{-1} + G_{1..m,*})_{1..(i-1),*} \\ G_{j,*} \\ (K^{-1} + G_{1..m,*})_{(i+1)..m,*} \end{vmatrix}}{\begin{vmatrix} K^{-1} + G_{1..m,*} \end{vmatrix}} = \frac{|\hat{G}|}{|\bar{G}|} \quad (4.21)$$

4.4. Sensitivity of the Outer Open-Loop Transfer Function Elements

It is the outputs which are loose after closure of the inner loop which will be fed back in the outer loop. The effective open-loop system for the outer loop is \bar{Q} , which is defined in Section 4.2. The transfer function elements of \bar{Q} must be checked to assess whether the inner loop closure has caused them to become structurally sensitive or phase sensitive. If they have become structurally sensitive or phase sensitive then this could have repercussions for the stability of the complete system once the outer loop has been closed.

In order to assess the sensitivity of $|\hat{G}|$ of Eqn (4.21) to changes in the transfer function elements of \hat{G} it would be desirable to re-write Eqn (4.21) in such a way that an MSF is defined so that ICA can be applied. This is the motive behind the development of Eqns (4.22) through (4.29). Support for this approach will follow afterwards.

For element $y_j/r_i = \bar{q}_{ji}$, where $j > m$, write,

$$\bar{q}_{ji} = \left(g_{ji} |\hat{G}^i| + |\hat{G}_i| \right) / |\bar{G}| \quad (4.22)$$

where \hat{G}^i is \hat{G} with row i and column i removed, and \hat{G}_i is \hat{G} with element (i,i) set to zero. Recall from Section 4.3 that $g_{ji} |\hat{G}^i|$ will always be positive as the numerator matrix is manipulated such that g_{ji} is a diagonal element.

Now, $|\hat{G}^i| = |\bar{G}^i|$ and so Eqn (4.22) can be written as,

$$\bar{q}_{ji} = g_{ji} \left(\frac{|\bar{G}^i|}{|\bar{G}|} \right) \left(1 - \left(-\frac{|\hat{G}_i|}{g_{ji}} |\hat{G}^i| \right) \right) \quad (4.23)$$

To simplify Eqn (4.23) consider Channel i of the inner system,

$$C_i = k_i g_{ii} (1 - \gamma_i) = k_i g_{ii} (1 + |\bar{G}_i| / g_{ii} |\bar{G}^i|) \quad (4.24)$$

And so C_i can be written as,

$$C_i = k_i \left| \frac{\bar{G}}{\bar{G}^i} \right| \quad (4.25)$$

where all elements of ${}_i\bar{G}$ are the same as \bar{G} except element (1,1) which is g_{ii} instead of $k_i^{-1} + g_{ii}$. Therefore,

$$1 + C_i = k_i \left| \frac{\bar{G}}{\bar{G}^i} \right| \quad (4.26)$$

Substituting Eqn (4.26) into Eqn (4.23)

$$\bar{q}_{ji} = k_i g_{ji} (1 / (1 + C_i)) \left(1 - \left(-\frac{|\hat{G}_i|}{g_{ji}} |\hat{G}^i| \right) \right) \quad (4.27)$$

Define,

$$\bar{\gamma}_{ji} = -\frac{|\hat{G}_i|}{g_{ji}} |\hat{G}^i| \quad (4.28)$$

So,

$$\bar{q}_{ji} = k_i g_{ji} \left(\frac{1}{1 + C_i} \right) (1 - \bar{\gamma}_{ji}) \quad j > m, i = 1, \dots, m \quad (4.29)$$

To support the use of the MSF defined in Eqn (4.28) as a structural and/or phase sensitivity measure, consider the case where the transfer function of interest is the transfer function between output j and input i where $j = i$. i.e. it is the transfer function of the closed loop Channel i . In that case, if one were to define an MSF, $\bar{\gamma}_{ji}$, for this transfer function then it would be equal to the MSF of the open loop Channel i , i.e. γ_i . It is known that the closeness of γ_i to the (1,0) point is an indication as to whether plant

uncertainty may cause Channel i to change its zero structure. If Channel i changes its zero structure then so will the closed loop Channel i , as they share the same zeros. The definition of $\bar{\gamma}_{ji}$ is therefore a zero structural sensitivity measure for the closed-loop Channel transfer functions, and it seems very reasonable to conclude that the definition is also valid as a zero structural sensitivity measure for the loose transfer functions.

The next question to ask is whether the $\bar{\gamma}_{ji}$ is a measure of phase sensitivity. Phase sensitivity can only occur to the detriment of stability margins at, or in some close vicinity of, the 0dB crossover of a particular transfer function element. If $\bar{\gamma}_{ji}$ is close to the (1,0) point then one can be quite certain that $(1-\bar{\gamma}_{ji})$ will exhibit phase sensitivity, as $\bar{\gamma}_{ji}$ is subject to variation. Strictly, it should be determined whether or not the correlation between the errors in the different elements of G is such that the variation in $k_j g_{ji}(1/1+C_i)$ cancels (or partly cancels) the variation in $(1-\bar{\gamma}_{ji})$. This is difficult to do generally, but one would expect to be able to avoid problems in practice by choosing the 0dB crossover frequencies of the 'outer' Channels to be distant from any problematic frequencies.

Once the transfer function elements which form \bar{Q} have been analysed using the above procedure and any problematic frequencies identified, then ICAD can be performed with confidence on \bar{Q} .

There are therefore three proposed criteria which should be met for a non-square system to be regarded as possessing stability robustness. These are,

- i) *The inner feedback system should be robust, as assessed using ICA.*
- ii) *The transfer function elements which form the open-loop transfer function matrix for the outer system, \bar{Q} , should not exhibit structural sensitivity and/or phase sensitivity with respect to variations in the plant elements. This sensitivity is assessed by analysis of $\bar{\gamma}_{ji}$.*

- iii) *The outer feedback system should be robust, with respect to the transfer function elements of \bar{Q} , as assessed using ICA.*

A simple conceptual example is now given to demonstrate the method.

Consider the case where the system has 2 inputs and 3 outputs and has 2 loop closures between outputs 1 and 2 and inputs 1 and 2 respectively on the inner system, but only one loop closure on the outer system. Say the outer loop will be closed around output 3 and input 1. Figure 4.2 shows a block diagram of this configuration,

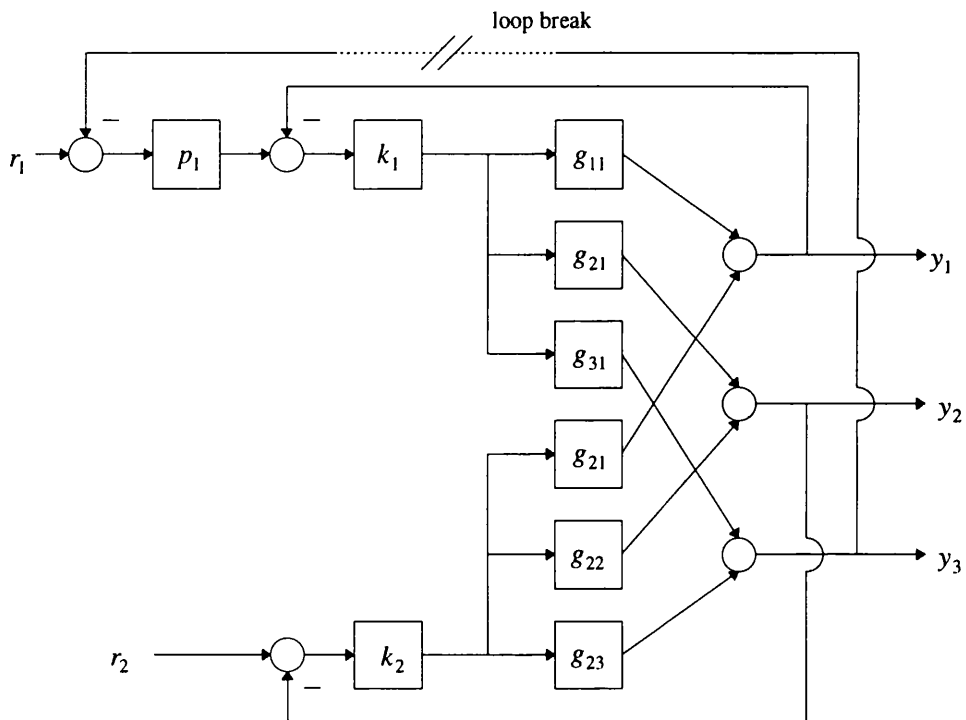


Figure 4.2. Block diagram of conceptual example.

\bar{Q} in this case will be a single transfer function given by,

$$\bar{q}_{31} = \frac{\begin{vmatrix} g_{31} & g_{32} \\ g_{21} & k_2^{-1} + g_{22} \end{vmatrix}}{\begin{vmatrix} k_1^{-1} + g_{11} & g_{12} \\ g_{21} & k_2^{-1} + g_{22} \end{vmatrix}} \quad (4.30)$$

which by the development above, can be expressed as,

$$\bar{q}_{31} = g_{31} \frac{k_2^{-1} + g_{22}}{\begin{vmatrix} k_1^{-1} + g_{11} & g_{12} \\ g_{21} & k_2^{-1} + g_{22} \end{vmatrix}} \left(1 - \frac{g_{21}g_{32}}{g_{31}(k_2^{-1} + g_{22})} \right) = k_1 g_{31} \left(\frac{1}{1 + C_1} \right) (1 - \bar{\gamma}_{31}) \quad (4.31)$$

where,

$$\frac{k_1}{1 + C_1} = \frac{k_2^{-1} + g_{22}}{\begin{vmatrix} k_1^{-1} + g_{11} & g_{12} \\ g_{21} & k_2^{-1} + g_{22} \end{vmatrix}} \quad (4.32)$$

$$\bar{\gamma}_{31} = \frac{g_{21}g_{32}}{g_{31}(k_2^{-1} + g_{22})} \quad (4.33)$$

The sensitivity of $1/(1+C_1)$ is determined by ICA of the inner feedback system. For $1/(1+C_1)$ to be insensitive it is sufficient that Channel 1 has adequate gain and phase margins and that the MSF of Channel 1 is far from the (1,0) point at frequencies of importance. In addition, the Nyquist plot of $\bar{\gamma}_{31}$ should be checked to determine whether it approaches the (1,0) point at any frequency. If $\bar{\gamma}_{31}$ approaches the (1,0) point at frequencies of importance then \bar{q}_{31} may exhibit structural and/or phase sensitivity. If \bar{q}_{31} exhibits sensitivity at frequencies of importance then the gain and phase margins of $p_1\bar{q}_{31}$ will not be valid as robustness measures.

4.5. Analysis Before The Inner Loop Has Been Designed

It is obviously of importance to the control engineer to be able to analyse the outer loop, if only approximately, before the inner loop has actually been designed. One way in which this can be done is to use the constrained variable method (Tischler [75]). That is, to assume that the inner loops have infinite bandwidth. An analysis of this kind will highlight potential structural and robustness problems. The equations developed in Section 4.3 will be amended appropriately in this Section.

Assuming infinite gain control on the inner loop, Eqn (4.17) becomes,

$$\frac{y_j}{r_i} = \frac{\begin{vmatrix} (G_{1..m,:})_{1..(i-1),:} \\ G_{j,:} \\ (G_{1..m,:})_{(i+1)..m,:} \end{vmatrix}}{|G_{1..m,:}|} = \frac{|\tilde{G}|}{|G_s|} \quad (4.34)$$

For element $y_j/r_i = q_{ji}$, where $j > m$, write,

$$q_{ji} = \frac{g_{ji}|\tilde{G}^i| + |\tilde{G}_i|}{|G_s|} \quad (4.35)$$

where \tilde{G}^i is \tilde{G} with row i and column i removed, and \tilde{G}_i is \tilde{G} with element (i,i) set to zero.

$$q_{ji} = \frac{g_{ji}|\tilde{G}^i|}{|G_s|} \left(1 - \frac{|\tilde{G}_i|}{g_{ji}|\tilde{G}^i|} \right) \quad (4.36)$$

Now, $|\tilde{G}^i| = |G_s^i|$ and so to simplify Eqn (4.36) consider approximate Channel i of the inner system,

$$\hat{C}_i = g_{ii}(1 - \hat{F}_i) \quad (4.37)$$

where,

$$\hat{\Gamma}_i = \frac{-|G_{si}|}{g_{ji}|G_s^i|} \quad (4.38)$$

And so \hat{C}_i can be written as,

$$\hat{C}_i = \frac{|G_s|}{|G_s^i|} \quad (4.39)$$

Substituting Eqn (4.39) into Eqn (4.36)

$$q_{ji} = g_{ji} \left(\frac{1}{\hat{C}_i} \right) \left(1 - \frac{-|\tilde{G}_i|}{g_{ji}|\tilde{G}^i|} \right) \quad (4.40)$$

Define,

$$\Gamma'_{ji} = \frac{-|\tilde{G}_i|}{g_{ji}|\tilde{G}^i|} \quad (4.41)$$

So,

$$q_{ji} = g_{ji} \left(\frac{1}{\hat{C}_i} \right) (1 - \Gamma'_{ji}) \quad j > m, i = 1, \dots, m \quad (4.42)$$

4.6. Summary

This Chapter has proposed a method in which a non-square system which can be decomposed into a square inner system and a square outer system can be assessed within the ICA framework. The effect on the sensitivity of the transfer function elements of the outer system, due to the closure of the inner systems loops is assessed by ICA of the inner system and the use of subsidiary multivariable structure functions which are defined in Section 4.4.

There are three proposed criteria which should be met for a non-square system to be regarded as possessing stability robustness. These are,

- i) *The inner feedback system should be robust, as assessed using ICA.*
- ii) *The transfer function elements which form the open-loop transfer function matrix for the outer system, \bar{Q} , should not exhibit structural sensitivity and/or phase sensitivity with respect to variations in the plant elements. This sensitivity is assessed by analysis of $\bar{\gamma}_{ji}$.*
- iii) *The outer feedback system should be robust, with respect to the transfer function elements of \bar{Q} , as assessed using ICA.*

The method developed in this Chapter for the analysis of non-square systems is applications driven, i.e. it has been developed to allow transparent design procedures, and fits in well with the overall philosophy of ICAD.

Individual Channel Analysis of State Space Systems

5.1. Introduction

One factor which may have limited the use of ICAD is its dependence on the transfer function representation of MIMO plants. The theory has been developed in terms of transfer function matrices and their determinants and, indeed, there are subtleties involved when using state space models in ICAD (Leithead and O'Reilly [33]). Yet, many plant models are most easily expressed in state space terms and many potential users would prefer to base their numerical computations on state space models, particularly aerospace control engineers who work extensively with state space models. This Chapter reviews the issues involved with using ICA on state space models and compares two methods for the computation of the MSFs based, respectively, on transfer functions and the direct use of state space models. The state space method uses existing techniques for the computation of transmission zeros and is found to be more convenient and numerically reliable.

The outline of this Chapter is as follows. Section 5.2 gives a brief review of applicable state space theory. Section 5.3 describes how the transmission zeros of a general m -input m -output system may be calculated. This is a pre-requisite for the development of the following Sections. Section 5.4 describes the manner in which the approximate MSF of a defined Channel 1, Γ_1 , is calculated using the two techniques stated above. Section 5.5 describes how the actual MSF of a defined Channel 1, γ_1 , can be calculated using the two techniques. Both Sections 5.4 and 5.5 briefly state how the developed methodology can be applied to general MSFs. Section 5.6 determines the way in which the zeros of a Channel and the transmission zeros of a plant are determined from the

appropriate MSFs. Section 5.7 gives an example of the two techniques applied to the calculation of the approximate MSF, Γ_1 , of an 8th order 4-input 4-output state space description of a helicopter and a comparison of the two techniques is made. Section 5.8 investigates the structural issues of the Channels and the MSFs.

It should be pointed out that this Chapter contains a wealth of notation. While every attempt has been made to make the Chapter as clear as possible, extra care should be paid to the descriptions of the notations as they are presented.

5.2. A Review of Applicable State Space Theory

This Section reviews a sufficient amount of state space theory for the reader unfamiliar with state space techniques to understand the remainder of the Chapter. For further details on state space theory the reader is referred to Maciejowski [43].

A linear system can be described by a general state space quadruple (A,B,C,D) which has m inputs and p outputs. The dynamics of such a system are described by the following two equations,

$$\dot{x} = Ax + Bu \tag{5.1}$$

$$y = Cx + Du \tag{5.2}$$

A , the system matrix, has dimension $n \times n$. The eigenvalues of the A matrix correspond to the dynamic modes of the system and are analogous to the poles of a single-input single-output system. B , the control matrix, has dimension $n \times m$. C , the observation matrix, has dimension $p \times n$. D has dimension $p \times m$ and is commonly a zero matrix. x , the state vector, has dimension $n \times 1$. u is an $m \times 1$ vector which describes the inputs to the system. y is a $p \times 1$ vector and describes the observed outputs of the system.

In state space theory the concept of *controllability* and *observability* have importance for control system design.

The controllability matrix C_0 is defined as,

$$C_o = [B \quad AB \quad A^2B \quad \cdots \quad A^{n-1}B] \quad (5.3)$$

If C_o has rank n then the system is controllable.

The observability matrix O_b is defined as,

$$O_b = \begin{bmatrix} C \\ CA \\ CA^2 \\ \vdots \\ CA^{n-1} \end{bmatrix} \quad (5.4)$$

If O_b has rank n then the system is observable

If a state space representation of a system is both controllable and observable then it is called a *minimal realisation*.

A transfer function matrix G can be derived from a state space model by the following equation,

$$G = C(sI - A)^{-1}B + D \quad (5.5)$$

Given a minimal state space representation, those complex frequencies at which G loses rank correspond to the frequencies of the transmission zeros. The transmission zeros of a multivariable system are analogous to the zeros of a single-input single-output system.

The matrix,

$$\tilde{N} = \begin{bmatrix} sI - A & B \\ -C & D \end{bmatrix} \quad (5.6)$$

is known as *Rosenbrock's system matrix* and it loses rank at those points in the complex plane which correspond to the transmission zeros of G , if the state space system from which G is derived is a minimal realisation. It is assumed for the remainder of this Chapter that all state space systems under consideration are minimal realisations.

5.3. Calculation of Plant Transmission Zeros

The purpose of this Section is to present two ways in which the transmission zeros of a system described by a state space model can be calculated. This is necessary, as will be seen, for the interpretation of the pole-zero structure of Γ_1 . The first way described is by means of a transfer function matrix derived from a state space model, and the second way is by consideration of the state space model only. The reason the transfer function matrix is considered is due to the fact that the development of ICAD has been based on transfer function representations of systems.

One can expand a transfer function matrix, G , derived from a state space model (Eqn (5.5)) as follows,

$$G = \begin{bmatrix} g_{11} & \cdots & g_{1m} \\ \vdots & \ddots & \vdots \\ g_{m1} & \cdots & g_{mm} \end{bmatrix} = \begin{bmatrix} \frac{N_{11}}{\phi} & \cdots & \frac{N_{1m}}{\phi} \\ \vdots & \ddots & \vdots \\ \frac{N_{m1}}{\phi} & \cdots & \frac{N_{mm}}{\phi} \end{bmatrix} = \frac{N}{\phi} \quad (5.7)$$

where,

$$\phi = |sI - A| \quad (5.8)$$

$$N_{ij} = |sI - A + B_{(*,j)}C_{(i,*)}| - (1 - D_{ij})|sI - A|, \quad i=1..m, j=1..m \quad (5.9)$$

where $B_{(*,j)}$ is column j of B , $C_{(i,*)}$ is row i of C and D_{ij} is element (i,j) of D . $| \cdot |$ is the determinant. The roots of ϕ are the eigenvalues of the A matrix.

$|G|$ can be calculated two ways (Leithead and O'Reilly [33]). The first is to calculate the determinant from the transfer function matrix given in Eqn (5.7),

$$|G|_{TF} = \frac{|N|}{\phi^m} \quad (5.10)$$

where the subscript TF denotes that the determinant is calculated from the transfer function matrix. m is the number of inputs (outputs) of the system.

The second is to calculate the determinant directly from the state space form of the model,

$$|G|_{ss} = |(sI - A)^{-1}| \cdot \begin{vmatrix} sI - A & B \\ -C & D \end{vmatrix} = \frac{|\tilde{N}|}{\phi} \quad (5.11)$$

Recall from Section 5.2 that \tilde{N} is the Rosenbrock system matrix.

By comparing Eqns (5.11) and (5.10), it is seen that the roots of $|N|$ must have the roots of ϕ^{m-1} as a factor, with the remaining roots being the transmission zeros of the system. More formally,

$$|N| = \phi^{m-1} |\tilde{N}| \quad (5.12)$$

5.4. The Approximate Multivariable Structure Function

This Section describes the significance of Eqn (5.12) in relation to a MSF which has been derived from a state space model. We can restrict ourselves, without loss of generality, to the specific case of the computation of Γ_1 because, by appropriately rearranging the rows (columns) of the C (B) matrix, any of the m Channels can be redefined as Channel 1. Γ_1 is defined as,

$$\Gamma_1 = \frac{-|G_1|}{g_{11}|G^1|} \quad (5.13)$$

where G_1 is G with element (1,1) set to zero, G^1 is G with row 1 and column 1 removed and g_{11} is element (1,1) of G . Explicitly writing Γ_1 ,

$$\Gamma_1 = - \frac{\begin{vmatrix} 0 & g_{12} & \cdots & g_{1m} \\ g_{21} & g_{22} & \cdots & g_{2m} \\ \vdots & \vdots & \ddots & \vdots \\ g_{m1} & g_{m2} & \cdots & g_{mm} \end{vmatrix}}{g_{11} \begin{vmatrix} g_{22} & \cdots & g_{2m} \\ \vdots & \ddots & \vdots \\ g_{m2} & \cdots & g_{mm} \end{vmatrix}} \quad (5.14)$$

As the plant model is originally a minimum order state space representation, the minimum order representation of $(1-\Gamma_1)$ can be written as,

$$(1 - \Gamma_1) = \frac{g_{11}|G^1|_{SS} + |G_1|_{SS}}{g_{11}|G^1|_{SS}} = \frac{|G|_{SS}}{g_{11}|G^1|_{SS}} \quad (5.15)$$

where,

$$g_{11} = N_{11}/\phi, \quad |G^1|_{SS} = |\tilde{N}^1|/\phi, \quad |G|_{SS} = |\tilde{N}|/\phi \quad (5.16)$$

\tilde{N}^1 is the Rosenbrock system matrix for the system with row 1 of C , column 1 of B and row 1 and column 1 of D removed.

Therefore,

$$(1 - \Gamma_1) = \frac{|\tilde{N}|/\phi}{N_{11}|\tilde{N}^1|} \quad (5.17)$$

It is seen then, that the zeros of $(1-\Gamma_1)$ consists of the transmission zeros of (A,B,C,D) and the eigenvalues of A .

5.4.1. Calculation of the Approximate MSF using the Transfer Function Matrix

To calculate Γ_1 from the transfer function matrix, using Eqn (5.10), the determinant of the numerator of the $m \times m$ matrix must be calculated. This follows from,

$$|G|_{TF} = g_{11}|G^1|_{TF} + |G_1|_{TF} \quad (5.18)$$

The denominator of $g_{11}|G^1|_{TF}$ is ϕ^m and the denominator of $|G_1|_{TF}$ is also ϕ^m . These denominators therefore cancel exactly in Eqn (5.13) and hence only the numerator determinants of $g_{11}|G^1|_{TF}$ and $|G_1|_{TF}$ need be calculated.

Note that the numerator of $(1-\Gamma_1)$ is the numerator of $|G|_{\text{TF}}$ and so, from Eqn (5.12) will be equal to $\phi^{m-1}|\tilde{N}|$.

It is found that exact cancellation occurs between some of the factors of the numerator and denominator of Γ_1 , as will be shown.

The zeros of $|G^1|_{\text{TF}}$ are the roots of $\phi^{m-2}|\tilde{N}^1|$, where the roots of $|\tilde{N}^1|$ are the transmission zeros of $|G^1|_{\text{SS}}$. ϕ^{m-2} is a factor because G^1 has $(m-1)$ inputs and $(m-1)$ outputs. Now focusing on the numerator of G_1 , expanding $|G_1|_{\text{TF}}$ down the first column of G_1 gives,

$$|G_1|_{\text{TF}} = \sum_{i=2}^m (-1)^{i+1} g_{i1} L_{i1} \quad (5.19)$$

where L_{i1} is the cofactor of g_{i1} . Because L_{i1} is the determinant of a $(m-1) \times (m-1)$ transfer function matrix its numerator will have ϕ^{m-2} as a factor and so $|G_1|_{\text{TF}}$ will have ϕ^{m-2} as a factor. ϕ^{m-2} is therefore a factor of both the numerator and the denominator of Γ_1 and hence those roots will exactly cancel. After cancellation of those roots, the zeros of $(1-\Gamma_1)$ will be the roots of,

$$\frac{\phi^{m-1}|\tilde{N}|}{\phi^{m-2}} = \phi|\tilde{N}| \quad (5.20)$$

as required from Eqn (5.17).

5.4.2. Calculation of the Approximate MSF using the State Space Model

Eqn (5.13) can be written as,

$$\Gamma_1 = \frac{-|G - Z_1|}{|G - P_1|} \quad (5.21)$$

where Z_1 is a zero matrix of dimension $m \times m$ except element (1,1) which is set to g_{11} , and P_1 is a zero matrix of dimension $m \times m$ except elements (2..m,1) which are set to $g_{21} \dots g_{m1}$.

Explicitly writing Z_1 and P_1 ,

$$Z_1 = \left[\begin{array}{c|c} g_{11} & 0_{1(m-1)} \\ \hline 0_{(m-1)1} & 0_{(m-1)(m-1)} \end{array} \right] \quad P_1 = \left[\begin{array}{c|c} 0 & 0_{1(m-1)} \\ \hline g_{21} & \\ \vdots & \\ g_{m1} & 0_{(m-1)(m-1)} \end{array} \right] \quad (5.22)$$

by referring to Eqn (5.13) it is seen that $-|G - Z_1|$ and $|G - P_1|$ are indeed the numerator and denominator of Γ_1 respectively.

$-Z_1$ can be written in state space form as,

$$-Z_1 = -C_Z(sI - A)^{-1} B_Z - D_Z \quad (5.23)$$

where,

$$C_Z = \left[\begin{array}{c} C_{(1,*)} \\ 0_{(m-1),n} \end{array} \right], \quad B_Z = \left[\begin{array}{cc} B_{(*,1)} & 0_{n,(m-1)} \end{array} \right], \quad D_Z = \left[\begin{array}{cc} d_{11} & 0_{1,(m-1)} \\ 0_{(m-1),1} & 0_{(m-1),(m-1)} \end{array} \right] \quad (5.24)$$

$G - Z_1$ can be written in state space form by putting (A, B, C, D) and $(A, B_Z, -C_Z, -D_Z)$ in parallel,

$$G - Z_1 = C'(sI - A')B' + D' \quad (5.25)$$

where,

$$A' = \begin{bmatrix} A & 0 \\ 0 & A \end{bmatrix} \quad (5.26)$$

$$B' = \begin{bmatrix} B \\ B_Z \end{bmatrix} \quad (5.27)$$

$$C' = [C \quad -C_Z] \quad (5.28)$$

$$D' = D - D_Z \quad (5.29)$$

$-P_1$ can be written in state space form as,

$$-P_1 = -C_P (sI - A)^{-1} B_P - D_P \quad (5.30)$$

where,

$$C_P = \begin{bmatrix} 0_{1,n} \\ C_{(2..m,*)} \end{bmatrix}, B_P = [B_{(*,1)} \quad 0_{n,(m-1)}], D_P = \begin{bmatrix} 0 & 0_{1,(m-1)} \\ d_{(2..m,1)} & 0_{(m-1),(m-1)} \end{bmatrix} \quad (5.31)$$

$G - P_1$ can be written in state space form by putting (A,B,C,D) and $(A_P,B_P,-C_P,-D_P)$ in parallel,

$$G - P_1 = C''(sI - A'')B'' + D'' \quad (5.32)$$

where,

$$A'' = \begin{bmatrix} A & 0 \\ 0 & A \end{bmatrix} \quad (5.33)$$

$$B'' = \begin{bmatrix} B \\ B_P \end{bmatrix} \quad (5.34)$$

$$C'' = [C \quad -C_P] \quad (5.35)$$

$$D'' = D - D_P \quad (5.36)$$

It is seen that both $G - Z_1$ and $G - P_1$ share common poles because $A' = A''$. These common poles will exactly cancel in Γ_1 . i.e.,

$$\Gamma_1 = \frac{\left| \begin{array}{cc} sI - A' & B' \\ -C' & D' \end{array} \right| / |sI - A'|}{\left| \begin{array}{cc} sI - A'' & B'' \\ -C'' & D'' \end{array} \right| / |sI - A''|} = \frac{\left| \begin{array}{cc} sI - A' & B' \\ -C' & D' \end{array} \right|}{\left| \begin{array}{cc} sI - A'' & B'' \\ -C'' & D'' \end{array} \right|} \quad (5.37)$$

The zeros and poles of Eqn (5.37) are calculated by calculating the transmission zeros of the (A', B', C', D') system and the (A'', B'', C'', D'') system respectively. Doing this does not actually give Γ_1 , but gives,

$$\Gamma_1' = \frac{\prod_{t=1}^f (s + z_t)}{\prod_{l=1}^v (s + p_l)} \quad (5.38)$$

where the $-z_t, t=1..f$, are the transmission zeros of (A', B', C', D') and the $-p_l, l=1..v$, are the transmission zeros of (A'', B'', C'', D'') .

Γ_1 is related to Γ_1' by,

$$\Gamma_1 = k_{\Gamma_1} \Gamma_1' \quad (5.39)$$

where k_{Γ_1} is a scalar gain which is still to be determined. To determine k_{Γ_1} one method, which is numerically reliable, is to determine the frequency, $\omega_{\Gamma_{\max}}$, at which Γ_1' has its largest magnitude and then calculate,

$$\Gamma_{\max} = \frac{\left| \begin{array}{cc} j\omega_{\Gamma_{\max}} I - A' & B' \\ -C' & D' \end{array} \right|}{\left| \begin{array}{cc} j\omega_{\Gamma_{\max}} I - A'' & B'' \\ -C'' & D'' \end{array} \right|} \quad (5.40)$$

k_{Γ_1} is then calculated from,

$$k_{\Gamma_1} = \Gamma_{\max} / \Gamma_1' (j\omega_{\Gamma_{\max}}) \quad (5.41)$$

Recall that,

$$1 - \Gamma_1 = \frac{|\tilde{N}| \phi}{N_{11} |\tilde{N}^1|} \quad (5.42)$$

Therefore,

$$\frac{\begin{vmatrix} s\mathbf{I} - A'' & B'' \\ -C'' & D'' \end{vmatrix} + \begin{vmatrix} s\mathbf{I} - A' & B' \\ -C' & D' \end{vmatrix}}{\begin{vmatrix} s\mathbf{I} - A'' & B'' \\ -C'' & D'' \end{vmatrix}} = \frac{|\tilde{N}|\phi}{N_{11}|\tilde{N}^1|} \quad (5.43)$$

As Γ_1 is calculated directly from state space algorithms no cancellations are required. Recall from Section 5.4.1 that the transfer function method created exactly cancelling poles and zeros which have to be removed by the user.

5.5. The Actual Multivariable Structure Function

It is important to determine the $m \times m$ system from which γ_i , the actual MSF of Channel 1, can be calculated and to determine the relationship between the poles and zeros of such a system, in the same way as G , the system from which Γ_1 is calculated, was analysed in Eqns (5.1) through (5.9). The technique developed in this Section can be used to calculate γ_i , $i=2..m$, by appropriate rearrangement of the rows (columns) of the C (B) matrix and of the controller matrix.

In the literature (Leithead and O'Reilly [34]), γ_i is usually written as,

$$\gamma_1 = -|\bar{G}_1|/g_{11}|\bar{G}^1| \quad (5.44)$$

where $\bar{G} = K^{-1} + G$, \bar{G}_1 is \bar{G} with element (1,1) set to zero. \bar{G}^1 is \bar{G} with row 1 and column 1 removed. K is written as,

$$K = \begin{bmatrix} k_1 & 0 & \dots & 0 \\ 0 & \ddots & \ddots & \vdots \\ \vdots & \ddots & \ddots & 0 \\ 0 & \dots & 0 & k_m \end{bmatrix} = \begin{bmatrix} \frac{n_{k_1}}{d_{k_1}} & 0 & \dots & 0 \\ 0 & \ddots & \ddots & \vdots \\ \vdots & \ddots & \ddots & 0 \\ 0 & \dots & 0 & \frac{n_{k_m}}{d_{k_m}} \end{bmatrix} \quad (5.45)$$

n_{k_i} is the numerator of controller k_i and d_{k_i} is the denominator of controller k_i , $i=1..m$.

γ_1 can also be written as,

$$\gamma_1 = - \left| \begin{array}{c} 0 \\ G_{(2..m,1)} \end{array} (I_m + GK)_{(*,2..m)} \right| / g_{11} |(I_m + GK)^1| \quad (5.46)$$

where $G_{(2..m,1)}$ is a column vector containing the elements $g_{21}..g_{m1}$, $(I_m + GK)_{(*,2..m)}$ is columns 2..m of $(I_m + GK)$ and $(I_m + GK)^1$ is $(I_m + GK)$ with row 1 and column 1 removed.

Defining,

$$\tilde{G} = \left[G_{(*,1)} \quad (I_m + GK)_{(*,2..m)} \right] \quad (5.47)$$

where $G_{(*,1)}$ is column 1 of G . γ_1 can then be alternatively defined as,

$$\gamma_1 = -|\tilde{G}_1| / g_{11} |\tilde{G}^1| \quad (5.48)$$

where the subscript 1 and superscript 1 are defined as with Eqn (5.44).

The form of Eqn (5.44) is usually used in theoretical work as it leads to simpler analytical expressions. However, it will be seen that the form of Eqn (5.48) is more convenient for computation.

In transfer function matrix form,

$$\tilde{G} = \left[\begin{array}{cccc} \frac{N_{11}}{\phi} & \frac{n_{k_2} N_{12}}{d_{k_2} \phi} & \dots & \frac{n_{k_m} N_{1m}}{d_{k_m} \phi} \\ \frac{N_{21}}{\phi} & \frac{d_{k_2} \phi + n_{k_2} N_{22}}{d_{k_2} \phi} & \dots & \frac{n_{k_m} N_{2m}}{d_{k_m} \phi} \\ \vdots & \vdots & \ddots & \vdots \\ \frac{N_{m1}}{\phi} & \frac{n_{k_2} N_{m2}}{d_{k_2} \phi} & \dots & \frac{d_{k_m} \phi + n_{k_m} N_{mm}}{d_{k_m} \phi} \end{array} \right] \quad (5.49)$$

The determinant of \tilde{G} from the transfer function matrix of Eqn (5.49) is given by,

$$|\tilde{G}|_{TF} = \frac{|\tilde{N}|}{\phi^m d_{k_2} \dots d_{k_m}} = \frac{|\tilde{N}|}{\phi^m \theta} \quad (5.50)$$

where $\theta = d_{k_2} \dots d_{k_m}$ and \check{N} is the matrix of numerators of \check{G} .

In order to express \check{G} in state space form one forms a state space representation of the controller matrix K , given as (a_k, b_k, c_k, d_k) , with k_1 set to 1. The eigenvalues of the state space representation of the controller will therefore be the roots of $d_{k_2} \dots d_{k_m}$, i.e the roots of θ . (a_k, b_k, c_k, d_k) is then put in series with (A, B, C, D) , forming (a, b, c, d) . d should then be replaced by $(I_m)^1 + d$, where $(I_m)^1$ is an identity matrix of dimension m with element $(1,1)$ set to zero.

The determinant of \check{G} from the state space representation $(a, b, c, ((I_m)^1 + d))$ is given by,

$$|\check{G}|_{ss} = \left| (sI - a)^{-1} \begin{vmatrix} sI - a & b \\ -c & (I_m)^1 + d \end{vmatrix} \right| = \frac{|\check{N}|}{\phi\theta} \quad (5.51)$$

where the roots of $|\check{N}|$ are the transmission zeros of $(a, b, c, ((I_m)^1 + d))$. It is seen from Comparing Eqns (5.51) and (5.50) it is seen that $|\check{N}|$ has ϕ^{m-1} as a factor, with the remaining roots being the transmission zeros of \check{G} . More formally,

$$|\check{N}| = \phi^{m-1} |\check{N}| \quad (5.52)$$

Finally, $(1 - \gamma_1)$ can be written as,

$$1 - \gamma_1 = \frac{g_{11} |\check{G}^1|_{ss} + |\check{G}_1|_{ss}}{g_{11} |\check{G}^1|_{ss}} = \frac{|\check{G}|_{ss}}{g_{11} |\check{G}^1|_{ss}} \quad (5.53)$$

where,

$$g_{11} = N_{11}/\phi, \quad |\check{G}^1|_{ss} = |\check{N}^1|/\theta\phi, \quad |\check{G}|_{ss} = |\check{N}|/\theta\phi \quad (5.54)$$

\check{N}^1 is the Rosenbrock system matrix of $(a, b, c, ((I_m)^1 + d))$ with row 1 of c , column 1 of b and row 1 and column 1 of $((I_m)^1 + d)$ removed.

Therefore,

$$1 - \gamma_1 = \frac{|\tilde{N}| \phi}{N_{11} |\tilde{N}^1|} \quad (5.55)$$

It is seen then, that the zeros of $(1-\gamma_1)$ consist of the transmission zeros of $(a,b,c,((I_m)^1+d))$ and the eigenvalues of the system A matrix.

5.5.1. Calculation of the Actual MSF using the Transfer Function Matrix

γ_1 is calculated from Eqn (5.49) as,

$$\gamma_1 = \frac{-\left(\phi^m d_{k_2} \dots d_{k_m}\right) \begin{vmatrix} 0 & n_{k_2} N_{12} & \dots & n_{k_m} N_{1m} \\ N_{21} & d_{k_2} \phi + n_{k_2} N_{22} & \dots & n_{k_m} N_{2m} \\ \vdots & \vdots & \ddots & \vdots \\ N_{m1} & n_{k_2} N_{m2} & \dots & d_{k_m} \phi + n_{k_m} N_{mm} \end{vmatrix}}{\left(\phi^m d_{k_2} \dots d_{k_m}\right) N_{11} \begin{vmatrix} d_{k_2} \phi + n_{k_2} N_{22} & \dots & n_{k_m} N_{2m} \\ \vdots & \ddots & \vdots \\ n_{k_2} N_{m2} & \dots & d_{k_m} \phi + n_{k_m} N_{mm} \end{vmatrix}} \quad (5.56)$$

γ_1 is written in full so one can see from Eqn (5.56) that, as with the approximate MSF Γ_1 , the denominators of the individual transfer function elements are not required in the calculation, as they can come outside the determinant expressions and be cancelled.

Because the zeros of $(1-\gamma_1)$ are the zeros of $|\tilde{G}|_{TF}$ it follows that ϕ^{m-1} is a factor of the numerator of $(1-\gamma_1)$. However, it is found that as with Γ_1 , the roots of ϕ^{m-2} are a factor of both the roots of the numerator and denominator of γ_1 , and so after cancellation of these roots, the zeros of $(1-\gamma_1)$ are $\phi |\tilde{N}|$ as required to agree with Eqn (5.51).

5.5.2. Calculation of the Actual MSF using the State Space Model

The method for calculating Γ_1 in Section 5.4 can be extended in a straight-forward manner to the calculation of γ_1 .

Defining the state space form of γ_1 as,

$$\gamma_1 = \frac{\begin{vmatrix} sI - a' & b' \\ -c' & d' \end{vmatrix}}{\begin{vmatrix} sI - a'' & b'' \\ -c'' & d'' \end{vmatrix}} \quad (5.57)$$

(a', b', c', d') is formed by putting the state space system of the controller (a_k, b_k, c_k, d_k) in series with (A', B', C', D') and adding $(I_m)^1$ to the resulting 'D' matrix. Likewise, (a'', b'', c'', d'') is formed by putting (a_k, b_k, c_k, d_k) in series with (A'', B'', C'', D'') and adding $(I_m)^1$ to the resulting 'D' matrix.

Recall that,

$$1 - \gamma_1 = \frac{|\tilde{N}| \phi}{N_{11} |\tilde{N}^1|} \quad (5.58)$$

Therefore,

$$\frac{\begin{vmatrix} sI - a'' & b'' \\ -c'' & d'' \end{vmatrix} + \begin{vmatrix} sI - a' & b' \\ -c' & d' \end{vmatrix}}{\begin{vmatrix} sI - a'' & b'' \\ -c'' & d'' \end{vmatrix}} = \frac{|\tilde{N}| \phi}{N_{11} |\tilde{N}^1|} \quad (5.59)$$

As γ_1 is calculated directly from state space algorithms no cancellations are required. Recall from Section 5.5.1 that the transfer function method created exactly cancelling poles and zeros which have to be removed by the user.

5.6. Determination of the Zeros of the Channels and the Plant from the Appropriate MSFs

This Section investigates the implications for the structure of the system of the fact that the zeros of $(1-\gamma_a)$, where γ_a is *any* MSF derived from a state space model, approximate or actual, contain the eigenvalues of the system A matrix.

Channel i of a system is written as,

$$C_i = k_i g_{ii} (1 - \gamma_i) \quad (5.60)$$

Expanding this in terms of the numerators and denominators yields,

$$C_i = \frac{n_{k_i} N_{ii}}{d_{k_i} \phi} \left(\frac{|\tilde{N}| \phi}{N_{ii} |\tilde{N}^i|} \right) = \frac{n_{k_i}}{d_{k_i}} \left(\frac{|\tilde{N}|}{|\tilde{N}^i|} \right) \quad (5.61)$$

It is seen from Eqn (5.61) that the roots of $(1-\gamma_i)$ which are the eigenvalues of the system A matrix *exactly* cancel in the Channel expression.

Let us now determine the relationship between the zeros of $(1-\Gamma_i)$ and the zeros of the plant.

The relationship is written as,

$$|G| = (1 - \Gamma_i) g_{ii} |G^i| \quad (5.62)$$

Expanding this in terms of the numerators and denominators yields,

$$|G| = \left(\frac{\phi |\tilde{N}|}{N_{ii} |\tilde{N}^i|} \right) \frac{N_{ii} |\tilde{N}^i|}{\phi^2} = \frac{|\tilde{N}|}{\phi} \quad (5.63)$$

Eqn (5.63) shows the manner in which the zeros of $(1-\Gamma_i)$ which are the eigenvalues of the system A matrix are *exactly* cancelled.

The number of RHPZs of Channel i can be calculated from (Leithead and O'Reilly [33]),

$$N = Z + P - Q \quad (5.64)$$

where N is the number of clockwise encirclements of the (1,0) point of γ_i , Z is the number of RHPZs of Channel i , P is the number of RHPPs of γ_i and Q is the number of RHP eigenvalues of the system A matrix.

Likewise, the number of RHP transmission zeros of the plant is equal to,

$$N = Z + P - Q \quad (5.65)$$

where N is the number of clockwise encirclements of the (1,0) point of Γ_i , Z is the number of RHP transmission zeros of G , P is the number of RHPPs of Γ_i and Q is the number of RHP eigenvalues of the system A matrix.

5.7. Applied Example of Computation of Approximate MSFs

This Section shows a comparison between the two techniques of Section 5.4.1 and 5.4.2 for calculating Γ_1 of a system which is described by a state space model. The calculations were performed using MATLAB[®]. Examples of MATLAB[®] routines to calculate approximate and actual MSFs using the state space method are given in Appendix VI.

The model under consideration is an 8th order state space model of a typical combat rotorcraft trimmed in forward flight at 30 knots. The state space model is given in Appendix III.

The calculation of Γ_1 was performed using both the transfer function matrix determinant technique and the state space technique. Using the transfer function matrix determinant technique, Γ_1 has 26 poles and 26 zeros, before pole-zero cancellation, whereas using the state space technique, Γ_1 has 10 poles and 10 zeros. The poles and zeros of Γ_1 calculated from the transfer function matrix determinant technique are listed in Table 5.1 and the poles and zeros of Γ_1 and the zeros of $(1-\Gamma_1)$ calculated from the state space technique are listed in Table 5.2.

It is seen from Table 5.1 that although it is known that ϕ^2 is a factor of both the numerator and denominator of Γ_1 (as the system is 4-input 4-output), numerical error has caused some of the known exact cancelling poles and zeros to be slightly different in value. For this example, these poles and zeros can be cancelled by using the MINREAL function of MATLAB[®] with a tolerance of 1e-5. For larger order systems, the numerical error becomes more pronounced and can render MINREAL unusable due to the need to set a high tolerance level, which in turn may cancel necessary dynamics. If this is the case, cancellation must be done by hand but this is tedious and unacceptable.

Table 5.1. Structure of Γ_1 calculated from transfer function technique.

| Zeros of Γ_1 (rad/s) | Poles of Γ_1 (rad/s) |
|-----------------------------|-----------------------------|
| -1.3063e+1 | -1.0841e+1 |
| -1.0791e+1 ± 1.1864e-6j | -1.0791e+1 |
| -7.2810e-1 ± 5.7686e+0j | -1.0791e+1 |
| -2.5464e+0 ± 1.4856e-7j | -2.5464e-0 |
| -3.2782e-1 ± 1.1102e+0j | -2.5464e+0 |
| -3.2782e-1 ± 1.1102e+0j | -2.2548e+0 |
| -4.7131e-1 ± 7.9133e-1j | -3.8907e-1 ± 1.1609e+0j |
| 4.2469e-1 | -3.2782e-1 ± 1.1102e+0j |
| 8.9927e-2 ± 4.6048e-1j | -3.2782e-1 ± 1.1102e+0j |
| 8.9927e-2 ± 4.6048e-1j | 8.9928e-2 ± 4.6048e-1j |
| -3.8731e-1 ± 1.5480e-8j | 8.9927e-2 ± 4.6048e-1j |
| 8.3728e-2 | 9.1813e-2 ± 3.9952e-1j |
| -3.5000e-2 ± 2.2442e-2j | -5.2020e-1 |
| -1.2796e-2 | -3.8731e-1 ± 6.9572e-8j |
| -3.2237e-4 | -4.1088e-2 |
| -3.2238e-4 | -8.7505e-3 |
| | -4.0199e-3 |
| | -3.2238e-4 |
| | -3.2237e-4 |

Table 5.2. Structure of Γ_1 and $(1-\Gamma_1)$ calculated from state space technique.

| Zeros of Γ_1 (rad/s) | Poles of Γ_1 (rad/s) | Zeros of $(1-\Gamma_1)$ (rad/s) |
|-----------------------------|-----------------------------|---------------------------------|
| -1.3063e+1 | -1.0841e+1 | -1.0791e+1 |
| -7.2810e-1 ± 5.7686e+0j | -2.2548e+0 | -2.5464e+0 |
| -4.7131e-1 ± 7.9133e-1j | -3.8907e-1 ± 1.1609e+0j | -3.2782e-1 ± 1.1102e+0j |
| 4.2469e-1 | -5.2020e-1 | 8.9927e-2 ± 4.6048e-1j |
| 8.3728e-2 | 9.1813e-2 ± 3.9952e-1j | -3.8731e-1 |
| -3.5000e-2 ± 2.2442e-2j | -4.1088e-2 | -4.2376e-2 |
| -1.2796 | -8.7505e-3 | -9.9461e-3 |
| | -4.0199e-3 | -3.2238e-4 |

It is seen from Table 5.2 that, as expected, Γ_1 is minimum order and the zeros of $(1-\Gamma_1)$ contain the roots of ϕ as a factor. The roots of ϕ are the eigenvalues of the plant's A matrix. Although only the first 5 significant figures are shown in Table 5.2, the zeros of $(1-\Gamma_1)$ which correspond to the eigenvalues of A are equal to the eigenvalues of A up to 12 significant figures.

Experience has shown that even with higher order plants the state space method maintains acceptable accuracy and there is no need to cancel poles and zeros, as with the transfer function matrix method. Note that the fact that the roots of ϕ are a factor of the zeros of $(1-\Gamma_1)$ is a convenient test to ensure that the zeros, poles and gain of Γ_1 have been computed correctly.

5.8. Summary

This Chapter has presented a comparison between two methods in which the MSFs as defined in ICAD theory can be calculated when the plant to be analysed is defined by a state space model. One method involves the calculation of the MSF using a transfer function matrix which has been derived from a state space model and the other method involves the calculation of the MSF by consideration of the state space model only. It is found that the transfer function matrix technique leads to the introduction of exactly

cancelling pole-zero pairs in the MSF which, in theory, exactly correspond to the eigenvalues of the state space A matrix. In practice, however, numerical problems may arise in the computation of these roots such that they no longer cancel within an acceptable tolerance. The state space method leads to a minimum order MSF, i.e. no cancellations are required, and in general leads to a more reliable and efficient solution to the calculation of the MSFs.

It is found that the zeros of $(1-\gamma_a)$, where γ_a is *any* MSF derived from a state space model, contain the eigenvalues of the system A matrix, regardless of the method use to calculate γ_a . These zeros are found to exactly cancel in the Channel and plant representations.

Controller Design Using Individual Channel Analysis

6.1. Introduction

The previous three Chapters have addressed the analysis of systems using Individual Channel Analysis (ICA), particularly a system which has a diagonal control law. Although ICA provides a wealth of information concerning the dynamical aspects of a plant it does not in itself provide an answer to the question of how one can use this information to design a control law.

The purpose of this Chapter is to describe how one can use the information from ICA of a plant in order to design a stabilising diagonal control law. Section 6.2 describes a design philosophy which is in concept straightforward, but which no multivariable technique to date has been able to address satisfactorily. Section 6.3 derives analytical expressions which are used to assess the *potential* for the successful design of a stabilising diagonal control law. Section 6.4 describes how one designs a stabilising diagonal control law for a minimum phase plant using what are known as *nested Channels*. Section 6.5 sets up sufficient conditions to guarantee the closed-loop stability of two classes of system and gives an example of how the design can be performed. Section 6.6 gives an example of the design of a control law for a system which has a low frequency RHP transmission zero. Section 6.7 describes how performance considerations can be included in the design procedure. Section 6.8 considers robustness issues when designing using nested Channels. Section 6.9 gives an example of using ICAD feedforward to increase the robustness of a system.

The descriptions of the design methods are not general but are for certain classes of system. These classes will be highlighted at the appropriate stages. It is hoped that the descriptions will allow the reader to appreciate how the method can in theory be extended to any class of system.

6.2. Design Philosophy

As the technique of ICAD involves the design of a diagonal control law, with each element being designed one after the other, the simplest concept for designing a controller of this type for an m -input m -output plant is as follows:

Design controller 1 and close its associated loop,

With controller 1 in place and its feedback loop closed, design controller 2 and close its associated loop.

With controllers 1 and 2 in place and their feedback loops closed, design controller 3 and close its associated loop.

⋮

With controllers 1..($m-1$) in place and their associated ($m-1$) loops closed, design controller m and close its associated loop.

This technique is fine in concept but the question arises as to how to ensure stability after the last loop has been closed, let alone achieve desirable performance.

The technique of Sequential Loop Closure (Mayne [47]) uses the above concept and attempts to resolve the question of how one stabilises the plant by requiring that the plant is stable after each loop closure. However, this technique has several shortcomings. First, the structure of the system can heavily influence the order in which the loops are closed. For example, if a transfer function element has nearly cancelling

RHPPs and RHPZs then this element would not be chosen as the first element to be stabilised, as this would be an extremely tiresome task. Second, the situation may arise where none of the diagonal elements can be stabilised by a natural¹ controller, hence forcing the designer to attempt to cancel RHPPs and/or RHPZs, which is inadmissible as exact cancellation of system poles and zeros by controller zeros and poles results in internal instability. Third, Sequential Loop Closure gives no information regarding which order the loops should be closed.

Sequential Loop Closure is regarded as being an unacceptable technique for a large class of systems and more elaborate neo-classical techniques such as Nyquist Array methods (Maciejowski [43]), Characteristic Loci (MacFarlane and Kouvaritikas [42]) and Quantitative Feedback Theory (Horowitz [24]) were developed to address some of the problems which Sequential Loop Closure highlighted.

However, these techniques although more successful than Sequential Loop Closure, lost track of the original straightforward sequential loop closure philosophy which should in principle be an effective design technique. In order for this design process to be effective, the structural issues of the plant are required to be resolved. i.e. the influence of RHPPs and RHPZs at each stage of loop closure need to be elucidated.

ICAD is the first technique to be successful in this respect and enables sequential design procedures which lead to designs which achieve the best performance attainable with diagonal, natural control. In addition, because the technique involves frequency domain loop-shaping, the controllers are not dependent on the order of the system and in the hands of a competent designer familiar with SISO loop shaping, results in control laws which are low order and highly effective.

¹ A natural controller is a controller which is stable and minimum phase.

6.3. Prerequisites for Developing a Design Procedure to Guarantee Closed-Loop Stability

In order to assess the potential for successfully designing a stabilising diagonal control law, an analytical expression is required;

This analytical expression should,

- i) be independent of the controllers.*
- ii) be compatible with the nested nature of the proposed design procedure.*
- iii) highlight key structural aspects of the system which the effects of the controllers can be related to.*

To determine the required form of the analytical expression consider a SISO system. The poles of a closed-loop SISO system are the zeros of $(1+kg)$, where k is the controller and g is the plant. If g has no RHPZs then in order to stabilise the closed-loop system kg would be designed such that $(1+kg)$ has the same number of RHPZs as g . If g has one RHPZ then in order to stabilise the closed-loop system kg would be designed such that $1+kg$ has one less RHPZ than g and so on. For a general multi-input multi-output system the closed-loop poles are the zeros of $|I + GK|$ and the transmission zeros of G are the zeros of $|G|$. If G has no RHP transmission zeros then in order to stabilise the closed-loop system K would be designed such that $|I + GK|$ has the same number of RHPZs as G has RHP transmission zeros. If G has one RHP transmission zero then in order to stabilise the closed-loop system K would be designed such that $|I + GK|$ has one less RHPZ than G has RHP transmission zeros and so on. If K is constrained to be diagonal the question arises as to how the necessary information can be extracted from G to allow each element of K to be designed sequentially, such that the zeros of $|I + GK|$ will have the correct relationship to the transmission zeros of G to guarantee closed-loop stability.

It is most appropriate to consider $|I + GK|$ first and create an expression which extracts each individual controller element such that the effect that each controller element has on the closed-loop system becomes transparent.

An appropriate expression is created as follows,

$$|I + GK| = (1 + k_1 g_{11})|\hat{G}_1| + |\hat{G}^1| = \left(1 + k_1 g_{11} + \frac{|\hat{G}^1|}{|\hat{G}_1|}\right)|\hat{G}_1| \quad (6.1)$$

$$\left(1 + k_1 g_{11} + \frac{|\hat{G}^1|}{|\hat{G}_1|}\right)|\hat{G}_1| = \left(1 + k_1 g_{11} \left(1 + \frac{|\hat{G}^1|}{k_1 g_{11} |\hat{G}_1|}\right)\right)|\hat{G}_1| = [1 + k_1 g_{11} (1 - \gamma_1)]|\hat{G}_1| \quad (6.2)$$

Define,

$$\hat{G} = I + GK \quad (6.3)$$

Complete expansion of $|\hat{G}|$ yields,

$$|\hat{G}| = [1 + k_1 g_{11} (1 - \gamma_1)] [1 + k_2 g_{22} (1 - \gamma_{12})] \dots \dots \dots [1 + k_{(m-1)} g_{(m-1)(m-1)} (1 - \gamma_{1..(m-1)})] [1 + k_m g_{mm}] \quad (6.4)$$

It is seen from Eqn (6.4) that the individual controllers have been extracted to some degree and it will be seen that Eqn (6.4) will allow the use of a sequential design technique.

Define,

$$C'_i = k_i g_{ii} (1 - \gamma_{1..i}) \quad (6.5)$$

C'_i is known as nested Channel i . $\gamma_{1..i}$ is defined as,

$$\gamma_{1..i} = \frac{-|\bar{G}_i^{1..(i-1)}|}{g_{ii} |\bar{G}^{1..i}|} \quad (6.6)$$

where $\bar{G} = K^{-1} + G$, $\bar{G}^{1..i}$ is \bar{G} with rows and columns (1..i) removed and $\bar{G}_i^{1..(i-1)}$ is \bar{G} with rows and columns (1..(i-1)) removed and element (i,i) set to zero. Note that by definition $\gamma_{1..m}$ is equal to zero.

Eqn (6.6) can be re-written as,

$$|\hat{G}| = [1 + C'_1][1 + C'_2] \dots [1 + C'_{(m-1)}][1 + C'_m] \quad (6.7)$$

It is now required to develop an expression for $|G|$ which is compatible with Eqn (6.7).

The appropriate expression is formed as follows,

$$|G| = g_{11}|G^1| + |G_1| = \left(1 + \frac{|G_1|}{g_{11}|G^1|}\right)g_{11}|G^1| = (1 - \Gamma_1)g_{11}|G^1| \quad (6.8)$$

$|G^1|$ can be expanded as follows,

$$|G^1| = g_{22}|G^{12}| + |G_2^1| = \left(1 + \frac{|G_2^1|}{g_{22}|G^{12}|}\right)g_{22}|G^{12}| = (1 - \Gamma_2)g_{22}|G^{12}| \quad (6.9)$$

The expansion continues until $|G|$ is expressed as,

$$|G| = (1 - \Gamma_1)g_{11}(1 - \Gamma_2)g_{22} \dots (1 - \Gamma_{(m-1)})g_{(m-1)(m-1)}g_{mm} \quad (6.10)$$

where,

$$\Gamma_i = -|G_i^{1..(i-1)}|/g_{ii}|G^{1..i}|, \quad i = 1..m \quad (6.11)$$

$G_i^{1..(i-1)}$ is G with element (i,i) set to zero and rows and columns (1..(i-1)) removed.

$G^{1..i}$ is G with rows and columns (1..i) removed. Note that by definition Γ_m is equal to zero.

The way in which Eqns (6.10) and (6.7) are used to design K , such that the closed-loop system is stable, is explained in the next Section.

6.4. Design using Nested Channels

To attempt to describe the way in which one would design a controller for an m -input m -output system, in general, would be a counter-productive exercise due to all possible permutations and combinations. The most expressive manner to describe a design technique is by example. As two of the ICAD designs in this thesis involve the design of a 4-input 4-output system, the way in which one would design for a 4-input 4-output system which has minimum phase transmission zeros is explained here in concept. A worked example of the design of a control law for a minimum phase 4-input 4-output helicopter is given in Chapter 7. It will be seen in this Chapter that the technique can be extended in a straightforward manner to a system with any number of inputs and outputs.

Eqns (6.10) and (6.7) are specialised for use on a 4-input 4-output system and are given as,

$$|G| = (1 - \Gamma_1)g_{11}(1 - \Gamma_2)g_{22}(1 - \Gamma_3)g_{33}g_{44} \quad (6.12)$$

$$|\hat{G}| = [1 + k_1g_{11}(1 - \gamma_1)][1 + k_2g_{22}(1 - \gamma_{12})][1 + k_3g_{33}(1 - \gamma_{123})][1 + k_4g_{44}] \quad (6.13)$$

Eqn (6.13) can alternatively be written as,

$$|\hat{G}| = [1 + C'_1][1 + C'_2][1 + C'_3][1 + C'_4] \quad (6.14)$$

A convenient form of notation is required to express the zeros and poles of a system,

$\overline{|x|}$ is interpreted as being '*the zeros of x* '. Notice that the vertical bars have 'tails' on the top, which implies the numerator of x .

$\underline{|x|}$ is interpreted as being '*the poles of x* '. Notice that the vertical bars have 'tails' on the bottom, which implies the denominator of x .

$\langle \overline{|x|} \rangle$ is interpreted as being '*the zeros of x which are not equal to the eigenvalues of the system A matrix*'.

where x is some SISO transfer function or a determinant of a transfer function matrix.

Recall from Chapter 5 that the zeros of $(1-\gamma_a)$, where γ_a is any MSF derived from a state space model, will contain the eigenvalues of the system A matrix. This Chapter exclusively deals with the design of controllers for multivariable systems whose individual elements have a common denominator. Systems described by state space models obviously fall into this category. This is by no means an impediment to the application of the following techniques as a large number of systems, particularly aircraft (both fixed-wing and rotary-wing), are described by state space models.

The relationship between the poles of the approximate nested MSFs and the actual nested MSFs is given in Table 6.1. The relationship between the poles and zeros of the nested Channels is given in Table 6.2. Tables 6.1 and 6.2 will be required to be referred to in the proceeding discussions.

Table 6.1. Relationship of nested MSFs.

| | |
|---|---|
| $[\Gamma_1] = [g_{11}] \cup \langle [1 - \Gamma_2] \rangle$ | $[\gamma_1] = [g_{11}] \cup [1 + C'_2]$ |
| $[\Gamma_2] = [g_{22}] \cup \langle [1 - \Gamma_3] \rangle$ | $[\gamma_{12}] = [g_{22}] \cup [1 + C'_3]$ |
| $[\Gamma_3] = [g_{33}] \cup [g_{44}]$ | $[\gamma_{123}] = [g_{33}] \cup [1 + k_4 g_{44}]$ |

Table 6.2. Relationship of nested Channels.

| | | |
|--------------------------|--|--|
| $[\hat{G}] = [1 + C'_1]$ | $[C'_1] = [k_1] \cup \langle [1 - \gamma_1] \rangle$ | |
| | $[C'_2] = [k_2] \cup \langle [1 - \gamma_{12}] \rangle$ | |
| | $[C'_3] = [k_3] \cup \langle [1 - \gamma_{123}] \rangle$ | |

To let the reader visualise where the relationships in Table 6.1 and 6.2 are coming from, consider Γ_1 and C_1 as examples.

Γ_1 is given as,

$$\Gamma_1 = \frac{-|G_1|}{g_{11}|G^1|} \quad (6.15)$$

It was shown in Chapter 5 that if the transfer function elements have a common denominator then these denominators cancel in the expression for Γ_1 . The roots of the denominator of Γ_1 thus consists of the zeros of g_{11} and the transmission zeros of G^1 . $|G^1|$ can be expressed as,

$$|G^1| = (1 - \Gamma_2)g_{22}|G^{12}| = \left(\frac{\phi|\tilde{N}^1|}{N_{22}|\tilde{N}^{12}|} \right) \frac{N_{22}|\tilde{N}^{12}|}{\phi^2} = \frac{|\tilde{N}^1|}{\phi} \quad (6.16)$$

The reader is referred to Chapter 5 for descriptions of the notations. From Eqn (6.16) it is seen that the transmission zeros of G^1 are those zeros of $(1 - \Gamma_2)$ which are not roots of the common denominator of the plant. Hence the poles of Γ_1 are the zeros of g_{11} and those zeros of $(1 - \Gamma_2)$ which are not equal to the roots of the common denominator of the plant.

It was shown in Chapter 5 that the zeros of C_1 are those zeros of $(1 - \gamma_1)$ which are not roots of the common denominator of the plant and the zeros of controller k_1 . Considering the poles of C_1 , recall from Chapter 5 that C_1 can be written as,

$$C_1 = k_1 g_{11} \left(1 + \frac{|\check{G}_1|}{g_{11}|\check{G}^1|} \right) = \frac{k_1 (g_{11}|\check{G}^1| + |\check{G}_1|)}{|\check{G}^1|} \quad (6.17)$$

It is seen from Eqn (6.17) that the poles of C_1 are the poles of controller k_1 and the zeros of $|\check{G}^1|$. The zeros of $|\check{G}^1|$ are equal to the zeros of $|\hat{G}^1|$. $|\hat{G}^1|$ can be expanded as in Eqn (6.1),

$$|\hat{G}^1| = [1 + C'_2] \hat{G}^{12} = \left(\frac{|\hat{N}^1|}{d_{k_2} |\hat{N}^{12}|} \right) \frac{|\hat{N}^{12}|}{\phi d_{k_3} d_{k_4}} = \frac{|\hat{N}^1|}{\phi d_{k_2} d_{k_3} d_{k_4}} \quad (6.18)$$

It is seen that the poles of C_1 are the poles of controller k_1 and the zeros of $[1 + C'_2]$.

There are some key points to note from Table 6.1.

The structure of $[\gamma_1]$ can only be different to the structure of $[\Gamma_1]$ if the structure of $[1 + C'_2]$ is different to the structure of $\langle [1 + \Gamma_2] \rangle$.

The structure of $[\gamma_{12}]$ can only be different to the structure of $[\Gamma_2]$ if the structure of $[1 + C'_3]$ is different to the structure of $\langle [1 + \Gamma_3] \rangle$.

The structure of $[\gamma_{123}]$ can only be different to the structure of $[\Gamma_3]$ if the structure of $[1 + k_4 g_{44}]$ is different to the structure of $[g_{44}]$.

As the controllers are constrained to be stable and minimum phase, the zero structure of the C'_i s, $i = 1..4$, can only be affected by the structure of the $\langle [1 - \gamma_{1..i}] \rangle$ s and the pole structure of the C'_i s can only be affected by the structure of the $[1 + C'_j]$ s, $j = 2..4$.

Recall that the structure refers to the number of unstable roots.

6.5. Conditions Sufficient for Closed-Loop Stability of a Minimum Phase Plant

This Section investigates sufficient conditions compatible with the proposed nested design procedure which will guarantee closed-loop stability for systems with certain characteristics. This Section is based on the existence theorems of Leithead and O'Reilly [34] and for a fuller mathematical treaty of this topic the reader should refer to [34].

6.5.1. MSF High Frequency Limits less than One

The plant under consideration is a minimum phase plant, in which all the Channel MSFs have a high frequency limit of magnitude less than one. The reason for the high frequency constraint will become evident. This class of system is considered in detail as it forms the foundation for consideration of other classes of system.

Conditions sufficient for this plant to be stable will now be explained. Referral to Tables 6.1 and 6.2 should be made when clarification of certain statements are required. It should be noted that although the proceeding discussion is somewhat repetitive, it is absolutely essential in order that the reader unfamiliar with ICAD understands the structural issues involved when designing a control law.

As the plant is minimum phase and because $[G] = \langle [1 - \Gamma_1] \rangle$, then $\langle [1 - \Gamma_1] \rangle$ are stable. If it can be arranged such that $\langle [1 - \gamma_1] \rangle$ are also stable then C'_1 will be minimum phase. Controller k_1 can then be designed in a straightforward manner to ensure that $(1+C'_1)$ has the same number of RHPZs as C'_1 has RHPZs. Because the poles of the closed loop system are the zeros of $(1+C'_1)$ the plant will be stable.

For $\langle [1 - \gamma_1] \rangle$ to be stable it is sufficient that the number of RHPPs of γ_1 is the same as the number of RHPPs of Γ_1 and that the encirclement count of the (1,0) point of γ_1 and Γ_1 is the same. The encirclement count of γ_1 and Γ_1 can only *potentially* be the same if the high frequency limit of Γ_1 is less than one. This is because control action will cause the high frequency limit of γ_1 to be zero.

In order that the number of RHPPs of γ_1 is the same as the number of RHPPs of Γ_1 it is required that the number of RHPZs of $(1+C'_2)$ is the same as the number of RHPZs of $\langle [1 - \Gamma_2] \rangle$.

For the number of RHPZs of $(1+C'_2)$ to be the same as the number of RHPZs of $\langle [1 - \Gamma_2] \rangle$ it is sufficient that the number of RHPZs of $\langle [1 - \gamma_{12}] \rangle$ is the same as the

number of RHPZs of $\langle [1 - \Gamma_2] \rangle$ and that controller k_2 is designed such that the number of RHPZs of $(1 + C'_2)$ is the same as the number of RHPZs of C'_2 .

For the number of RHPZs of $\langle [1 - \gamma_{12}] \rangle$ to be the same as the number of RHPZs of $\langle [1 - \Gamma_2] \rangle$ it is sufficient that the number of RHPPs of γ_{12} is the same as the number of RHPPs of Γ_2 and that the encirclement count of the (1,0) point of γ_2 and Γ_2 is the same.

In order that the number of RHPPs of γ_2 is the same as the number of RHPPs of Γ_2 it is required that the number of RHPZs of $(1 + C'_3)$ is the same as the number of RHPZs of $\langle [1 - \Gamma_3] \rangle$.

For the number of RHPZs of $(1 + C'_3)$ to be the same as the number of RHPZs of $\langle [1 - \Gamma_3] \rangle$ it is sufficient that the number of RHPZs of $\langle [1 - \gamma_{123}] \rangle$ is the same as the number of RHPZs of $\langle [1 - \Gamma_3] \rangle$ and that controller k_3 is designed such that the number of RHPZs of $(1 + C'_3)$ is the same as the number of RHPZs of C'_3 .

For the number of RHPZs of $\langle [1 - \gamma_{123}] \rangle$ to be the same as the number of RHPZs of $\langle [1 - \Gamma_3] \rangle$ it is sufficient that the number of RHPPs of γ_{123} is the same as the number of RHPPs of Γ_3 and that the encirclement count of the (1,0) point of γ_{123} and Γ_3 is the same.

In order that the number of RHPPs of γ_{123} is the same as the number of RHPPs of Γ_3 it is required that the number of RHPZs of $(1 + k_4 g_{44})$ is the same as the number of RHPZs of g_{44} .

The above discussion is summarised generally in Condition 6.1.

Condition 6.1.

In order to stabilise a minimum phase plant whose MSFs have a high frequency limit of less than one, it is sufficient that the $\gamma_{1..j}$ s have the same pole structure and encirclement count as the Γ_j s and that the number of RHPZs of the $(1 + C'_i)$ s are the same as the number of RHPZs of the C'_i s.

Notice that because the sufficient conditions are general, they are valid irrespective of the ordering of the input-output pairs of the system. Also, it is hoped that by describing the technique on a 4-input 4-output system that the reader can visualise how one would extend the technique to a system with m-inputs and m-outputs.

6.5.1.1. Designing to Meet the Sufficient Conditions

Now that sufficient conditions have been established to ensure the stability of the closed-loop system., the question arises as to how one achieves these conditions. One method is as follows:

6.5.1.1.1. Design of Controller k_4

The design proceeds by designing controller k_4 first followed by the other controllers in reverse order. k_4 is to be designed such that the number of RHPZs of $(1+k_4g_{44})$ is the same as the number of RHPZs of g_{44} , thus ensuring that the pole structure of γ_{123} is the same as the pole structure of Γ_3 . This is a relatively straightforward procedure and, in addition, the designer should ensure that the loop gain below the chosen crossover frequency is as high as is practically possible, i.e. the controller gain should be made high at frequencies below crossover. The reason for this is explained below.

The equations for Γ_3 and γ_{123} are written explicitly as,

$$\Gamma_3 = \frac{g_{34}g_{43}}{g_{33}g_{44}} \quad (6.19)$$

$$\gamma_{123} = \frac{g_{34}g_{43}}{g_{33}(k_4^{-1} + g_{44})} \quad (6.20)$$

If the gain of controller k_4 is made high at low to mid frequencies then γ_{123} will be approximately equal to Γ_3 in this region and so the encirclements of the (1,0) point of γ_{123} and Γ_3 will be the same in the low to mid frequency region. In order to ensure that the total number of encirclements of the (1,0) point of γ_{123} and Γ_3 is the same, it is only required to check that the behaviour of γ_{123} in the high frequency region does not induce additional encirclements of the (1,0) point relative to Γ_3 . If the high frequency behaviour is benign then the sufficient conditions concerning the structure of C'_3 will have been met by the design of controller k_4 .

6.5.1.1.2. Design of Controller k_3

k_3 is to be designed such that the number of RHPZs of $(1+C'_3)$ is the same as the number of RHPZs of C'_3 , thus ensuring that the pole structure of γ_{12} is the same as the pole structure of Γ_2 . This is a relatively straightforward procedure and, in addition, the designer should ensure that the loop gain below the chosen crossover frequency is as high as is practically possible, i.e. the controller gain should be made high at frequencies below crossover. The reason for this is explained below.

The equations for Γ_2 and γ_{12} are written explicitly as,

$$\Gamma_2 = - \frac{\begin{vmatrix} 0 & g_{23} & g_{24} \\ g_{32} & g_{33} & g_{34} \\ g_{42} & g_{43} & g_{44} \end{vmatrix}}{g_{22}} \frac{\begin{vmatrix} g_{33} & g_{34} \\ g_{43} & g_{44} \end{vmatrix}}{g_{22}} \quad (6.21)$$

$$\gamma_{12} = - \frac{\begin{vmatrix} 0 & g_{23} & g_{24} \\ g_{32} & k_3^{-1} + g_{33} & g_{34} \\ g_{42} & g_{43} & k_4^{-1} + g_{44} \end{vmatrix}}{g_{22}} \frac{\begin{vmatrix} k_3^{-1} + g_{33} & g_{34} \\ g_{43} & k_4^{-1} + g_{44} \end{vmatrix}}{g_{22}} \quad (6.22)$$

If the gain of controller k_3 is made high at low to mid frequencies then γ_{12} will be approximately equal to Γ_2 in this region (remember that k_4 has high gain at low to mid frequencies also) and so the encirclements of the (1,0) point of γ_{12} and Γ_2 will be the same in the low to mid frequency region. In order to ensure that the total number of encirclements of the (1,0) point of γ_{12} and Γ_2 is the same, it is only required to check that the behaviour of γ_{12} in the high frequency region does not induce additional encirclements of the (1,0) point relative to Γ_2 . If the high frequency behaviour is benign then the sufficient conditions concerning the structure of C'_2 will have been met by the design of controller k_3 .

6.5.1.1.3. Design of Controller k_2

k_2 is to be designed such that the number of RHPZs of $(1+C'_2)$ is the same as the number of RHPZs of C'_2 , thus ensuring that the pole structure of γ_1 is the same as the pole structure of Γ_1 . This is a relatively straightforward procedure and, in addition, the designer should ensure that the loop gain below the chosen crossover frequency is as high as is practically possible, i.e. the controller gain should be made high at frequencies below crossover. The reason for this is as follows:

The equations for Γ_1 and γ_1 are written explicitly as,

$$\Gamma_1 = - \frac{\begin{vmatrix} 0 & g_{12} & g_{13} & g_{13} \\ g_{21} & g_{22} & g_{23} & g_{24} \\ g_{31} & g_{32} & g_{33} & g_{34} \\ g_{41} & g_{42} & g_{43} & g_{44} \end{vmatrix}}{g_{11}} \begin{vmatrix} g_{22} & g_{23} & g_{24} \\ g_{32} & g_{33} & g_{34} \\ g_{42} & g_{43} & g_{44} \end{vmatrix} \quad (6.23)$$

$$\gamma_1 = \frac{\begin{vmatrix} 0 & g_{12} & g_{13} & g_{13} \\ g_{21} & k_2^{-1} + g_{22} & g_{23} & g_{24} \\ g_{31} & g_{32} & k_3^{-1} + g_{33} & g_{34} \\ g_{41} & g_{42} & g_{43} & k_4^{-1} + g_{44} \end{vmatrix}}{\begin{vmatrix} k_2^{-1} + g_{22} & g_{23} & g_{24} \\ g_{11} & g_{32} & k_3^{-1} + g_{33} & g_{34} \\ g_{42} & g_{43} & k_4^{-1} + g_{44} \end{vmatrix}} \quad (6.24)$$

If the gain of controller k_2 is made high at low to mid frequencies then γ_1 will be approximately equal to Γ_1 in this region (remember that k_3 and k_4 have high gain at low to mid frequencies also) and so the encirclements of the (1,0) point of γ_1 and Γ_1 will be the same in the low to mid frequency region. In order to ensure that the total number of encirclements of the (1,0) point of γ_1 and Γ_1 is the same, it is only required to check that the behaviour of γ_1 in the high frequency region does not induce additional encirclements of the (1,0) point relative to Γ_1 . If the high frequency behaviour is benign then the sufficient conditions concerning the structure of C'_1 will have been met by the design of controller k_2 .

6.5.1.1.4. Design of Controller k_1

Controller k_1 is then designed such that the number of RHPZs of $(1+C'_1)$ is the same as the number of RHPZs of C'_1 . The closed loop system will therefore be stable as required and, in addition, high performance control below 0dB crossover frequencies is achievable.

Of course, the controllers designed using ICAD do not have to be high performance² controllers in order to stabilise a plant. The sufficient conditions for stability could be achieved by low performance controllers for certain plants. This would be determined by further analysis of the system.

² In this context, a high performance controller is a controller which enables the open-loop Channel to have gain greater than one at all frequencies below crossover, regardless of the crossover frequency.

Notice that the above procedure does not require bandwidth separation or particular ordering of the input-output pairs. However, if the specifications require bandwidth separation then the lowest bandwidth Channel would be chosen as Channel 1 and the highest bandwidth Channel would be chosen as Channel m , for a general m -input m -output plant. The reason for this is due to the fact that loop-interaction on Channel n will be low at the crossover frequency of Channel n due to the lower crossover frequencies of Channels $1..(n-1)$. Therefore, at crossover, nested Channel n will be approximately the same as actual Channel n . This means that the design iterations will be minimised.

6.5.2. MSF High Frequency Limits greater than One

The situation may arise where one or more of the $\gamma_{1,i}$ s have a high frequency limit which is greater than one. A specific example of this would be the situation where Γ_1 induces an anti-clockwise encirclement at high frequency in order to maintain the minimum phase nature of the plant. Because controllers induce gain drop off at high frequencies it would not be possible to cause Γ_1 and γ_1 to have the same number of encirclements, hence γ_1 would have one less anti-clockwise encirclement of the (1,0) point than Γ_1 . If γ_1 is designed to have the same pole structure as Γ_1 then $(1-\gamma_1)$ would have one RHPZ. The bandwidth of Channel 1 would therefore be limited by this RHPZ. Leithead and O'Reilly [34] state that this situation results in a significant bandwidth separation being required. This bandwidth separation should be big enough to render Channel 1 robust to changes in the location of the RHPZ.

A simple 2-input 2-output example will now be shown to demonstrate the way in which one would stabilise such a plant and the performance issues which arise. The same considerations described in the example can be applied to a general m -input m -output system. Leithead and O'Reilly [34] deal with the general situation in more theoretical detail.

The plant is given below in transfer function matrix form.

$$G = \frac{1}{(s + 1)(s + 10)} \begin{bmatrix} 6(s - 2) & 1.3(s + 0.1) \\ 2(s + 10) & 3(s + 10) \end{bmatrix} \tag{6.25}$$

The determinant of G can be written as,

$$|G| = (1 - \gamma)g_{11}g_{22} \tag{6.26}$$

Table 6.3 shows the structure of the parameters of Eqn (6.26) and Figure 6.1 shows the Nyquist plot of γ .

Table 6.3. Structure of parameters of Eqn (6.26)

| | RHPZs (rad/s) | RHPPs (rad/s) |
|----------------|---------------|---------------|
| $ G $ | – | – |
| $(1 - \gamma)$ | – | 2.0 |
| g_{11} | 2.0 | – |
| g_{22} | – | – |

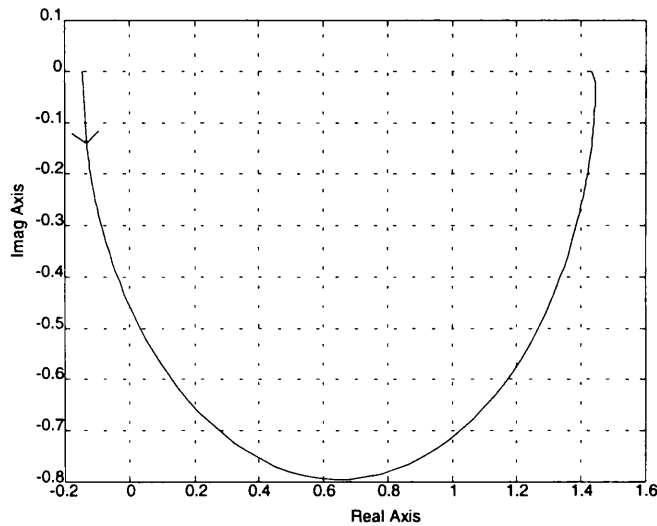


Figure 6.1. Nyquist plot of γ .

Let us say that the initial specifications of the system require that Channel 1 and Channel 2 have 0dB crossovers of 4 rad/s each and that high performance is required.

i.e. the gains of the Channels must be greater than one below their 0dB crossover frequencies.

Before proceeding with the design, the action of the controllers will be described qualitatively. If k_2 is designed such that $(1+k_2g_{22})$ has the same number of RHPZs as k_2g_{22} , then $(1+ k_2g_{22})$ will have no RHPZs and therefore γ_{h_2} will have one RHPP. However, the gain drop-off of k_2 will cause γ_{h_2} to have one less anticlockwise encirclement of the (1,0) point than γ . This means that $(1-\gamma_{h_2})$ will have one RHPZ. This RHPZ will occur in the vicinity of the crossover region of k_2g_{22} . Channel 1 will therefore have a RHPZ approximately at the 0dB crossover of k_2g_{22} and so Channel 1 will require a 0dB crossover well below this frequency to provide a degree of robustness. These issues will become clearer in the design process.

k_2 is designed such that $(1+ k_2g_{22})$ has the same number of RHPZs as k_2g_{22} . In addition the 0dB crossover of k_2g_{22} is placed at 4 rad/s to give a good 'first try' for the controller (this is discussed in more detail in Section 6.7). k_2 is given by,

$$k_2 = \frac{120(s + 1)}{s(s + 100)} \quad (6.27)$$

Table 6.4 shows the zero structure of $(1+ k_2g_{22})$ and k_2g_{22} and they are seen to be the same. Figure 6.2 shows the bode plot of k_2g_{22} and it is seen that the 0dB crossover frequency is 4 rad/s.

Table 6.4. Zero structure of k_2g_{22} and $(1+k_2g_{22})$.

| | RHPZs (rad/s) |
|-----------------|---------------|
| k_2g_{22} | – |
| $(1+k_2g_{22})$ | – |

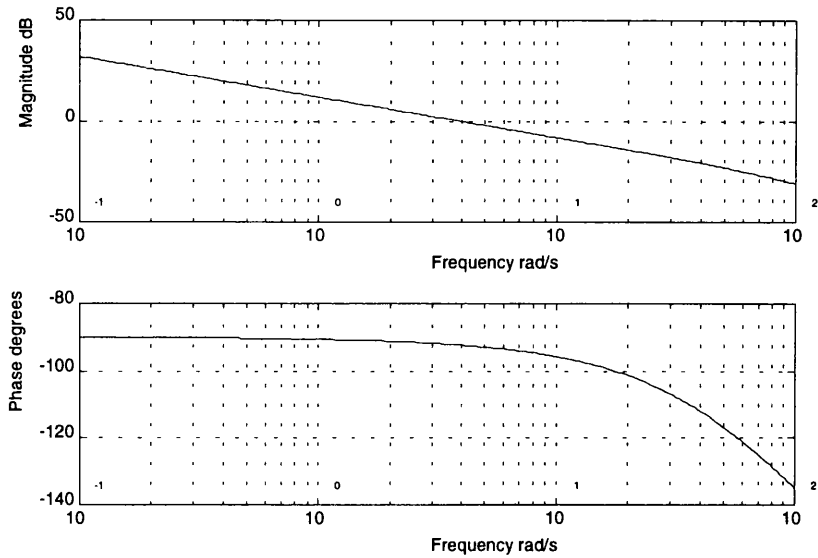
Figure 6.2. Bode plot of k_2g_{22} .

Figure 6.3 shows the Nyquist plot of γ and γ_{h_2} . Notice that γ_{h_2} has one less anti-clockwise encirclement count of the (1,0) point than γ , as expected.

Table 6.5 shows the structure of $(1-\gamma_{h_2})$ and $(1-\gamma)$ and it is seen that $(1-\gamma_{h_2})$, and hence Channel 1, has a RHPZ at approximately 3.8 rad/s.

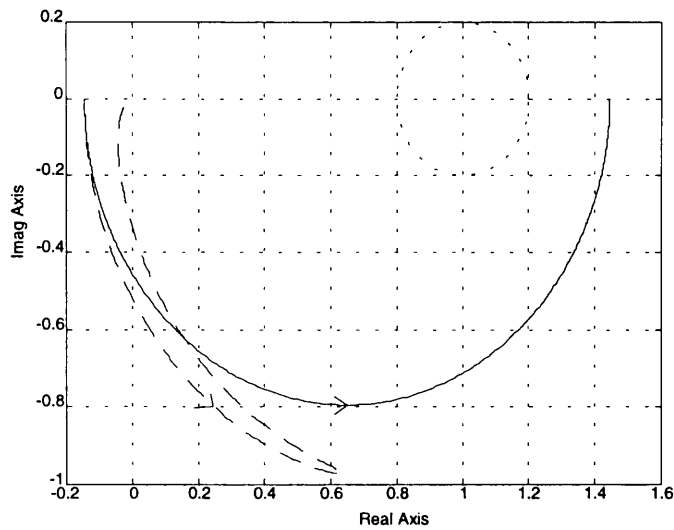
Figure 6.3. Nyquist plot of γ (solid) and γ_{h_2} (dashed).

Table 6.5. Zero structure of $(1-\gamma)$ and $(1-\gamma h_2)$.

| | RHPZs (rad/s) |
|------------------|---------------|
| $(1-\gamma)$ | – |
| $(1-\gamma h_2)$ | 3.8011 |

The 0dB crossover of Channel 1 is therefore constrained to be less than 3.8 rad/s and should be placed sufficiently far from this frequency to provide an adequate degree of robustness. The initial specifications in this situation would be required to be reviewed.

The 0dB crossover of Channel 1 was chosen to be 1 rad/s and controller k_1 is given by,

$$k_1 = \frac{-1}{s} \quad (6.28)$$

Table 6.6 shows the zero structure of $(1+C_1)$ and C_1 . It is seen that $(1+C_1)$ has no RHPZs and hence the system is nominally stable.

Table 6.6. Zero structure of C_1 and $(1+C_1)$.

| | RHPZs (rad/s) |
|---------|---------------|
| C_1 | 3.8011 |
| $1+C_1$ | – |

Figure 6.4 shows the Bode plot of Channel 2 for this design and it is seen that the 0dB crossover is 4 rad/s and is the same as $k_2 g_{22}$. This is expected as h_1 , and hence γh_1 , has gain significantly lower than 0dB at 4 rad/s. Therefore at the crossover frequency of Channel 2, $C_2 \approx k_2 g_{22}(1 - 0) = k_2 g_{22}$.

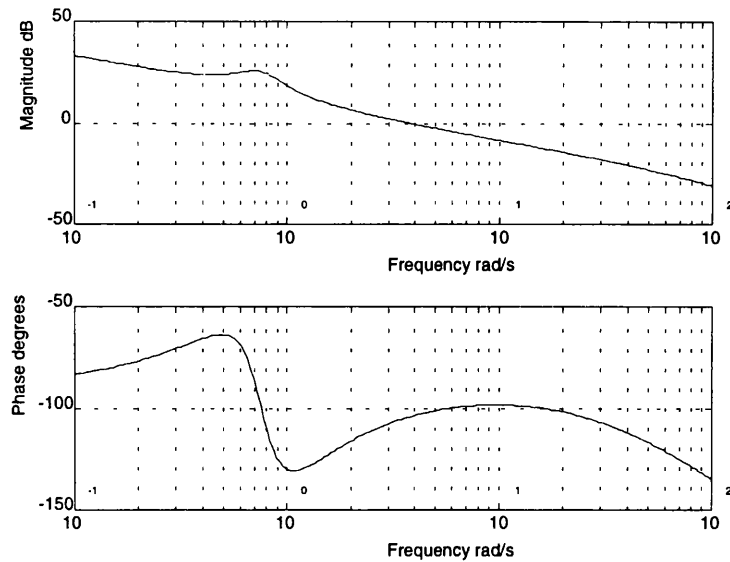


Figure 6.4. Bode plot of Channel 2.

One solution to the problem of requiring bandwidth separation would be to re-assign the input output pairings, i.e. input 1 controls output 2 and vice versa. This would ensure that the high frequency limit of γ was less than one. However, such re-assignment may not be possible in a practical situation.

What arises from consideration of such systems is a need to amend the sufficient conditions for closed loop stability described in Section 6.5. For a system where one or more MSFs have a high frequency limit greater than one the sufficient conditions for stability are stated below as Condition 6.2. Condition 6.2 is effectively a general summary of the preceding example.

Condition 6.2.

In order to stabilise a minimum phase plant where one or more of the MSFs have a high frequency limit of greater than one, it is sufficient that the number of RHPZs of the $(1+C'_i)$ s are the same as the number of RHPZs as the $(1-\Gamma_i)$ s.

Where the high frequency limit of $\gamma_{1..i}$ is less than one it is sufficient that the number of RHPPs of $\gamma_{1..i}$ is the same as the number of RHPPs of Γ_i and that the encirclement counts of the $(1,0)$ point of $\gamma_{1..i}$ and Γ_i is the same, in order to ensure that the zero structure of C'_i is the same as the required zero structure of $(1+C'_i)$. This makes the design of k_i relatively straightforward. Where the high frequency limit of $\gamma_{1..i}$ is greater than one it is sufficient that the number of RHPPs of $\gamma_{1..i}$ is the same as the number of RHPPs of Γ_i and that $\gamma_{1..i}$ has one less anti-clockwise encirclement count of the $(1,0)$ point as Γ_i . C'_i will have a RHPZ at approximately the bandwidth frequency of C'_{i+1} and so k_i should be designed such that C'_i has lower bandwidth than C'_{i+1} in order to ensure the correct zero structure of $(1+C'_i)$.

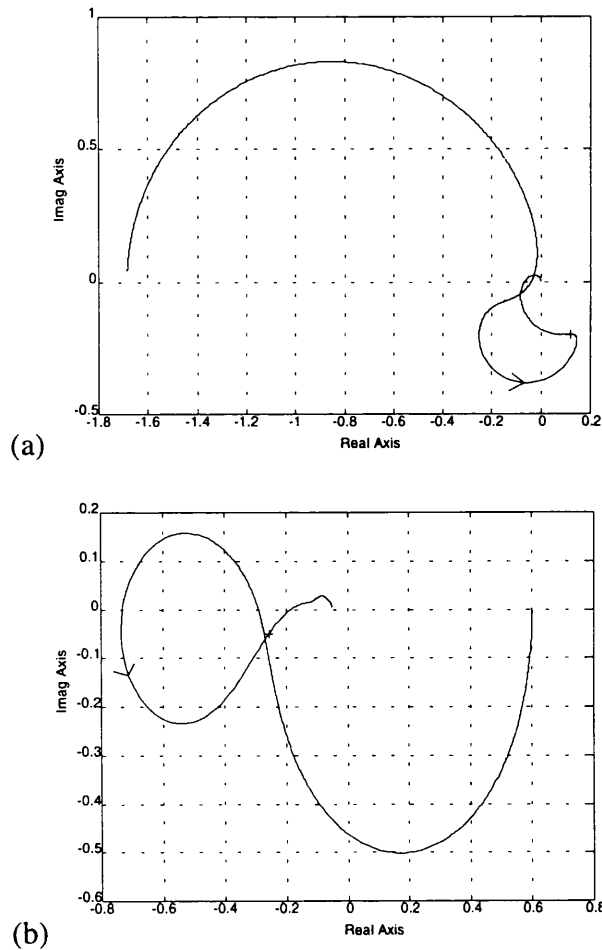
6.6. Example of Designing for Closed-Loop Stability of a Non-Minimum Phase Plant

For a plant which has RHP transmission zeros, the control engineer would use Eqn (6.7) to determine the ‘source’ of the RHP transmission zeros and would assess the control action necessary to design a stable closed-loop system.

This Section gives an example of the procedure one can adopt to determine the way in which a plant with a RHP transmission zero which is at a ‘frequency of interest’ can be stabilised. i.e. a frequency which is of dynamical importance.

The example is a perturbed version of an 8th order helicopter at 30 knots forward flight where the control and stability derivatives have been varied such that a RHP transmission zero has appeared at approximately 0.06 rad/s. The state space model of this system is given in Appendix V.

Figure 6.5 shows the nested approximate MSFs and Table 6.7 shows the structure of the parameters of Eqn (6.14) for this example.



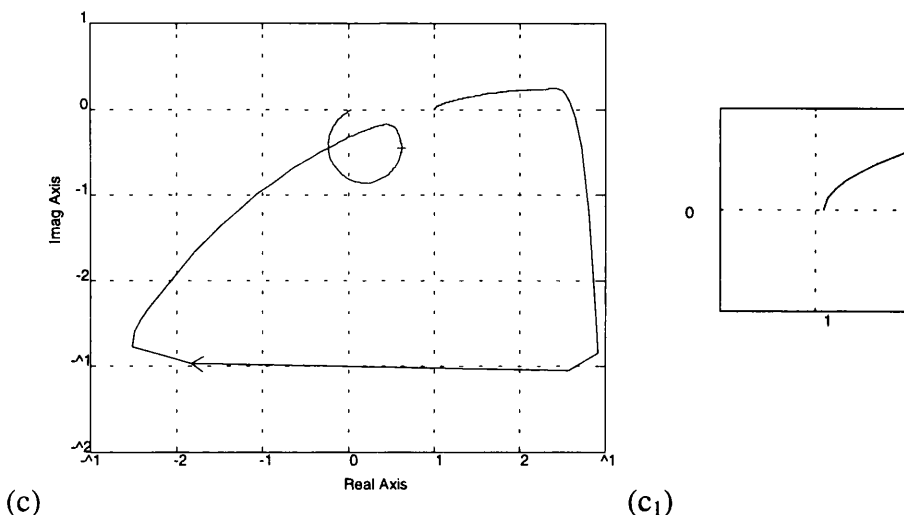


Figure 6.5. Nyquist plot of (a) Γ_1 , (b) Γ_2 ,

(c) Γ_3 , (c₁) Expansion of (1,0) region of (c)

(scaling is not shown on the expansion as its only purpose is to show which side of the (1,0) point the low frequency limit is on)

Table 6.7. Structure of parameters of Eqn (6.14).

| | RHPZs (rad/s) | RHPPs (rad/s) |
|------------------|---|--|
| $ G $ | 6.1636e-2 | 1.7242e-1 ± 6.5498e-1j |
| $(1 - \Gamma_1)$ | 1.7242e-1 ± 6.5498e-1j → 6.1636e-2 | 1.4961e-1 ± 6.0721e-1j → 6.2600e-2 |
| $(1 - \Gamma_2)$ | 1.7242e-1 ± 6.5498e-1j 6.2600e-2 ← | 1.2597e-1 ± 6.4857e-1j → 6.5317e-2 |
| $(1 - \Gamma_3)$ | 1.7242e-1 ± 6.5498e-1j 1.2597e-1 ± 6.4857e-1j 6.5317e-2 ← | 1.6052e-1 ± 6.6535e-1j 1.3505e-1 ± 6.4113e-1j |
| g_{11} | 1.4961e-1 ± 6.0721e-1j | 1.7242e-1 ± 6.5498e-1j |
| g_{22} | - | 1.7242e-1 ± 6.5498e-1j |
| g_{33} | 1.6052e-1 ± 6.6535e-1j | 1.7242e-1 ± 6.5498e-1j |
| g_{44} | 1.3505e-1 ± 6.4113e-1j | 1.7242e-1 ± 6.5498e-1j |

Table 6.7 shows the origin of the RHP transmission zero being traced. It is seen that it originates in the zeros of $(1-\Gamma_3)$. The question now is how can the plant be stabilised and what trade-offs must be made?

Inspecting Table 6.7 and Figure 6.5 it is seen that the RHPZ of $(1-\Gamma_3)$ at $6.3517\text{e-}2$ rad/s is caused by a clockwise encirclement of the $(1,0)$ point of Γ_3 . If it can be arranged such that γ_{123} has the same pole structure as Γ_3 , but one less clockwise encirclement count of the $(1,0)$ point, then this RHPZ will disappear from the actual system, which is very desirable as the system will in effect become minimum phase, hence enabling the use of the design procedure of Section 6.5.1.1 for controllers $k_3..k_1$. To make γ_{123} have the same pole structure as Γ_3 it is required that $(1+k_4g_{44})$ has the same number of RHPZs as g_{44} . In order that γ_{123} has one less encirclement count of the $(1,0)$ point it is required that the gain of k_4 is made less than one at low frequency such that γ_{123} will move to the other side of the $(1,0)$ point as required. This observation comes from,

$$\gamma_{123} = \frac{g_{34}g_{43}}{g_{33}(k_4^{-1} + g_{44})} \quad (6.29)$$

It is seen from Eqn (6.29) that if k_4 is made sufficiently less than one at some frequency then this will decrease γ_{123} relative to Γ_3 , which is required.

From the above considerations, sufficient conditions to stabilise the closed-loop system are as follows:

k_4 should be designed such that the number of RHPZs of $1+k_4g_{44}$ is the same as the number of RHPZs of g_{44} and such that γ_{123} will not encircle the $(1,0)$ point. This ensures that $(1-\gamma_{123})$, and hence, C'_3 has one less RHPZ than $(1-\Gamma_3)$.

$k_1..k_3$ should be designed such that the number of RHPZs of the $(1+C'_j)s$, $j = 1..3$, are the same as the number of RHPZs of the C'_j s and the $\gamma_{1..f}$ s, $f = 1,2$, have the same number of encirclement counts of the $(1,0)$ point as the Γ_f s.

A design which meets the sufficient requirements is now presented.

k_4 is designed to be,

$$k_4 = \frac{-5s}{(s + 0.1)(s + 40)} \quad (6.30)$$

Notice that k_4 has a zero at the origin, thus fixing the structural problem. The cost of doing this is that Channel 4 will not have high performance.

Table 6.8 shows the zero structure of g_{44} and $(1+k_4g_{44})$. It is seen that the structures are the same as required. Figure 6.6 shows the Nyquist plot of γ_{123} . It is seen that γ_{123} does not encircle the (1,0) point and hence $(1-\gamma_{123})$ has one less RHPZ than $(1-\Gamma_3)$.

Table 6.8. Zero structure of g_{44} and $(1+k_4g_{44})$.

| | RHPZs (rad/s) |
|-----------------|----------------------------|
| g_{44} | $1.3505e-1 \pm 6.4113e-1j$ |
| $(1+k_4g_{44})$ | $1.4135e-1 \pm 6.3961e-1j$ |

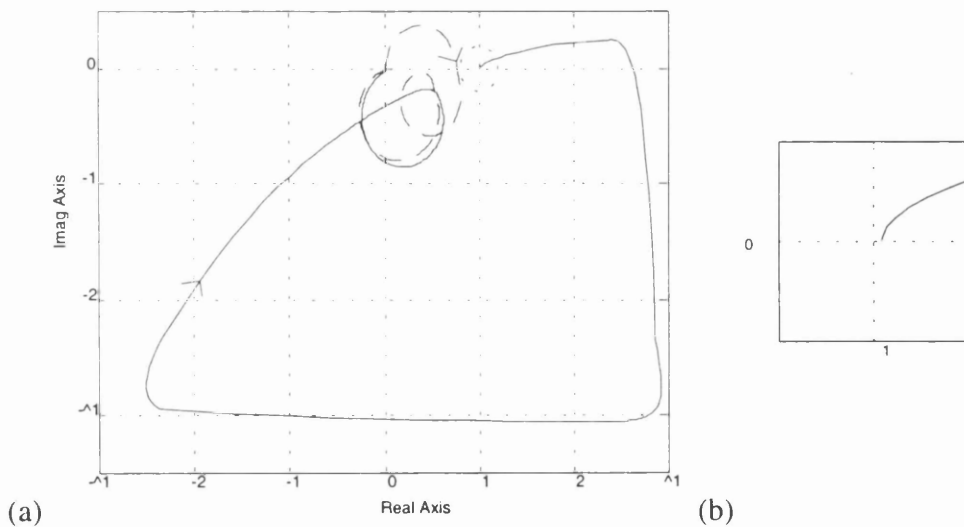


Figure 6.6. (a) Nyquist plot of Γ_3 (solid) and γ_{123} (dashed)
(b) Expansion of (1,0) region.

k_3 is designed to be,

$$k_3 = \frac{-2(s+1)}{s(s+40)} \quad (6.31)$$

Table 6.9 shows the zero structure of C'_3 and $(1+C'_3)$. It is seen that the structures are the same as required. Figure 6.7 shows the Nyquist plots of γ_{12} and Γ_2 and it is seen that their encirclement counts of the (1,0) point are the same as required.

Table 6.9. Zero structure of C'_3 and $(1+C'_3)$.

| | RHPZs (rad/s) |
|------------|----------------------------|
| C'_3 | $1.3582e-1 \pm 6.4373e-1j$ |
| $(1+C'_3)$ | $1.3590e-1 \pm 6.4502e-1j$ |

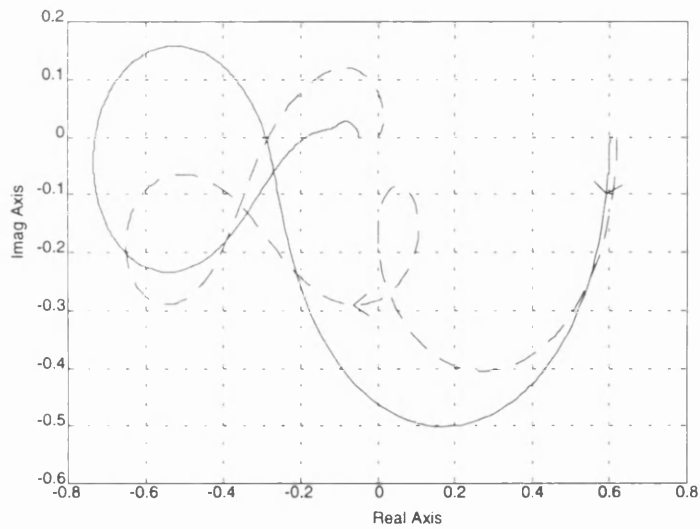


Figure 6.7. Nyquist plot of Γ_2 (solid) and γ_{12} (dashed).

k_2 is designed to be,

$$k_2 = \frac{5(s+1)^2(s+2)^2}{s(s+0.001)(s+6)^2(s+40)} \quad (6.32)$$

Table 6.10 shows the structure of C'_2 and $(1+C'_2)$. It is seen that the structures are the same as required. Figure 6.8 shows the Nyquist plots of γ_1 and Γ_1 and it is seen that their encirclement counts of the $(1,0)$ point are the same as required.

Table 6.10. Zero structure of C'_2 and $(1+C'_2)$.

| | RHPZs (rad/s) |
|------------|---------------|
| C'_2 | – |
| $(1+C'_2)$ | – |

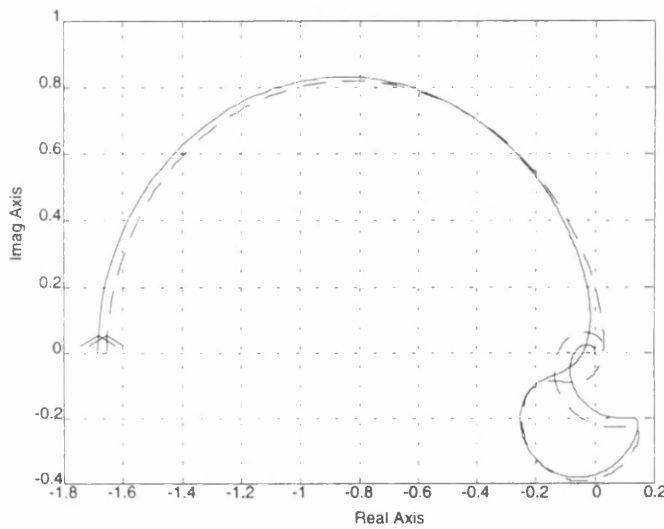


Figure 6.8. Nyquist plot of Γ_1 (solid) and γ_1 (dashed).

Finally, k_1 is designed to be,

$$k_1 = \frac{0.4(s+1)}{s(s+10)} \quad (6.33)$$

Table 6.11 shows the structure of C'_1 and $(1+C'_1)$. It is seen that they are the same as required and that $(1+C'_1)$ has no RHPZs. The closed-loop system is therefore stable.

Table 6.11. Zero structure of C'_1 and $(1+C'_1)$.

| | RHPZs (rad/s) |
|------------|---------------|
| C'_1 | – |
| $(1+C'_1)$ | – |

Because only k_4 was required to have low gain at low frequency, only Channel 4 exhibits low performance. The other 3 Channels all have high performance controllers.

6.7. Performance Considerations when Designing using Nested Channels

From an engineering viewpoint, one would guess that it makes sense to place the 0dB crossover frequencies of the nested Channels at the desired 0dB crossover frequencies of the Channels. For the first iteration of design this would give a good first try for the controllers, and the controllers could be fine tuned, if desired, once all the controllers are in place.

In order to give this engineering viewpoint more of an analytical basis, a technique from Leithead and O'Reilly [39] for a 2-input 2-output system is extended for use on a 4-input 4-output system.

Leithead and O'Reilly [39] note a very interesting relationship between the sensitivity of the closed-loop Channels and the sensitivity of the closed-loop subsystems. This relationship is given below,

$$\frac{1 - T_1}{1 - h_1} = \frac{1 - T_2}{1 - h_2} \quad (6.34)$$

T_1 and T_2 are the closed-loop Channels 1 and 2 respectively and h_1 and h_2 are the closed-loop subsystems k_1g_{11} and k_2g_{22} respectively.

What Eqn (6.34) tells us is that the ratio of the sensitivities of the closed-loop Channels with their respective closed-loop subsystems is the same. This leads to a 2-input

2-output version of the nested Channel design technique which can cater for performance requirements. The design approach may proceed as follows:

k_2 is designed such that h_2 has approximately the performance requirements desired of Channel 2.

k_1 is then designed such that the performance requirement of T_1 is met.

The ratio of $(1-T_1)/(1-h_1)$ is checked and if the ratio is benign, the performance requirements of T_2 will be very near to that which is desired. The ratio will be 'benign' if it is close to 0dB. How close is subjective and the designer must use his/her judgement to decide. However, as a rule of thumb one can regard a deviation of ± 5 dB from 0dB as being non-benign in the crossover region of the actual Channels. At other frequencies larger margins are allowable without noticeable degradation in performance. If the ratio is regarded as non-benign, the information given by the ratio equality of Eqn (6.34) can be used to refine the design.

This method works particularly well when the magnitude of loop interaction is relatively low on one, or both, of the Channels at the desired Channel crossover frequencies. The case where the loop interaction is low on one of the Channels would be the situation where there was bandwidth separation of the two Channels with, for example, Channel 2 being higher bandwidth than Channel 1. At the crossover frequency of Channel 2 the loop interaction would be small due to the gain drop-off of h_1 .

When the magnitude of the loop interaction at the desired crossover frequencies is not low one can either algebraically calculate the required gain and phase of the controllers to achieve the desired Channel crossover frequencies or alternatively one can use the above method as it stands and refine the controllers in further iterations of the design process. The algebraic technique is given in Leithead and O'Reilly [39].

The above method can be extended to general MIMO systems. The technique will be extended for use on a 4-input 4-output system in this Section and this should give the reader sufficient insight into how it can be extended generally. In the proceeding discussion the superscript relates to which feedback loops are closed. The subscript

relates to the Channel and the T indicates that the Channel is closed. No superscript on the T indicates that *all* loops are closed.

Controller k_4 is designed such that h_4 is close to the performance requirements of T_4 . Controller k_3 is then designed such that T_3^{34} is close to the requirements of T_3 . The following ratio equality can then be checked,

$$\frac{1 - T_3^{34}}{1 - h_3} = \frac{1 - T_4^{34}}{1 - h_4} \quad (6.35)$$

If the ratio $(1 - T_3^{34})/(1 - h_3)$ is benign then T_4^{34} will be close to the performance requirements of T_4 . If $(1 - T_3^{34})/(1 - h_3)$ is not benign then refinements can be made before controller k_2 is designed. Controller k_2 is then designed such that T_2^{234} is close to the requirements of T_2 .

The following two ratio equalities can then be checked,

$$\frac{1 - T_2^{234}}{1 - T_2^{24}} = \frac{1 - T_3^{234}}{1 - T_3^{34}} \quad (6.36)$$

$$\frac{1 - T_2^{234}}{1 - T_2^{23}} = \frac{1 - T_4^{234}}{1 - T_4^{34}} \quad (6.37)$$

If $(1 - T_2^{234})/(1 - T_2^{24})$ is benign then T_3^{234} will be close to the requirements of T_3 . In addition, If $(1 - T_2^{234})/(1 - T_2^{23})$ is benign then T_4^{234} will be close to the requirements of T_4 . If either of the ratios is not benign then refinements can be made before controller k_1 is designed.

Finally, controller k_1 is designed such that the performance requirements of T_1 are met.

The following three ratio equalities can then be checked,

$$\frac{1 - T_1}{1 - T_1^{134}} = \frac{1 - T_2}{1 - T_2^{234}} \quad (6.38)$$

$$\frac{1 - T_1}{1 - T_1^{124}} = \frac{1 - T_3}{1 - T_3^{234}} \quad (6.39)$$

$$\frac{1 - T_1}{1 - T_1^{123}} = \frac{1 - T_4}{1 - T_4^{234}} \quad (6.40)$$

If the three ratios are benign then the performance requirements of all four Channels will have been closely met and the design will require only minor amendment. If one or more of the ratios are not benign then refinements to the design can be made. The above technique essentially justifies the sufficiency of placing the 0dB crossovers of the nested Channels at the desired 0dB crossover frequencies of the actual Channels, particularly if the magnitude of loop-interaction is relatively low. If loop-interaction is not low, the information given by the ratio equalities can be used to refine the design. Note that the above technique only explicitly caters for on-axis performance. If off-axis performance, or cross-coupling, is found to be deficient after the feedback design process is complete, then a prefilter outside the loop can be designed to achieve the desired off-axis responses.

6.8. Robustness Issues Arising from the Use of Nested Channels

This Section describes the manner in which one can ‘design in’ stability robustness using the nested Channel design process. The following observations have been made by Leithead and O’Reilly for the 2-input 2-output case and a generalisation to the m -input m -output case is presented here. For a 2-input 2-output plant, Leithead and O’Reilly [39] show that an appropriate measure of closed loop stability robustness is as follows,

Condition 6.3.

An appropriate measure of stability robustness for a 2-input 2-output system can be made by assessment of the phase and gain margins for the open-loop subsystem k_2g_{22} together with the phase and gain margins for the open loop Channel C_1 , provided that the Nyquist plot of the multivariable structure function γ_1 (which can also be written as γ_2) does not go near the $(1,0)$ point at frequencies of importance.

To visualise this, consider Channel 1 of a 2-input 2-output plant, given as,

$$C_1 = k_1g_{11}(1 - \gamma_2) \quad (6.41)$$

Now, let us say that γ_2 is sufficiently far from the $(1,0)$ point such that plant variation will not make γ_2 change its encirclement count of the $(1,0)$ point. The only way in which a RHPZ can possibly be introduced into Channel 1 is if the number of RHPPs of h_2 changes such that the number of RHPZs of $(1-\gamma_2)$ changes. If the gain and phase margins of k_2g_{22} are big enough such that plant variation cannot change the number of RHPZs of $(1+k_2g_{22})$, and hence the number of RHPPs of h_2 , then Channel 1 cannot change structure. Also, because γ_2 is far from the $(1,0)$ point, Channel 1 will not exhibit phase sensitivity. If Channel 1 has adequate gain and phase margins then the RHPZ structure of $(1+C_1)$ will be invariant and hence the closed-loop system is stability robust.

The above argument is directly extendible to the m-input m-output case and stated below is sufficient conditions for closed-loop stability robustness of an m-input m-output plant.

Condition 6.4.

For an m -input m -output plant to possess stability robustness:

The gain and phase margins of the C_i' s ($i = 1..m$) should be adequate.

The $\gamma_{1..i}$ s should not be close to the (1,0) point at frequencies of importance.

These conditions are justifiable by the same considerations described in the 2-input 2-output example given above.

It is seen then that one can 'design in' robustness during the design procedure. This ability potentially allows the design of diagonal control laws which will guarantee closed-loop stability in the face of known bounded errors. This aspect of ICAD is not dealt with in detail in this thesis. However, Chapter 10 lays down possible guidelines for the development of this technique. Because the designs in this thesis are control laws for linear helicopter models where the error bounds of the helicopter models are not known, 'adequate' gain and phase margins will be designed for. Gain margins and phase margins of at least 5dB and 40 degrees respectively are regarded as being adequate.

Once the first iteration of design is complete and the nested Channels have been designed to have adequate robustness margins, it is likely that the controllers will be tuned such that the desired 0dB crossover frequencies of the Channels are achieved. Once this is done, as a final check to determine whether the system still possesses stability robustness, it is sufficient to ensure that the Channel gain and phase margins are adequate and that the Channel MSFs are far from the (1,0) point. The Channel gain and phase margins will of course be checked during the tuning procedure, as the specifications for the system will undoubtedly place gain and phase margin requirements on the Channels. Justification of the use of Channel gain and phase margins as robustness measures is made in Chapter 3.

6.9. A Look at ICAD Feedforward

ICAD Feedforward is a technique which exists in ICAD theory (Leithead and O'Reilly [35]) and is the way in which non-diagonal control is introduced into ICAD. Although none of the helicopter control system designs in this thesis use ICAD feedforward (hereon referred to as simply 'feedforward'), as it was not found to be necessary, the technique is included here to give the reader some insight into one of its possible uses. Leithead and O'Reilly [35] state that there are three uses for feedforward. These are: to improve the structure of a system, to decouple a systems feedback signals and to render a non-robust system robust. No attempt is made in this thesis to explain the first two uses, the reader is referred to [35] in this instance. However, the use of feedforward as a method to improve the robustness of a system will be described.

For simplicity, only a 2-input 2-output plant is considered here. The block diagram shown in Figure 6.9 is felt to be the most transparent representation of a feedforward configuration. In Figure 6.9 the feedforward elements are f_{12} and f_{21} . The term 'feedforward' in this context implies that the plant G is replaced by $(G+F)$ so far as the design of the diagonal feedback controller is concerned, where,

$$F = \begin{bmatrix} 0 & f_{12} \\ f_{21} & 0 \end{bmatrix} \quad (6.42)$$

For instance, if one can design f_{21} such that it is exactly equal to $-g_{21}$ then it seen from Figure 6.9 that the error signal e_2 will be zero. Physically, this situation means that the system will not generate any control action in order to alter the off-axis dynamics which come through g_{21} . Hence, the dynamics of $g_{21}r_1$ will show themselves, unaltered, at output y_2 .

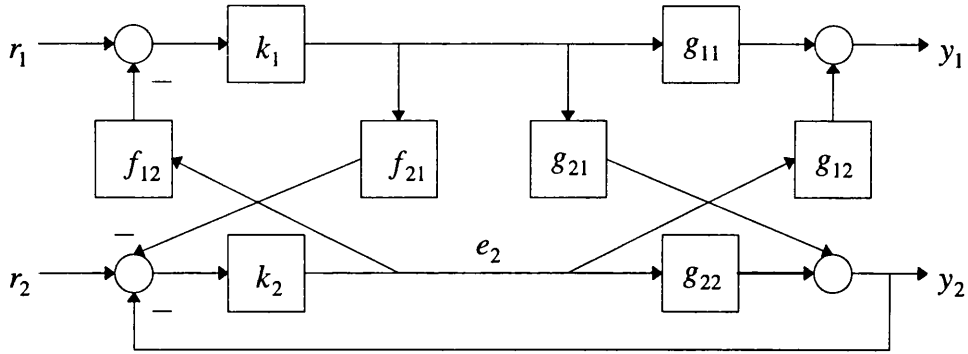


Figure 6.9. Block diagram of feedforward configuration.

The benefit of ‘hiding’ the off-axis dynamics from the feedback system is that the plant inputs will ‘think’ that they are dealing with two uncoupled systems, g_{11} and g_{22} . Hence any robustness problem that may arise due to loop interaction, i.e. the MSF of the Channels closely approaching the (1,0) point, is no longer an issue.

Of course, the above example is an extreme case where complete decoupling of the off-axis signals of the feedback system will occur between g_{11} and g_{22} . In practice, this extremity is not required as one need only ‘trim’ the troublesome off-axis signal at the required frequency in order to ease the robustness problem. This means that a degree of off-axis control will still be possible.

The approximate MSF of the plant without feedforward is given by,

$$\gamma = \frac{g_{12}g_{21}}{g_{11}g_{22}} \quad (6.43)$$

The amended MSF of the plant with feedforward is given by (Leithead and O’Reilly [35]),

$$\gamma_f = \frac{(f_{12} + g_{12})(f_{21} + g_{21})}{g_{11}g_{22}} \quad (6.44)$$

If γ is close to the (1,0) point at some frequency then the simplest, and perhaps most appropriate, manner in which f_{12} and f_{21} are to be chosen is to ensure that they have the dynamical characteristics of g_{12} and g_{21} respectively at the required frequency, but are scaled so as to move the MSF no more than is deemed necessary. Taking an extreme

example, let us suppose that γ is exactly on the (1,0) point at some frequency and it has been determined that this situation is a definite robustness problem. Let us also say that by moving the MSF a distance of 0.19 to the left of the (1,0) point will render the system robust. By choosing $f_{12} = -0.1g_{12}$ and $f_{21} = -0.1g_{21}$ then the nominal γ_f will be

$$\gamma_f = \frac{(-0.1g_{12} + g_{12})(-0.1g_{21} + g_{21})}{g_{11}g_{22}} = \frac{0.81g_{12}g_{21}}{g_{11}g_{22}} \quad (6.45)$$

It is seen from Eqn (6.45) that the nominal γ_f has been moved the appropriate distance.

Exactly matching the dynamical characteristics of elements g_{12} and g_{21} at a specific frequency, while ensuring that the gains of the feedforward elements are small at all other frequencies could lead to not only a larger than necessary feedforward controller, but also a very stressed engineer. It is usually sufficient to ensure that the dynamical characteristics are within some 'close' vicinity of the actual dynamical characteristics and this can lead to simpler feedforward elements

6.9.1. Applied Example

This Section investigates the longitudinal dynamics of a helicopter trimmed at 80 knots forward flight. The state space model is given in Appendix IV.

Figure 6.10 shows the approximate MSF of the longitudinal subsystem and it is seen that γ just enters the non-robust region at approximately 0.35 rad/s. Realistically, this situation is unlikely to warrant the use of feedforward, but in order to demonstrate the technique we shall proceed.

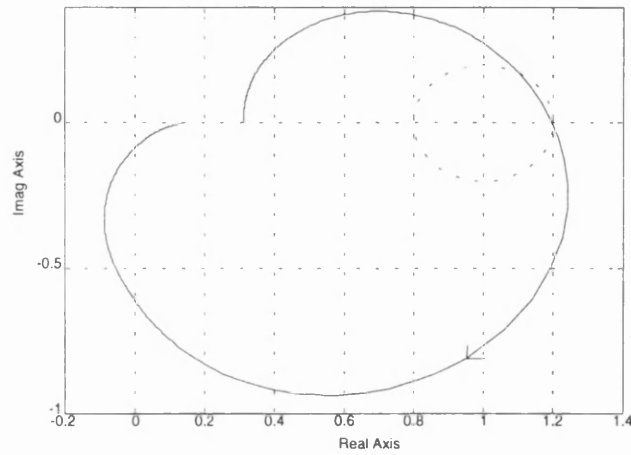


Figure 6.10. Nyquist plot of approximate MSF of longitudinal subsystem.

Let us say that it is required that the amended MSF is moved to a position where it is *at least* 0.25 from the (1,0) point. In order to do this one looks at the bode plots of g_{12} and g_{21} and pays specific attention to 0.35 rad/s. Figure 6.11 shows the bode plot of g_{12} .

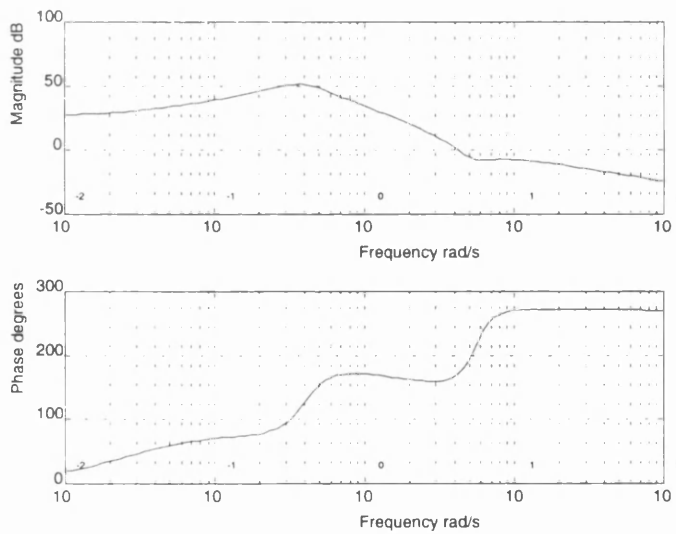


Figure 6.11. Bode plot of g_{12} .

It is seen from Figure 6.11 that g_{12} has a gain of approximately 50dB and a phase of approximately 125° at 0.35 rad/s. g_{21} was found to have a gain of approximately 47dB and a phase of approximately 160° at 0.35 rad/s. To render the system robust it is

sufficient to 'trim' g_{12} and g_{21} by 5% each. As stated above, it is counter-productive for the control engineer to attempt to design the required feedforward elements to be *exactly* $-0.5g_{12}$ and $-0.5g_{21}$ respectively. It is also required that the feedforward elements have low gain at frequencies outwith 0.35 rad/s in order to minimise the change to the system. From classical control considerations it is known that a transfer function which has the form,

$$f = \frac{ks^2}{(s + p)^4} \quad (6.46)$$

will have a phase of 0° at its peak at p rad/s if its sign is positive and a phase of -180° if its sign is negative. In addition, the gain will drop off at -40 dB/decade either side of the peak at p rad/s. k is a scalar gain. Because it is required that f_{12} and f_{21} have a gain of approximately 25dB and 21dB respectively and a phase of -120° and -160° respectively in the perfect case, then it seems that the use of transfer functions of the form of Eqn (6.46) will be sufficient to move γ_f appropriately far from the (1,0) point at 0.35 rad/s. The feedforward elements were designed to be,

$$f_{12} = \frac{-8.9s^2}{(s + 0.35)^4} \quad (6.47)$$

$$f_{21} = \frac{-5.8s^2}{(s + 0.35)^4} \quad (6.48)$$

which gave gains at 0.35 rad/s of 25.2dB and 21.4dB which will give a gain reduction of approximately 5% and phases, as expected, of -180° at 0.35 rad/s. Although the phases are not the exact requirements they are within some 'close' vicinity of the perfect requirements. Figure 6.12 shows the original MSF, γ , and the amended MSF, γ_f , and it is seen that the amended MSF has indeed moved to a distance greater than 0.25 at frequencies around 0.35 rad/s as required. It is seen then, that simple feedforward elements have been successful in increasing the robustness level of the system.

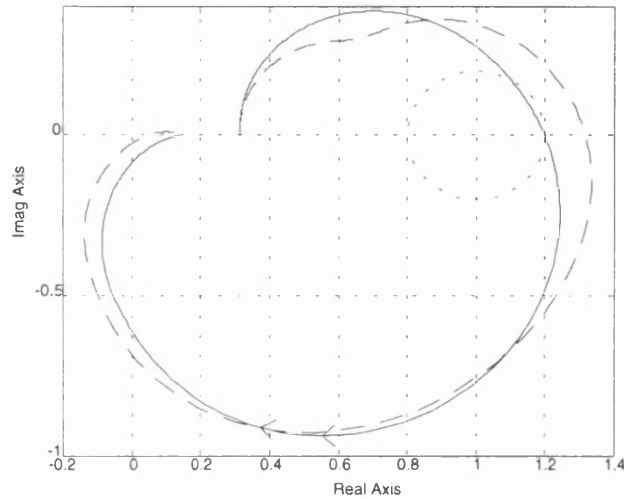


Figure 6.12. Nyquist plot of γ (solid) and γ_f (dashed).

ICA of the amended system showed that there were no structural problems in designing a high performance controller. The controllers were designed to be,

$$k_1 = \frac{10(s+1)}{s(s+100)} \quad (6.49)$$

$$k_2 = \frac{24(s+1)(s+15)}{s(s+10.5)(s+100)} \quad (6.50)$$

The gain and phase margins of the Channels are shown in Table 6.12. and are seen to be good.

Table 6.12. Channel gain and phase margins.

| | GM (dB) | PM (deg) |
|-----------|----------|----------|
| Channel 1 | ∞ | 75.5 |
| Channel 2 | 23.9 | 56.4 |

Because the feedforward elements only have significant gain around 0.35 rad/s the gain and phase margins at the input of the plant are very near those at the output of the plant.

From these results the feedback system can be regarded as possessing stability robustness. Figure 6.13 shows the response of the system with feedforward and without feedforward for a commanded step input into the pitch Channel. It is seen that there is noticeable degradation in the on-axis and off-axis responses for the system which includes feedforward in comparison to the system without feedforward.

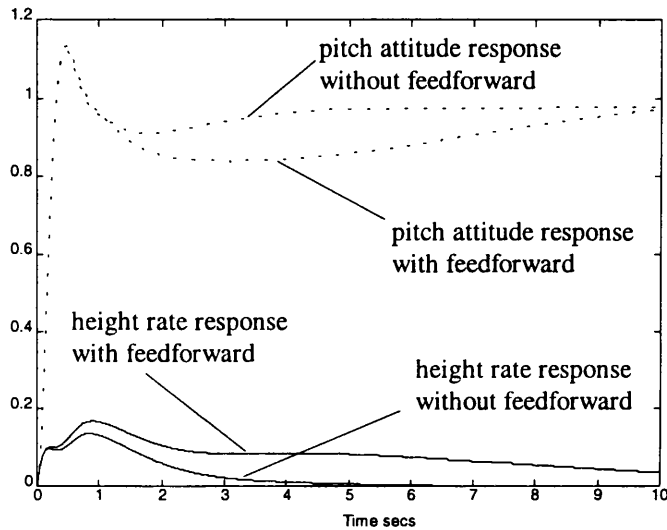


Figure 6.13. Response of system with and without feedforward to commanded step input in pitch Channel.

Although the feedforward elements trimmed the off-axis signals by only 5% each at approximately 0.35 rad/s it is seen from Figure 6.13 that the responses are deficient by considerably more than 5% over the time scale shown. It is seen from this particular example that, in general, careful consideration must be given as to whether it is worth attempting to achieve more stability robustness, as it is possible that serious degradation in off-axis performance can occur. Within the context of military flight control, it is generally accepted that a pilot would rather have a high performance aircraft which may exhibit slow divergence in comparison to a stability robust aircraft whose performance is deficient in the short term and requires additional pilot compensation. An aircraft whose performance is deficient in the short term will not provide Level 1 Handling Qualities. If possible instability is an issue, further analysis would be required to assess the rate of divergence of any unstable modes.

6.10. Summary

It has been shown in this Section that ICA is a powerful technique to elucidate structural issues of both minimum phase and non-minimum phase systems, allowing the sequential design of diagonal control laws which the control engineer will know will provide the best attainable performance. In the non-minimum phase worked example given in Section 6.6, it was seen that only the controller of Channel 4 was required to be low performance while the other 3 Channels were able to have high performance control. This is not a general result but is system specific. For minimum phase plants where the limits of the MSFs as s tends to infinity are less than one, the ordering of the input output pairs does not alter the sufficient conditions for stability. However, for non-minimum phase plants it is not known, until after detailed analysis, where the RHP transmission zero, or zeros, originate and so no general sufficient conditions for stability can be presented. An example of how one can trace the RHP transmission zero is given in Section 6.6. A brief introduction to ICAD feedforward was given to show how the robustness of a multivariable system could be improved. However, it was shown that small improvements in robustness could lead to unacceptable degradation in off-axis response and so careful consideration must be given before applying feedforward to a system.

7.1. Introduction

Attitude Command Attitude Hold (ACAH) systems are required for Level 1 handling in degraded visual cue environments (UCE=2) for all Mission Task Elements (MTEs) defined in ADS-33D [3]. An ACAH system does not offer the agility of a Rate Command system, which is discussed in Chapter 8, but this decrease in agility is traded-off for an increase in the level of stabilisation of the helicopter. The reader familiar with helicopter flight control may feel that a Rate Command system would be the most natural starting point to demonstrate ICAD, as it involves the least stabilisation. However, ICA highlights an interesting effect at low frequency when observing rates. This effect requires special attention and the author feels that the reader should first be exposed to the analysis and design of a system which does not exhibit this effect. In addition, this Chapter will describe the ICAD design procedure step-by-step. The literature tends to focus primarily on the design of ACAH control laws (see for example Garrard and Liebst [13], Gribble [15], Manness and Murray-Smith [46], Takahashi [72] and Walker and Postlethwaite [78]), and so this Chapter will form a sound basis for the reader who wishes to compare design techniques.

The structure of this Chapter is as follows. Section 7.2 considers what is required of the design of an ACAH system and determines specifications to meet these requirements. Section 7.3 presents the results of an approximate sensitivity analysis of the system. Section 7.4 determines the conditions for stability and achievable performance of a diagonal control law. Section 7.5 describes the design of the diagonal control law.

Section 7.6 analyses the ACAH system. Section 7.7 describes the design of a pre-compensator and Section 7.8 assesses the Handling Qualities.

7.2. Design Considerations

Before proceeding with the analysis of the ACAH system it is relevant to consider what is required to be achieved by the design before it is determined by analysis whether these requirements are attainable.

The first requirement of the design is that it is an ACAH system. i.e. a commanded input in δ_{long} or δ_{lat} will respectively yield a proportional pitch or roll attitude and, in addition, the system must regulate the pitch and roll attitudes to their trim values when there are no commanded inputs.

Because angular rate signals are available to the system it is desirable to feed back a blend of the appropriate rates with the attitudes in order to provide phase lead at low noise levels to the feedback system. By using a blend of this type, the phase lead requirements of the controller will be reduced. In addition to providing phase lead, the stability derivatives M_q and L_p will be augmented by feeding back the pitch and roll rates respectively. This provides additional damping of the pitch and roll responses.

In straight and level flight,

$$q \approx \dot{\theta} \quad (7.1)$$

$$p \approx \dot{\phi} \quad (7.2)$$

Taking the pitch attitude as an example. If one were to produce a linear blend of the pitch attitude and pitch rate of the form,

$$\theta + kq \approx \theta(1 + ks) \quad (7.3)$$

then it is seen that a stable zero has effectively been introduced to the θ response at k^{-1} rad/s.

As the required 0dB crossovers are envisaged to be above 1 rad/s, k will be set to one for both the pitch and roll responses, hence introducing an effective zero at 1 rad/s in each of the attitude Channels. This will provide appropriate phase lead at the frequencies of interest for design, without compromising the ability of the system to track and regulate the attitudes below 1 rad/s.

There is a sensitivity issue involved concerning the blending of outputs. For instance, does adding two signals together create a signal which will be sensitive to plant variation? As far as the blending of pitch and roll attitudes with their corresponding rates are concerned, one may think that there is no sensitivity problem because the angular rates are approximately the derivatives of the attitudes in straight and level flight and any sensitivity exhibited in an attitude will be exhibited in the corresponding angular rate. However, *approximately* is not *exactly* and it will now be shown that at low frequencies problems can potentially arise.

Two example helicopters are considered, which will be called model 1 and model 2 respectively. Both relate to 30 knots forward flight, the state space model of which is given in Appendix III. The observed outputs of model 1 are $\{\dot{h}, \theta, \phi, r\}$ and the observed outputs of model 2 are $\{\dot{h}, q, \phi, r\}$. Figure 7.1 shows the Nyquist plot of the MSFs of θ/θ_{1s} of model 1 (which will be exactly the same as $\dot{\theta}/\theta_{1s}$) and q/θ_{1s} of model 2. It is seen that at low frequencies there is a notable difference while at higher frequencies, above approximately 0.3 rad/s, the two plots merge into each other. This implies that at higher frequencies $\dot{\theta}$ is in fact very nearly equal to q but at lower frequencies $q \neq \dot{\theta}$.

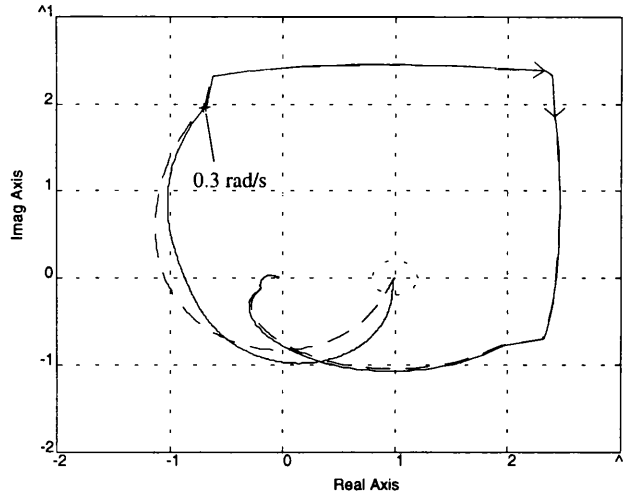


Figure 7.1. Nyquist plots of MSFs of $\theta/\delta_{\text{long}}$ (solid) and q/δ_{long} (dashed).

The reason for this discrepancy is explained by considering the equations which relate the angular rates to the derivatives of the attitudes, given in linear form as,

$$q = \dot{\theta} \cos \Phi_0 - \dot{\psi} \cos \Theta_0 \sin \Phi_0 \quad (7.1)$$

$$p = \dot{\phi} - \dot{\psi} \sin \Theta_0 \quad (7.2)$$

Inspecting Eqn (7.1) it is seen that the discrepancy at low frequency of Figure 7.1 must be due to the term containing $\dot{\psi}$ becoming significant. This can be easily checked by inspection of the Bode plots of the response. Figure 7.2 shows the bode plot of q/θ_{1s} and Figure 7.3 shows the Bode plot of $\dot{\theta} \cos \Phi_0/\theta_{1s}$ and $\dot{\psi} \cos \Theta_0 \sin \Phi_0/\theta_{1s}$. It is seen that $\dot{\psi} \cos \Theta_0 \sin \Phi_0$ is indeed significant at low frequencies but becomes insignificant at frequencies above approximately 0.2 rad/s. This correlates well with the behaviour of the MSF plots of Figure 7.1 which are seen to merge at approximately 0.3 rad/s.

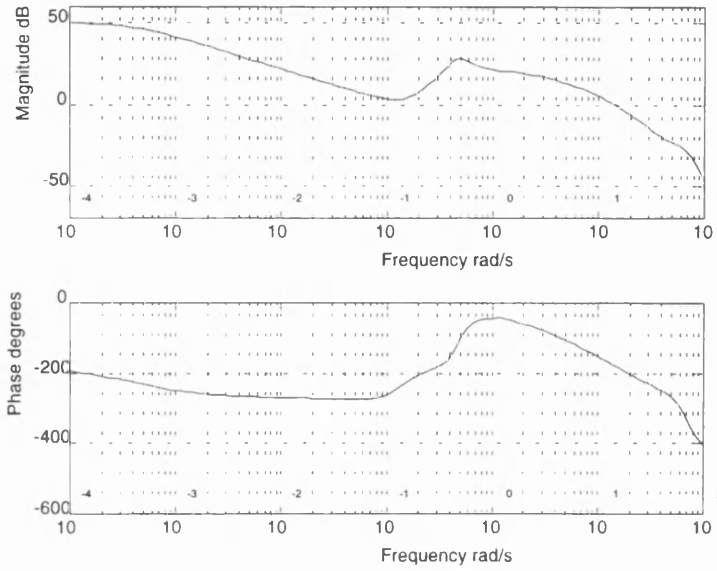


Figure 7.2. Bode plot of q/θ_{1s} .

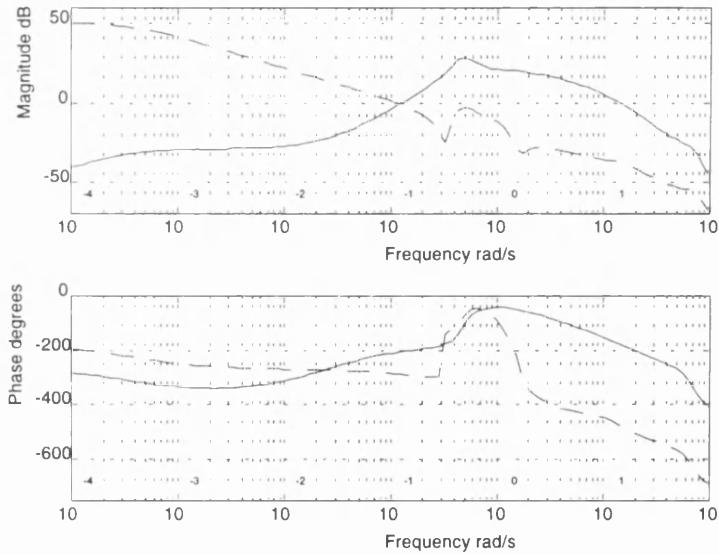


Figure 7.3. Bode plots of $\dot{\theta} \cos \Phi_0/\theta_{1s}$ (solid) and $\dot{\psi} \cos \Theta_0 \sin \Phi_0/\theta_{1s}$ (dashed).

This behaviour at low frequencies is very interesting but its significance within the context of ICAD is not yet fully understood. However, it is seen that regardless of whether one observes the pitch attitude or the pitch rate, an increase in sensitivity at low frequency is evident. This was also observed when comparing two systems which observed roll attitude and roll rate respectively. Therefore, in this situation, blending the

attitudes with rates will not introduce sensitivity which does not already exist. In addition, this sensitivity is evident only at low frequencies, below about 0.005 rad/s. Any unstable modes which *may* arise due to this potential sensitivity will be at low frequencies and can be easily controlled by the pilot with a minimal increase in workload. This question of possible low frequency unstable modes and their effect on pilot workload will be addressed in more detail in Section 7.6.

Before the controllers have been designed, it is possible to approximately determine the phase limited bandwidth from an approximate *open-loop* Channel frequency response. In order to do this, three values are required.

These are,

- i) The desired 0dB crossover frequency, ω_{0dB} .
- ii) The desired phase margin.
- iii) The desired -180° crossover frequency, ω_{-180° .

The phase of the approximate *closed-loop* Channel *i* at ω_{0dB} can be calculated from i) and ii) by the following equation,

$$\varphi_{CLi} = \angle \left(-e^{j\eta_i} / (1 - e^{j\eta_i}) \right) \quad (7.3)$$

where φ_{CLi} is the closed-loop phase of Channel *i* at ω_{0dB} , \angle denotes the angle and η_i is the phase margin of Channel *i*. The -180° crossover frequency of Channel *i*, ω_{-180° , will be the same as the closed loop Channel *i* -180° degree crossover frequency. This is because $C_i(j\omega_{-180^\circ})$ is a negative real number whose magnitude is less than one, and so the closed loop, $C_i(j\omega_{-180^\circ}) / (1 + C_i(j\omega_{-180^\circ}))$, will also be a negative real number and hence has a phase of -180° . If it is assumed that the closed loop phase decrease between ω_{0dB} and ω_{-180° is linear on the logarithmic scale then an approximation of the phase limited bandwidth can be made. Therefore, specifications for the open loop Channels should include not only a designated 0dB crossover frequency and phase margin, but also a -180° crossover frequency, the values being set to achieve a required phase limited bandwidth.

The Handling Qualities bandwidths of the pitch roll and yaw attitudes are required to be Level 1. Because it is the bandwidth of the θ , ϕ and ψ responses, rather than $(\theta+q)$, $(\phi+p)$ and r , which is of interest, appropriate amendments must be made to the approximate closed loop phase plots generated by consideration of the chosen feedback signals. The θ and ϕ responses are effectively the $(\theta+q)$ and $(\phi+p)$ responses, but each with an additional pole at 1 rad/s. The ψ response is effectively the r response, but with a pole at the origin. The phase response of the effective pole can be superimposed on the approximate closed-loop phase plots of the $(\theta+q)$, $(\phi+p)$ and r and superposition used to calculate the approximate phase behaviour of the θ , ϕ and ψ responses. The Handling Qualities phase limited bandwidth is defined as being the frequency at which the closed loop attitude phase responses are -135° . Because the -135° phase of the approximate θ , ϕ and ψ responses may not be within the frequency range between ω_{0dB} and ω_{-180° of the approximate $(\theta+q)$, $(\phi+p)$ and r responses, due to the phase decrease introduced by the effective poles, it is sufficient to extrapolate the response to the frequency at which the phase is -135° , ω_{-135° . In most cases ω_{-135° will be close enough to ω_{0dB} such that linear extrapolation is locally valid. In addition to calculating the approximate phase limited bandwidth, one can also calculate an approximation to the phase delay. This is most useful in the approximation of the roll attitude response as ADS-33D puts specific upper limits on the allowable phase delay for Level 1 and Level 2, unlike the pitch and yaw attitude responses where there is no defined upper limits on the phase delay requirements. The approximation is rather crude due to the need to linearly extrapolate over a frequency range of which there is little, *a-priori* knowledge, but it serves a purpose in that it can let the designer know of any serious shortcomings in the proposed open-loop specifications.

The approximate phase plot should be extrapolated to the frequency which is double ω_{-180° , i.e. $2\omega_{-180^\circ}$ and the phase at $2\omega_{-180^\circ}$ determined. To determine the approximate phase delay the following equation is used,

$$\tau_p = \frac{\text{abs}(\phi_{2\omega_{-180^\circ}} + 180^\circ)}{57.3(2\omega_{-180^\circ})} \quad (7.4)$$

where $\phi_{2\omega_{-180^\circ}}$ is the approximate phase at $2\omega_{-180^\circ}$.

Taking the roll attitude response as an example, to meet Level 1 Handling Qualities bandwidth requirements it is required that the Handling Qualities bandwidth, which is defined as the lesser of the phase limited bandwidth and the gain limited bandwidth, is greater than 2.5 rad/s and that the phase delay is less than 0.112 seconds. Specifying ω_{0dB} to be 3.2 rad/s, ω_{-180° to be 13 rad/s and the phase margin to be 50 degrees, Figure 7.4 shows the approximate closed-loop phase response of the roll attitude. The approximate phase limited bandwidth was calculated to be 3.1 rad/s and the approximate phase delay was calculated to be 0.10 secs. These values are within the Level 1 region.

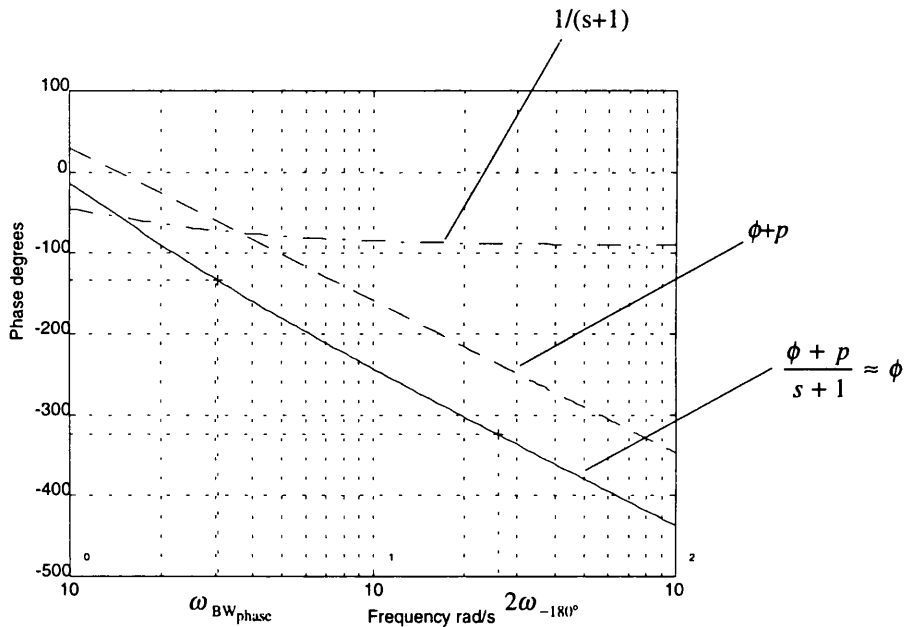


Figure 7.4. Approximate closed-loop phase of roll attitude response.

As a rule of thumb, if one designs the $(\theta+q)$ and $(\phi+p)$ Channels to have gain margins of at least 10 dB then the phase limited bandwidths of the attitude responses are likely to be less than the gain limited bandwidths, which is preferred for an ACAH system. This is in order that the pilot has a gain margin of at least 6dB available, hence reducing the possibility of pilot induced oscillations (PIOs) when manoeuvring aggressively.

Table 7.1 shows the open-loop specifications for the design with the approximate Handling Qualities parameters. The '×' on the Channel 1 specification for ω_{-180° means that it can be placed arbitrarily as there is no Handling Qualities bandwidth requirement for the height rate response. These specifications are for guidance only and there is no requirement on the designer to meet them exactly, or interpret them as being lower limits which must be met. It is usually sufficient that the appropriate parameters of the final design are within some 'close' vicinity of the open-loop specifications. How 'close' is subjective and is left to the designer's judgement. In the event that the first iteration of the design does not meet the Handling Qualities requirements it is likely that the number of further iterations required will be substantially reduced, as opposed to a design where no consideration of the approximate Handling Qualities parameters have been made.

Table 7.1. Approximate open-loop Channel specifications.

| | ω_{0dB} (rad/s) | ω_{-180° (rad/s) | $\omega_{BW_{phase}}$ (rad/s) | PM (deg) | GM (dB) |
|-----------|------------------------|-------------------------------|-------------------------------|----------|---------|
| Channel 1 | 1.0 | × | n/a | 55.0 | 20.0 |
| Channel 2 | 3.0 | 10.0 | 2.9 | 50.0 | 10.0 |
| Channel 3 | 3.2 | 13.0 | 3.1 | 50.0 | 10.0 |
| Channel 4 | 5.0 | 20.0 | 4.0 | 55.0 | 20.0 |

The helicopter model is a 19th order state space representation of a typical combat rotorcraft trimmed at 30 knots forward flight. 30 knots was chosen as it is in the middle of the low-speed range, and this was judged to be a good starting point. The model has 9 rigid body states, 6 rotor states and 4 actuator states. The state space model is given in Appendix III.

7.3. Approximate Sensitivity Analysis

The helicopter with the appropriate observations is given in transfer function form by,

$$G = C_{\text{acah}}(sI - A)^{-1}B \quad (7.5)$$

hence,

$$\begin{bmatrix} \dot{h} \\ \theta + q \\ \phi + p \\ r \end{bmatrix} = G \begin{bmatrix} \theta_0 \\ \theta_{1s} \\ \theta_{1c} \\ \theta_{0T} \end{bmatrix} = \begin{bmatrix} g_{11} & g_{12} & g_{13} & g_{14} \\ g_{21} & g_{22} & g_{23} & g_{24} \\ g_{31} & g_{32} & g_{33} & g_{34} \\ g_{41} & g_{42} & g_{43} & g_{44} \end{bmatrix} \begin{bmatrix} \theta_0 \\ \theta_{1s} \\ \theta_{1c} \\ \theta_{0T} \end{bmatrix} \quad (7.6)$$

Table 7.2 shows the structure of the transmission zeros and eigenvalues of the system.

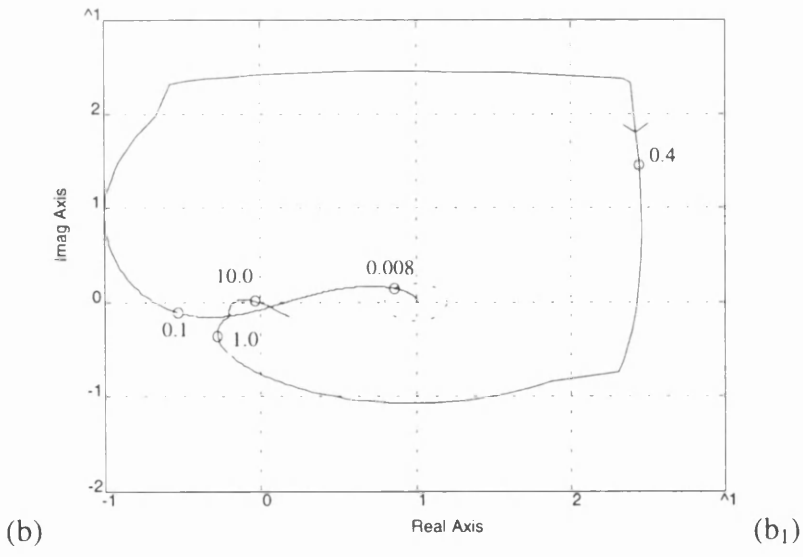
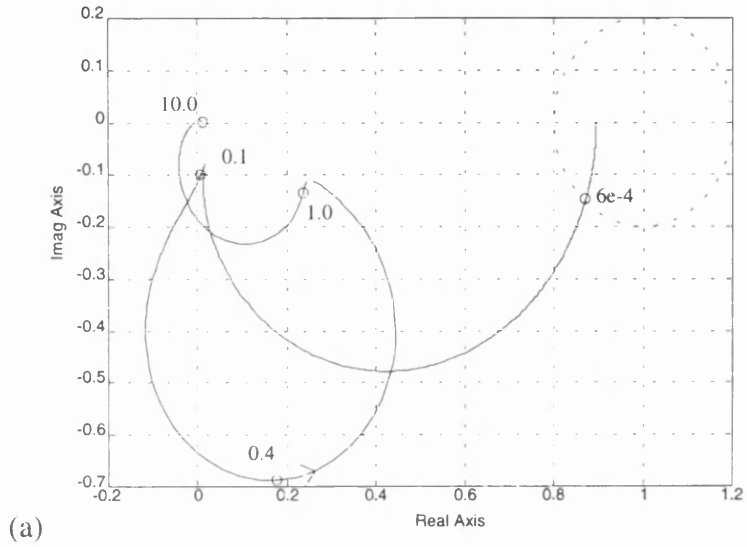
Table 7.2. Structure of G .

| | RHP Transmission Zeros (rad/s) | RHP Eigenvalues (rad/s) |
|-----|--------------------------------|-------------------------|
| G | 1.4234e+5 | 9.1439e-2 ± 4.6032e-1j |

For analysis and design purposes, the highest frequency which will be considered is 30 rad/s and all frequencies up to and including 30 rad/s will be regarded as *frequencies of interest*. 30 rad/s is sufficiently far above the desired crossover frequencies and will adequately highlight the effects of the modelled rotor modes at the frequency range over which the ACAH feedback system will be operational. One need not consider RHP (transmission) zeros which are above frequencies of interest. This is because the Channels will have gain less than one at such frequencies, causing the RHPZs to have no dynamical significance. This means that the high frequency RHP transmission zero at 1.4234e+5 rad/s can be disregarded and the helicopter can be regarded as being a minimum-phase system. In addition, any approximate MSFs under consideration will be plotted up to 30 rad/s and, for analysis and design purposes, the values of the MSFs at 30 rad/s will be taken as the high frequency limits.

The approximate sensitivity analysis involves inspecting the approximate Channel MSFs to determine whether there is a potential robustness problem due to the multivariable structure of the helicopter.

Figure 7.5 shows the Nyquist plots of the approximate Channel MSFs.



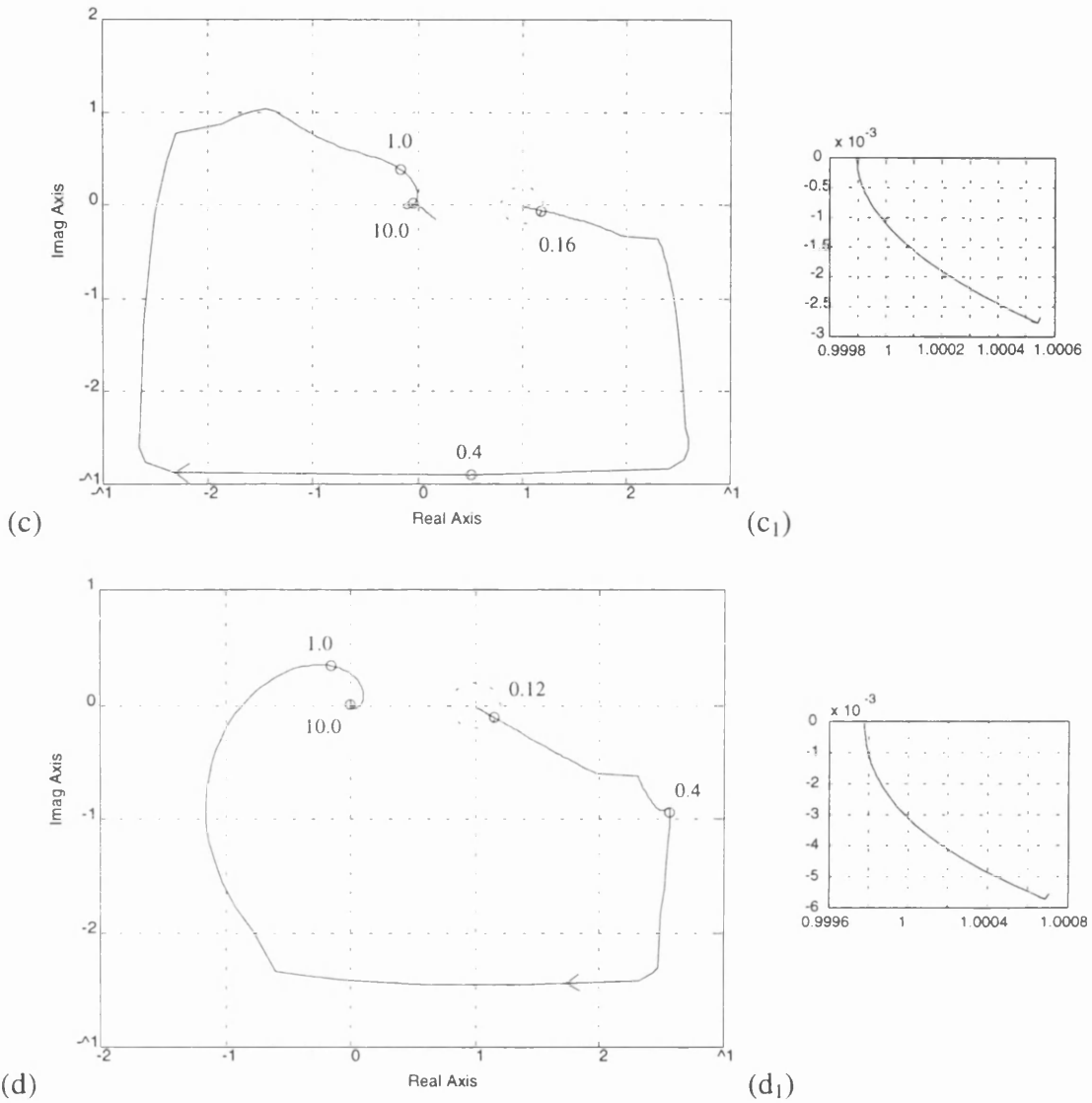


Figure 7.5. Nyquist plots of (a) \hat{G}_1 , (b) \hat{G}_2 , (b1) Expansion of (1,0) region of (b), (c) \hat{G}_3 , (c1) Expansion of (1,0) region of (c), (d) \hat{G}_4 , (d1) Expansion of (1,0) region of (d).

(all plots are shown up to 30 rad/s, frequencies shown on plots are in rad/s)

It can be concluded from this sensitivity analysis that the actual system will exhibit potential stability robustness problems only at low frequencies, below 0.16 rad/s, if high performance control is used. It is seen that the MSFs of \hat{G}_j , $j=2..4$, go very close to the (1,0) point but do not go exactly to (1,0), and so the encirclement counts of the (1,0) point are well defined.

7.4. Stabilisation and Potential Performance of the ACAH System

From Section 7.2 it was determined that the 0dB crossover frequencies of the Channels should respectively be 1 rad/s, 3 rad/s, 3.2 rad/s and 5 rad/s. As mentioned in Chapter 6, for systems whose Channels are defined to have different bandwidths, the most appropriate numbering of the Channels is such that the lowest bandwidth Channel is defined as Channel 1 and the highest bandwidth Channel is defined as Channel 4. It turns out that the requirements of the system naturally impose numbering on the Channels which is compatible with this philosophy.

In order to determine the achievable performance of the system one begins with the equation,

$$|G| = g_{11}(1 - \Gamma_1)g_{22}(1 - \Gamma_2)g_{33}(1 - \Gamma_3)g_{44} \quad (7.7)$$

and relates it to the following equation,

$$|\hat{G}| = [1 + k_1g_{11}(1 - \gamma_1)].[1 + k_2g_{22}(1 - \gamma_{12})].[1 + k_3g_{33}(1 - \gamma_{123})].[1 + k_4g_{44}] \quad (7.8)$$

The zeros of $|\hat{G}|$ are the poles of the closed-loop system.

By the definition of the nested Channels in Chapter 6.

$$|\hat{G}| = [1 + C'_1].[1 + C'_2].[1 + C'_3].[1 + C'_4] \quad (7.9)$$

The physical interpretation of the nested Channels is as follows,

C'_1 is the transfer function describing \dot{h} due to δ_{coll} when the height rate loop is open but the $(\theta+q)$, $(\phi+p)$ and yaw rate loops are closed. C'_1 is equal to C_1 .

C'_2 is the transfer function describing $(\theta+q)$ due to δ_{long} when the height rate loop and $(\theta+q)$ loops are open but the $(\phi+p)$ and the yaw rate loops are closed.

C'_3 is the transfer function describing $(\phi+p)$ due to δ_{lat} when the height rate, $(\theta+q)$ and $(\phi+p)$ loops are open but the yaw rate loop is closed.

C'_4 is the transfer function describing r due to δ_{tail} when all the feedback loops are open. C'_4 is equal to $k_4 g_{44}$.

Eqn (7.7) explicitly relates the behaviour of the diagonal transfer function elements and the Γ_i s, $i = 1..4$, to the structure of $|G|$, the zeros of which are the transmission zeros of the open-loop helicopter. Eqn (7.8) explicitly relates the nested Channels to the structure of $|\hat{G}|$, the zeros of which are the poles of the closed-loop system. The way in which these equations are used will now be explained.

Before the controllers have been designed, one uses Eqn (7.7) to assess the *potential* for stabilisation and achievable performance. The rotorcraft has no non-minimum phase transmission zeros and so the zeros of $|G|$ are all stable. It is required that the poles of the closed-loop system are stable. The poles of the closed-loop system, as mentioned previously, are the zeros of $|\hat{G}|$.

Conditions sufficient for the zeros of $|\hat{G}|$ to be stable are as follows. The $\gamma_{1..i}$ s should have the same pole structure and encirclement count of the Γ_i s and the number of RHPZs of the $(1+C'_i)$ s should be the same as the number of RHPZs of the C'_i s. These sufficient conditions are explained in detail in Chapter 6.

Γ_1 , Γ_2 and Γ_3 are written explicitly as,

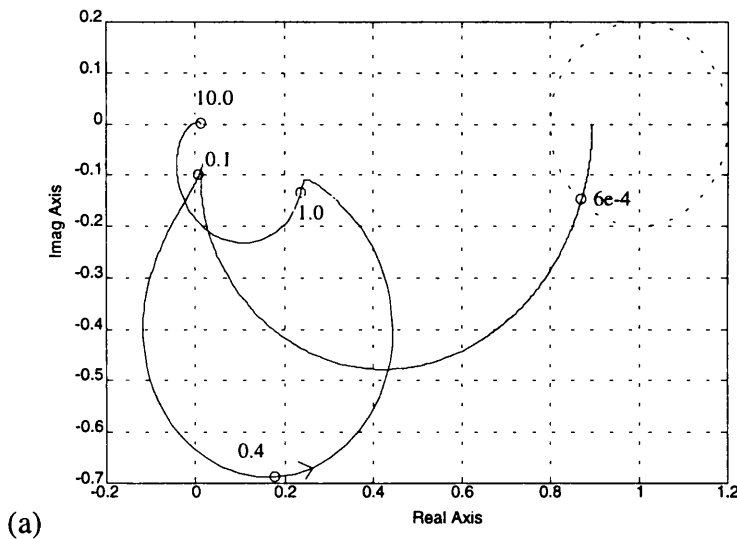
$$\Gamma_1 = - \frac{\begin{vmatrix} 0 & g_{12} & g_{13} & g_{14} \\ g_{21} & g_{22} & g_{23} & g_{24} \\ g_{31} & g_{32} & g_{33} & g_{34} \\ g_{41} & g_{42} & g_{43} & g_{44} \end{vmatrix}}{g_{11}} \begin{vmatrix} g_{22} & g_{23} & g_{24} \\ g_{32} & g_{33} & g_{34} \\ g_{42} & g_{43} & g_{44} \end{vmatrix} \quad (7.10)$$

$$\Gamma_2 = - \frac{\begin{vmatrix} 0 & g_{23} & g_{24} \\ g_{32} & g_{33} & g_{34} \\ g_{42} & g_{43} & g_{44} \end{vmatrix}}{g_{22}} \frac{\begin{vmatrix} g_{33} & g_{34} \\ g_{43} & g_{44} \end{vmatrix}}{g_{22}} \quad (7.11)$$

$$\Gamma_3 = \frac{g_{34}g_{43}}{g_{33}g_{44}} \quad (7.12)$$

Recall that by definition, Γ_4 is equal to zero.

Figure 7.6 shows the Nyquist plots of Γ_1 , Γ_2 and Γ_3 . Shown on Figure 7.7 are discrete frequency points and it is seen that the magnitude of the MSFs above 1 rad/s is small, hence loop interaction is small, and so designing the 0dB crossovers of the Channels at the frequencies specified in Table 7.1 will not pose any difficulties. Table 7.3 shows the structures of the parameters of Eqn (7.7). The nested nature of the Γ_j , $j=1..3$, is evident. Notice that the zeros of the $(1-\Gamma_j)$ s contain RHPZs which *exactly* correspond to the eigenvalues of the system and so can be disregarded in the structural assessment. Details of this phenomenon are described in more detail in Chapter 5.



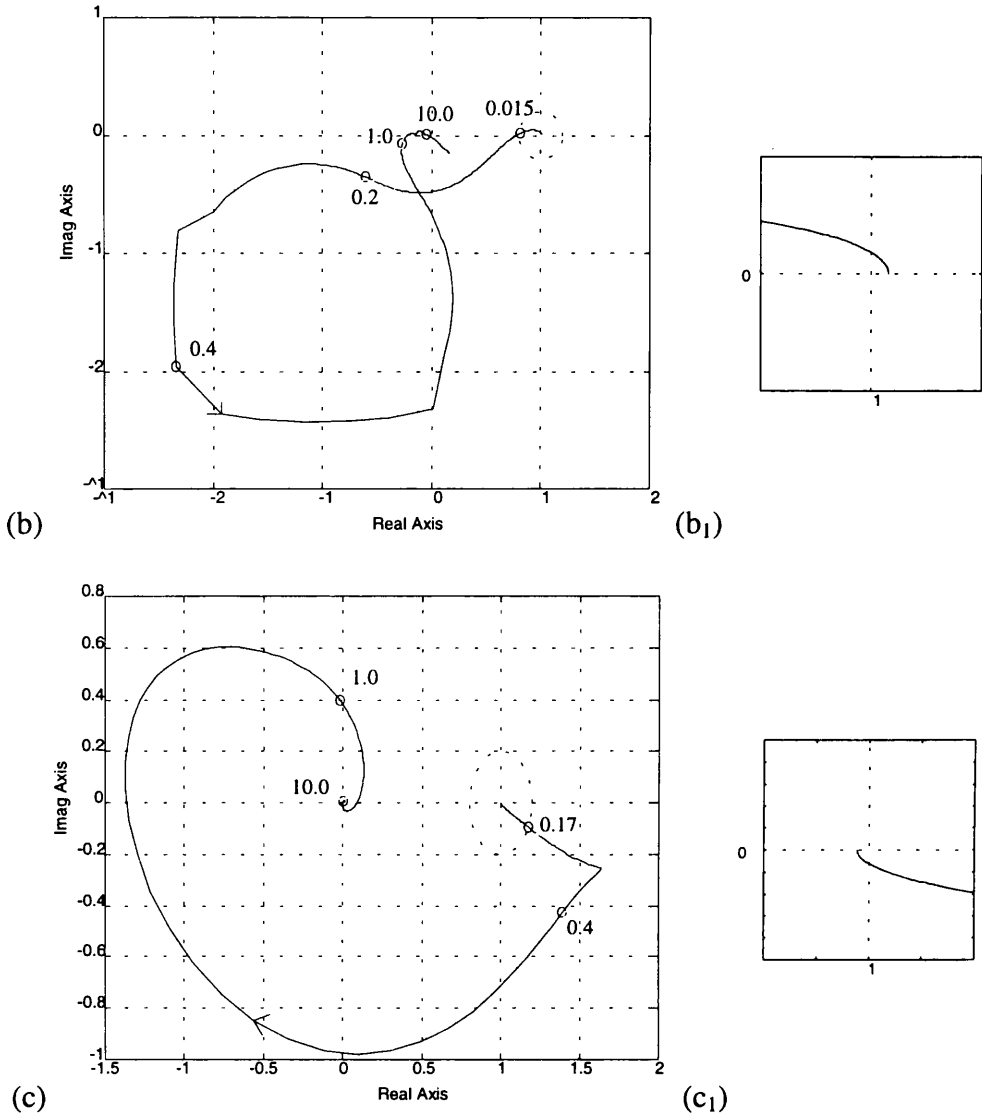


Figure 7.6. Nyquist plot of (a) Γ_1 , (b) Γ_2 , (b₁) Expansion of (1,0) region of Γ_2
 (c) Γ_3 , (c₁) Expansion of (1,0) region of Γ_3

(All plots are shown up to 30 rad/s. Frequencies are in rad/s. The expansions are not scaled as their only purpose is to show which side of the (1,0) point the MSFs are on.)

Table 7.3. Structure of parameters of Eqn (7.7).

| | RHPZs (rad/s) | RHPPs (rad/s) |
|------------------|--|--|
| $ G $ | – | $9.1439e-2 \pm 4.6032e-1j$ |
| $(1 - \Gamma_1)$ | $9.1439e-2 \pm 4.6032e-1j$ | $9.2078e-2 \pm 3.9896e-1j$ |
| $(1 - \Gamma_2)$ | $9.1439e-2 \pm 4.6032e-1j$ | $3.9534e-2 \pm 4.0786e-1j$ $1.9633e-2$ |
| $(1 - \Gamma_3)$ | $9.1439e-2 \pm 4.6032e-1j$ $3.9534e-2 \pm 4.0786e-1j$ | $1.1838e-1 \pm 4.9502e-1j$ $8.7159e-2 \pm 3.7749e-1j$ |
| g_{11} | $9.2078e-2 \pm 3.9896e-1j$ | $9.1439e-2 \pm 4.6032e-1j$ |
| g_{22} | $1.9633e-2$ | $9.1439e-2 \pm 4.6032e-1j$ |
| g_{33} | $1.1838e-1 \pm 4.9502e-1j$ | $9.1439e-2 \pm 4.6032e-1j$ |
| g_{44} | $8.7159e-2 \pm 3.7749e-1j$ | $9.1439e-2 \pm 4.6032e-1j$ |

From Table 7.3 it is seen that g_{33} , g_{44} and $(1-\Gamma_3)$ have non-cancelling RHPZs and this tells us that *potentially* the helicopter cannot be stabilised by high performance control of the lateral system only. This makes sense as the unstable poles of the system can be interpreted as being an unstable phugoid mode and hence originates in the longitudinal dynamics. High performance lateral control will therefore be unable to stabilise this mode. However, closure of loops 2, 3 and 4 will potentially stabilise the helicopter, as will closure of all four loops.

If one designs high performance control, then at frequencies below the desired 0dB crossovers the $\gamma_{l,i}$ s will be arbitrarily close to the Γ_i s in the low to mid frequency range. Also, the controllers will be designed such that the $(1+C'_i)$ s have the same number of RHPZs as the C'_i s. All that remains is to check that the encirclements of the (1,0) point of the $\gamma_{l,i}$ s at high frequency are the same as that of the Γ_i s. Figure 7.6 shows the value of the Γ_i s at 1 rad/s. It is seen that the high frequency regions of the Γ_i s' are comfortably far from the (1,0) point and are, indeed, quite close to the origin. As the $\gamma_{l,i}$ s will be arbitrarily close to the Γ_i s in the low to mid frequency region and

then attenuate to the origin in the high frequency region, the number of encirclement counts of the $\gamma_{1..i}$ s will be the same as the Γ_i s.

The design should start with controller k_4 and end with controller k_1 . At each stage it is sufficient to place the 0dB crossovers of the nested Channels at the desired 0dB crossovers of the actual Channels. This gives a good first try for the controllers. Once the first iteration of design is complete, the design can be fine tuned if desired.

Note that the above method is different from Sequential Loop Closure (Mayne [47]), as mentioned in Chapter 6, as stability of the system after each loop closure is not required. Closed-loop stability is only required after all 4 loops are closed. This however, does not imply that the system will destabilise if one loop fails. Infact, recall from Table 7.3 that the system will potentially remain closed-loop stable if loop 1 is opened. Further analysis would be required to determine system integrity. System integrity is a topic which is outwith the scope of this thesis, but which is discussed in Leithead and O'Reilly [34].

7.5. Feedback Controller Design

The design of the diagonal controller will be shown here step-by-step to let the reader see how the sufficient conditions for closed-loop stability, stated in the previous Section, are achieved and also how performance considerations are included in the design process.

Controller k_4 is to be designed such that the number of RHPZs of $(1+k_4g_{44})$ (recall that k_4g_{44} is C'_4) are the same as the number of RHPZs of g_{44} . In addition the low to mid frequency gain of k_4 should be made high to ensure that γ_{123} will be close to Γ_3 in the low to mid frequency region and also so that Channel 4 will exhibit good performance robustness in the low to mid frequency range.

One would normally inspect the Nyquist plots to ensure that the correct number of encirclement counts for the required structure have been made. However, because of

the large gains at low frequencies which are exhibited in the nested Channels, it is very difficult to present these plots in a way that will be clear to the reader that the correct encirclement counts have been made. Because of this, only the bode plots of the nested Channels will be shown and the structures will be shown in tabular form.

Bode plots enable the designer to see the *local* gain and phase properties of the transfer function being shaped, i.e. the relationship of magnitude and phase with frequency is made explicit, and so are a very powerful graphical tool for loop-shaping design.

k_{4g44} is shaped to closely correspond to the desired shape of Channel 4. The ‘desired’ shape of an open-loop response is essentially: high gain at low frequency, good attenuation of gain at high frequency and a smooth transition over the specified 0dB region, with gain and phase margins as specified.

Figure 7.7 shows the Bode plots of C'_4 with k_4 set to one and with k_4 designed as,

$$k_4 = \frac{-0.7(s + 2)}{s(s + 25)} \quad (7.13)$$

(the bode plots of the nested Channels will be shown with the dynamic controllers and also with the controllers set to one, to let the reader see the loop-shaping effect of the controllers). Table 7.4 shows the metrics of C'_4 and relates them to the approximate specifications of Table 7.1. It is seen that the metrics are within some close vicinity of the specifications. Table 7.5 shows the zero structure of C'_4 and $(1+C'_4)$ and it is seen that they are the same, as required. This means that the pole structure of γ_{123} will be the same as the pole structure of Γ_3 .

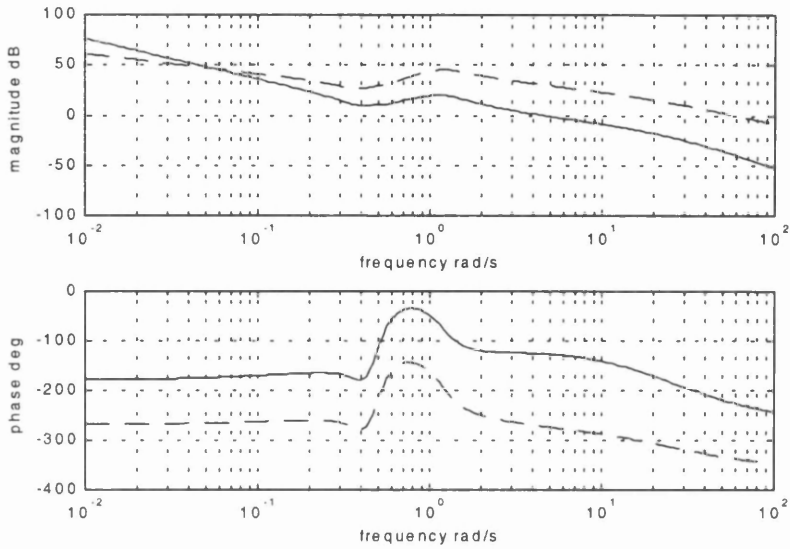


Figure 7.7. Bode plot of g_{44} (dashed) and k_4g_{44} (solid).

TABLE 7.4. Comparison of C'_4 metrics with C_4 approximate specifications.

| | GM (dB) | PM (deg) | 0dB crossover (rad/s) | -180° crossover (rad/s) |
|--------------------|---------|----------|-----------------------|--------------------------------|
| $C'_4 (k_4g_{44})$ | 16.9 | 54.4 | 4.5 | 23.8 |
| C_4 specs. | 20.0 | 55.0 | 5.0 | 20.0 |

TABLE 7.5. Zero structures of C'_4 and $(1+C'_4)$

| | RHPZs |
|------------|----------------------------|
| C'_4 | $8.7159e-2 \pm 3.7749e-1j$ |
| $(1+C'_4)$ | $7.2926e-2 \pm 3.7618e-1j$ |

Figure 7.8 shows the Nyquist plots of Γ_3 and γ_{123} . It is seen that the encirclement count of the (1,0) point of each is the same and so the zero structure of $(1-\gamma_{123})$ is the same as the zero structure of $(1-\Gamma_3)$.

The reader should note that the designer does not have a large amount of freedom in shaping the MSFs. The main aim is to ensure that the actual MSFs which arise during design work have the required properties to ensure that the sufficient conditions for closed-loop stability is adhered to. Performance objectives are achieved by shaping the (nested) Channels.

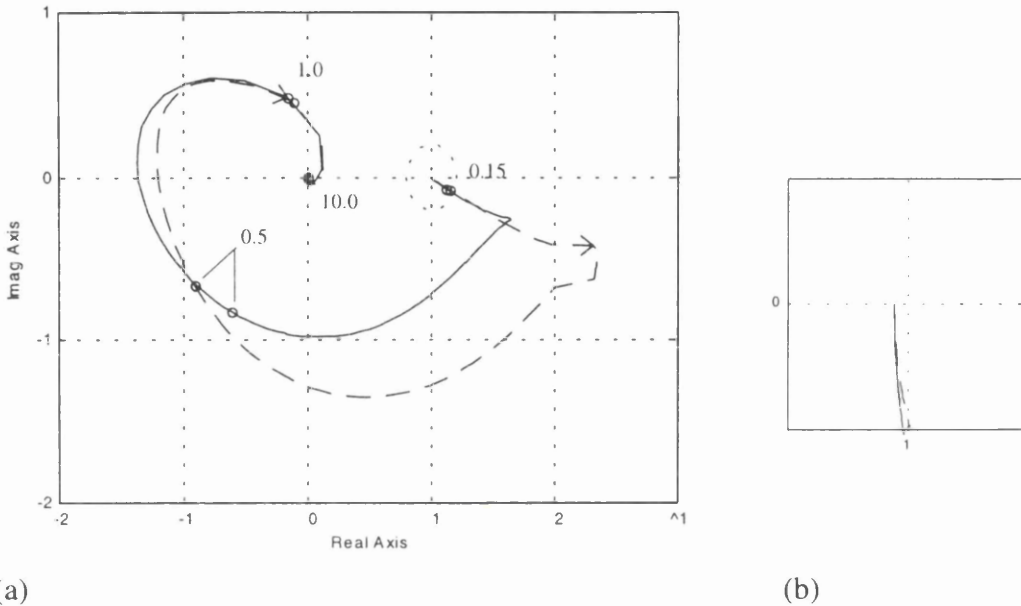


Figure 7.8. (a) Nyquist plot of Γ_3 (solid) and γ_{123} (dashed)
 (b) Expansion of (1,0) region
(frequencies shown are in rad/s)

Controller k_3 is designed such that the number of RHPZs of $(1+C'_3)$ are the same as the number of RHPZs of C'_3 . The zeros of C'_3 are the zeros of $(1-\gamma_{123})$ which are not the eigenvalues of the system, due to exact cancellation, and so C'_3 will have 2 RHPZs. In addition, the low to mid frequency gain of k_3 is made high to ensure that γ_{12} will be close to Γ_2 in the low to mid frequency region and also so that Channel 3 will exhibit good performance robustness in the low to mid frequency range.

Figure 7.9 shows the Bode plots of C'_3 with k_3 set to one and with k_3 designed as,

$$k_3 = \frac{-0.3(s+1)(s+4.2)}{s(s+0.001)(s+90)} \quad (7.14)$$

Table 7.6 shows the metrics of C'_3 and relates them to the approximate specifications of Table 7.1. It is seen that the metrics are within some close vicinity of the specifications. Table 7.7 shows the zero structure of C'_3 and $(1+C'_3)$ and it is seen that they are the same as required. Γ_2 and γ_{12} therefore have the same pole structure.

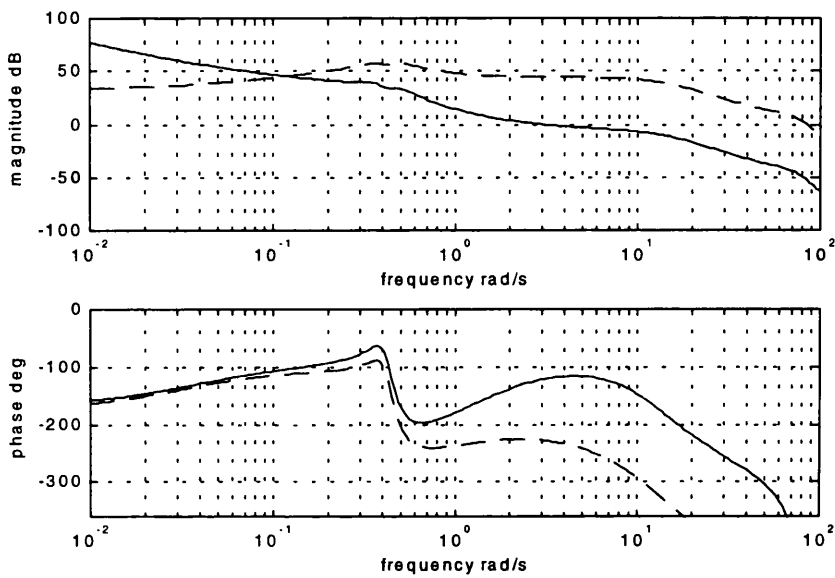


Figure 7.9. Bode plot of C'_3 without controller (dashed) and C'_3 with controller (solid).

TABLE 7.6. Comparison of C'_3 metrics with C_3 approximate specifications.

| | GM (dB) | PM (deg) | 0dB crossover (rad/s) | -180° crossover (rad/s) |
|--------------|---------|----------|-----------------------|--------------------------------|
| C'_3 | 10.4 | 58.6 | 3.1 | 13.9 |
| C_3 specs. | 10.0 | 50.0 | 3.2 | 13.0 |

TABLE 7.7. Zero structure of C'_3 and $(1+C'_3)$

| | RHPZs |
|------------|----------------------------|
| C'_3 | $4.5112e-2 \pm 4.2185e-1j$ |
| $(1+C'_3)$ | $4.5440e-2 \pm 4.2252e-1j$ |

Figure 7.10 shows the Nyquist plots of Γ_2 and γ_{12} . It is seen that the encirclement count of the (1,0) point of each is the same and so the zero structure of $(1-\gamma_{12})$ is the same as the zero structure of $(1-\Gamma_2)$.

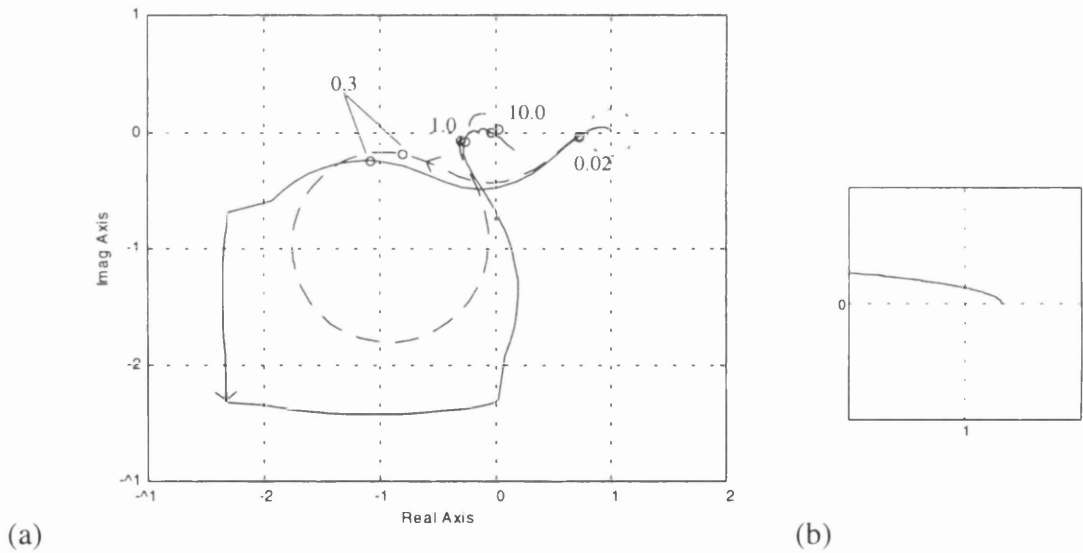


Figure 7.10. (a) Nyquist plot of Γ_2 (solid) and γ_{12} (dashed)
 (b) Expansion of (1,0) region
 (frequencies shown are in rad/s)

Controller k_2 is designed such that the number of RHPZs of $(1+C'_2)$ are the same as the number of RHPZs of C'_2 . The zeros of C'_2 are the zeros of $(1-\gamma_2)$ which are not the eigenvalues of the system and so C'_2 will have no RHPZs. In addition the low to mid frequency gain of k_2 is made high to ensure that γ_1 will be close to Γ_1 in the low to mid frequency region and also so that Channel 2 will exhibit good performance robustness in the low to mid frequency range.

Figure 7.11 shows the Bode plots of C'_2 with k_2 set to one and with k_2 designed as,

$$k_2 = \frac{0.45(s+1)(s+1.1)(s+2)}{s(s+0.001)(s+3.4)(s+40)} \quad (7.15)$$

Table 7.8 shows the metrics of C'_2 and relates them to the approximate specifications of Table 7.1. It is seen that the metrics are within some close vicinity of the specifications. Table 7.9 shows the RHPZs of C'_2 and the RHPZs of $(1+C'_2)$. It is seen that they have the same structure, therefore the pole structure of γ_1 is the same as the pole structure of Γ_1 .

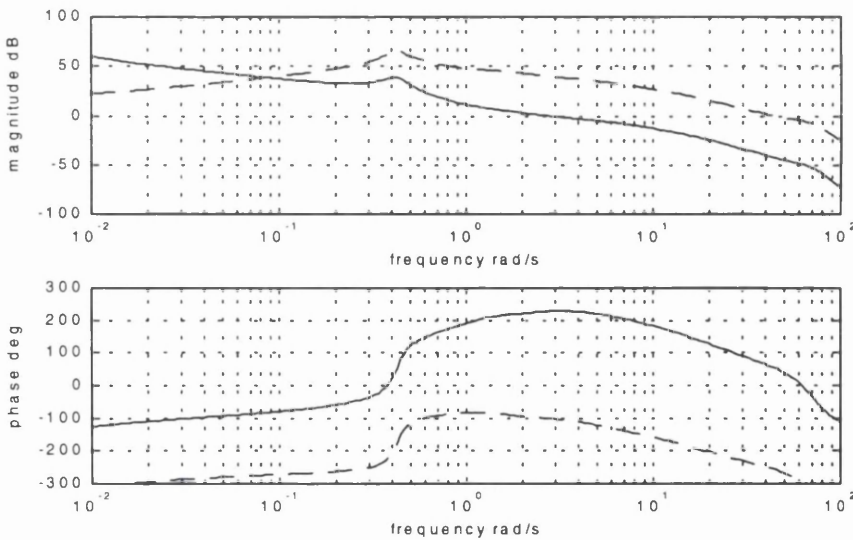


Figure 7.11. Bode plot of C'_2 without controller (dashed) and C'_2 with controller (solid).

TABLE 7.8. Comparison of C'_2 metrics with C_2 approximate specifications

| | GM (dB) | PM (deg) | 0dB crossover (rad/s) | -180° crossover (rad/s) |
|--------------|---------|----------|-----------------------|--------------------------------|
| C'_2 | 13.4 | 48.2 | 2.7 | 10.4 |
| C_2 specs. | 10.0 | 50.0 | 3.0 | 10.0 |

TABLE 7.9. Zero structure of C'_2 and $(1+C'_2)$

| | RHPZs |
|------------|-------|
| C'_2 | – |
| $(1+C'_2)$ | – |

Figure 7.12 shows the Nyquist plots of Γ_1 and γ_1 . It is seen that the encirclement count of the (1,0) point of each is the same and so the zero structure of $(1-\gamma_1)$ is the same as the zero structure of $(1-\Gamma_1)$. Table 7.9 shows the structure of $(1-\gamma_1)$ and $(1-\Gamma_1)$ and it is seen that the structures are the same.

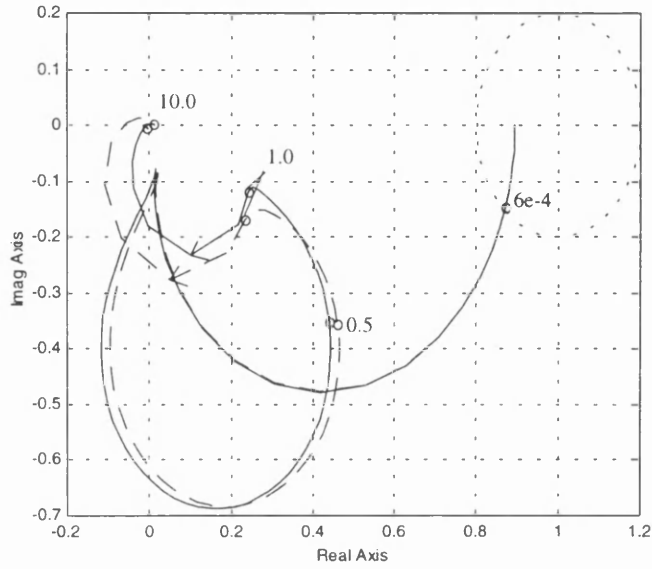


Figure 7.12. Nyquist plot of Γ_1 (solid) and γ_1 (dashed).
(frequencies shown are in rad/s)

Controller k_1 is designed such that the number of RHPZs of $(1+C'_1)$ are the same as the number of RHPZs of C'_1 . The zeros of C'_1 are the zeros of $(1-\gamma_1)$ which are not the eigenvalues of the system and so C'_1 will have no RHPZs. The closed-loop system will therefore be stable. In addition, as C'_1 is the same as C_1 , the metrics derived from this loop-shape will be the actual metrics of C_1 . After these metrics have been designed to closely correspond to the specifications, one then inspects the metrics of the actual Channels $C_2..C_4$ (as all controllers will be in place) to ensure that they are close to the specifications. As the levels of loop-interaction are low at the Channel 0dB crossover frequencies it is envisaged that the metrics of $C_2..C_4$ will closely correspond to the metrics of $C'_2..C'_4$ and will therefore be close to specification.

Figure 7.13 shows the Bode plots of C'_1 with k_1 set to one and with k_1 designed as,

$$k_1 = \frac{0.13(s+1)}{s(s+10)} \quad (7.16)$$

Table 7.10 shows the metrics of C'_1 and relates them to the approximate specifications of Table 7.1. It is seen that the metrics are within some close vicinity of the

specifications. Table 7.11 shows the RHPZs of C'_1 and the RHPZs of $(1+C'_1)$. It is seen that closed-loop Channel 1, and hence the plant, is stable.

TABLE 7.10. Comparison of C'_1 metrics with C_1 approximate specifications

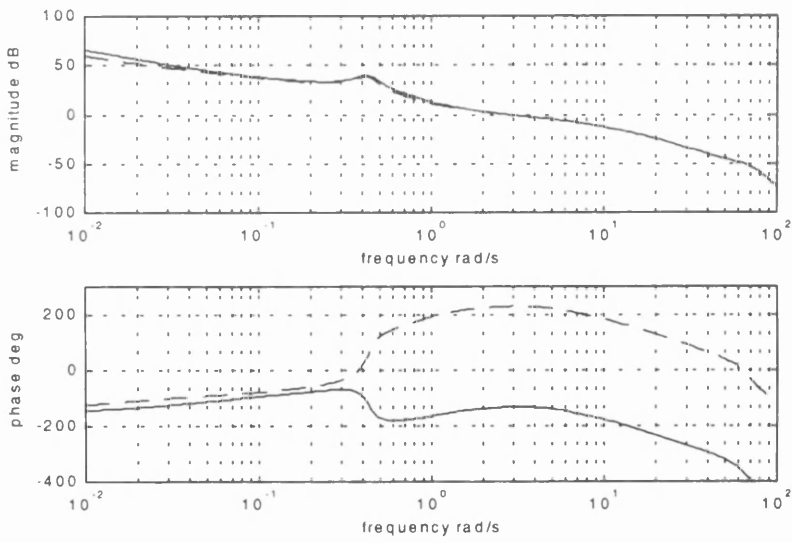
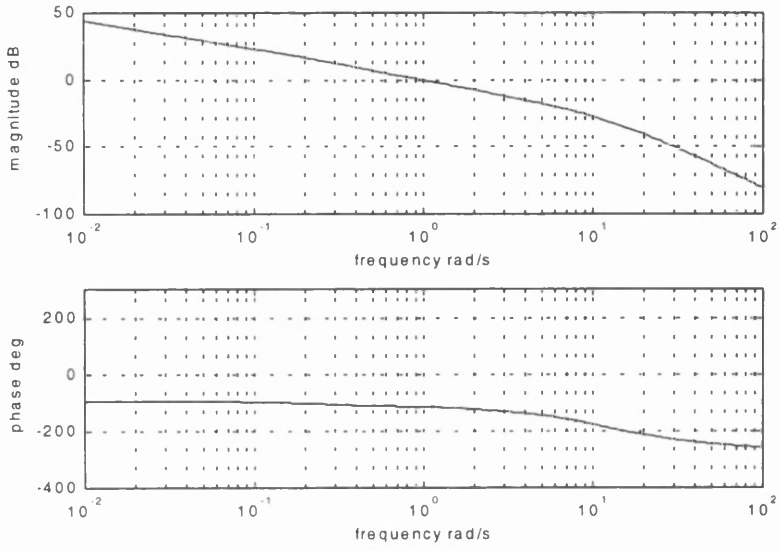
| | GM (dB) | PM (deg) | 0dB crossover (rad/s) | -180° crossover (rad/s) |
|--------------|---------|----------|-----------------------|-------------------------|
| C'_1 | 28.4 | 65.6 | 1.0 | × |
| C_1 specs. | 20.0 | 55.0 | 1.0 | × |

Table 7.11. Zero structure of C'_1 and $(1+C'_1)$

| | RHPZs (rad/s) |
|------------|---------------|
| C'_1 | - |
| $(1+C'_1)$ | - |

7.6. Individual Channel Analysis

Now that the feedback design is complete, one must ensure that the performance and robustness designed into the nested Channels is exhibited in the actual Channels. If not, then further iterations of design will be required. Figure 7.13 shows the Bode plots of Channels $C_1..C_4$ overlaid on the Bode plots of $C'_1..C'_4$. It is seen that C'_1 exactly matches C_1 as they are one and the same, C'_2 and C'_3 closely match C_2 and C_3 over the frequency range specified, and C_4 and C'_4 have noticeable differences in the low to mid frequency range only. Table 7.4 compares the metrics of $C_1..C_4$ with the metrics of $C'_1..C'_4$ and as expected they are seen to closely correspond to each other. Figure 7.14 show the actual MSFs of $C_1..C_4$.



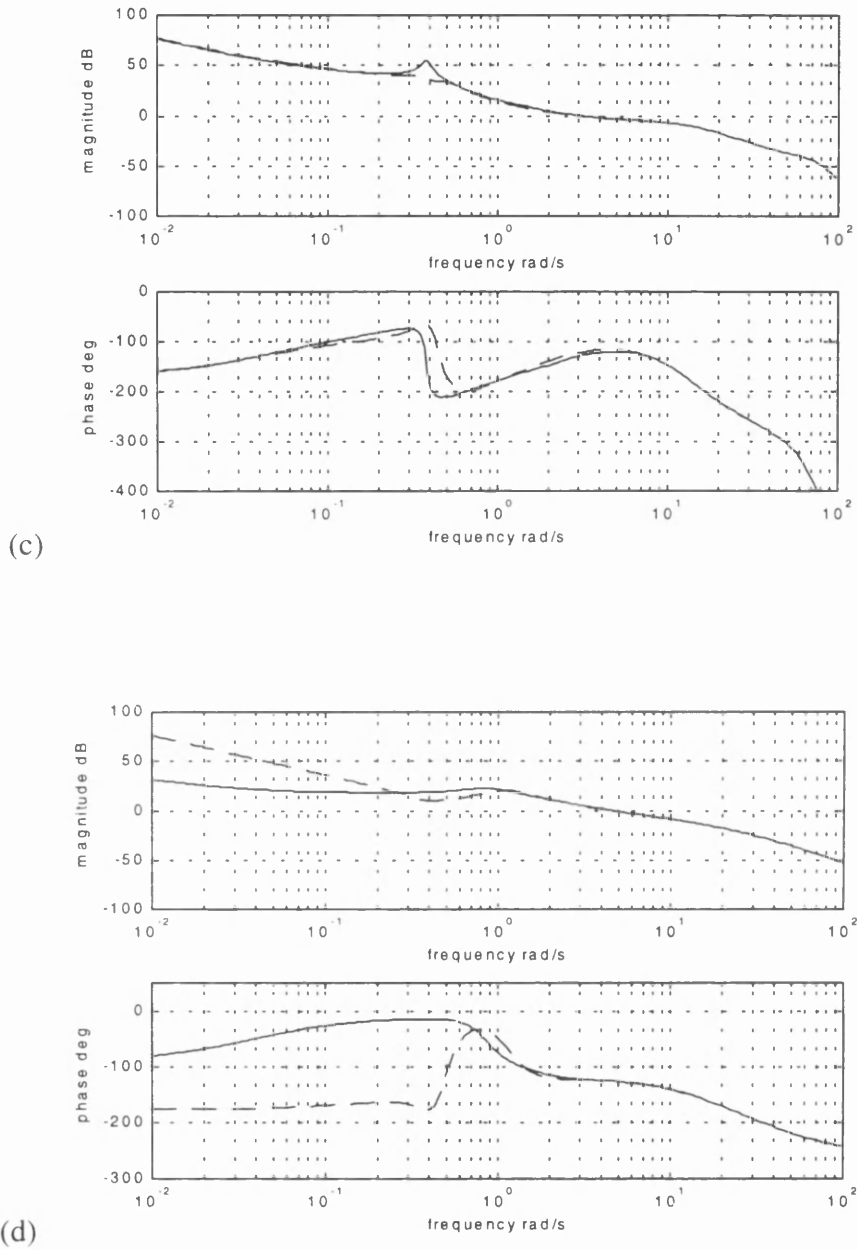
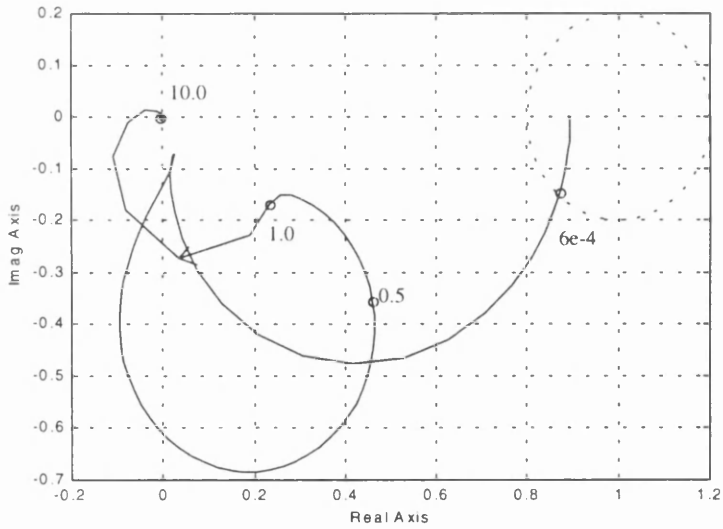


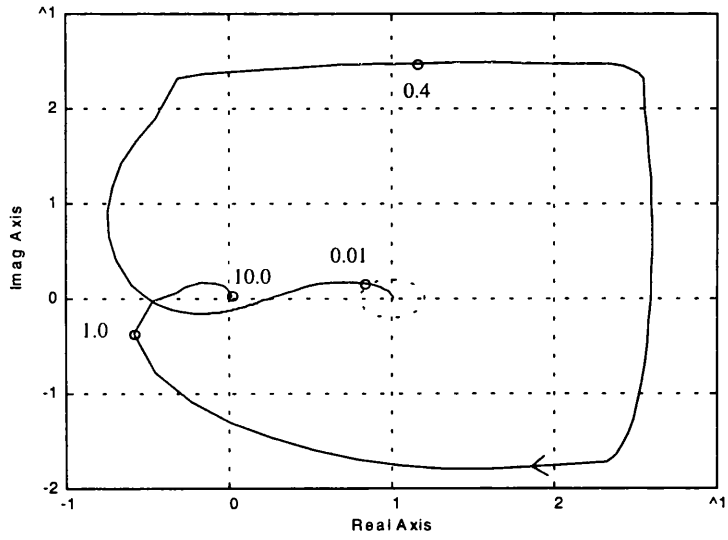
Figure 7.13. Bode plot of (a) C_1 (solid) and C_1' (dashed), (b) C_2 (solid) and C_2' (dashed), (c) C_3 (solid) and C_3' (dashed), (d) C_4 (solid) and C_4' (dashed).

TABLE 7.12. Comparison of metrics of actual Channels and nested Channels

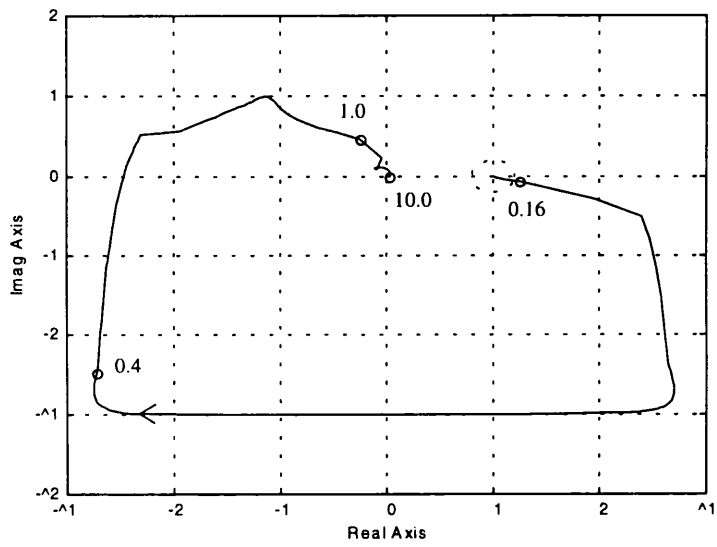
| | GM (dB) | PM (deg) | 0dB crossover (rad/s) | -180° crossover (rad/s) |
|--------|---------|----------|-----------------------|-------------------------|
| C_1 | 28.4 | 65.6 | 1.0 | × |
| C'_1 | 28.4 | 65.6 | 1.0 | × |
| C_2 | 13.4 | 47.8 | 2.7 | 10.4 |
| C'_2 | 13.4 | 48.2 | 2.7 | 10.4 |
| C_3 | 10.4 | 52.0 | 3.1 | 13.9 |
| C'_3 | 10.4 | 58.6 | 3.1 | 13.9 |
| C_4 | 20.6 | 54.3 | 4.6 | 23.7 |
| C'_4 | 16.9 | 54.4 | 4.5 | 23.8 |



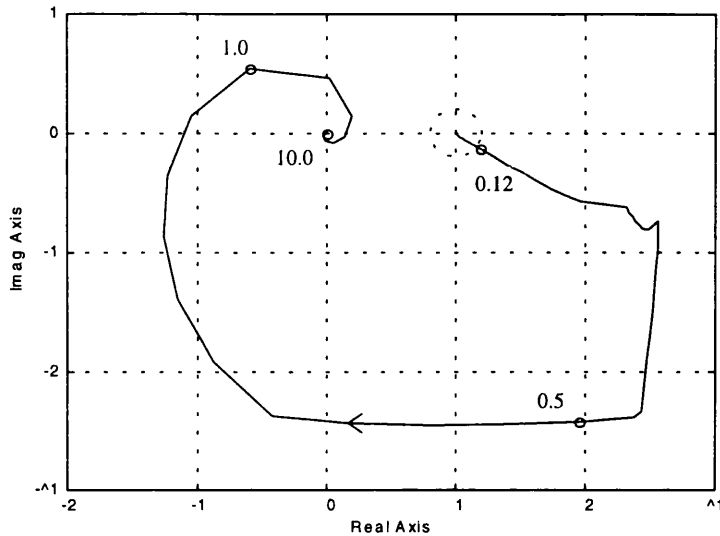
(a)



(b)



(c)



(d)

Figure 7.14. Nyquist plot of (a) γ_1 , (b) γ_2 , (c) γ_3 , (d) γ_4 .
(frequencies shown are in rad/s)

It is seen from Figure 7.14 that the MSFs enter the non-robust region at frequencies not greater than 0.16 rad/s. It can be concluded that the system is expected to possess stability robustness except at frequencies below 0.16 rad/s. Any potential unstable modes which may arise below 0.16 rad/s are not regarded as being a problem due to the fact that the pilot is more than capable of controlling low frequency unstable modes with a minimal increase in workload.

To add some weight to this statement, errors will be purposely introduced into the helicopter dynamics with the sole intention of causing a RHPZ to develop at approximately 0.1 rad/s in the roll Channel and 0.01 rad/s in the pitch Channel. The response of the helicopter to inputs in each of the axes will then be assessed. This example is of course a worse case scenario. The error introduced was an additive transfer function matrix, given as,

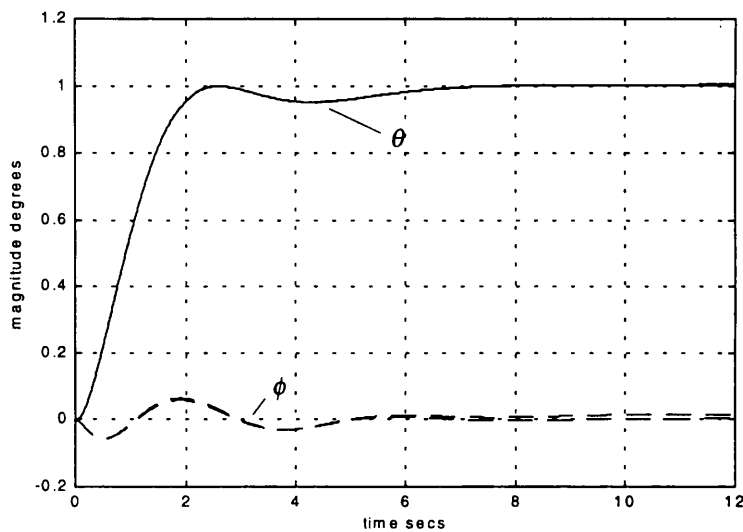
$$G_{\text{add}} = \begin{bmatrix} 0 & 0 & 0 & 0 \\ 0 & \frac{-0.005}{(s+0.005)(s+0.005)} & 0 & 0 \\ 0 & 0 & \frac{5}{(s+0.5)(s+0.5)} & 0 \\ 0 & 0 & 0 & 0 \end{bmatrix} \quad (7.17)$$

Table 7.13 shows the structure of the closed-loop Channels with the errors introduced.

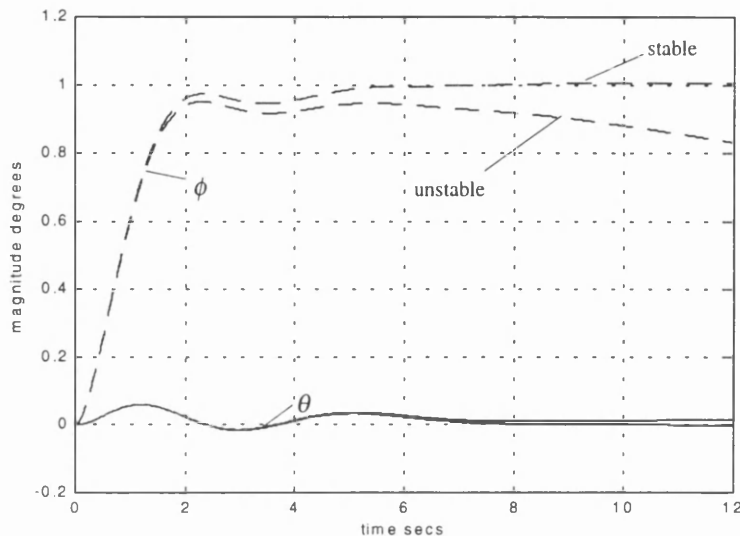
Table 7.13. Structure of perturbed closed-loop Channels.

| | RHPZs (rad/s) | RHPPs (rad/s) |
|-----------|---------------|---------------|
| Channel 1 | 1.1419e-1 | 1.1430e-1 |
| | 1.1253e-2 | 1.1246e-2 |
| Channel 2 | 1.1425e-1 | 1.1430e-1 |
| | 1.1252e-2 | 1.1246e-2 |
| Channel 3 | 1.1455e-1 | 1.1430e-1 |
| | 1.1246e-2 | 1.1246e-2 |
| Channel 4 | 1.1867e-1 | 1.1430e-1 |
| | 1.1248e-2 | 1.1246e-2 |

Figure 7.15 shows the pitch and roll attitude responses due to commanded pitch and roll attitudes of 5° for both the nominal system and the perturbed system. It is seen that the instability in the pitch response does not dramatically show itself during the 20 seconds shown and the instability in the roll response is evident after 2 seconds.



(a)



(b)

Figure 7.15. Comparison of linear time responses of stable and unstable system due to commanded step inputs in: (a) Pitch Channel, (b) Roll Channel.

ADS-33D states that the pitch and roll attitude responses due to commanded step inputs should remain essentially constant between 6 and 12 seconds. It is seen that this is essentially achieved for both responses.

The question that needs to be answered at this stage is why are the responses so well behaved over such a long time scale? An unstable pole at 0.1 rad/s would normally be expected to cause much faster divergence than is shown on Figure 7.15. The answer comes from consideration of the structures of the Channels shown in Table 7.13. It is seen from Table 7.13 that although the responses are unstable, the unstable poles are sitting very close to the unstable zeros and this is effectively contributing to damping out the unstable mode. It is known that automatic controllers would be unable to effectively stabilise such an unstable mode but a pilot is an extremely adaptive controller and would easily compensate for such a slow instability. In addition, a pilot will 'sense' more states than the control law has access to and therefore will not observe the same zeros. It is also noted that the dynamics of a real helicopter will be continually changing and so the instability, if it occurs, may not exist long enough for it to even begin to be noticeable to the pilot. Any slow unstable responses which *may* occur due to the effects of loop interaction are therefore of no concern. The gain and

phase margins of the Channels are therefore valid as robustness measures and the ACAH system can be regarded as possessing stability robustness.

7.7. Pre-Compensation

It was found necessary to implement a decoupling filter outside the feedback system to reduce the yaw rate due to collective. To reduce this response one can design a pre-filter matrix which has unity elements on the diagonal and an off-axis element which corresponds to the response which is to be reduced. If the feedback system is written as,

$$T = (I + GK)^{-1} GK \quad (7.18)$$

then the closed-loop yaw rate due to collective response is described by element t_{41} .

Writing T and the pre-filter P in full,

$$Q = \begin{bmatrix} t_{11} & t_{12} & t_{13} & t_{14} \\ t_{21} & t_{22} & t_{23} & t_{24} \\ t_{31} & t_{32} & t_{33} & t_{34} \\ t_{41} & t_{42} & t_{43} & t_{44} \end{bmatrix} \begin{bmatrix} 1 & 0 & 0 & 0 \\ 0 & 1 & 0 & 0 \\ 0 & 0 & 1 & 0 \\ p_{41} & 0 & 0 & 1 \end{bmatrix} = \begin{bmatrix} t_{11} + t_{14}p_{41} & t_{12} & t_{13} & t_{14} \\ t_{21} + t_{24}p_{41} & t_{22} & t_{23} & t_{24} \\ t_{31} + t_{34}p_{41} & t_{32} & t_{33} & t_{34} \\ t_{41} + t_{44}p_{41} & t_{42} & t_{43} & t_{44} \end{bmatrix} \quad (7.19)$$

It is desired to reduce the magnitude of element $q_{41}=t_{41}+t_{44}p_{41}$. Theoretically, one could reduce q_{41} to exactly zero by setting,

$$p_{41} = \frac{-t_{41}}{t_{44}} \quad (7.20)$$

but designing such a filter is impractical in practice. One need only reduce the gain of q_{41} at the frequency at which the troublesome coupling occurs and this can reduce the dynamical demand on p_{41} significantly.

Figure 7.16 shows a Bode plot of $(-t_{41}/t_{44})$ and also p_{41} , designed as,

$$p_{41} = \frac{-4s}{(s+3)(s+6)} \quad (7.21)$$

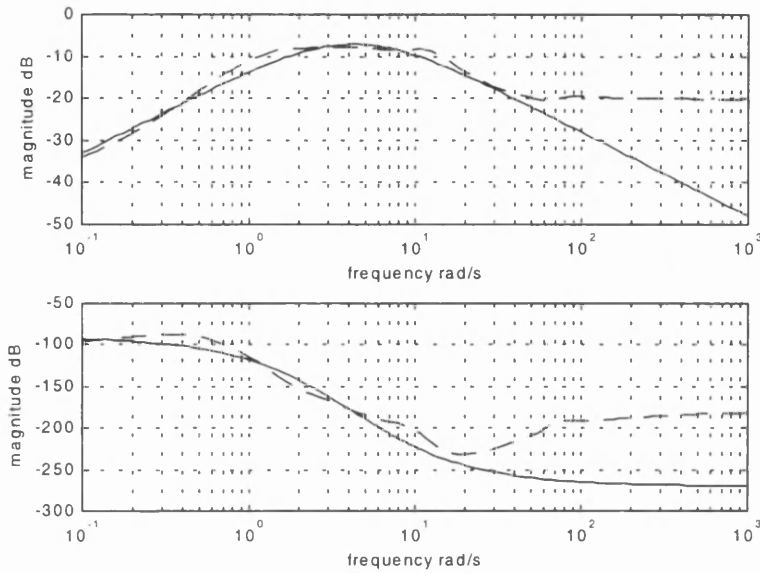


Figure 7.16. Bode plot of p_{41} (solid) and $(-t_{41}/t_{44})$ (dashed).

It is seen from Figure 7.16 that p_{41} closely matches $(-t_{41}/t_{44})$ over the frequency range which contains the magnitude peak. This is sufficient to substantially reduce the coupling in the transient region, as is seen in Figure 7.17.

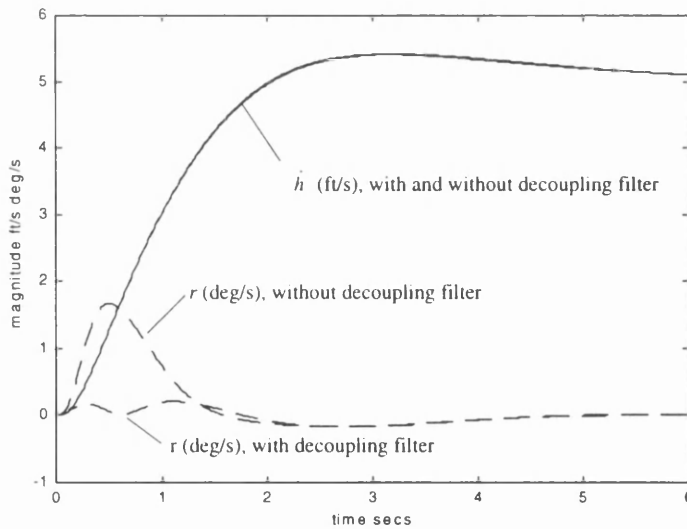


Figure 7.17. Linear response of \dot{h} (solid) and r (dashed) due to a commanded height rate of 5 ft/s, with and without decoupling filter.

A shaping filter for the height rate response given as,

$$s_h = \frac{7.14(s + 0.7)}{(s + 0.5)(s + 10)} \quad (7.22)$$

was designed to reduce the overshoot of the height rate response.

Figure 7.18 shows a block diagram of the complete system. Note that p_{41} has been renamed d_{yaw_coll} . Figure 7.19 shows the response of the system to step commands in each axis for the nominal model at 30 knots.

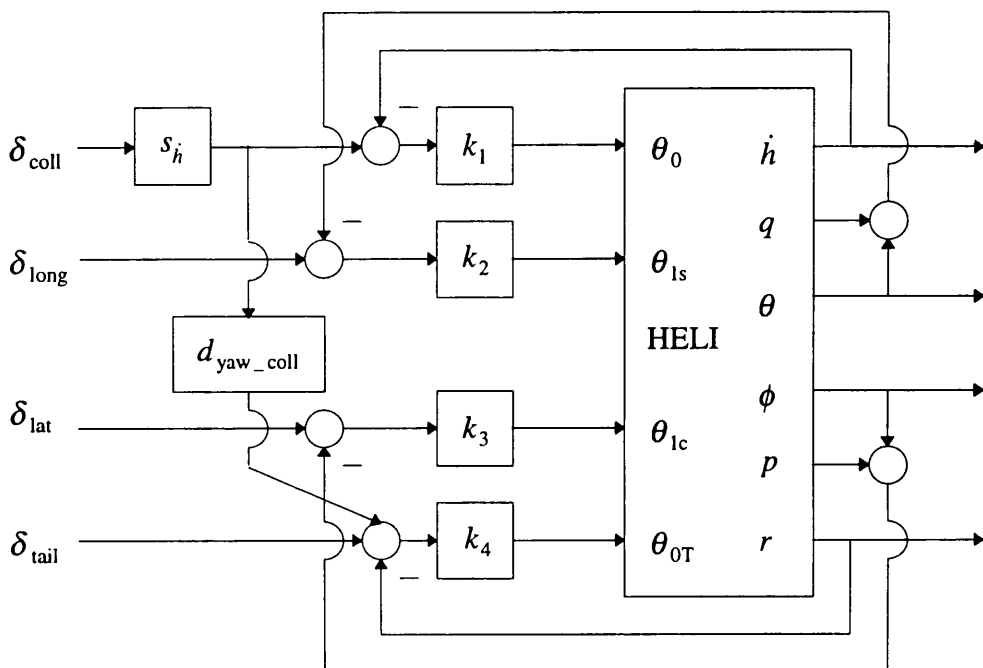
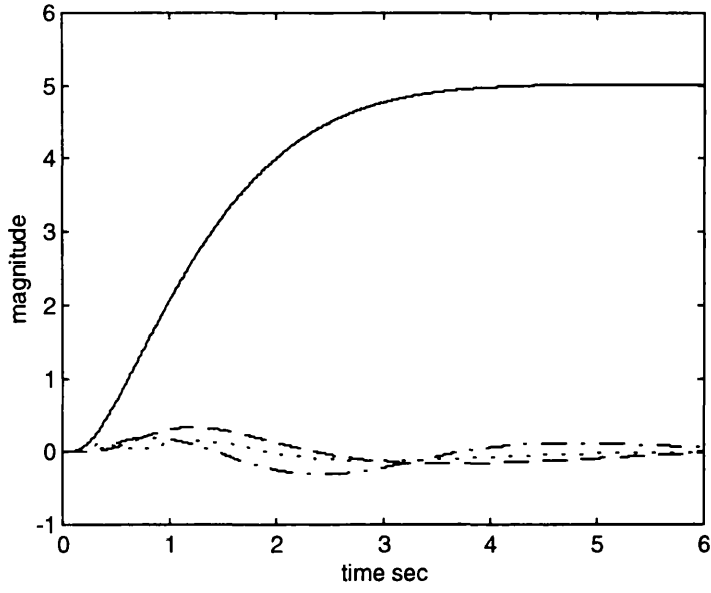
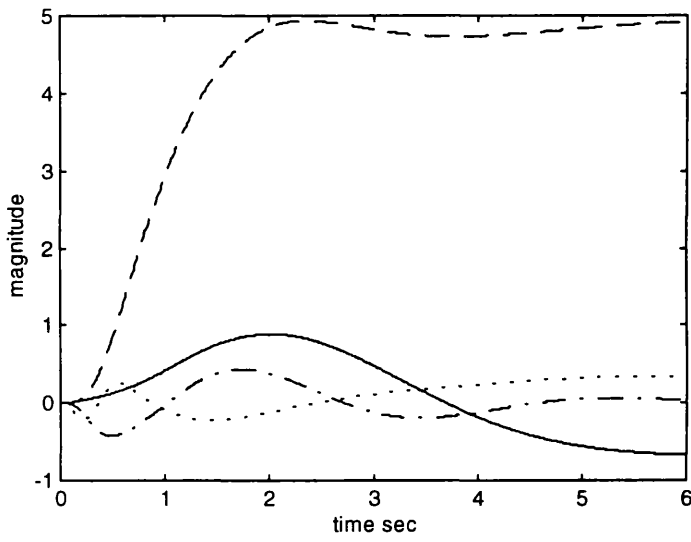


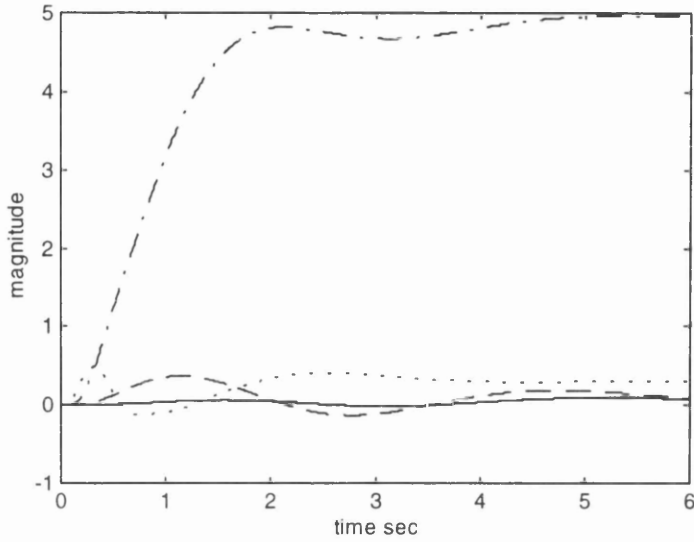
Figure 7.18. Block diagram of ACAH system.



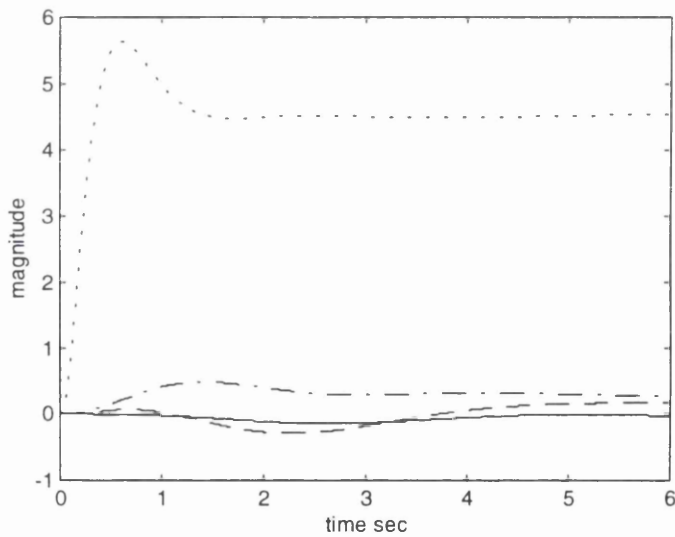
(a)



(b)



(c)



(d)

Figure 7.19. Linear time response of ACAH system at 30 knots to (a) height rate command of 5 ft/s, (b) pitch attitude command of 5° , (c) roll attitude command of 5° , (d) yaw rate command of $5^\circ/\text{s}$.

(\dot{h} ft/s (solid), θ deg (dashed), ϕ deg (dash-dotted), r deg/s (dotted))

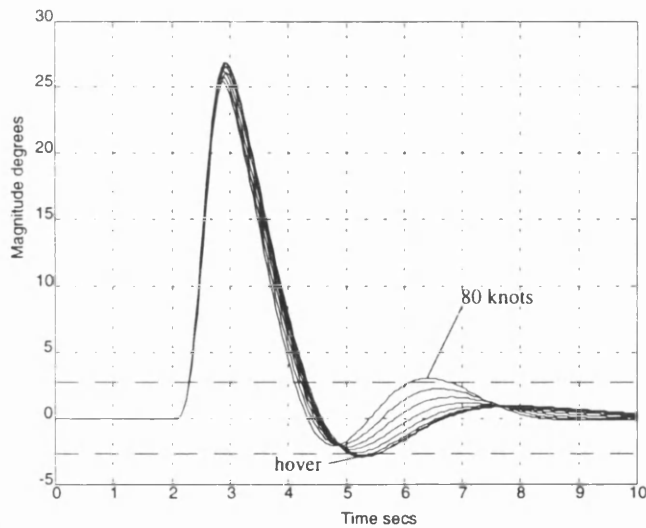
7.8. Handling Qualities Assessment

7.8.1. Attitude Hold

For Attitude Hold response it is required that the pitch attitude returns to within $\pm 10\%$ of the peak excursion, following a pulse input, in less than 20 seconds for UCE=1. The roll attitude is required to return to within 10% of peak in less than 10 seconds

This test is performed using the non-linear helicopter model HELISIM. The pulse input used in this case is of duration 0.4 seconds and height 75° .

It is seen from Figure 7.20 that the attitudes return to within 10% of the peak excursion within 10 seconds. Level 1 requirements for Attitude Hold are met for both the pitch and roll attitudes. Note that the input is applied after 2 seconds and the responses are referred to a zero datum for clarity. The reason for the 2 second delay is to check the trim of the helicopter.



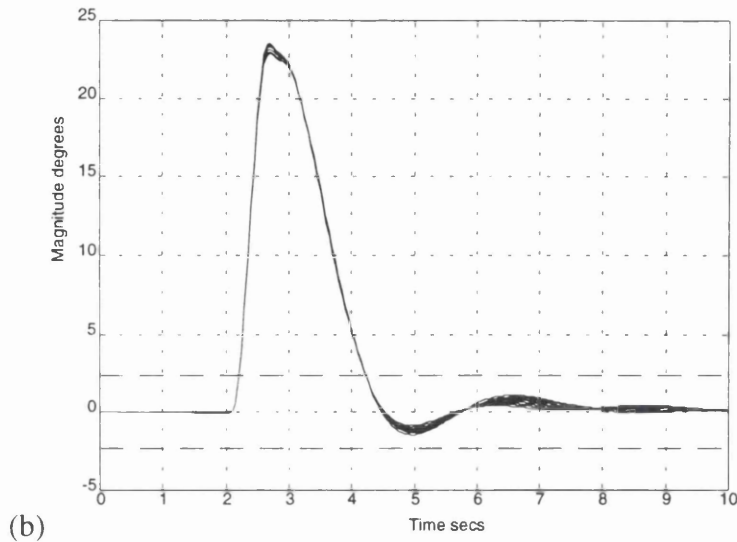
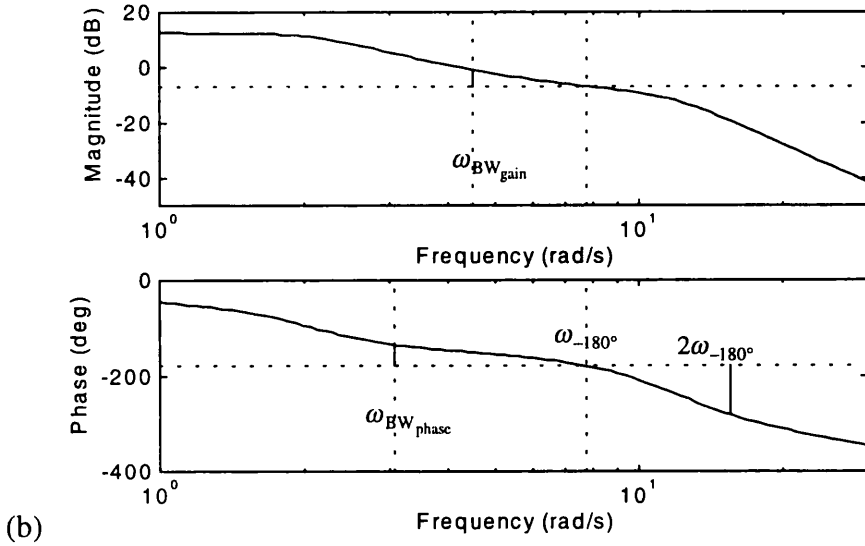
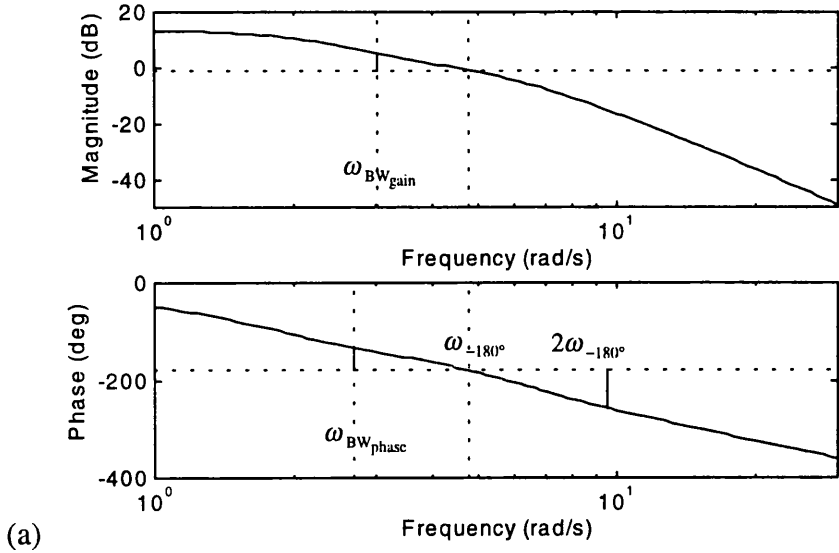


Figure 7.20. Non-linear response of (a) pitch attitude to commanded pulse from hover to 80 knots, (b) roll attitude to commanded pulse from hover to 80 knots.

7.8.2. Small Amplitude Attitude Changes

As mentioned in Chapter 2, the criterion for small amplitude attitude changes is measured in terms of Handling Qualities bandwidths and phase delays. The measurements are taken from the closed-loop frequency responses of the attitudes due to their primary inputs, i.e. $\theta/\delta_{\text{long}}$, ϕ/δ_{lat} and $\psi/\delta_{\text{tail}}$. Figure 7.21 shows the bode plots of $\theta/\delta_{\text{long}}$, ϕ/δ_{lat} and $\psi/\delta_{\text{tail}}$ at 30 knots. Shown on Figure 7.21 are the phase limited bandwidths and the gain limited bandwidth. It is seen that each response is phase limited.



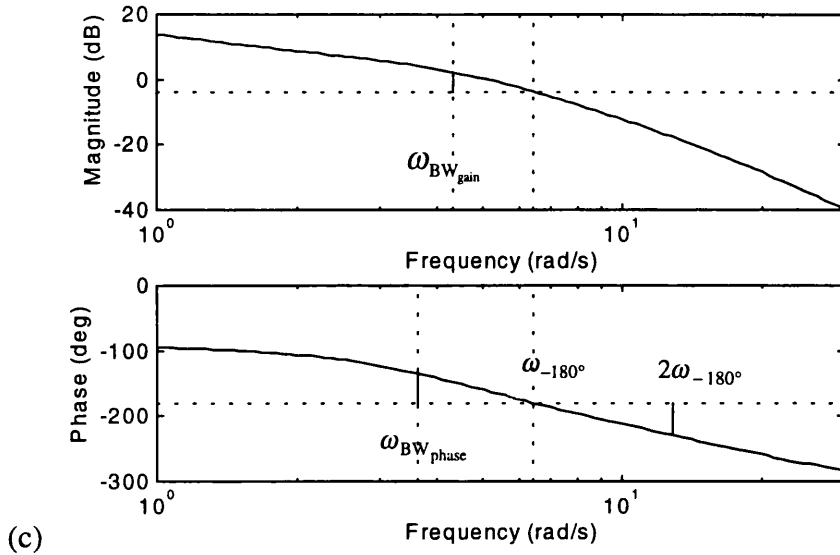


Figure 7.21. Bode plots of (a) $\theta/\delta_{\text{long}}$, (b) ϕ/δ_{lat} , (c) $\psi/\delta_{\text{tail}}$ at 30 knots, with Handling Qualities parameters shown.

It is seen from Figure 7.21 that the phase limited bandwidth is less than the gain limited bandwidth for each response and so the phase limited bandwidth is defined as the Handling Qualities bandwidth. The pilot therefore has at least 6dB of gain margin available in each attitude axis which reduces the risk of pilot induced oscillations when manoeuvring aggressively. Figure 7.22 shows the small amplitude criteria from hover to 80 knots for target acquisition and tracking in low speed and air combat in forward flight, the most stringent requirements, which share the same boundaries. It is seen that Level 1 is met for all three attitude responses from hover to 80 knots.

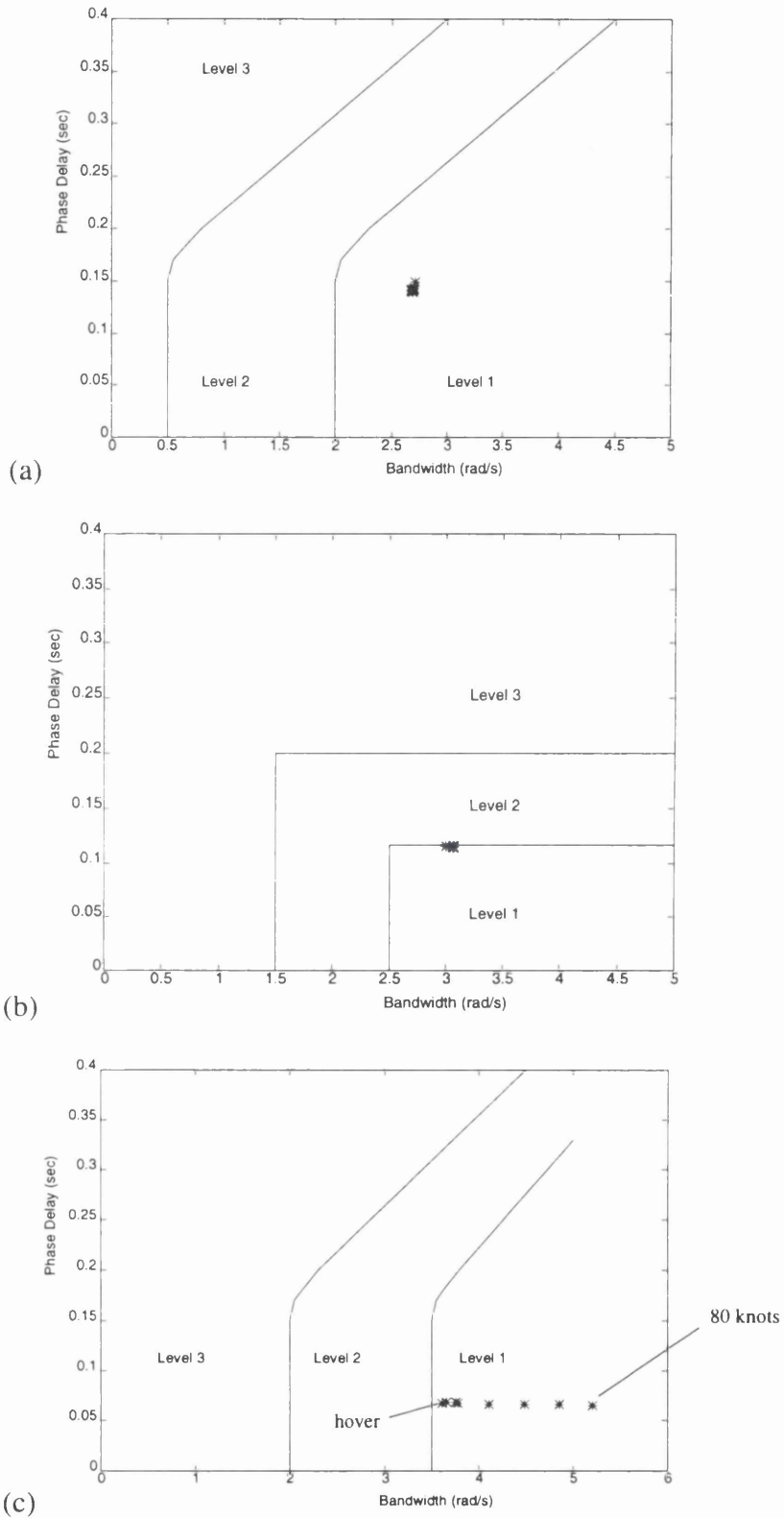


Figure 7.22. Handling Qualities bandwidth and phase delay assessment for Pitch attitude, (b) Roll attitude, (c) Yaw attitude.

(a)

7.8.3. Mid Term Response

The Mid-Term response relates to the effective damping factor of the pitch and roll attitudes in response to pulse controller inputs in the appropriate axis. To meet Level 1 the effective damping factor must be greater than 0.35. Figure 7.23 shows the effective damping factors of the pitch and roll attitudes in response to pulse inputs from hover to 40 knots, the hover and low speed criterion. The 'stars' are the pitch responses and the 'crosses' are the roll responses. Figure 7.24 shows the effective damping factors of the roll attitude response to a pulse input from 50 to 80 knots, the forward flight criterion. The responses are seen to be within the Level 1 region.

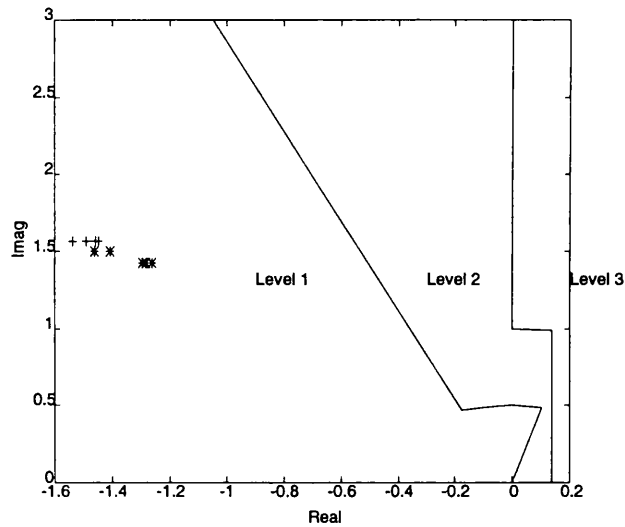


Figure 7.23. Mid-Term assessment of pitch and roll attitude responses.
Hover and low speed.

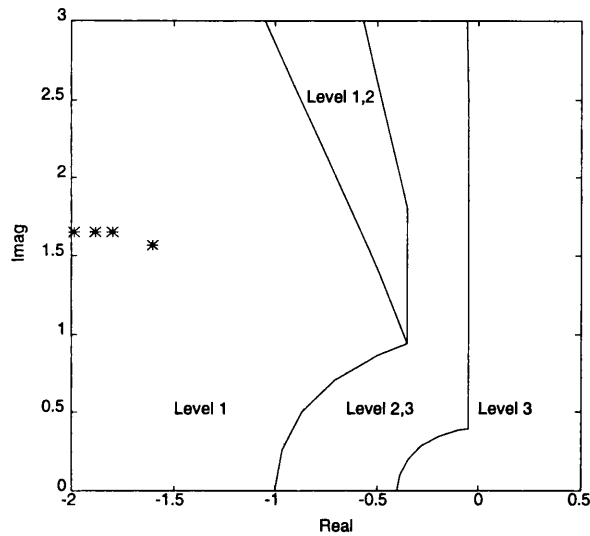


Figure 7.24. Mid-Term assessment of roll attitude response. Forward flight.

7.8.4. Interaxis Coupling

The hover and low speed flight regime places requirements on the yaw rate due to collective. Figure 7.25 shows the yaw rate due to collective responses from hover to 40 knots. It is seen that Level 1 is met.

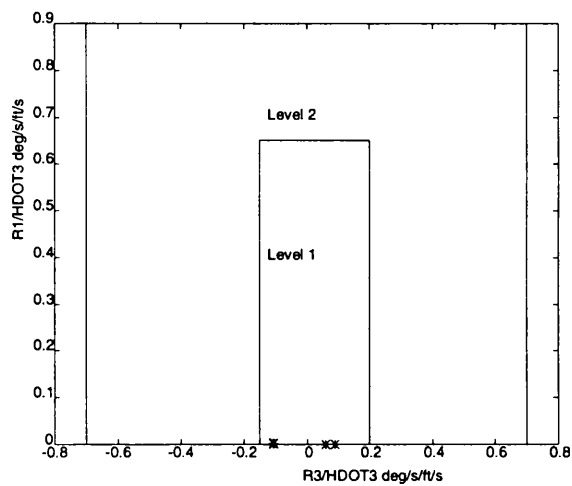


Figure 7.25. Assessment of yaw rate due to collective.

The requirements on pitch due to roll and roll due to pitch state that to meet Level 1 the peak off-axis response over the first four seconds must be less than 25% of the on-axis response at 4 seconds. Figure 7.26 shows the pitch and roll responses due to commanded attitude step inputs of 30° in δ_{long} and δ_{lat} respectively. It is seen that the coupling in each case is less than 25%.

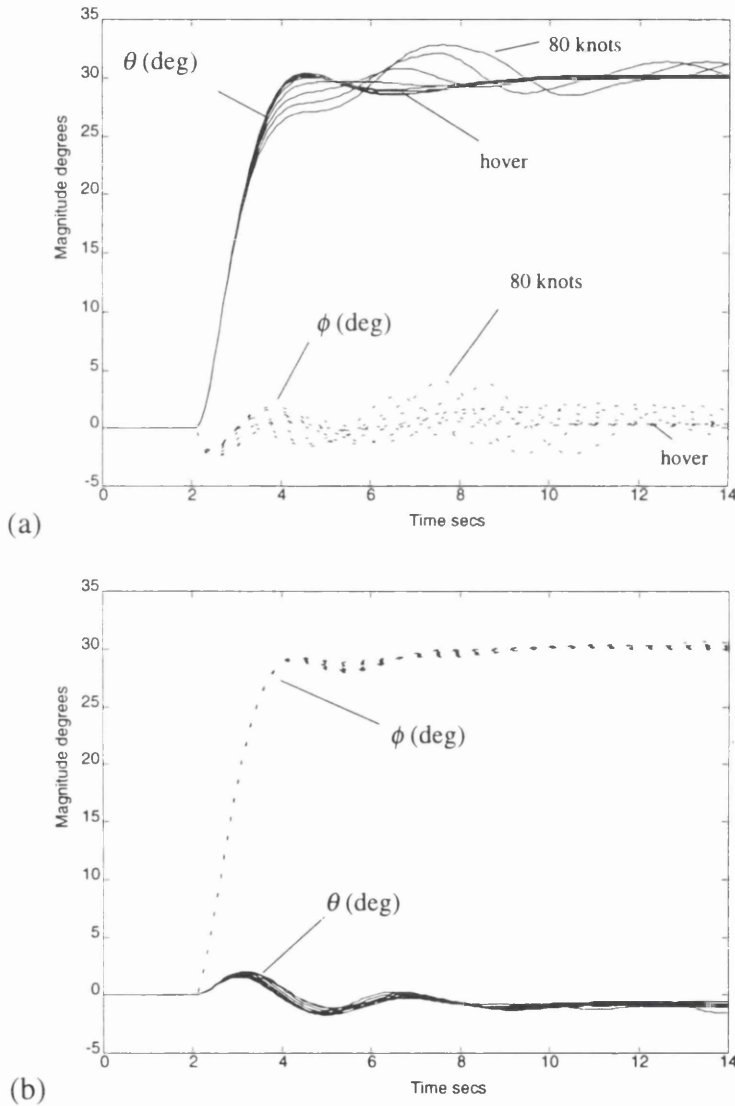


Figure 7.26. (a) Non-linear response of commanded pitch attitude step of 30° .
 (b) Non-linear response of commanded roll attitude step of 30° .

In forward flight there is a requirement on the ratio of the peak change in pitch attitude and the peak normal acceleration for collective inputs. For large collective inputs the

absolute value of the peak change in pitch attitude, θ_{peak} , to the peak change in normal acceleration, $n_{z_{\text{peak}}}$, should not be greater than 0.5 deg/ft/sec^2 in the up direction.

Table 7.14 shows $\left| \theta_{\text{peak}} / n_{z_{\text{peak}}} \right|$ from 50 to 80 knots for a commanded height rate step of 30 ft/s. It is seen that Level 1 is met.

Table 7.14. Values of $\left| \theta_{\text{peak}} / n_{z_{\text{peak}}} \right|$ for commanded height rate step of 30 ft/s.

| Forward Velocity (knots) | $\left \theta_{\text{peak}} / n_{z_{\text{peak}}} \right $ (deg/ft/sec ²) |
|--------------------------|--|
| 50 | 0.1964 |
| 60 | 0.2188 |
| 70 | 0.2368 |
| 80 | 0.2530 |

7.8.5. Response to Collective

In hover and low speed flight, the height rate response is to have a qualitative first order appearance for the first five seconds following a step input on the collective inceptor. The response is to be fitted to an ideal first order response and have a coefficient of determination between 0.97 and 1.03. In addition, the equivalent rise time must be less than 5 secs and the equivalent time delay must be less than 0.2 secs to meet Level 1. Using a commanded height rate step of 5 ft/s, Table 7.15 shows the spread of the coefficient of determination (CD), equivalent rise time, $T_{\dot{h}_{\text{eq}}}$, and equivalent time delay, $\tau_{\dot{h}_{\text{eq}}}$, from hover to 40 knots. Level 1 is met for all criteria.

Table 7.15. Height rate response parameters from hover to 40 knots.

| | CD | $T_{i_{eq}}$ | $\tau_{i_{eq}}$ |
|-------------------------|-------------|--------------|-----------------|
| \dot{h}/δ_{coll} | 0.987-0.992 | 1.593-1.715 | 0.170-0.191 |

7.9. Summary

This Chapter has assessed the application of ICAD to the design of a helicopter ACAH system at 30 knots straight and level flight. It was found that by blending angular rates to their corresponding attitudes phase lead was conveniently made available to the feedback system. However, the body referenced angular rates are not the exact derivatives of their corresponding earth referenced attitudes and it was found that one must assess the sensitivity of the combination, particularly at low frequencies where the pitch and roll angular rates are effectively the derivative of the rate of change of the heading angle.

ICA established that the desired Channel bandwidths could be achieved using a diagonal control law. However, a possible lack of stability robustness due to loop interaction was observed at low frequencies which could introduce low frequency unstable modes. As this lack of robustness occurred at frequencies below 0.15 rad/s it was not regarded as being a problem due to the fact that the pilot is capable of stabilising low frequency unstable modes with a minimal increase in workload. It was shown that a ‘worse case’ divergence was fairly benign.

Although the fixed diagonal control law had only 11 states and the two element pre-filter had only 4 states, the system was found to meet Level 1 Handling Qualities Requirements from hover to 80 knots for both the small amplitude and moderate amplitude criteria, showing that high order complex control is not necessary to achieve high performance.

In conclusion, ICAD has been found to be very well suited to the design of a helicopter ACAH system.

8.1. Introduction

Rate systems offer the least stabilisation of all response types (ADS-33D [3]) but are sufficient to meet Level 1 Handling Qualities requirements in a good visual cue environment (UCE=1), for all Mission Task Elements (MTEs) where the pilot is fully attentive to completion of the task. Rate systems are desirable where high agility is required.

The structure of this Chapter is as follows. Section 8.2 considers what is required of the design of a rate system and determines specifications to meet these requirements. Section 8.3 performs an approximate sensitivity analysis of the rate system. Section 8.4 considers the behaviour of the system at zero frequency. Section 8.5 determines the achievable performance of the feedback control law. Section 8.6 presents the control law. Section 8.7 assesses the feedback system using ICA. Section 8.8 assesses the Handling Qualities.

8.2. Design Considerations

Before proceeding with the analysis of the system it is relevant to consider what is required to be achieved by the design before it is determined by analysis whether these requirements are attainable.

The first requirement of the design is that it is a Rate Command system. i.e. a commanded step input will yield a proportional rate in the appropriate axis. Although there is no requirement in ADS-33D as to the duration of time that the proportional rate must last, let us say for a commanded step input the corresponding rate should hold for at least 6 seconds. This is more than adequate as rate responses, especially large rate responses, are unlikely to be required for more than a few seconds.

The Handling Qualities bandwidths for the pitch, roll and yaw attitudes are required to be Level 1. Because the system to be designed is a rate system, appropriate consideration must be made to the bandwidths of the rate Channels as the closed-loop rate responses will be different to the closed-loop attitude responses. The technique described in Section 7.2 can be used to determine the approximate open-loop Channel specifications to achieve Level 1 phase bandwidth requirements. These specifications are listed in Table 8.1.

Table 8.1. Approximate open-loop Channel specifications.

| | ω_{0dB} (rad/s) | ω_{-180° (rad/s) | $\omega_{BW_{phase}}$ (rad/s) | PM (deg) | GM (dB) |
|-----------|------------------------|-------------------------------|-------------------------------|----------|---------|
| Channel 1 | 1.0 | × | n/a | 55.0 | 20.0 |
| Channel 2 | 3.0 | 12.0 | 2.4 | 55.0 | 10.0 |
| Channel 3 | 3.5 | 13.0 | 2.8 | 55.0 | 10.0 |
| Channel 4 | 5.0 | 20.0 | 4.0 | 55.0 | 20.0 |

8.3. Approximate Sensitivity Analysis

The rotorcraft model is a 19th order state space representation of a typical combat rotorcraft trimmed at 30 knots forward flight. The model has nine rigid body states, 6 rotor states and 4 actuator states. The model is given in Appendix III.

The rate system is given in transfer function matrix form by,

$$G = C_{\text{rate}}(sI - A)^{-1}B \quad (8.1)$$

hence,

$$\begin{bmatrix} \dot{h} \\ q \\ p \\ r \end{bmatrix} = G \begin{bmatrix} \theta_0 \\ \theta_{1s} \\ \theta_{1c} \\ \theta_{0T} \end{bmatrix} = \begin{bmatrix} g_{11} & g_{12} & g_{13} & g_{14} \\ g_{21} & g_{22} & g_{23} & g_{24} \\ g_{31} & g_{32} & g_{33} & g_{34} \\ g_{41} & g_{42} & g_{43} & g_{44} \end{bmatrix} \begin{bmatrix} \theta_0 \\ \theta_{1s} \\ \theta_{1c} \\ \theta_{0T} \end{bmatrix} \quad (8.2)$$

The structure of G is shown in Table 9.2.

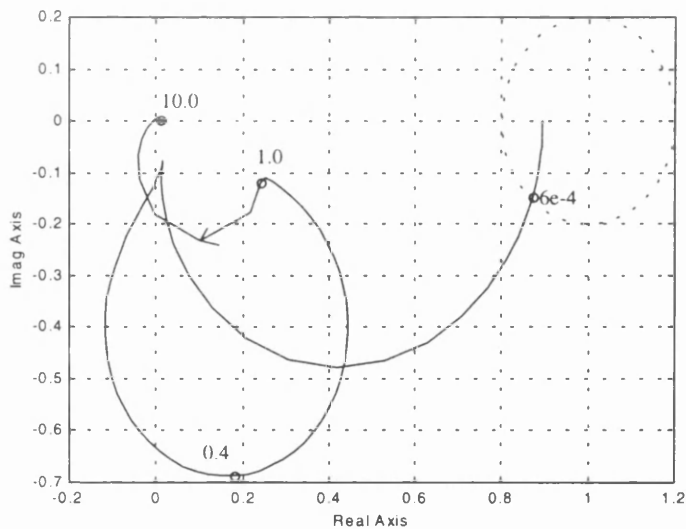
Table 8.2. Structure of G .

| | RHP Transmission Zeros (rad/s) | RHP Eigenvalues (rad/s) |
|-----|--------------------------------|-------------------------|
| G | 7.2150e-12 2.4175e-14 | 9.1439e-2 ± 4.6032e-1j |

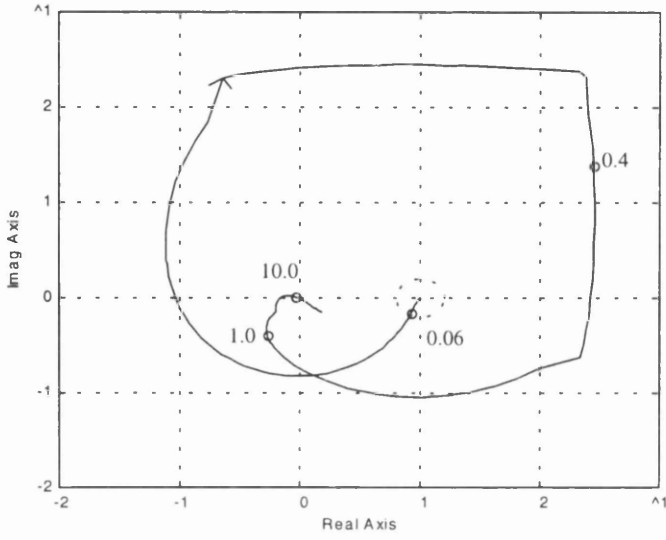
It is seen from Table 8.2 that the system has two RHP transmission zeros but that they are extremely close to the origin. It is likely that these transmission zeros are at zero rad/s exactly and it is important to determine analytically if this is so, as it may have consequences for the interpretation of any results obtained within the ICAD framework. This is dealt with in the next Section.

The approximate sensitivity analysis involves inspecting the approximate Channel MSFs defined in Chapter 3 to determine whether there is a potential robustness problem due to the multivariable structure of the helicopter.

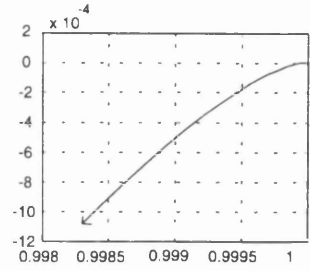
Figure 8.1 shows the Nyquist plots of the approximate MSFs $\hat{\Gamma}_i$, $i=1..4$. It is seen that all the MSFs are within the non-robust region at low frequencies only, $\hat{\Gamma}_4$ being in the non-robust region for the widest spectrum, up to a frequency of 0.15 rad/s. This means that the rate command system will potentially suffer from a stability robustness problem at frequencies not exceeding 0.15 rad/s, if high gain feedback control is implemented. As mentioned in Chapter 6, this potential lack of stability robustness at low frequency is not important as a pilot can stabilise any low frequency unstable modes, which may develop, with a minimal increase in workload. An additional observation of interest is that the low frequency limits of $\hat{\Gamma}_j$, $j=2..4$, approach the (1,0) point *very* closely at low frequencies and look as though they may be approaching the (1,0) point exactly. This low frequency behaviour will be investigated in more detail in the next Section.



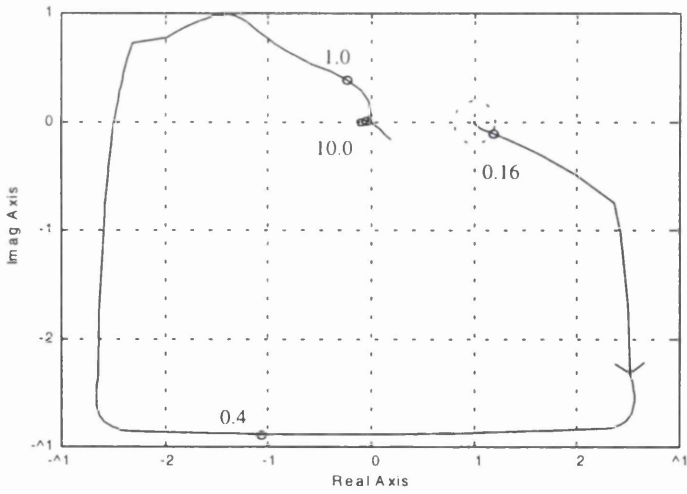
(a)



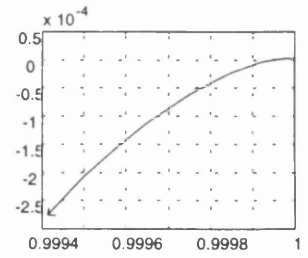
(b)



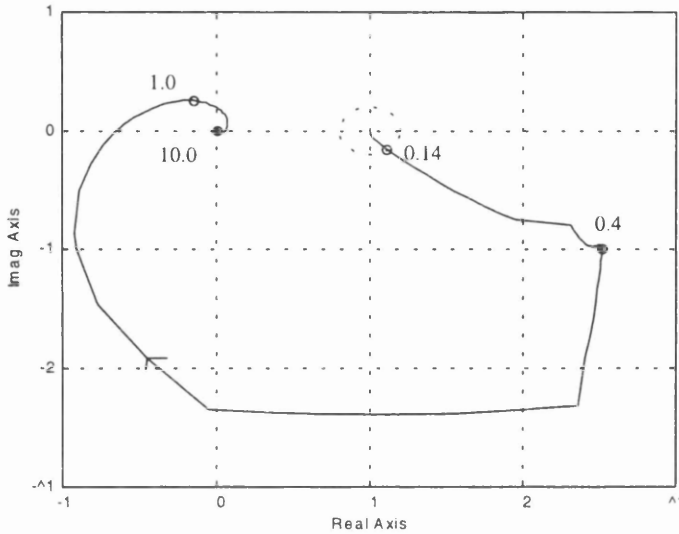
(b₁)



(c)



(c₁)



(d)

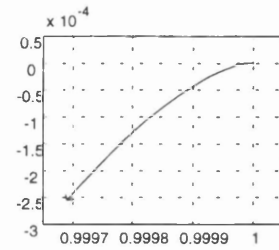
(d₁)

Figure 8.1. Nyquist plot of (a) $\hat{\Gamma}_1$, (b) $\hat{\Gamma}_2$, (b₁) Expansion of (1,0) region of (b), (c) $\hat{\Gamma}_3$, (c₁) Expansion of (1,0) region of (c), (d) $\hat{\Gamma}_4$, (d₁) Expansion of (1,0) region of (d).

(plots are shown up to 30 rad/s, frequencies shown are in rad/s)

8.4. System Behaviour at Zero Frequency

In order to investigate the transmission zeros of the system and the low frequency behaviour of $\hat{\Gamma}_j$, $j=2..4$, the state space model of the rigid body dynamics only will be investigated. This is sufficient as it is the rigid body states that are of interest, and as the rotor and actuator modes are faster than the rigid body modes they have negligible influence on the low frequency dynamics. In addition, the mathematics are simplified considerably by considering rigid body states only.

The transmission zeros of a state space system are the roots of the determinant of the Rosenbrock system matrix \tilde{N} , where,

$$\tilde{N} = \begin{bmatrix} sI - A & B \\ -C & D \end{bmatrix} \quad (8.3)$$

Expanding \tilde{N} symbolically,

$$\tilde{N} = \begin{bmatrix} s - a_{11} & a_{12} & a_{13} & a_{14} & a_{15} & a_{16} & 0 & 0 & b_{11} & b_{12} & b_{13} & 0 \\ a_{21} & s - a_{22} & a_{23} & a_{24} & a_{25} & a_{26} & a_{27} & 0 & b_{21} & b_{22} & b_{23} & 0 \\ a_{31} & a_{32} & s - a_{33} & 0 & a_{35} & a_{36} & 0 & 0 & b_{31} & b_{32} & b_{33} & 0 \\ 0 & 0 & a_{43} & s & 0 & 0 & 0 & a_{48} & 0 & 0 & 0 & 0 \\ a_{51} & a_{52} & a_{53} & a_{54} & s - a_{55} & a_{56} & a_{57} & a_{58} & b_{51} & b_{52} & b_{53} & b_{54} \\ a_{61} & a_{62} & a_{63} & 0 & a_{65} & s - a_{66} & 0 & a_{68} & b_{61} & b_{62} & b_{63} & b_{64} \\ 0 & 0 & a_{73} & 0 & 0 & a_{76} & s & a_{78} & 0 & 0 & 0 & 0 \\ a_{81} & a_{82} & a_{83} & 0 & a_{85} & a_{86} & 0 & s - a_{88} & b_{81} & b_{82} & b_{83} & b_{84} \\ -c_{11} & -c_{12} & 0 & -c_{14} & -c_{15} & 0 & -c_{17} & 0 & 0 & 0 & 0 & 0 \\ 0 & 0 & -c_{23} & 0 & 0 & 0 & 0 & 0 & 0 & 0 & 0 & 0 \\ 0 & 0 & 0 & 0 & 0 & -c_{36} & 0 & 0 & 0 & 0 & 0 & 0 \\ 0 & 0 & 0 & 0 & 0 & 0 & 0 & -c_{48} & 0 & 0 & 0 & 0 \end{bmatrix} \quad (8.4)$$

Consider the case where $s = 0$. \tilde{N} has two linearly dependent rows, row 10 and row 11. That is, these two rows can be described by a scaled combination of other rows. The rank of this matrix is therefore deficient by two, which means that there are two transmission zeros at $\omega = 0$. The linear dependence will now be shown.

$$\begin{bmatrix} 0 \\ 0 \\ -c_{23} \\ 0 \\ 0 \\ 0 \\ 0 \\ 0 \\ 0 \\ 0_{4,1} \end{bmatrix}' = -\frac{c_{23}}{a_{43}} \begin{bmatrix} 0 \\ 0 \\ a_{43} \\ 0 \\ 0 \\ 0 \\ 0 \\ a_{48} \\ 0_{4,1} \end{bmatrix}' - \frac{c_{23}a_{48}}{c_{48}a_{43}} \begin{bmatrix} 0 \\ 0 \\ 0 \\ 0 \\ 0 \\ 0 \\ 0 \\ -c_{48} \\ 0_{4,1} \end{bmatrix}' \quad (8.5)$$

$$\begin{bmatrix} 0 \\ 0 \\ 0 \\ 0 \\ 0 \\ -c_{36} \\ 0 \\ 0 \\ 0 \\ 0_{4,1} \end{bmatrix}' = -\frac{c_{36}}{a_{76}} \begin{bmatrix} 0 \\ 0 \\ a_{73} \\ 0 \\ 0 \\ a_{76} \\ 0 \\ a_{78} \\ 0_{4,1} \end{bmatrix}' + \frac{c_{36}a_{73}}{a_{76}a_{43}} \begin{bmatrix} 0 \\ 0 \\ 0 \\ 0 \\ 0 \\ 0 \\ 0 \\ a_{48} \\ 0_{4,1} \end{bmatrix}' - \frac{(c_{36}a_{78}a_{43} - c_{36}a_{73}a_{48})}{a_{76}a_{43}c_{48}} \begin{bmatrix} 0 \\ 0 \\ 0 \\ 0 \\ 0 \\ 0 \\ 0 \\ -c_{48} \\ 0_{4,1} \end{bmatrix}' \quad (8.6)$$

Note that the linear dependence is not a function of the B matrix.

Now that it has been shown that the frequency of two of the transmission zeros is indeed *exactly* zero rad/s it is of importance to assess the behaviour of the MSFs at $\omega = 0$.

The approximate MSFs of the 4 Channels are,

$$\hat{T}_i = \frac{|G_i|}{g_{ii}|G^i|}, \quad i = 1..4 \quad (8.7)$$

where G_i is G with element (i,i) set to zero, G^i is G with row i and column i removed and g_{ii} is element (i,i) of G .

Consider the Rosenbrock system matrix (RSM) of the G^i , $i = 1..4$. The RSM of G^1 is \tilde{N} with row 9 and column 9 removed. This subsystem has two linearly dependent rows, the rows containing $-c_{23}$ and $-c_{36}$, and so has two transmission zeros at $\omega = 0$. Inspection of Eqns (8.10) and (8.11) make this apparent as row 10 and row 11 of \tilde{N} do not depend on row 9 or column 9. The RSM of G^2 is \tilde{N} with row 10 and column 10 removed. This subsystem has one linearly dependent row, the row containing $-c_{36}$, and so has one transmission zero at $\omega = 0$. This is apparent as row 11 does not depend on row 10 or column 10. The RSM of G^3 is \tilde{N} with row 11 and column 11 removed. This subsystem has one linearly dependent row, the row containing $-c_{23}$, and so has one transmission zero at $\omega = 0$. This is apparent as row 10 does not depend on row 11 or column 11. Finally, the RSM of G^4 is \tilde{N} with row 12 and column 12 removed. As Eqns (8.5) and (8.6) are both dependent on c_{48} , which is not included in G^4 , it may seem that G^4 has no linearly dependent rows. However, row 11 of G^4 can also be expressed as,

$$\begin{bmatrix} 0 \\ 0 \\ 0 \\ 0 \\ 0 \\ -c_{36} \\ 0 \\ 0 \\ 0_{4,1} \end{bmatrix}' = -\frac{c_{36}}{a_{76}} \begin{bmatrix} 0 \\ 0 \\ a_{73} \\ 0 \\ a_{76} \\ 0 \\ 0 \\ a_{78} \\ 0_{4,1} \end{bmatrix}' + \frac{c_{36}a_{73}}{a_{76}a_{43}} \begin{bmatrix} 0 \\ 0 \\ a_{43} \\ 0 \\ 0 \\ 0 \\ 0 \\ a_{48} \\ 0_{4,1} \end{bmatrix}' - \frac{(c_{36}a_{78}a_{43} - c_{36}a_{73}a_{48})}{a_{76}a_{43}c_{48}} \begin{bmatrix} 0 \\ 0 \\ -c_{23} \\ 0 \\ 0 \\ 0 \\ 0 \\ 0 \\ 0_{4,1} \end{bmatrix}' \quad (8.8)$$

Eqn (8.13) is not dependent on c_{48} and therefore G^4 has one zero at $\omega = 0$.

Because the G^i , $i = 1..4$, all have at least one zero at the origin then this implies that their determinants at zero frequency are zero.

Therefore,

$$|G(0)| = g_{ii}(0)|G^i(0)| + |G_i(0)| = 0 \quad ,i = 1..m \quad (8.9)$$

Because it has been shown that $|G(0)|$ and the $|G^i(0)|$ are equal to zero then this means that the $|G_i(0)|$ are also equal to zero. Therefore the values of the \hat{T}_i 's are *indeterminate* at zero frequency, i.e. $\hat{T}_i = 0/0 = ?$, if one attempts to calculate the values numerically. However, if one calculates the poles and zeros of \hat{T}_i , exact cancellation between the poles and zeros at the origin will occur and the limits of the \hat{T}_i as s tends to zero can be determined. Of course, it would be a tedious undertaking to attempt to calculate the poles and zeros analytically to determine the exact limits. Computation by computer has been found through experience to be sufficiently accurate for the task, particularly if the state space method described in Chapter 5 is used.

It is found that the limits as s tends to zero of the $(1-\hat{T}_i)s$, $i = 1..4$, are $1.0e-1$, $1e-6$, $1e-8$ and $1e-10$ respectively. It is seen that the limits of the \hat{T}_j 's, $j = 2..4$, are very close to one.

To determine whether the \hat{T}_j 's go to *exactly* (1,0) at zero frequency, consider the linear equations of motion relating the angular rates to the derivatives of the Euler angles,

$$q = \dot{\theta} \cos \Phi_0 + \dot{\psi} \cos \Theta_0 \sin \phi_0 \quad (8.10)$$

$$p = \dot{\phi} - \dot{\psi} \sin \Theta_0 \quad (8.11)$$

$$r = -\dot{\theta} \sin \Phi_0 + \dot{\psi} \cos \Theta_0 \cos \phi_0 \quad (8.12)$$

At zero frequency $\dot{\theta}$ and $\dot{\phi}$ are found to be zero and so q , p and r are given by,

$$(q)_{\omega=0} = (\dot{\psi})_{\omega=0} \cos \Theta_0 \sin \phi_0 \quad (8.13)$$

$$(p)_{\omega=0} = (\dot{\psi})_{\omega=0} \sin \Theta_0 \quad (8.14)$$

$$(r)_{\omega=0} = (\dot{\psi})_{\omega=0} \cos \Theta_0 \cos \phi_0 \quad (8.15)$$

It is seen from Eqns (8.13) to (8.15) that the angular rates at zero frequency are determined exclusively by $\dot{\psi}$, scaled by some constant factor. This means that the limits of the $\hat{\Gamma}_j s$, $j = 2..4$, will tend to exactly (1,0) as s tends to zero. To demonstrate that this is the case, the calculation of the limit of $\hat{\Gamma}_2$ as s tends to zero is shown below.

$$\begin{aligned} [\hat{\Gamma}_2]_{\lim_{s \rightarrow 0}} &= \frac{\begin{vmatrix} \dot{h}_{\delta_{\text{coll}}} & \dot{h}_{\delta_{\text{long}}} & \dot{h}_{\delta_{\text{lat}}} & \dot{h}_{\delta_{\text{tail}}} \\ a\dot{\psi}_{\delta_{\text{coll}}} & 0 & a\dot{\psi}_{\delta_{\text{lat}}} & a\dot{\psi}_{\delta_{\text{tail}}} \\ b\dot{\psi}_{\delta_{\text{coll}}} & b\dot{\psi}_{\delta_{\text{long}}} & b\dot{\psi}_{\delta_{\text{lat}}} & b\dot{\psi}_{\delta_{\text{tail}}} \\ c\dot{\psi}_{\delta_{\text{coll}}} & c\dot{\psi}_{\delta_{\text{long}}} & c\dot{\psi}_{\delta_{\text{lat}}} & c\dot{\psi}_{\delta_{\text{tail}}} \end{vmatrix}}{\begin{vmatrix} \dot{h}_{\delta_{\text{coll}}} & \dot{h}_{\delta_{\text{lat}}} & \dot{h}_{\delta_{\text{tail}}} \\ a\dot{\psi}_{\delta_{\text{long}}} & b\dot{\psi}_{\delta_{\text{coll}}} & b\dot{\psi}_{\delta_{\text{lat}}} & b\dot{\psi}_{\delta_{\text{tail}}} \\ c\dot{\psi}_{\delta_{\text{coll}}} & c\dot{\psi}_{\delta_{\text{lat}}} & c\dot{\psi}_{\delta_{\text{tail}}} \end{vmatrix}} = \dots \\ &= \frac{\begin{vmatrix} \dot{h}_{\delta_{\text{coll}}}/\dot{\psi}_{\delta_{\text{coll}}} & \dot{h}_{\delta_{\text{long}}}/\dot{\psi}_{\delta_{\text{long}}} & \dot{h}_{\delta_{\text{lat}}}/\dot{\psi}_{\delta_{\text{lat}}} & \dot{h}_{\delta_{\text{tail}}}/\dot{\psi}_{\delta_{\text{tail}}} \\ 1 & 0 & 1 & 1 \\ abc\dot{\psi}_{\delta_{\text{long}}} & \dot{\psi}_{\delta_{\text{coll}}} & \dot{\psi}_{\delta_{\text{lat}}} & \dot{\psi}_{\delta_{\text{tail}}} \\ 1 & 1 & 1 & 1 \\ 1 & 1 & 1 & 1 \end{vmatrix}}{\dots \begin{vmatrix} \dot{h}_{\delta_{\text{coll}}}/\dot{\psi}_{\delta_{\text{coll}}} & \dot{h}_{\delta_{\text{lat}}}/\dot{\psi}_{\delta_{\text{lat}}} & \dot{h}_{\delta_{\text{tail}}}/\dot{\psi}_{\delta_{\text{tail}}} \\ abc\dot{\psi}_{\delta_{\text{long}}} & \dot{\psi}_{\delta_{\text{coll}}} & \dot{\psi}_{\delta_{\text{lat}}} & \dot{\psi}_{\delta_{\text{tail}}} \\ 1 & 1 & 1 & 1 \\ 1 & 1 & 1 & 1 \end{vmatrix}} = \dots \\ &= \frac{abc\dot{\psi}_{\delta_{\text{long}}} \dot{\psi}_{\delta_{\text{coll}}} \dot{\psi}_{\delta_{\text{lat}}} \dot{\psi}_{\delta_{\text{tail}}} \cdot 0}{abc\dot{\psi}_{\delta_{\text{long}}} \dot{\psi}_{\delta_{\text{coll}}} \dot{\psi}_{\delta_{\text{lat}}} \dot{\psi}_{\delta_{\text{tail}}} \cdot 0} = \frac{abc\dot{\psi}_{\delta_{\text{long}}} \dot{\psi}_{\delta_{\text{coll}}} \dot{\psi}_{\delta_{\text{lat}}} \dot{\psi}_{\delta_{\text{tail}}}}{abc\dot{\psi}_{\delta_{\text{long}}} \dot{\psi}_{\delta_{\text{coll}}} \dot{\psi}_{\delta_{\text{lat}}} \dot{\psi}_{\delta_{\text{tail}}}} = 1 \end{aligned} \quad (8.16)$$

where $a = \cos \Theta_0 \sin \phi_0$, $b = \sin \Theta_0$ and $c = \cos \Theta_0 \cos \phi_0$.

Because the Nyquist plots of the $\hat{\Gamma}_j s$, $j = 2..4$, are on the (1,0) point at zero frequency, the number of encirclements of the (1,0) point is indeterminate. Hence no information about the structure of the zeros of $(1 - \hat{\Gamma}_j)$ is available if one inspects the Nyquist plots

of the \hat{F}_j s only. This is seemingly an impediment to applying ICA but this will be covered in more detail in the following Section.

8.5. Stabilisation and Potential Performance of the Rate System

From Section 8.2 it was determined that 0dB crossover frequencies of the Channels should respectively be 1 rad/s, 3 rad/s, 3.5 rad/s and 5 rad/s. As mentioned in Chapter 5, for systems whose Channels are defined to have different bandwidths, the numbering of the Channels should be done in the order of lowest bandwidth as Channel 1 and highest bandwidth as Channel 4. It turns out that the requirements of the system naturally impose numbering on the Channels which is compatible with this philosophy.

In order to determine the conditions for closed-loop stability and achievable performance of the system, one expands the determinant of the open-loop system as follows,

$$|G| = g_{11}(1 - \Gamma_1)g_{22}(1 - \Gamma_2)g_{33}(1 - \Gamma_3)g_{44} \quad (8.17)$$

and relates this to the determinant of the return difference which is expanded as follows,

$$|\hat{G}| = [1 + k_1g_{11}(1 - \gamma_1)].[1 + k_2g_{22}(1 - \gamma_{12})].[1 + k_3g_{33}(1 - \gamma_{123})].[1 + k_4g_{44}] \quad (8.18)$$

which can be written as,

$$|\hat{G}| = [1 + C'_1].[1 + C'_2].[1 + C'_3].[1 + C'_4] \quad (8.19)$$

The physical interpretation of the nested Channels is as follows:

C'_1 is the transfer function describing \dot{h} due to δ_{coll} when the height rate loop is open but the pitch rate, roll rate and yaw rate loops are closed. C'_1 is equal to C_1 .

C'_2 is the transfer function describing q due to δ_{long} when the height rate loop and pitch rate loops are open but the roll rate and yaw rate loops are closed.

C'_3 is the transfer function describing p due to δ_{lat} when the height rate, pitch rate and roll rate loops are open but the yaw rate loop is closed.

C'_4 is the transfer function describing r due to δ_{tail} when all the feedback loops are open. C'_4 is equal to $k_4 g_{44}$.

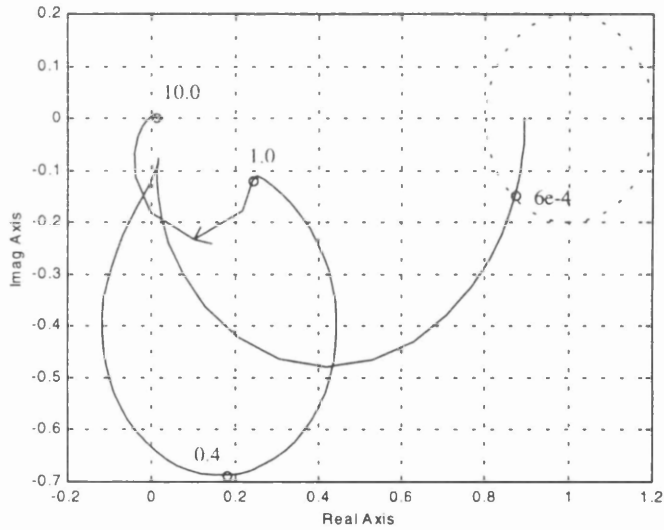
Eqn (8.17) explicitly relates the behaviour of the diagonal transfer function elements and the Γ_j to the structure of $|G|$, the zeros of which are the transmission zeros of the open-loop helicopter. Eqn (8.19) explicitly relates the nested Channels to the structure of $|\hat{G}|$, the zeros of which are the poles of the closed-loop system.

Recall that the system has no RHP transmission zeros. This means that the zeros of $|G|$ are all stable. It is required that the poles of the closed-loop system, and hence the zeros of $|\hat{G}|$, are stable.

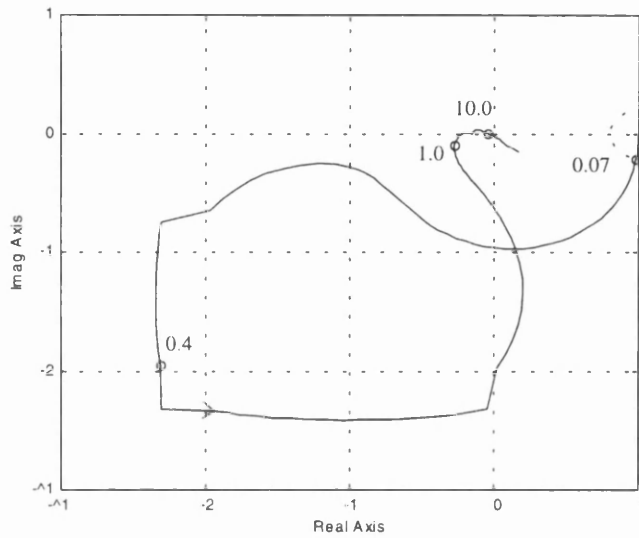
Conditions sufficient for the zeros of $|\hat{G}|$ to be stable are as follows: The $\gamma_{1..i}$ should have the same pole structure and encirclement count of the (1,0) point as the Γ_j . Hence the number of RHPZs of $(1-\gamma_{1..i})$ will be the same as the number of RHPZs of $(1-\Gamma_j)$. In addition, the number of RHPZs of the $(1+C'_j)$ s should be the same as the number of RHPZs of the C'_j s. Note that these conditions are exactly the same as the conditions required to stabilise the ACAH system of Chapter 7.

Figure 8.2 shows the Nyquist plots of Γ_1 , Γ_2 and Γ_3 . Γ_1 , Γ_2 and Γ_3 are written explicitly in Section 7.4. Notice that the magnitude of the MSFs are low at frequencies above 1 rad/s. This means that loop interaction at the desired Channel 0dB crossover frequencies will be low, which will simplify the design process. Table 8.3. shows the structures of the parameters of Eqn (8.17). The nested nature of the Γ_j s, $j = 2..4$, is clearly evident. Recall that the zeros of the $(1-\Gamma_j)$ s contain RHPZs which exactly

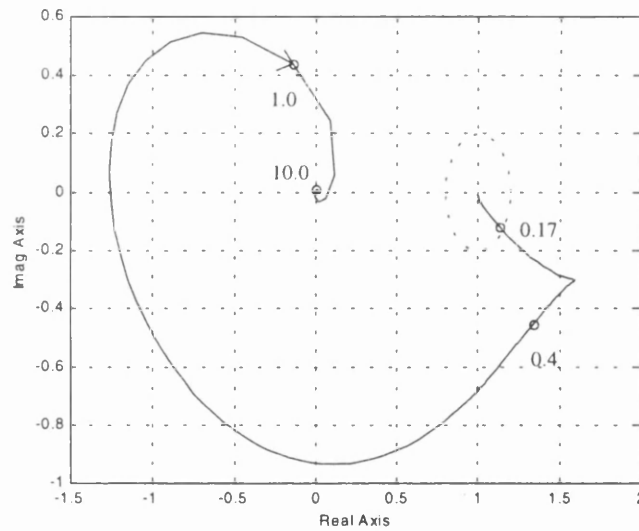
correspond to the RHPPs of the plant. These RHPZs *exactly* cancel with the poles of $g_{22}\dots g_{44}$ and so can be disregarded in the structural assessment. From Table 8.3 it is seen that g_{33} , g_{44} and $(1-T_3)$ have non-cancelling RHPZs and this tells us that *potentially* the plant cannot be stabilised by high performance control of the lateral system only. This observation was also noted for the ACAH system and is due to the unstable poles of the system originating in the longitudinal dynamics. High performance lateral control will therefore be unable to stabilise this mode. However, closure of loops 2, 3 and 4 will potentially stabilise the plant, as will closure of all four loops.



(a)



(b)



(c)

Figure 8.2. Nyquist plots of (a) Γ_1 , (b) Γ_2 and (c) Γ_3 .

(plots are shown up to 30 rad/s. frequencies shown are in rad/s)

Table 8.3. Structure of parameters of Eqn (8.17).

| | RHPZs (rad/s) | RHPPs (rad/s) |
|------------------|--|---|
| $ G $ | – | $9.1439e-2 \pm 4.6032e-1j$ |
| $(1 - \Gamma_1)$ | $9.1439e-2 \pm 4.6032e-1j$ | $9.2078e-2 \pm 3.9896e-1j$ |
| $(1 - \Gamma_2)$ | $9.1439e-2 \pm 4.6032e-1j$ | $3.9680e-2 \pm 4.0827e-1j$ $1.0753e-1$ |
| $(1 - \Gamma_3)$ | $9.1439e-2 \pm 4.6032e-1j$ $3.9680e-2 \pm 4.0827e-1j$ | $1.1510e-1 \pm 4.9125e-1j$ $8.7159e-2 \pm 3.7749e-1j$ $4.0159e-2$ |
| g_{11} | $9.2078e-2 \pm 3.9896e-1j$ | $9.1439e-2 \pm 4.6032e-1j$ |
| g_{22} | $1.0753e-1$ | $9.1439e-2 \pm 4.6032e-1j$ |
| g_{33} | $1.1510e-1 \pm 4.9125e-1j$ | $9.1439e-2 \pm 4.6032e-1j$ |
| g_{44} | $8.7159e-2 \pm 3.7749e-1j$ | $9.1439e-2 \pm 4.6032e-1j$ |

Because Γ_2 and Γ_3 are exactly (1,0) at zero frequency a slight problem is encountered as the zeros of $(1-\Gamma_2)$ and $(1-\Gamma_3)$ cannot be determined by inspection of the Nyquist plots of Γ_2 and Γ_3 alone. However, it is known by direct calculation what the zeros of $(1-\Gamma_2)$ and $(1-\Gamma_3)$ are. For closed-loop stability it is required that the zeros of $(1-\gamma_{12})$ and $(1-\gamma_{123})$ have the same zero structure as $(1-\Gamma_2)$ and $(1-\Gamma_3)$ respectively. To achieve this it is sufficient that $\gamma_{12}(0)$ and $\gamma_{123}(0)$ are exactly equal to one and that γ_{12} and γ_{123} are arbitrarily close to Γ_2 and Γ_3 over the low to mid frequency range. This is done by ensuring that h_2 , h_3 and h_4 are exactly one at zero frequency and that they are arbitrarily close to one over the low to mid frequency range.

To achieve the required zero frequency conditions k_2 , k_3 and k_4 should have integral control and $g_{22}(0)$, $g_{33}(0)$ and $g_{44}(0)$ should be checked to insure that they are non-zero. $g_{22}(0)$, $g_{33}(0)$ and $g_{44}(0)$ were calculated to be -3873.9, 19092.0 and -30423.0 respectively. The zero frequency conditions are therefore achievable.

All that remains is to check that the encirclements of the (1,0) point at high frequencies of the $\gamma_{1..i}$ s are the same as that of the Γ_i s. Figure 8.2 highlights discrete frequency

points on the Γ_i s and it is seen that the high frequency regions of the Γ_i s are comfortably far from the (1,0) point at mid to high frequencies. As the $\gamma_{1..i}$ s will be arbitrarily close to the Γ_i s in the low to mid frequency region and then attenuate to the origin in the high frequency region, the number of encirclement counts of the $\gamma_{1..i}$ s at high frequency will be the same as the Γ_i s.

8.6. Control Law

It is not the aim of this Section to provide a step-by-step description of the design of the control law, but merely to state the control law parameters. The reason for this is because the design *procedure* is identical to the design procedure of the ACAH control law, which is presented in detail in Section 7.5. The step-by-step guide of Section 7.5 can be used as a foundation for the design of control laws for any system which share equivalent conditions for achieving stability and desired performance.

The diagonal control law is given as,

$$k_1 = \frac{0.1(s+1)}{s(s+10)} \quad (8.20)$$

$$k_2 = \frac{0.45(s+1)(s+2)(s+3.4)}{s(s+0.001)(s+8.4)(s+25)} \quad (8.21)$$

$$k_3 = \frac{-0.28(s+0.7)(s+7)}{s(s+0.001)(s+100)} \quad (8.22)$$

$$k_4 = \frac{-(s+1)^2}{s(s+0.001)(s+30)} \quad (8.23)$$

As with the ACAH control law, a decoupling filter was required to reduce the yaw rate due to collective. A shaping filter for the height rate was necessary after implementation of the decoupler. The decoupling filter is given as,

$$d_{\text{yaw_coll}} = \frac{-2s}{(s + 3)(s + 6)} \tag{8.24}$$

and the shaper is given as,

$$s_{\dot{h}} = \frac{1.2(s + 1)}{(s + 0.6)(s + 2)} \tag{8.25}$$

Figure 8.3 shows a block diagram of the complete system.

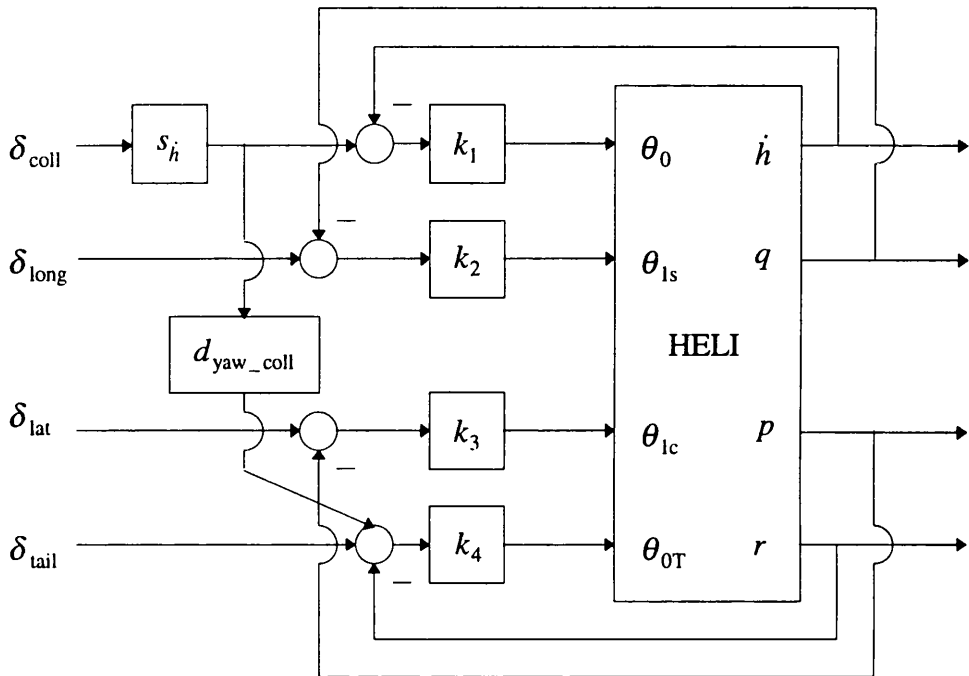
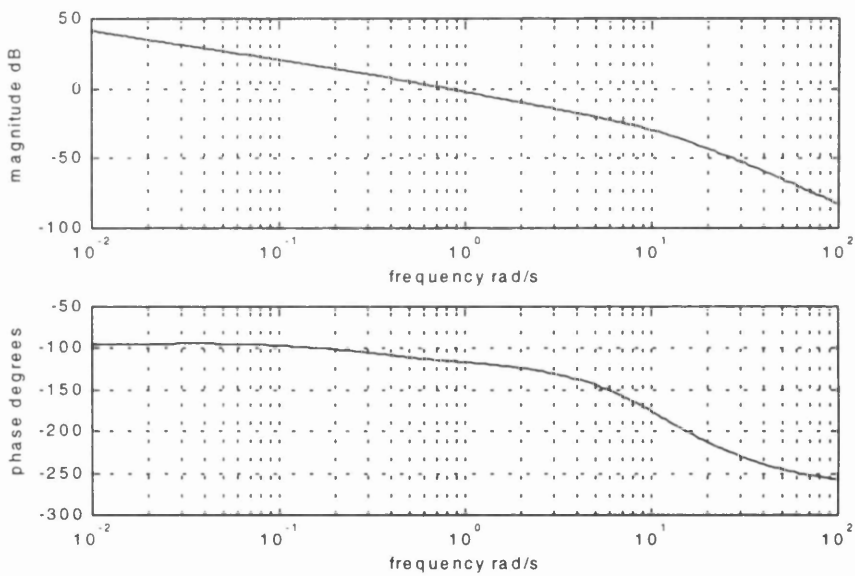


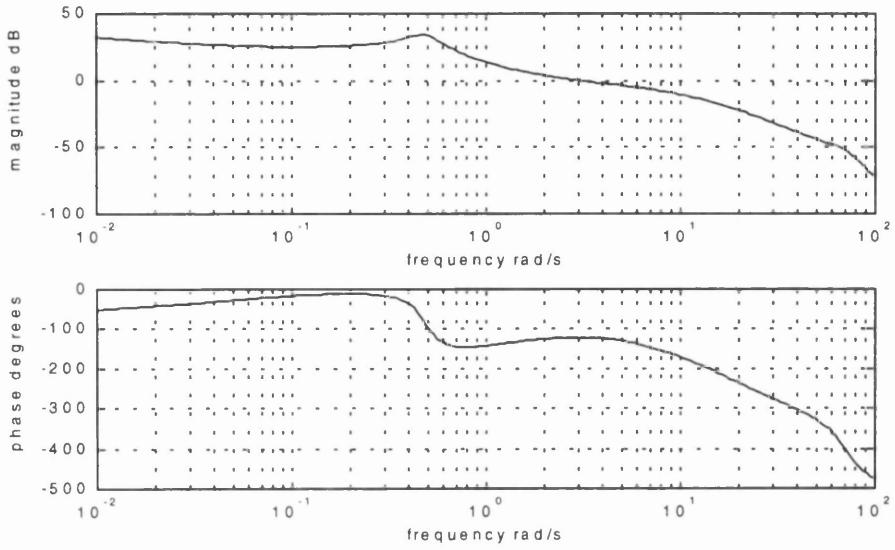
Figure 8.3. Block diagram of Rate Command system.

8.7. Individual Channel Analysis

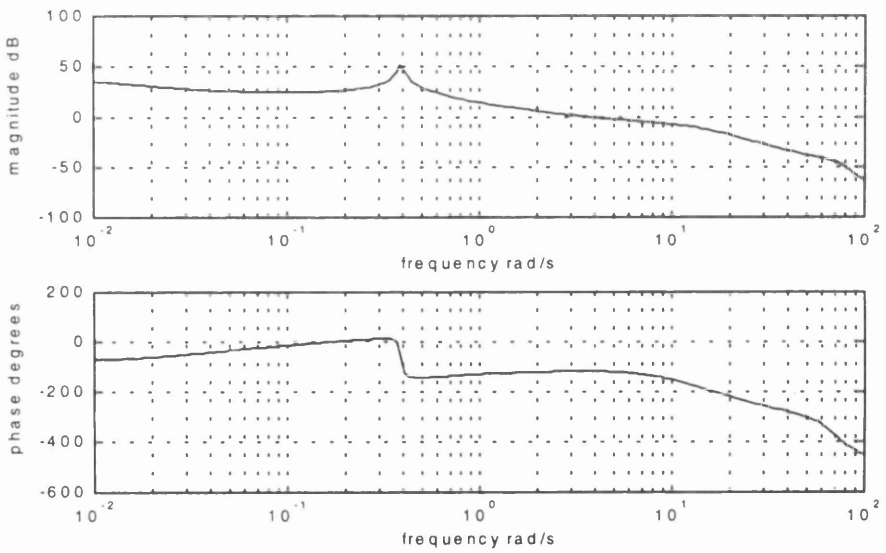
Figure 8.4 shows the bode plots of the Channels and it is seen that they are good by classical design criteria. i.e. high gain at frequencies below crossover (but not at very low frequencies), smooth slope over the 0dB region and steep attenuation of gain at high frequency. Also the gain and phase margins are adequate and the phase of the Channels exhibit adequate 'flatness' in the region of the 0dB frequency. By making the phase as flat as possible in this region the transient response is improved.



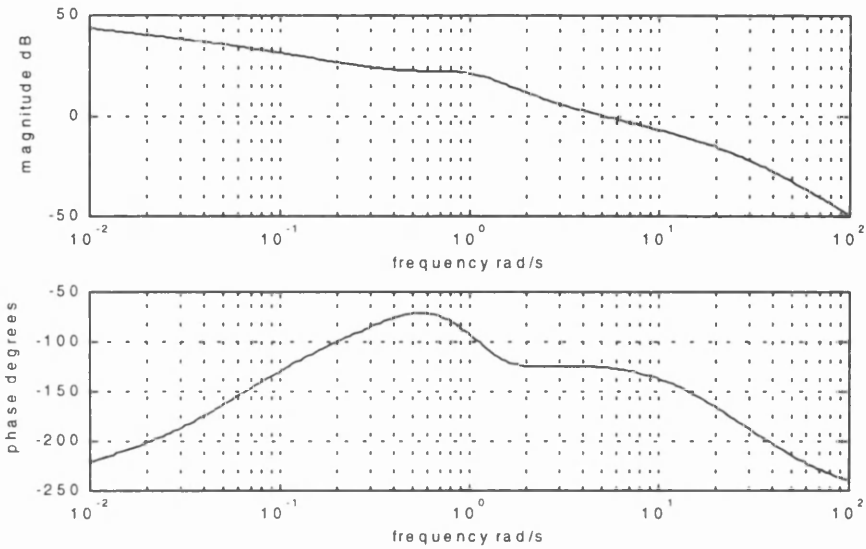
(a)



(b)



(c)



(d)

Figure 8.4. Bode plot of (a) Channel 1, (b) Channel 2, (c) Channel 3, (d) Channel 4.

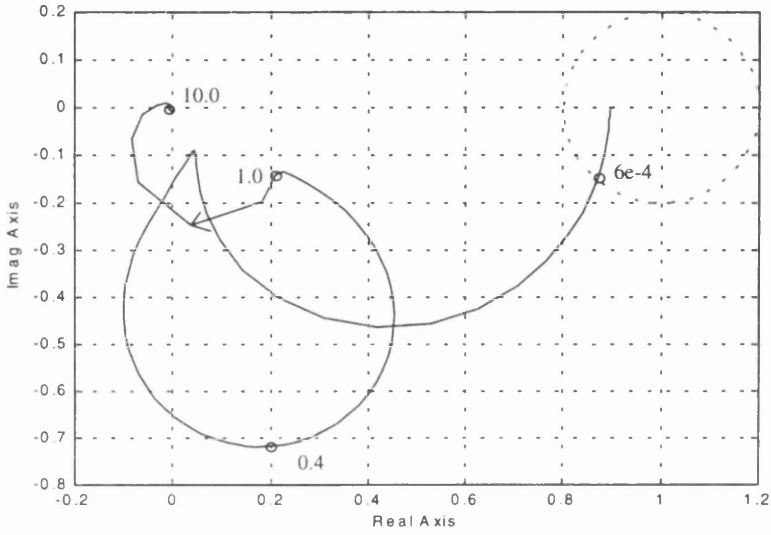
Table 8.4 shows the phase and gain margins and crossover frequencies of the Channels. It is seen that all gain and phase margins are adequate. Also shown on Table 8.4 is the Handling Qualities bandwidths of the closed-loop attitude responses. The bandwidths are phase limited and meet Level 1 requirements.

Table 8.4. Channel parameters of final design

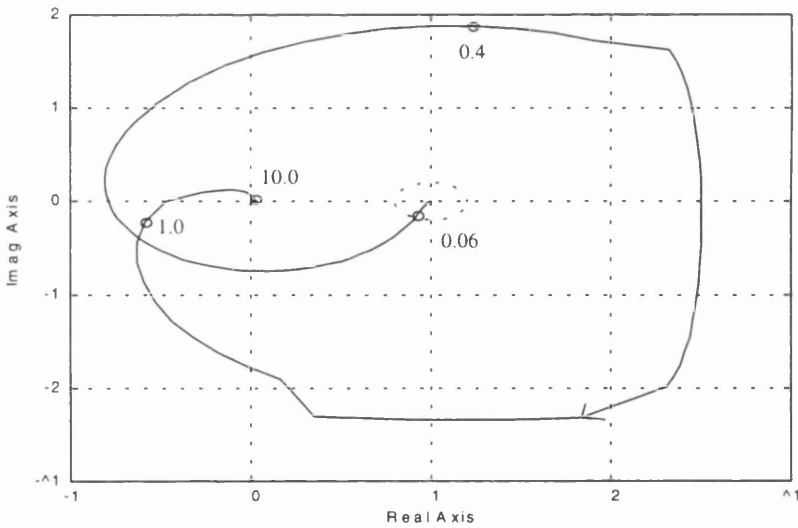
| | ω_{0dB} (rad/s) | ω_{180} (rad/s) | ω_{phase} (rad/s) | PM (deg) | GM (deg) |
|-----------|------------------------|------------------------|--------------------------|----------|----------|
| Channel 1 | 0.8 | n/a | n/a | 64.9 | 30.6 |
| Channel 2 | 3.0 | 11.3 | 2.2 | 59.2 | 12.1 |
| Channel 3 | 3.6 | 13.4 | 2.7 | 63.5 | 10.8 |
| Channel 4 | 5.1 | 26.1 | 3.9 | 54.3 | 20.0 |

However, the Channel gain and phase margins will only be valid as robustness measures if the MSFs of each Channel are sufficiently distant from the (1,0) point at frequencies of importance.

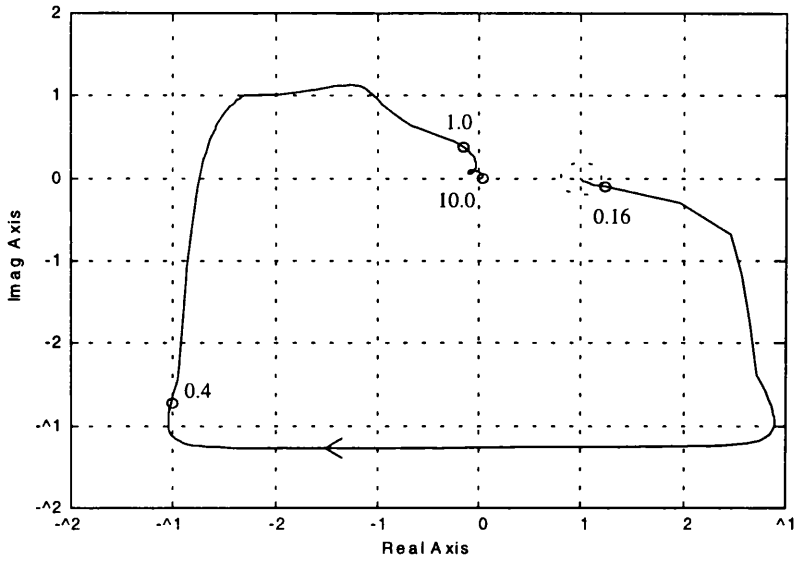
Figure 8.5 shows the actual MSFs of the Channels and it is seen that each MSF enters the non-robust region at low frequencies only. γ_3 is in the non-robust region for the widest spectrum; up to a frequency of 0.16 rad/s.



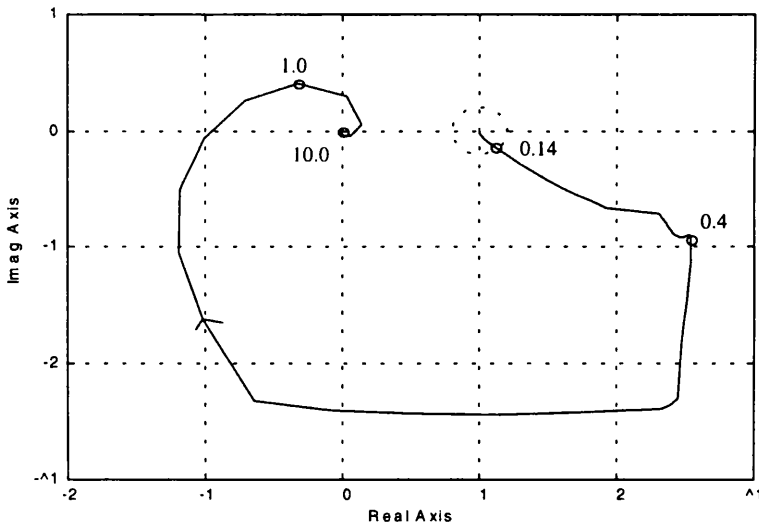
(a)



(b)



(c)



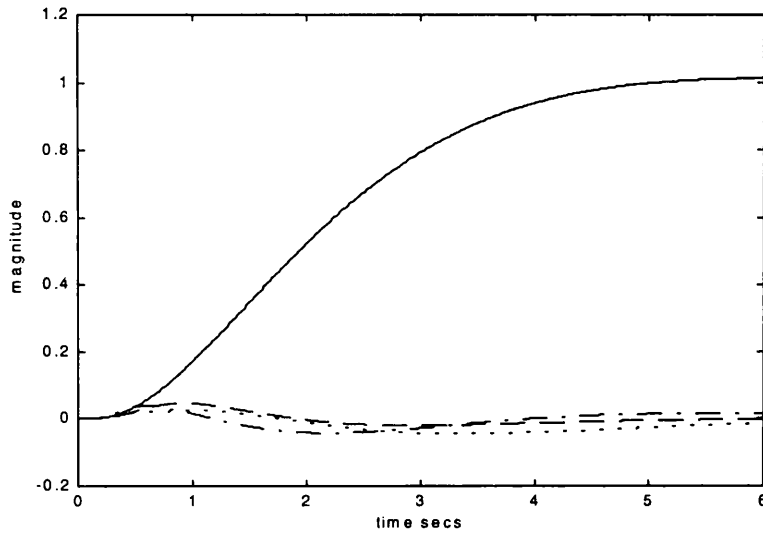
(d)

Figure 8.5. Nyquist plot of (a) γ_1 , (b) γ_2 , (c) γ_3 , (d) γ_4 .
(frequencies shown are in rad/s)

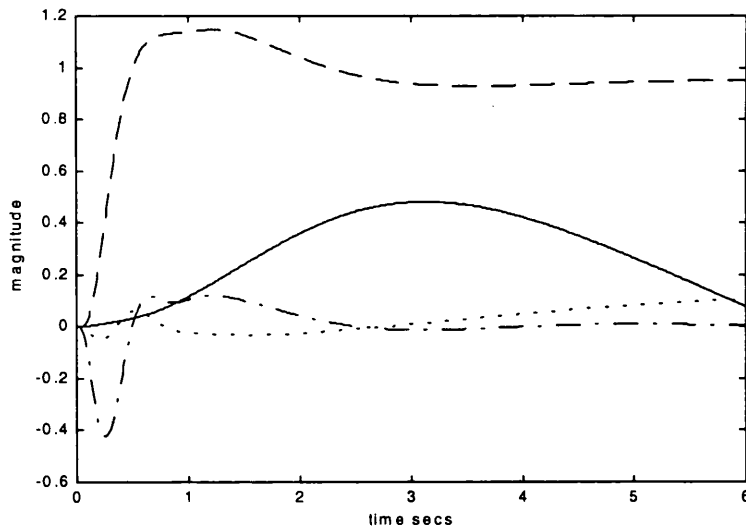
There is therefore a possible lack of stability robustness due to loop interaction at low frequency which could introduce low frequency unstable modes. As this lack of robustness occurs at frequencies below 0.16 rad/s it is not regarded as being a problem due to the fact that the pilot is capable of stabilising low frequency unstable modes with

a minimal increase in workload. The gain and phase margins of the Channels are therefore valid as robustness measures and the Rate Command system can be regarded as possessing stability robustness.

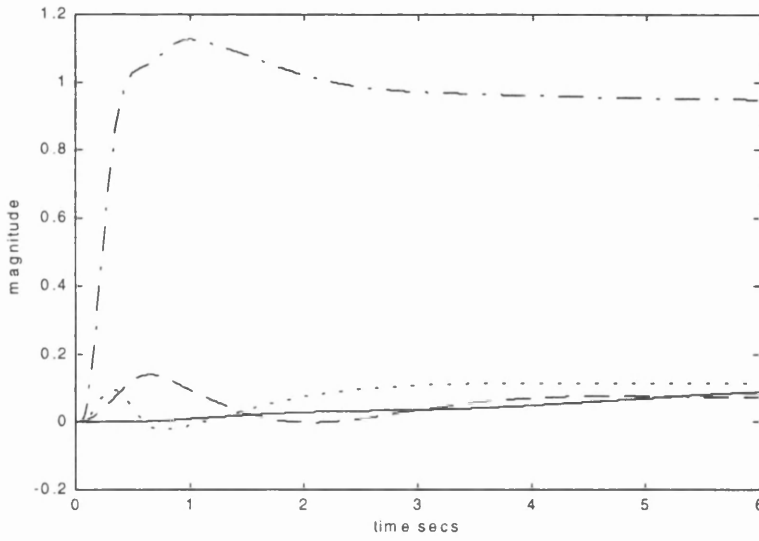
Figure 8.6 shows small amplitude step responses of the linear system at 30 knots.



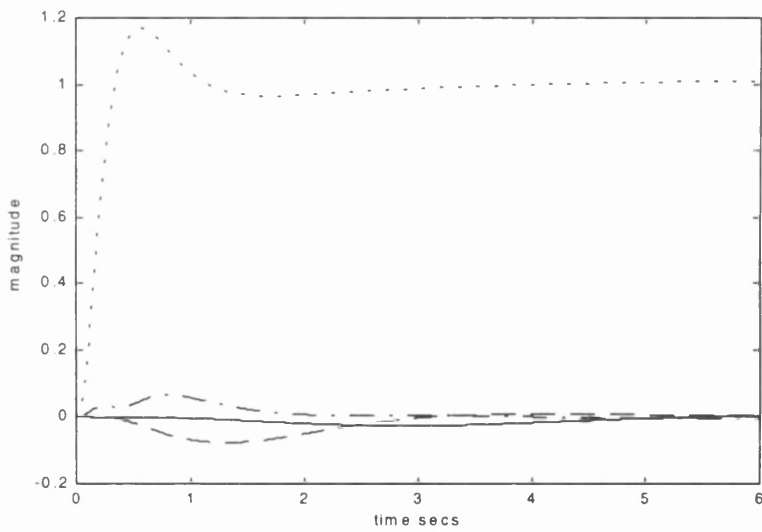
(a)



(b)



(c)



(d)

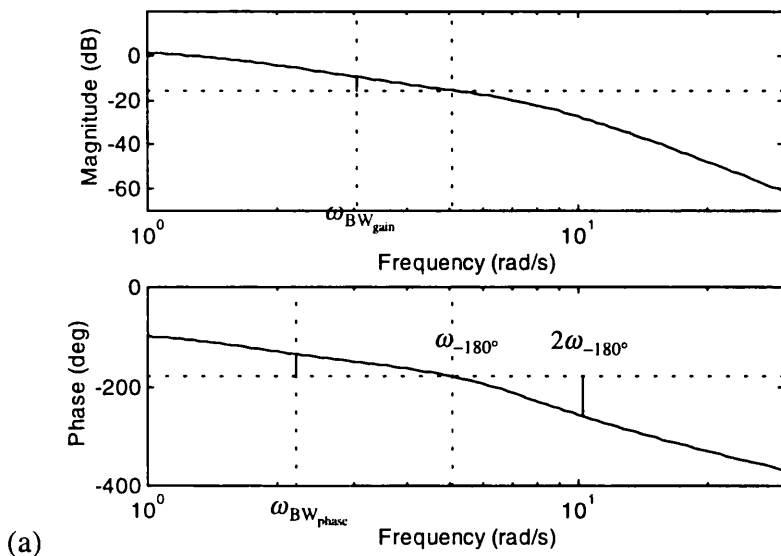
Figure 8.6. Small amplitude time histories of (a) 1ft/s height rate command, (b) 1°/s pitch rate command, (c) 1°/s roll rate command, (d) 1°/s yaw rate command.

(\dot{h} ft/s (solid line), q °/s (dashed line), p °/s (dash-dotted line), r °/s (dotted line))

8.8. Handling Qualities Assessment

8.8.1. Small Amplitude Attitude Changes

As mentioned in Chapter 2 the criteria for small amplitude attitude changes are measured in terms of Handling Qualities bandwidths and phase delays. The measurements are taken from the closed-loop frequency responses of the attitudes due to their primary inputs i.e., $\theta/\delta_{\text{long}}$, ϕ/δ_{lat} and $\psi/\delta_{\text{tail}}$. Figure 8.7 shows the Bode plots of $\theta/\delta_{\text{long}}$, ϕ/δ_{lat} and $\psi/\delta_{\text{tail}}$ for 30 knots. Notice that there is integral action, which is expected as the system is Rate Command. Shown on Figure 8.7 is the phase limited bandwidth, the gain limited bandwidth and the parameters for calculating the phase delay. It is seen from Figure 8.7 that the phase limited bandwidth is less than the gain limited bandwidth and so the phase limited bandwidth is defined as the Handling Qualities bandwidth. Figure 8.8 shows the small amplitude criteria from hover to 80 knots for target acquisition and tracking in low speed and air combat in forward flight, the most stringent requirements, which share the same boundaries. It is seen that Level 1 is met for all three attitude responses over the flight range.



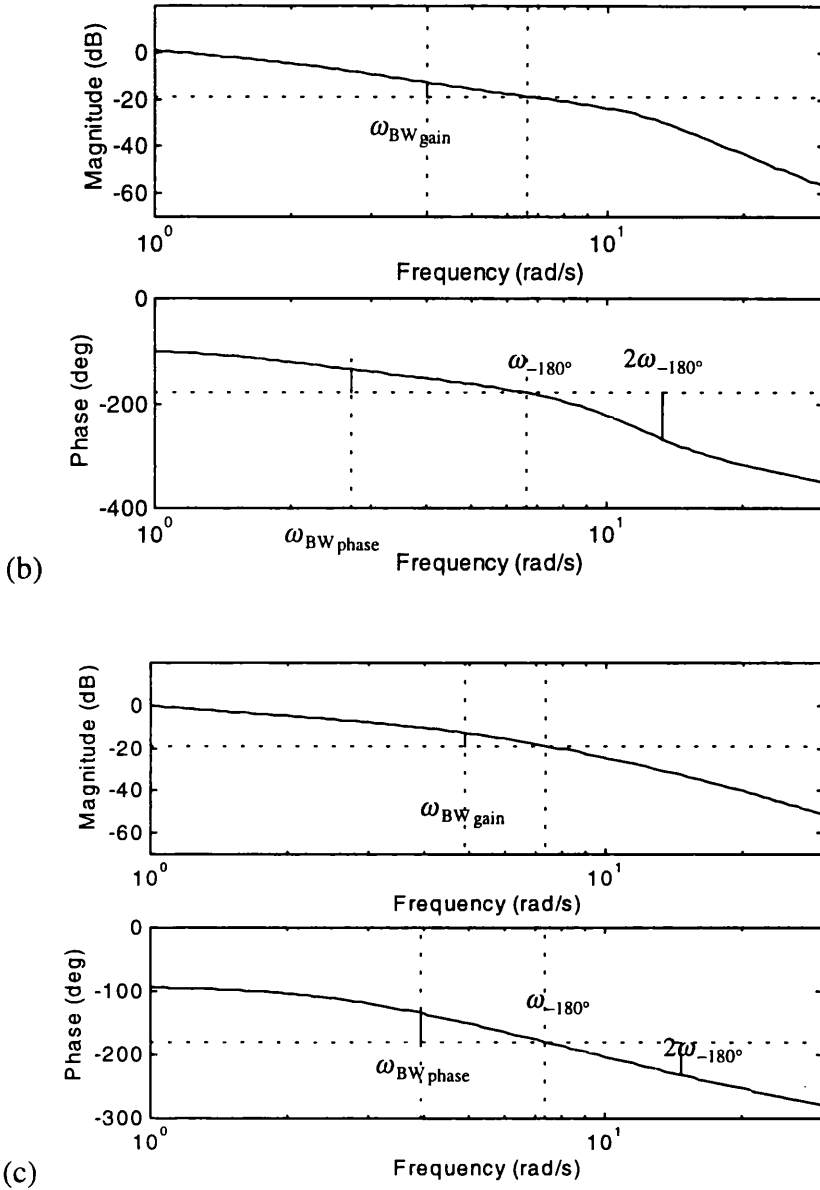


Figure 8.7. Bode plot of (a) $\theta/\delta_{\text{long}}$, (b) ϕ/δ_{lat} , (c) $\psi/\delta_{\text{tail}}$, with Handling Qualities parameters shown.

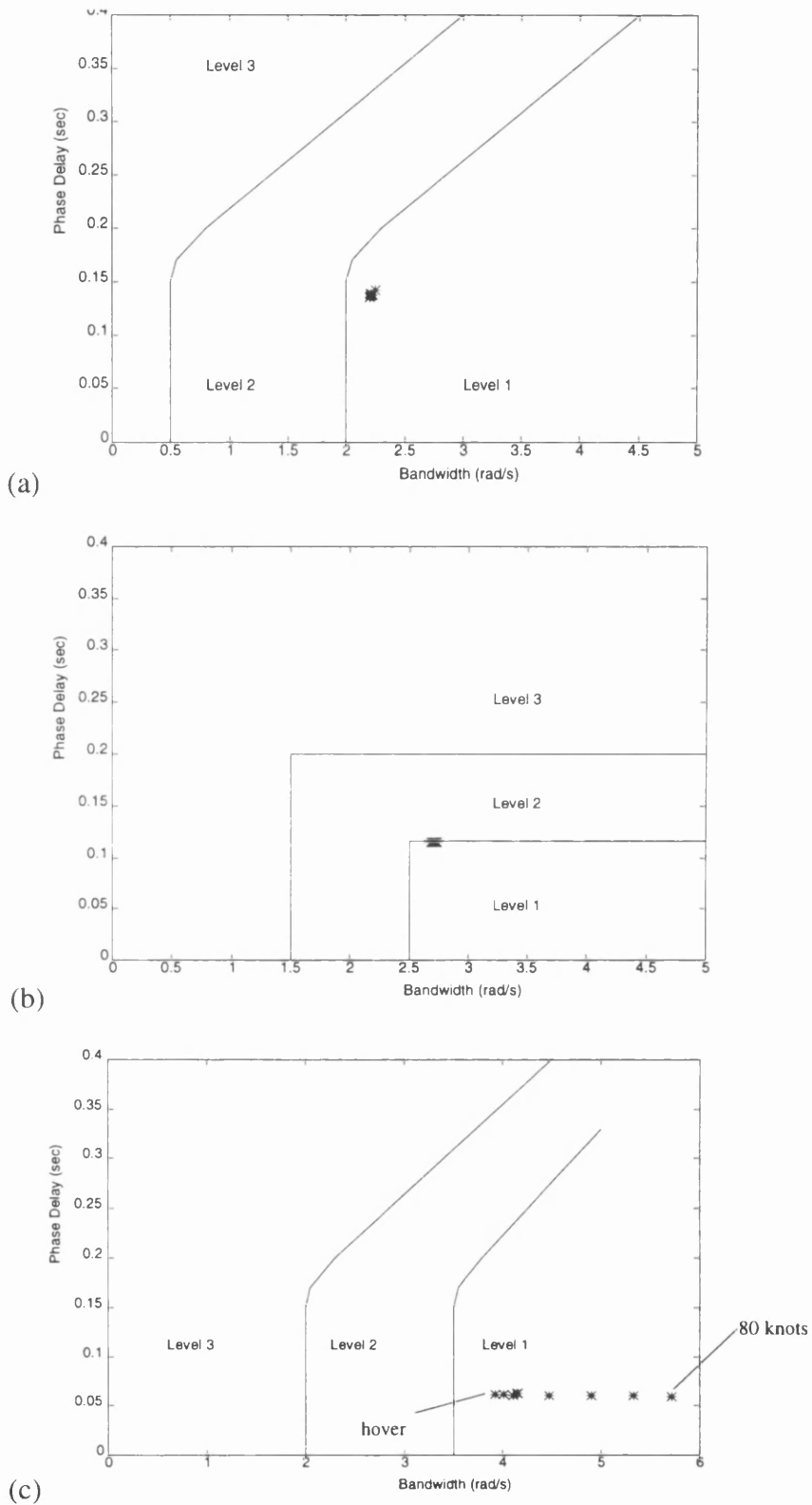
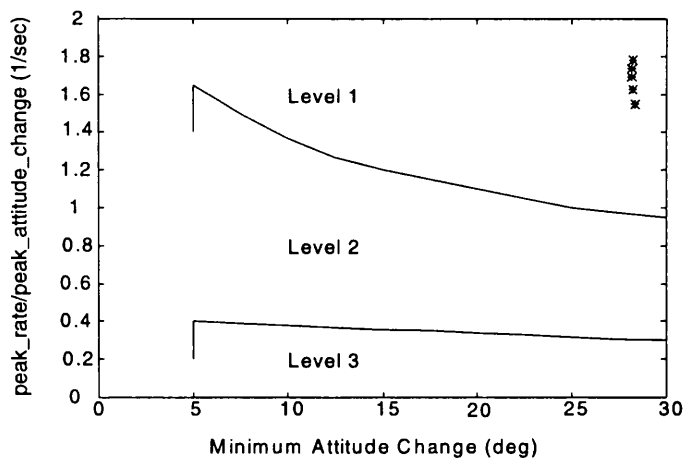


Figure 8.8. Handling Qualities bandwidth and phase delay assessment for: (a) Pitch attitude, (b) Roll attitude, (c) Yaw attitude.

8.8.2. Moderate Amplitude Attitude Changes

The moderate amplitude attitude criteria relates to how ‘quick’ moderate amplitude attitudes can be achieved. It is assessed by measuring the ratio of the peak rate due to a change in the attitude and relating this quantity to the minimum attitude change, i.e. the lowest peak in the transient region. Because the system is Rate Command, pulse control inputs can be used to induce attitude changes. ADS-33D states that the ‘*attitude changes shall be made as rapidly as possible*’. Let us say that attitude changes of 30° are to be commanded and that a rapid pilot’s input for an attitude change of this magnitude, in all axes, can be simulated as an ideal pulse with a pulse width of 0.4 sec and height of 75° . This pulse is expected to cause the actuator rate limits to be hit for a substantial amount of the time and so the helicopter will be operating near the limit of its manoeuvring capability. Figure 8.9. shows the moderate amplitude assessment for the pitch, roll and yaw attitude responses for target acquisition and tracking in hover and low speed flight. Figure 8.10 shows the moderate amplitude assessment of the roll responses for air combat in forward flight. It is seen that Level 1 is met for all responses.



(a)

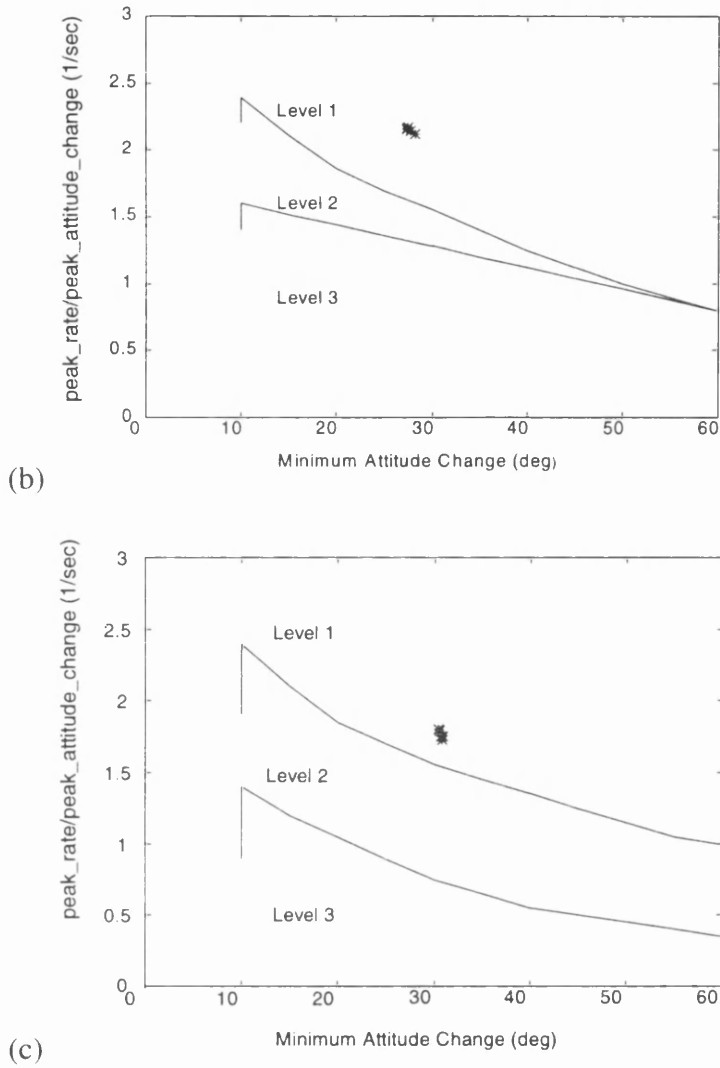


Figure 8.9. Non-linear Moderate Amplitude assessment for hover and low speed of (a) Pitch attitude, (b) Roll attitude, (c) Yaw attitude

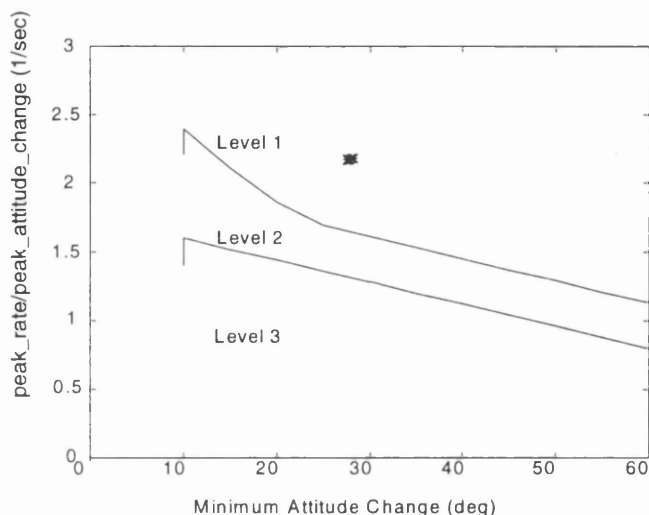


Figure 8.10. Non-Linear Moderate Amplitude assessment of roll attitude for forward flight.

8.8.3. Mid-Term Response

The Mid-Term response relates to the effective damping factor of the pitch and roll attitudes in response to pulse controller inputs in the appropriate axis. To meet Level 1 the effective damping factor must be greater than 0.35. Figure 8.11 shows the effective damping factors of the pitch and roll rates in response to pulse inputs from hover to 40 knots, the low speed criterion and Figure 8.12 shows the effective damping factors of the roll rate in response to a pulse input from 50 to 80 knots, the forward flight criterion. In Figure 8.11, the 'stars' are the pitch responses and the 'crosses' are the roll responses. It is seen that the responses are within the Level 1 region.

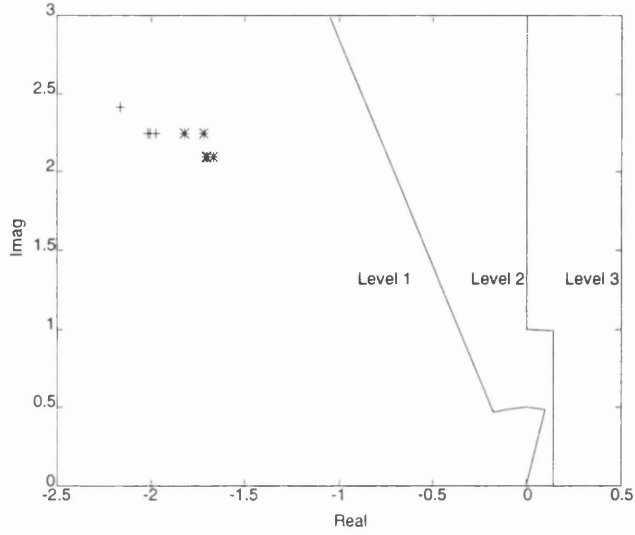


Figure 8.11. Mid-Term assessment of pitch rate and roll rate responses. Hover and low speed.

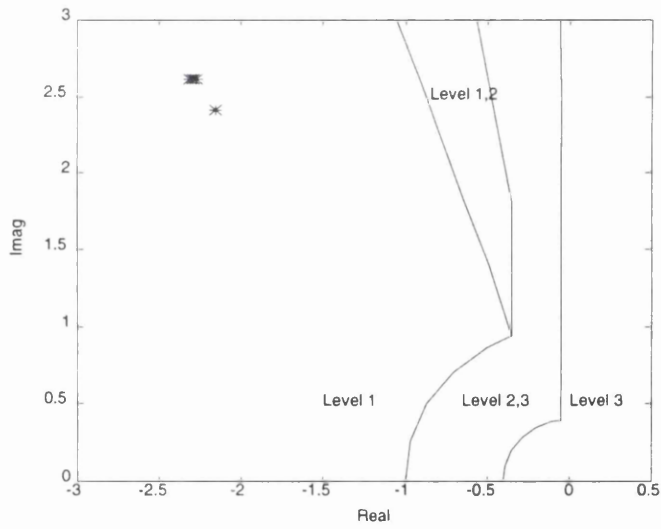


Figure 8.12. Mid-Term assessment of roll rate response. Forward flight.

8.8.4. Interaxis Coupling

The hover and low speed flight regime places requirements on the yaw rate due to collective. Figure 8.13 shows the yaw rate due to collective responses from hover to 40 knots. It is seen that Level 1 is met.

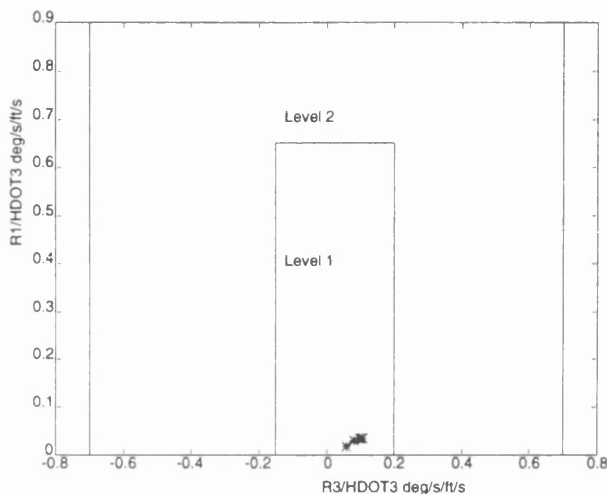


Figure 8.13. Assessment of yaw rate due to collective

The requirements on pitch due to roll and roll due to pitch state that to meet Level 1 the peak off-axis response over the first 4 seconds must be less than 25% of the on-axis response at four seconds. Figure 8.14 shows the pitch and roll responses due to the commanded pulse input of Section 8.8.2 in δ_{ong} and δ_{lat} respectively. It is seen that the coupling in each case is less than 25%.

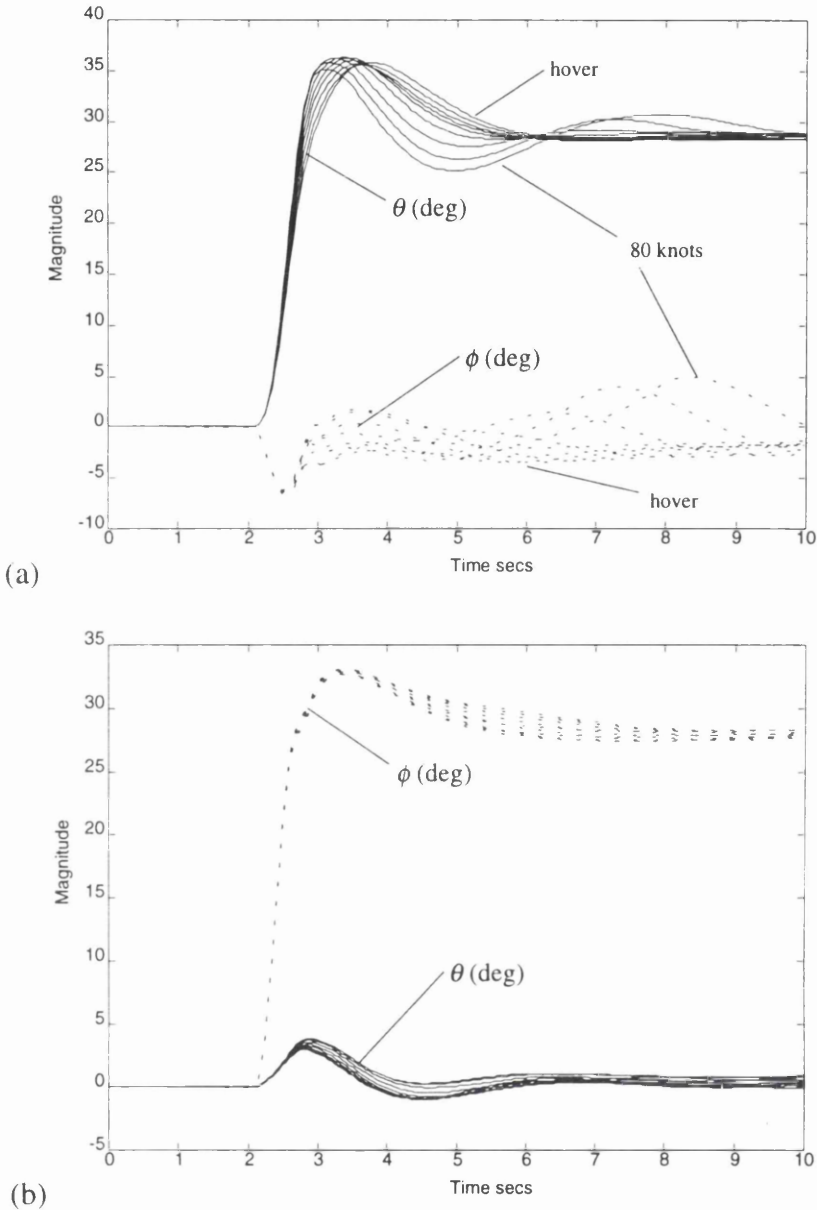


Figure 8.14. (a) Response of commanded pitch attitude of 30°
 (b) Response of commanded roll attitude of 30°

In forward flight there is a requirement on the allowable peak normal acceleration due to the peak change in pitch attitude for collective inputs. For large collective inputs the absolute value of the peak change in pitch attitude, θ_{peak} , to the peak change in normal acceleration, $n_{z_{peak}}$, should not be greater than 0.5 deg/ft/sec² in the up direction.

Table 8.5 shows $\left| \theta_{peak} / n_{z_{peak}} \right|$ at 50 and 80 knots for a commanded height rate of 30 ft/s. It is seen that Level 1 is met.

Table 8.5. Values of $\left| \theta_{\text{peak}} / n_{z_{\text{peak}}} \right|$ for commanded height rate of 30 ft/s

| Forward Velocity (knots) | $\left \theta_{\text{peak}} / n_{z_{\text{peak}}} \right $ (deg/ft/sec ²) |
|--------------------------|--|
| 50 | 0.1995 |
| 80 | 0.2541 |

8.8.5. Response to Collective

In hover and low speed flight, the height rate response is to have a qualitative first order appearance for the first five seconds following a step input on the collective inceptor. The response is to be fitted to an ideal first order response and have a coefficient of determination between 0.97 and 1.03. In addition, the equivalent rise time must be less than 5 secs and the equivalent time delay must be less than 0.2 secs to meet Level 1. Using a commanded height rate of 5 ft/s, Table 8.6 shows the spread of the coefficient of determination (CD), equivalent rise time, $T_{\dot{h}_{\text{cq}}}$, and equivalent time delay, $\tau_{\dot{h}_{\text{cq}}}$, from hover to 40 knots. Level 1 is met for all criteria.

Table 8.6. Height rate response parameters from hover to 40 knots

| | CD | $T_{\dot{h}_{\text{cq}}}$ | $\tau_{\dot{h}_{\text{cq}}}$ |
|----------------------------------|-------------|---------------------------|------------------------------|
| $\dot{h} / \delta_{\text{coll}}$ | 0.970-0.990 | 0.845-1.434 | 0.124-0.144 |

8.9. Summary

This Chapter has assessed the application of ICAD to the design of a helicopter Rate Command System at 30 knots straight and level flight. It was found that the state space model contains two transmission zeros at zero frequency when observing height rate and the angular rates. The existence of the transmission zeros at zero frequency rendered the MSFs of the system indeterminate at zero frequency, requiring a limit analysis to be performed. It was found that the limits of the MSFs of the angular rate Channels tended towards (1,0) as s tended towards zero.

ICA established that the desired Channel bandwidths could be achieved using a diagonal control law. However, a possible lack of stability robustness due to loop interaction was observed at low frequency which could introduce low frequency unstable modes. As this lack of robustness occurred at frequencies below 0.16 rad/s it was not regarded as being a problem due to the fact that the pilot is capable of stabilising low frequency instabilities with a minimal increase in workload.

Although the fixed diagonal control law had only 12 states and the two element pre-filter had only 4 states, the system was found to meet Level 1 quantitative Handling Qualities requirements from hover to 80 knots for both the small amplitude and moderate amplitude criteria, showing that high order, complex control is not a necessity.

In conclusion, ICAD has been found to be very well suited to the design of a helicopter Rate Command system.

Translational Rate Command

9.1. Introduction

Translational Rate Command (TRC) involves controlling the earth referenced forward and side velocities using the helicopter's cyclic control. TRC is required for Level 1 handling in severely degraded visual cue environments (UCE=3) for tasks such as a precision hover. Handling Qualities requirements for TRC systems suggest that the design should comprise an inner attitude loop with TRC control as an outer loop. This forms a non-square system and hence the methodology developed in Chapter 4 can be applied.

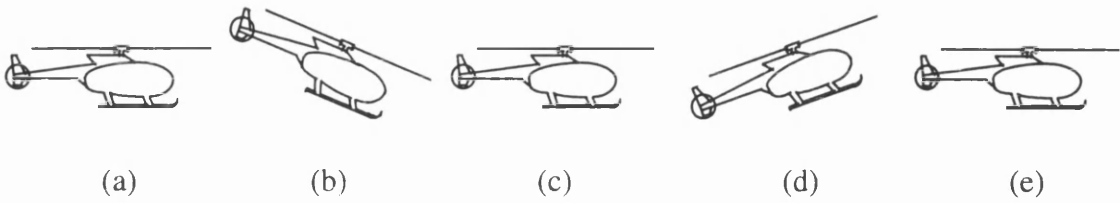
The outline of this Chapter is as follows. Section 9.2 discusses the design issues of the TRC system. Section 9.3 discusses the ACAH system which is used as an inner loop and assesses its robustness in the hover condition. Section 9.4 presents the analysis and design of the TRC system. Section 9.5 assesses the relevant Handling Qualities. Section 9.6 describes and presents the results of a 'practical' robustness test for the TRC system.

9.2. Design Considerations

The natural starting point of the analysis and design process is to consult the specifications in order to determine the form of the required controller. ADS-33D [3] states that,

- “ i) Constant pitch and roll controller force and deflection inputs shall produce a proportional steady translational rate, with respect to the earth, in the appropriate direction.*
- ii) The translational rate response to step cockpit pitch (roll) control position or force inputs shall have an equivalent rise time no less than 2.5 sec and no greater than 5 sec.*
- iii) The pitch and roll attitude shall not exhibit objectionable overshoots in response to a step cockpit controller input.”*

Statement ii) indicates that the -3dB bandwidth of the Translational Rate responses should be approximately 0.4 rad/s. Statement iii) suggests that the pitch and roll attitudes are required to be controlled in some manner. The primary inputs for the control of pitch and roll, i.e. longitudinal cyclic and lateral cyclic, are the same as for the forward and lateral velocities respectively. One can visualise this by considering the following. If the helicopter pitches nose down then its lift vector will rotate in the same direction, hence increasing the component of forward force. The forward velocity of the helicopter will therefore increase. Figure 9.1 shows graphically the manner in which a helicopter would move forward by some distance.



(a) Hover, (b) Nose down to increase forward velocity, (c) Nose up to trim at required forward velocity, (d) Nose up to reduce forward velocity, (e) Nose down to trim at hover.

Figure 9.1. Helicopter moving from one position to another.

Likewise, if the helicopter rolls in a positive sense (clockwise if sitting in the cockpit and facing forwards) then the lift vector will rotate clockwise hence increasing the component of side force. The lateral velocity of the helicopter will therefore increase in a positive sense.

The proposed control structure therefore consists of an inner and an outer loop. The inner loop will involve the control of pitch and roll attitude as the translational rates cannot be controlled if the attitudes are not stabilised (Hoh [22]), and the outer loop will involve the control of the translational velocities.

The inner attitude loop will be of ACAH form with the usual height rate and yaw rate control, and following Chapter 7, \dot{h} , $(\theta+q)$, $(\phi+p)$ and r are fed back to θ_0 , θ_{1s} , θ_{1c} and θ_{0T} respectively, via a diagonal control law. Although the height rate and yaw rate loops are not 'inner' loops for the TRC system the system including these loops will nonetheless be referred to as the inner system, as the loops are designed without regard for the velocity responses. The outer loop constitutes TRC augmentation in which forward velocity and lateral velocity are fed back to the inputs of the pitch and roll Channels respectively, via a diagonal controller. The proposed feedback control structure is shown in block diagram form in Figure 9.2.

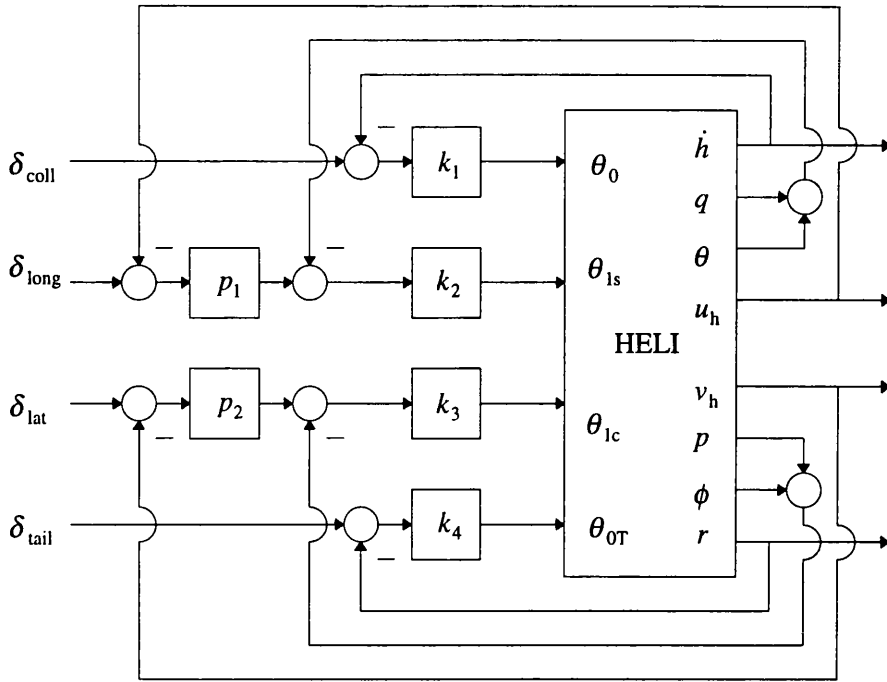


Figure 9.2. Block diagram of proposed TRC feedback system

In this case, the helicopter model, G , is a 6×4 transfer function matrix. The open-loop helicopter is given as,

$$\begin{bmatrix} \dot{h} \\ \theta + q \\ \phi + p \\ r \\ u_h \\ v_h \end{bmatrix} = \begin{bmatrix} g_{11} & g_{12} & g_{13} & g_{14} \\ g_{21} & g_{22} & g_{23} & g_{24} \\ g_{31} & g_{32} & g_{33} & g_{34} \\ g_{41} & g_{42} & g_{43} & g_{44} \\ g_{51} & g_{52} & g_{53} & g_{54} \\ g_{61} & g_{62} & g_{63} & g_{64} \end{bmatrix} \begin{bmatrix} \theta_0 \\ \theta_{1s} \\ \theta_{1c} \\ \theta_{0T} \end{bmatrix} \quad (9.1)$$

The character of u_h and v_h , the velocities to be controlled by the TRC system, will now be explained. ADS-33D states that '*constant pitch and roll controller force and deflection inputs shall produce a proportional steady translational rate, with respect to the earth, in the appropriate direction*'. In this context, 'earth referenced' means ground speed and not airspeed, and in the 'appropriate direction' means that the ground speed should be relative to the orientation of the aircraft, i.e. body-referenced groundspeed as opposed to earth-referenced groundspeed.

In non-linear form, the body-referenced forward and lateral ground velocities, U_h , and V_h respectively, are given by,

$$U_h = U \cos \Theta + V \sin \Phi \sin \Theta + W \cos \Phi \sin \Theta \quad (9.2)$$

$$V_h = V \cos \Phi - W \sin \Phi \quad (9.3)$$

The linearised perturbations from trim are,

$$u_h = u \cos \Theta_0 + v \sin \Phi_0 \sin \Theta_0 + w \cos \Phi_0 \sin \Theta_0 \quad (9.4)$$

$$v_h = v \cos \Phi_0 - w \sin \Phi_0 \quad (9.5)$$

In hover Θ_0 is 0.07371 rad and Φ_0 is -0.05412 rad and so,

$$u_h = (9.9728e - 1)u - (3.9836e - 3)v + (7.3535e - 2)w \quad (9.6)$$

$$v_h = (9.9853e - 1)v + (5.4094e - 2)w \quad (9.7)$$

There are some points to make at this stage. The system, when it is designed, will be expected to regulate w to zero (as $w \approx -\dot{h}$) and also to decouple u_h due to v_h and v_h due to u_h . This means that for manoeuvres for which the deviation of pitch and roll attitude from trim are small enough such that the approximations $\cos \theta(\cos \phi) \approx 1$ and $\sin \theta(\sin \phi) \approx \theta(\phi)$ can be used, then, in the absence of wind, $u_h \approx u$ and $v_h \approx v$. This implies that the control of u and v , as opposed to u_h and v_h , will be sufficiently accurate to meet the Handling Qualities requirements. However, for the sake of not taking any chances, particularly when large-amplitude manoeuvres are to be considered, the horizontal-plane velocities will be controlled.

9.3. Individual Channel Analysis of the Inner Attitude System

As the ACAH system of Chapter 7 was found to meet Level 1 Handling Qualities requirements at hover it will be used as the inner system. In order that the attitude system at hover is robust the Channel gain and phase margins must be adequate and the Channel MSFs must be far from the (1,0) point at frequencies of importance. Figure 9.3 shows the actual MSF of the pitch Channel, γ_2 . It is seen that γ_2 is within the 'non-robust' region only at frequencies below 0.005 rad/s. Plant uncertainty could cause γ_2 to traverse the (1,0) point and introduce a RHPZ into C_2 , thus causing a potential stability problem. As this sensitivity is at frequencies below 0.005 rad/s it is not regarded as being a problem due to the fact that any low frequency instabilities that occur can be compensated for by the pilot with a minimal increase in workload. The other three actual MSFs were found to be comfortably distant from the (1,0) point at frequencies above 0.02 rad/s. The gain and phase margins of the Channels are shown in Table 9.1.

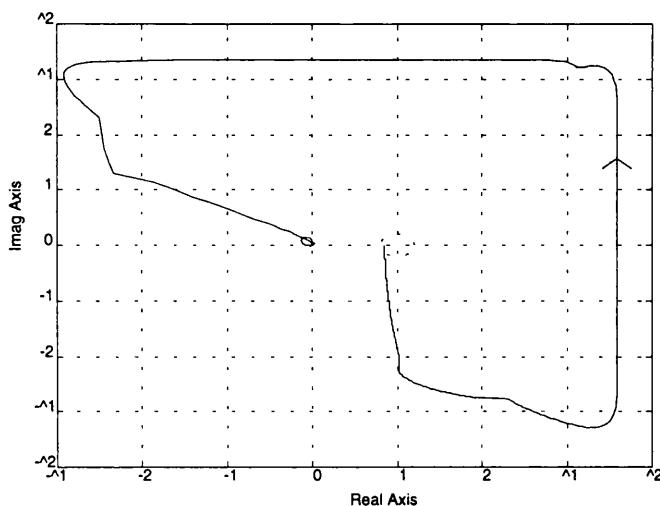


Figure 9.3. Nyquist plot of γ_2 of the inner attitude system.

Table 9.1. Gain and phase margins of Channels of the inner attitude system.

| TF | GM (dB) | PM (deg) |
|-----------|---------|----------|
| Channel 1 | 30.09 | 51.79 |
| Channel 2 | 13.08 | 44.41 |
| Channel 3 | 12.56 | 44.48 |
| Channel 4 | 18.82 | 50.43 |

Because the gain and phase margins are adequate and the γ s do not approach the (1,0) point at frequencies of importance, the inner attitude system can be regarded as possessing stability robustness.

9.4. TRC System

The loose transfer function elements which constitute the open-loop for the outer feedback system must be assessed to determine whether the closure of the inner loops have caused them to become structurally and/or phase sensitive. If such sensitivity exists then there is the possibility that the outer loop could exhibit stability robustness problems. Using the notation of Chapter 4, the open-loop outer system is given as,

$$\begin{bmatrix} u_h \\ v_h \end{bmatrix} = \begin{bmatrix} \bar{q}_{52} & \bar{q}_{53} \\ \bar{q}_{62} & \bar{q}_{63} \end{bmatrix} \begin{bmatrix} u_2 \\ u_3 \end{bmatrix} = \bar{Q} \begin{bmatrix} u_2 \\ u_3 \end{bmatrix} \quad (9.8)$$

The structure of \bar{Q} is given in Table 9.2. It is seen that the system has 2 RHP, very poorly damped, transmission zeros at approximately 5 rad/s. These transmission zeros are definitely an impediment to attaining arbitrarily high bandwidth, but as Channel bandwidths of approximately 0.4 rad/s will meet the performance specifications these transmission zeros are unlikely to affect the stability of the system. ICA will elucidate this observation.

Table 9.2. Structure of \bar{Q}

| | RHP Transmission Zeros (rad/s) | RHPPs (rad/s) |
|-----------|--------------------------------|---------------|
| \bar{Q} | $2.5053e-3 \pm 5.2844e+0j$ | – |

Manness and Murray-Smith [46], in applying Eigenstructure Assignment to the design of a TRC system, quite rightly noted that the non-minimum phase zeros introduced by the observation of forward and side velocities constrain what can be achieved by the control system. Because the requirements for TRC in ADS-33D put such a low bandwidth requirement on the TRC responses, it seems that there is an implicit assumption that the dynamics of a rotorcraft, in general, exhibit non-minimum phase characteristics when translational rates are observed.

As \bar{Q} is square, square ICAD theory can be applied.

Define the MSF for \bar{Q} ,

$$\bar{\gamma} = \bar{q}_{53}\bar{q}_{62}/\bar{q}_{52}\bar{q}_{63} \quad (10.9)$$

The TRC controller is given as,

$$P = \begin{bmatrix} p_1 & 0 \\ 0 & p_2 \end{bmatrix} \quad (10.10)$$

and so the closed loop subsystems are,

$$h_{52} = p_1\bar{q}_{52}/(1 + p_1\bar{q}_{52}) \quad (10.11)$$

$$h_{63} = p_2\bar{q}_{63}/(1 + p_2\bar{q}_{63}) \quad (10.12)$$

9.4.1. Analysis of the Loose Transfer Functions

The sensitivity of the transfer function elements of \bar{Q} must be determined, although as we shall see, it may not be necessary to check the sensitivity of the off-diagonal elements, \bar{q}_{53} and \bar{q}_{62} . To determine this, Figure 9.4 shows the Nyquist plot of $\bar{\gamma}$ up to 2 rad/s,

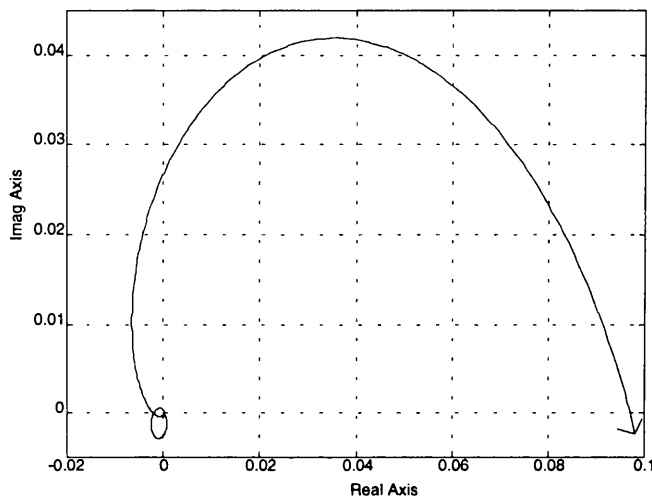


Figure 9.4. Nyquist plot of $\bar{\gamma}$ up to 2 rad/s.

It is seen that $\bar{\gamma}$ does not encircle the (1,0) point at low frequency and, once control action is introduced, $\bar{\gamma}_{52}$ and $\bar{\gamma}_{63}$ will have magnitudes comfortably less than once at frequencies up to the desired 0dB crossover frequencies of the TRC Channels. This is known because the TRC Channels can meet the performance requirements with crossover frequencies at approximately 0.4 rad/s, hence the gains of h_{52} and h_{63} will be dropping off around this frequency.

Because $\bar{\gamma}$ is of such small magnitude over the frequency range of importance, the structural sensitivity of \bar{q}_{53} and \bar{q}_{62} need not be determined as the zero structure of $\bar{\gamma}$ will not affect the structure of $(1-\bar{\gamma})$. Also, the phase sensitivity of \bar{q}_{53} and \bar{q}_{62} need

not be determined as any phase sensitivity exhibited in $\bar{\gamma}$ will have a minimal effect on the phase of $(1-\bar{\gamma})$.

It is only required to check the sensitivity of \bar{q}_{52} and \bar{q}_{63} . \bar{q}_{52} and \bar{q}_{63} are expressed as,

$$\bar{q}_{52} = k_2 g_{52} \left(\frac{1}{1+C_2} \right) (1-\bar{\gamma}_{52}) \quad (9.13)$$

$$\bar{q}_{63} = k_3 g_{63} \left(\frac{1}{1+C_3} \right) (1-\bar{\gamma}_{63}) \quad (9.14)$$

where C_2 and C_3 are the pitch and roll Channels of the inner system.

$\bar{\gamma}_{52}$ and $\bar{\gamma}_{63}$ are written explicitly as,

$$\bar{\gamma}_{52} = - \frac{\begin{vmatrix} g_{11}/h_1 & g_{12} & g_{13} & g_{14} \\ g_{51} & 0 & g_{53} & g_{54} \\ g_{31} & g_{32} & g_{33}/h_3 & g_{34} \\ g_{41} & g_{42} & g_{43} & g_{44}/h_4 \end{vmatrix}}{g_{52} \begin{vmatrix} g_{11}/h_1 & g_{13} & g_{14} \\ g_{31} & g_{33}/h_3 & g_{34} \\ g_{41} & g_{43} & g_{44}/h_4 \end{vmatrix}} \quad (9.15)$$

$$\bar{\gamma}_{63} = - \frac{\begin{vmatrix} g_{11}/h_1 & g_{12} & g_{13} & g_{14} \\ g_{21} & g_{22}/h_2 & g_{23} & g_{24} \\ g_{61} & g_{62} & 0 & g_{64} \\ g_{41} & g_{42} & g_{43} & g_{44}/h_4 \end{vmatrix}}{g_{63} \begin{vmatrix} g_{11}/h_1 & g_{12} & g_{14} \\ g_{21} & g_{22}/h_2 & g_{24} \\ g_{41} & g_{42} & g_{44}/h_4 \end{vmatrix}} \quad (9.16)$$

For \bar{q}_{52} and \bar{q}_{63} to be insensitive to plant variation it is sufficient that C_2 and C_3 have adequate gain and phase margins and that the MSFs of C_2 and C_3 are far from the (1,0) point at frequencies of importance and, in addition, $\bar{\gamma}_{52}$ and $\bar{\gamma}_{63}$ should be distant from the (1,0) point at frequencies of importance.

From ICA of the attitude system in Section 9.3 it has already been established that the gain and phase margins of C_2 and C_3 are adequate and that the MSFs of C_2 and C_3 are distant from the (1,0) point at frequencies of importance. It is only required then, to assess the closeness of $\bar{\gamma}_{52}$ and $\bar{\gamma}_{63}$ to the (1,0) point.

Figure 9.5 shows $\bar{\gamma}_{52}$ and $\bar{\gamma}_{63}$. It is seen that the (1,0) point is approached quite closely by $\bar{\gamma}_{52}$ at some frequency but $\bar{\gamma}_{63}$ is sufficiently far from the (1,0) point at all frequencies.

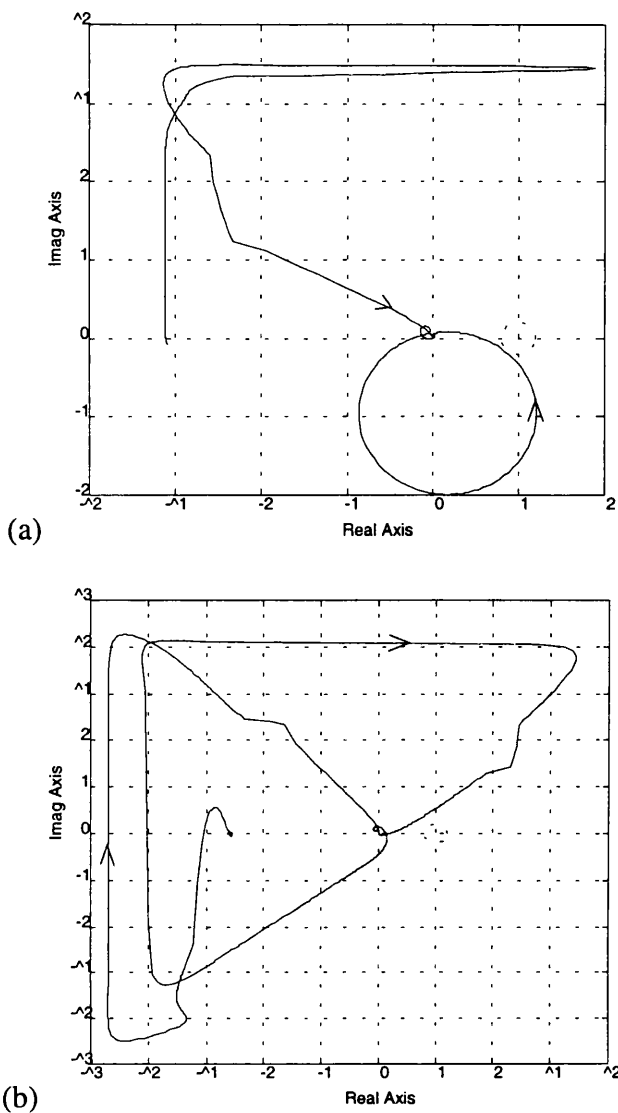


Figure 9.5. Nyquist plot of (a) $\bar{\gamma}_{52}$, (b) $\bar{\gamma}_{63}$.

To determine at what frequency the closeness of $\bar{\gamma}_{52}$ to the (1,0) point occurs, Figure 9.6 shows a magnitude Bode plot of frequency versus $abs(1 - \bar{\gamma}_{52})$. It is seen that $\bar{\gamma}_{52}$ approaches the (1,0) point at around 5 rad/s and is displaying the characteristics of a poorly damped zero complex pair. In fact, an unstable zero complex pair of \bar{q}_{52} is situated at $0.002 \pm 5.309j$ rad/s. The closeness of $\bar{\gamma}_{52}$ to the (1,0) point has indicated that there is possible structural and phase sensitivity at approximately 5 rad/s. However, although full ICA has not yet been performed on \bar{Q} , preliminary indications are that because the bandwidths of the Channels are to be approximately 0.4 rad/s and $\bar{\gamma}$ is

small up to 2 rad/s, $p_1\bar{q}_{52}$ will have a 0dB crossover at approximately 0.4 rad/s. Hence the sensitivity at 5 rad/s is of no consequence as the gain of $p_1\bar{q}_{52}$ will have attenuated sufficiently at 5 rad/s.

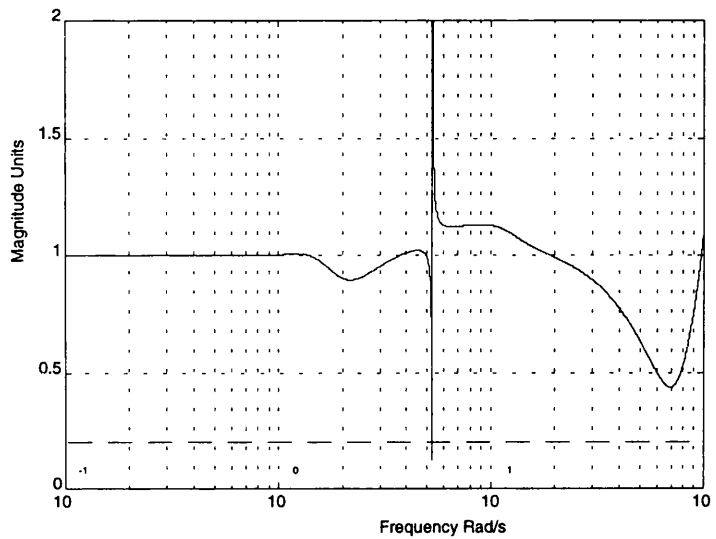


Figure 9.6. Magnitude Bode plot of $\text{abs}(1 - \bar{\gamma}_{52})$.

It can be concluded from these findings that the inner attitude system will not have a detrimental effect on the stability robustness of the outer system, and hence the complete system.

9.4.2. Stabilisation and Potential Performance of the TRC System

As the velocity Channels are likely to have comparable bandwidths of approximately 0.4 rad/s the numbering of the Channels can be done in any order. In this case, the forward velocity Channel will be assigned as Channel 1 and the side velocity Channel will be assigned as Channel 2.

In order to determine the conditions for stability and achievable performance of the TRC system one begins with the equation,

$$|\bar{Q}| = \bar{q}_{52}(1 - \bar{\gamma})\bar{q}_{63} \quad (9.17)$$

and relates this to the following equation,

$$|\hat{Q}| = [1 + p_1\bar{q}_{52}(1 - \bar{\gamma} \cdot h_{63})].[1 + p_2\bar{q}_{63}] \quad (9.18)$$

where,

$$|\hat{Q}| = |I + \bar{Q}P| \quad (10.19)$$

Figure 9.7 shows the Nyquist plot of $\bar{\gamma}$ and Table 9.3 shows the structures of the parameters of Eqn (9.17).

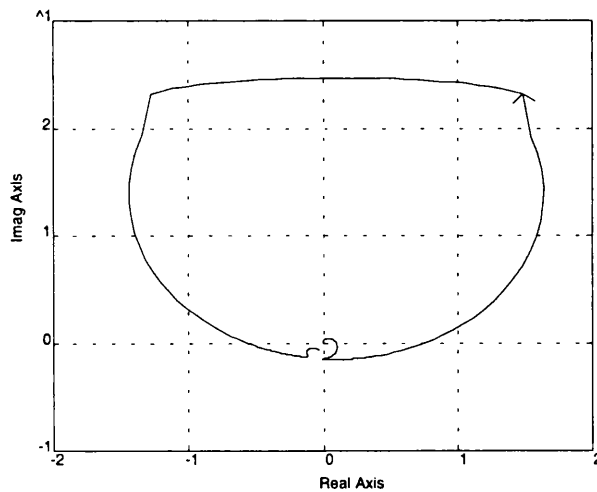


Figure 9.7. Nyquist plot of $\bar{\gamma}$.

Table 9.3. Structure of parameters of Eqn (9.17).

| | RHPZs (rad/s) | RHPPs (rad/s) |
|----------------------|----------------------------|----------------------------|
| $ \bar{Q} $ | $2.5053e-3 \pm 5.2844e+0j$ | – |
| $(1 - \bar{\gamma})$ | $2.5053e-3 \pm 5.2844e+0j$ | $7.9104e-3 \pm 5.3066e+0j$ |
| \bar{q}_{52} | $7.9104e-3 \pm 5.3066e+0j$ | – |
| \bar{q}_{63} | – | – |

Conditions sufficient for the zeros of $|\hat{Q}|$, and hence the poles of the closed-loop plant, to be stable are as follows: p_2 should be designed such that the zeros of $(1 + p_2 \bar{q}_{63})$ are the same as the zeros of \bar{q}_{63} . Therefore the zeros of $(1 + p_2 \bar{q}_{63})$ will be stable. $\bar{\gamma} h_{63}$ will therefore have 2 RHPPs and as h_{63} is to be designed to have a bandwidth of approximately 0.4 rad/s, $\bar{\gamma} h_{63}$ will not encircle the (1,0) point. The zeros of $(1 - \bar{\gamma} h_{63})$ and hence the zeros of $p_1 \bar{q}_{52} (1 - \bar{\gamma} h_{63})$ will contain 2 RHPZs at approximately 5 rad/s. $p_1 \bar{q}_{52} (1 - \bar{\gamma} h_{63})$ will have no RHPPs because the RHPPs of $\bar{\gamma}$ exactly cancel with the RHPZs of \bar{q}_{52} . p_1 is then designed such that $p_1 \bar{q}_{52} (1 - \bar{\gamma} h_{63})$ does not encircle the (-1,0) point and has a 0dB crossover of approximately 0.4 rad/s. The system will therefore be stable and high performance is achievable at frequencies below 0.4 rad/s in both Channels.

9.4.3. Controller Design

Controller p_2 is designed so that the nested lateral velocity Channel ($p_2 \bar{q}_{63}$) closely matches the desired shape for the actual lateral velocity Channel ($p_2 \bar{q}_{63} (1 - \bar{\gamma} h_{52})$). Figure 9.8 shows the bode plot of \bar{q}_{63} and $p_2 \bar{q}_{63}$ with p_2 designed as,

$$p_2 = \frac{9(s + 0.14)(s + 0.2)}{s(s + 0.29)(s + 10)} \quad (9.20)$$

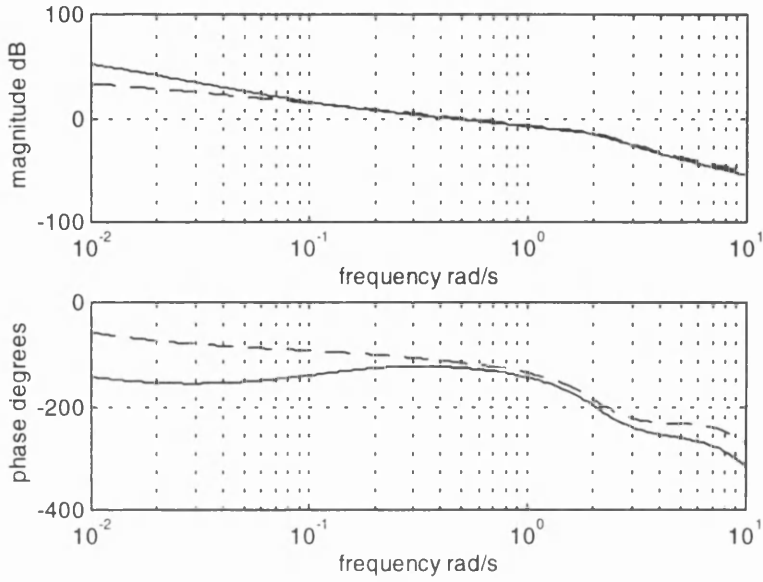


Figure 9.8. Bode plot of $p_2\bar{q}_{63}$ (solid) and \bar{q}_{63} (dashed).

Table 9.4 shows the zero structure of \bar{q}_{63} and $(1+p_2\bar{q}_{63})$ and it is seen that they have the same structure. $\bar{\gamma} h_{63}$ therefore has the same pole structure of $\bar{\gamma}$ as required.

Table 9.4. Zero structure of \bar{q}_{63} and $(1+p_2\bar{q}_{63})$.

| | RHPZs (rad/s) |
|-----------------------|---------------|
| \bar{q}_{63} | — |
| $(1+p_2\bar{q}_{63})$ | — |

Figure 9.9 shows the Nyquist plot of $\bar{\gamma}$ and $\bar{\gamma} h_{63}$. It is seen that they encircle the (1,0) point the same number of times and hence the zero structure of $(1-\bar{\gamma} h_{63})$ is the same as the zero structure of $(1-\bar{\gamma})$ as required.

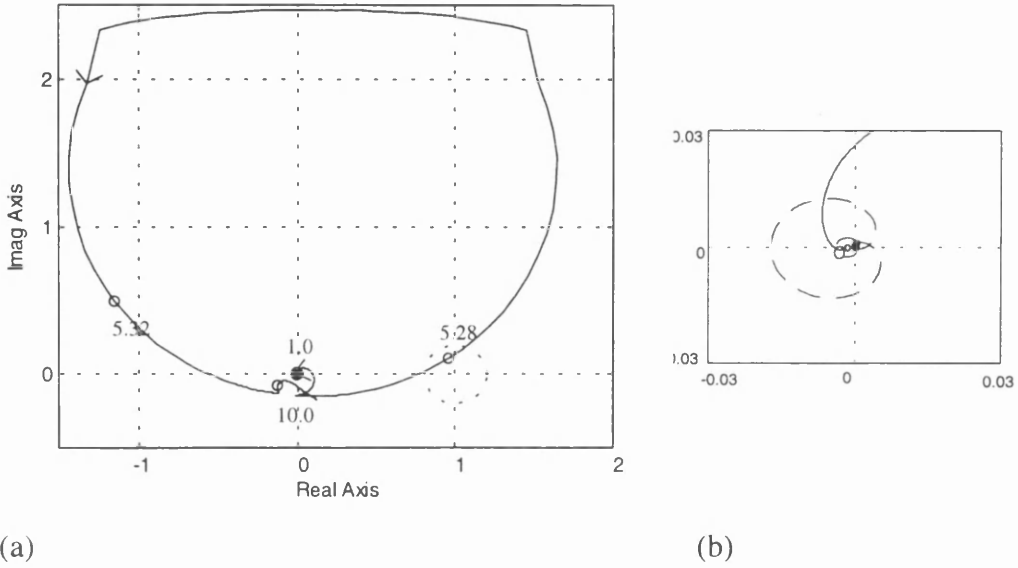


Figure 9.9. (a) Nyquist plot of $\bar{\gamma}$ (solid) and $\bar{\gamma} h_{63}$ (dashed - refer to (b)),
 (b) Expansion of (0,0) region of (a).
 (frequencies shown in rad/s, plots shown up to 30 rad/s)

Controller p_1 is designed on the actual longitudinal velocity Channel ($p_1 \bar{q}_{52} (1 - \bar{\gamma} \cdot h_{63})$) and is given as,

$$p_1 = \frac{-9(s + 0.1)}{s(s + 10)} \tag{9.21}$$

Figure 9.10 shows the bode plot of the longitudinal velocity Channel with the controller set to one and with the controller as defined in Eqn (9.21). Table 9.5 shows the zero structure of $p_1 \bar{q}_{52} (1 - \bar{\gamma} \cdot h_{63})$ and $(1 + p_1 \bar{q}_{52} (1 - \bar{\gamma} \cdot h_{63}))$. It is seen that the closed-loop system is stable.

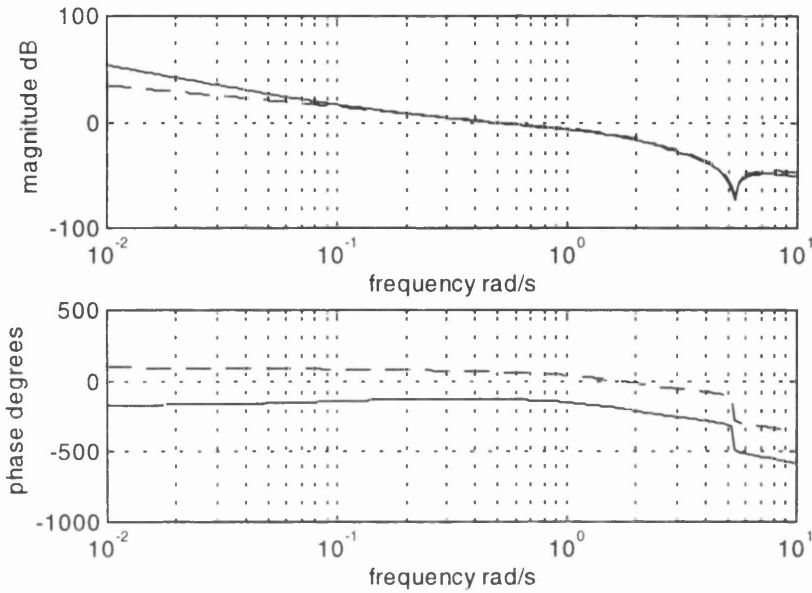


Figure 9.10. Bode plot of $p_1\bar{q}_{52}(1-\bar{\gamma}.h_{63})$ (solid) and $\bar{q}_{52}(1-\bar{\gamma}.h_{63})$ (dashed).

Table 9.5. Zero structure of $p_1\bar{q}_{52}(1-\bar{\gamma}.h_{63})$ and $(1+p_1\bar{q}_{52}(1-\bar{\gamma}.h_{63}))$.

| | RHPZs (rad/s) |
|--|----------------------------|
| $p_1\bar{q}_{52}(1-\bar{\gamma}.h_{63})$ | $8.2214e-1 \pm 5.3066e+0j$ |
| $(1+p_1\bar{q}_{52}(1-\bar{\gamma}.h_{63}))$ | — |

A decoupling filter was required to reduce the yaw rate due to collective response. Shaping filters were required for the height rate, forward velocity and side velocity Channels.

The decoupler is given as,

$$d_{\text{yaw_coll}} = \frac{-4s}{(s+3)(s+6)} \quad (9.22)$$

and the shapers are given as,

$$s_h = \frac{11.4(s+0.57)}{(s+0.3)(s+20)} \quad (9.23)$$

$$s_{u_h} = \frac{-5.1(s + 0.35)}{(s + 0.18)(s + 10)} \tag{9.24}$$

$$s_{v_h} = \frac{4.6(s + 0.5)}{(s + 0.24)(s + 10)} \tag{9.25}$$

Notice the negative sign on s_{u_h} . This is so that the helicopter will move forwards (positive response) if the cyclic stick is pushed forward (negative input), as required.

The complete system is shown in block diagram form in Figure 9.11.

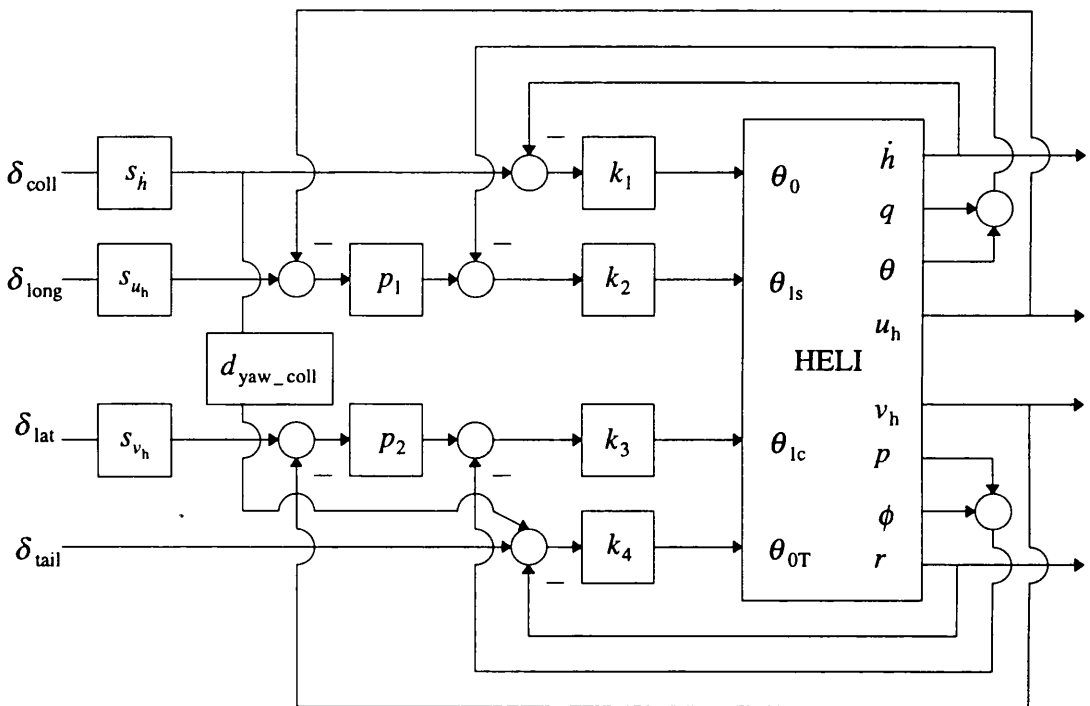


Figure 9.11. Block diagram of TRC system.

9.4.4. Individual Channel Analysis

The gain and phase margins of the Channels are shown in Table 9.6 and are seen to be good. The $\bar{\gamma}h_j$ s ($j = 52,63$) are shown in Figure 9.12 and are seen to be nowhere near the critical (1,0) point. Therefore the Channel gain and phase margins are valid as robustness measures.

Because the inner attitude system is robust, and the interaction of the attitude augmentation on the outer loop elements does not cause sensitivity problems, the complete design can be regarded as possessing stability robustness.

Table 9.6. Gain and phase margins of TRC Channels.

| | GM (dB) | PM (deg) |
|---|---------|----------|
| $p_1 \bar{q}_{52} (1 - \bar{\gamma}h_{63})$ | 11.5 | 51.1 |
| $p_2 \bar{q}_{63} (1 - \bar{\gamma}h_{52})$ | 11.6 | 55.5 |

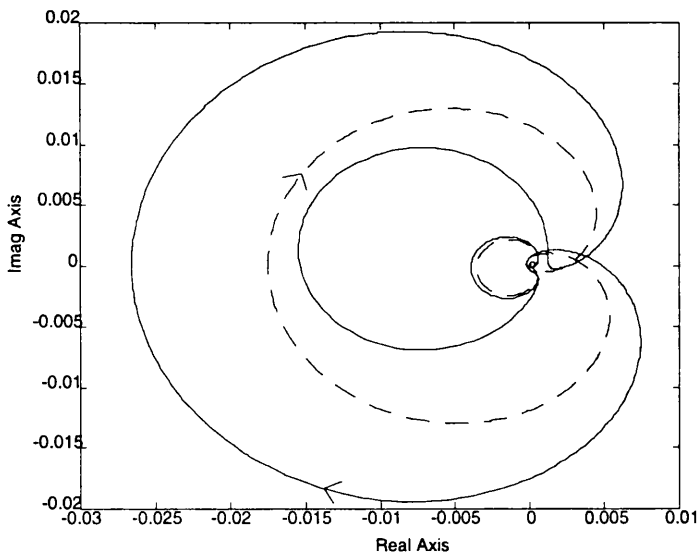
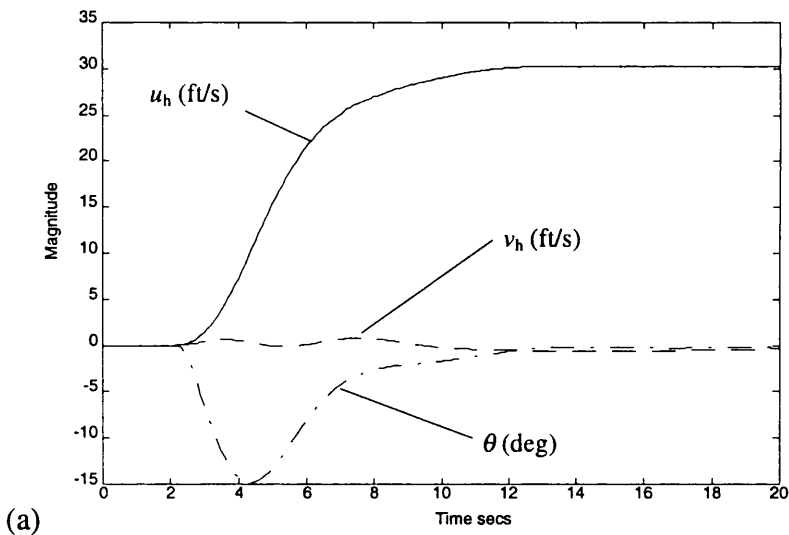


Figure 9.12. Nyquist plot of $\bar{\gamma}h_{63}$ (solid) and $\bar{\gamma}h_{52}$ (dotted).

9.5. Handling Qualities Assessment

The non-linear helicopter model HELISIM was used to assess the time responses of the system. The forward velocity and side velocity responses due to commanded inputs of 30 ft/s are shown in Figure 9.13 (for clarity, only off axis responses of Handling Qualities importance are shown).

The rise times (calculated as being the time to reach 0.632 of the steady state values) are approximately 3.7 secs and 4.0 secs for the u_h and v_h responses respectively, and both responses are seen to have qualitative first order appearances. Note that the pitch and roll responses of Figure 9.13 are required to achieve the commanded forward and side velocities and hence are not objectionable. The responses meet Level 1 requirements. It is clearly evident from Figure 9.13 that the helicopter must pitch down (negative pitch) to establish a forward velocity, and roll clockwise (positive roll) to establish a side velocity to starboard.



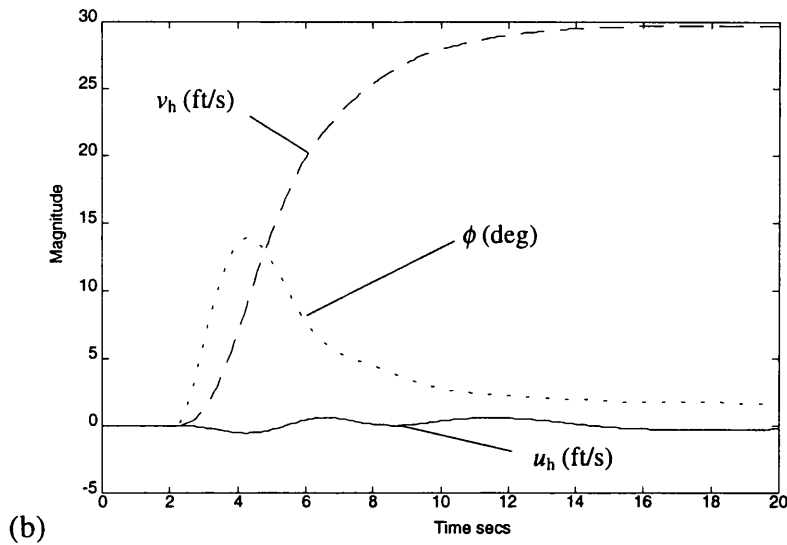


Figure 9.13. (a) Non-linear response due to commanded forward velocity of 30 ft/s.
 (b) Non-linear response due to commanded side velocity of 30 ft/s.

9.6. Elliptical Turn Robustness Test

This Section describes a robustness test of the TRC system known as an Elliptical Turn Test (Osder and Caldwell [57]) using the non-linear helicopter model HELISIM. The robustness check involves the helicopter initially being in hover. A forward velocity command between 10 and 50 knots is then introduced, and once the helicopter is established at its commanded velocity a tail rotor input of 1 rad/s [57] is introduced which is applied long enough for the helicopter to rotate through *at least* 360 degrees. During this rotation the cyclic control must be sinusoidally adjusted such that the helicopter will attempt to maintain its original earth referenced velocity. A diagram of this manoeuvre is shown in Figure 9.14.

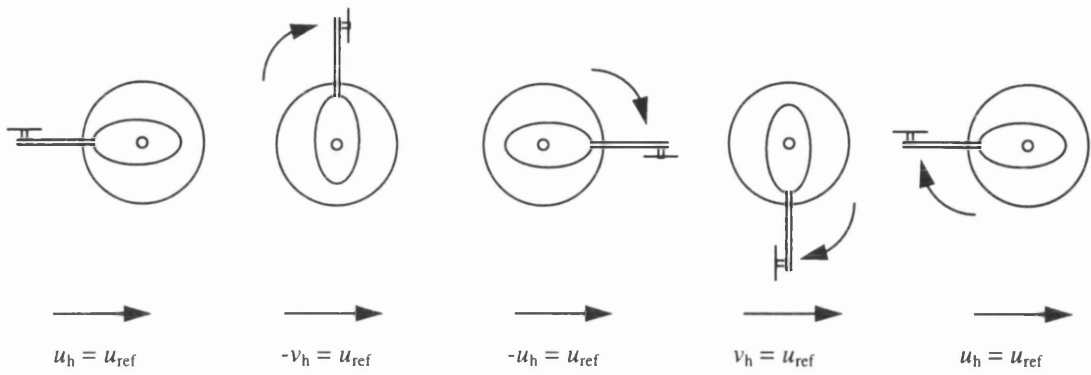


Figure 9.14. Elliptical Turn

How closely the helicopter can maintain this reference velocity vector whilst rotating is a measure of the system's practical robustness (Osder and Caldwell [57]).

Because the TRC system has rise times of approximately 4 secs on each of its velocity Channels this must be taken into consideration when deciding at what reference velocity the test can be performed at. For instance, because of the abruptness of the tail rotor input, it is unlikely that the horizontal-plane velocity responses will be achieved quickly enough to track the reference velocity vector for a reference velocity of more than 20 knots. For this reason it was decided to perform the test for a reference velocity of 30 ft/s, which is approximately 18 knots.

Considering the ideal case where the reference velocity is 30 ft/s, the velocity Channels and the yaw rate Channel have infinite bandwidth and perfect tracking of commanded response. If a yaw rate of 1 rad/s is commanded, then in order to track the reference velocity vector the instantaneous horizontal-plane velocities will vary as,

$$v_{\text{ref}} = -30\sin(t) \text{ ft/s} \quad (9.26)$$

$$u_{\text{ref}} = 30\cos(t) \text{ ft/s} \quad (9.27)$$

Because the system is not ideal, some trial and error is required to achieve the correct magnitude of response in order to attempt to track the reference velocity vector. It was also required to introduce a shaping filter into the yaw rate Channel. Figure 9.15 shows the yaw rate response to a commanded yaw rate of 5 deg/s when no shaping filter is in

place. It is seen that the transient is by no means objectionable, but for the elliptical turn manoeuvre the initial overshoot is likely to cause the helicopter to obtain a yaw attitude which will be out of phase with the sinusoid inputs. This will cause the rotorcraft to obtain a larger than necessary component of earth referenced side velocity whilst performing the manoeuvre, with a consequent decrease in the earth referenced forward velocity. By eliminating this overshoot the system will perform better, although due to the non-zero rise times of the responses, not ideally.

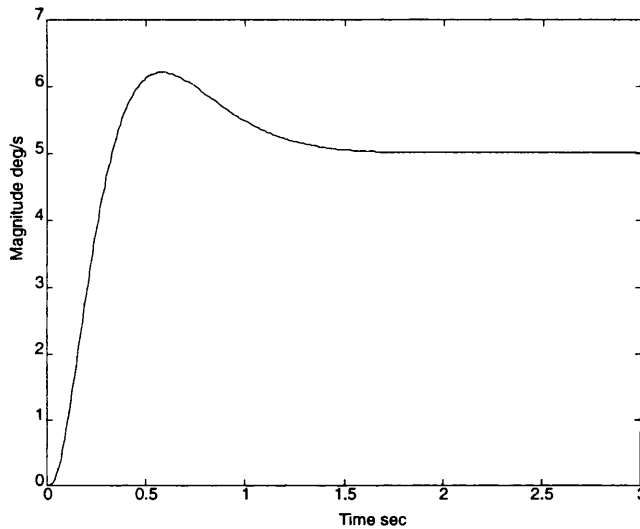


Figure 9.15. Non-linear yaw rate response due to commanded yaw rate of 5 deg/s with no shaping filter.

The yaw rate shaper is given as,

$$s_r = \frac{60(s^2 + 4s + 13)}{(s^2 + 5.66s + 13.03)(s + 60)} \tag{9.28}$$

Figure 9.16 shows the yaw response due to a commanded yaw rate of 5 deg/s with the shaping filter. It is seen that the overshoot has been reduced. The Handling Qualities bandwidth and phase delay of the yaw attitude response with s_r in place still met Level 1 requirements.

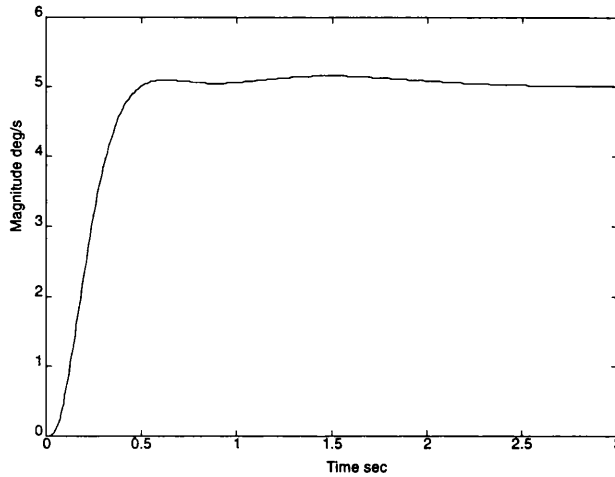


Figure 9.16. Non-linear yaw rate response due to commanded yaw rate of 5 deg/s with shaping filter.

The actual commanded velocities and yaw rate during the elliptical turn were chosen to be,

$$v_{\text{ref-actual}} = -45\sin(t) \text{ ft/s} \quad (9.29)$$

$$u_{\text{ref-actual}} = 45\cos(t) \text{ ft/s} \quad (9.30)$$

$$r_{\text{actual}} = 1 \text{ rad/s} \quad (9.31)$$

The high values of $v_{\text{ref-actual}}$ and $u_{\text{ref-actual}}$ are required to achieve the necessary size of the helicopter velocities to track the reference velocity vector.

The elliptical turn test inputs were applied 14 seconds after the commanded forward velocity, thus giving the helicopter time to achieve its reference velocity vector. By applying the elliptical turn test inputs for 19 seconds, the helicopter was able to turn through 3 full rotations. After 19 seconds of the elliptical turn test inputs, the input reverted back to the initial forward velocity command of 30 ft/s. Figure 9.17 shows the earth referenced forward and side velocities.

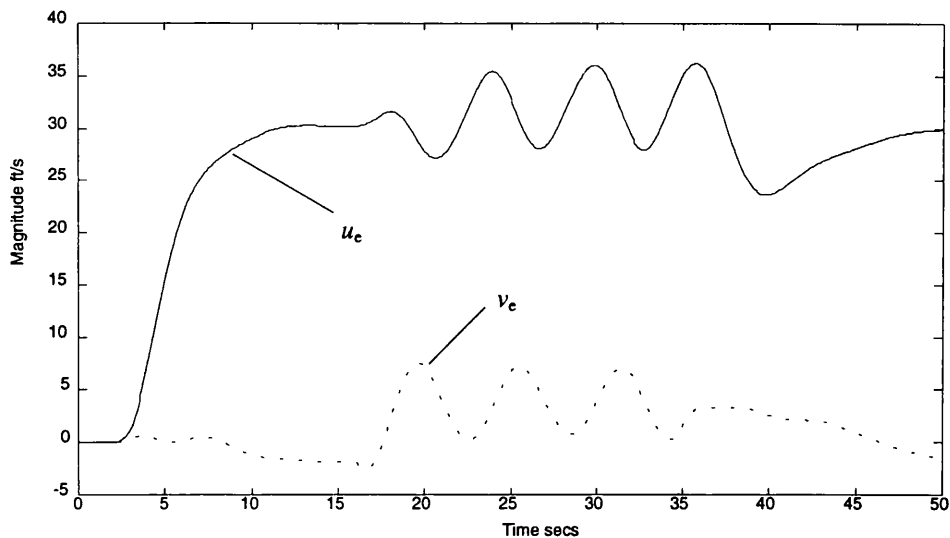


Figure 9.17. Earth referenced forward and side velocities

It is seen from Figure 9.17 that the earth referenced velocity vector is tracked relatively well, the error being oscillatory (as expected) with a magnitude of approximately 5 ft/sec peak-peak. This error is comparable to the example given in Osder and Caldwell [57], which was flown at 30 knots and exhibited peak-peak oscillations of 10 ft/s on the earth referenced velocity. However, as the model used in [57] is configured as an Apache AH-64 and not the combat rotorcraft under consideration here, no conclusions can be drawn from a comparison. However, the results presented here are regarded as being very encouraging.

Figure 9.18 shows the flight path of the helicopter and it is seen that the reference heading is held quite well.

Figure 9.19 shows the body-referenced ground velocities. It is seen the peaks of the oscillations are approximately ± 30 ft/s as required. Also, because the bandwidths of the u_h and v_h Channels are comparable, the required phase difference between the responses hold very well. If the bandwidths were different, problems would be encountered with maintaining the earth referenced velocity if using pure sine and cosine cyclic inputs in off-line simulation. In practice, the pilot would adapt correspondingly.

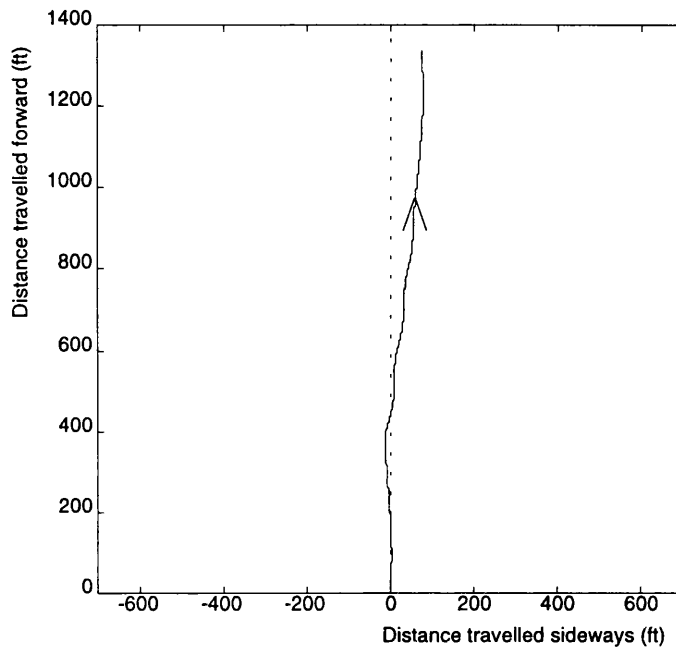
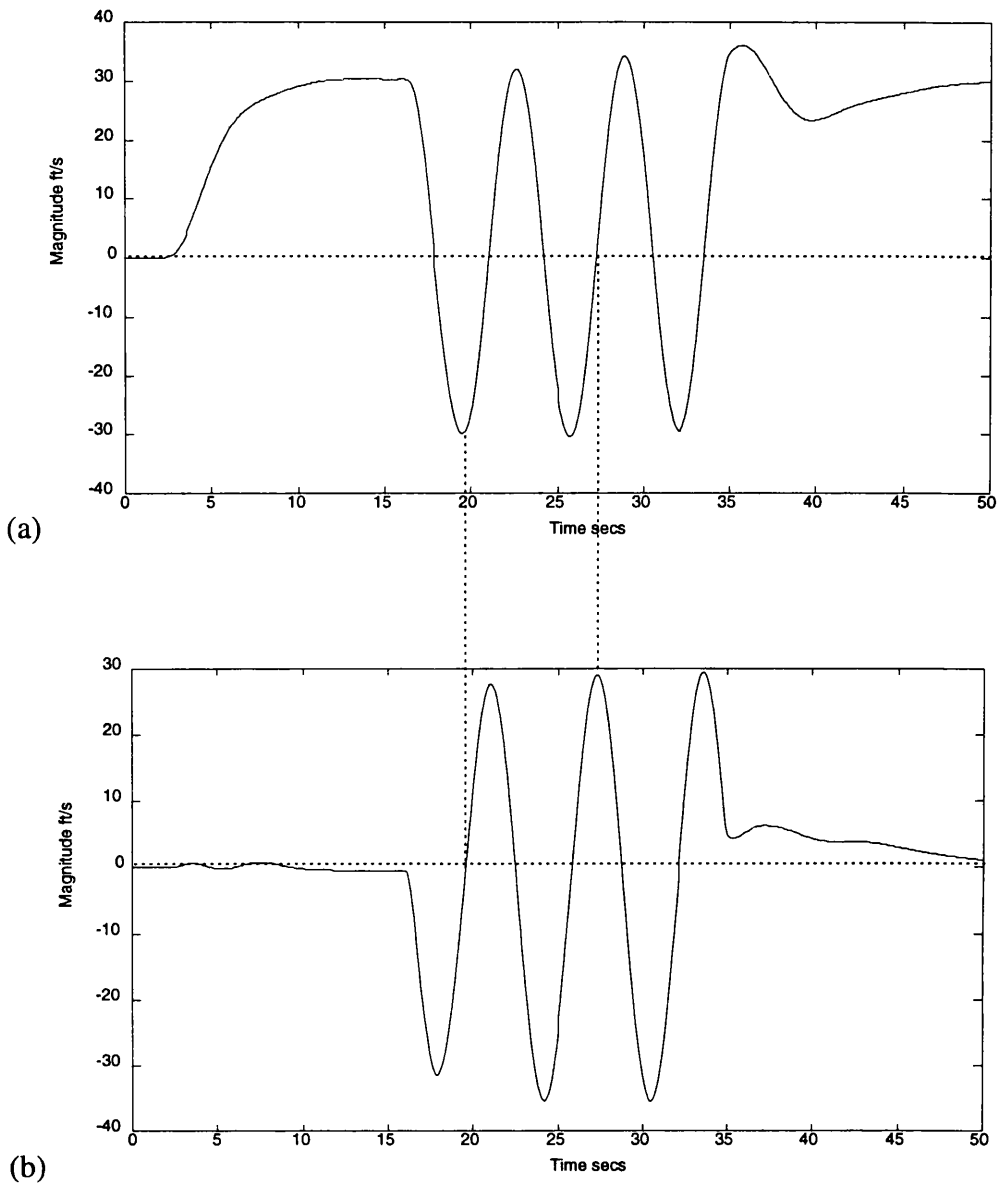


Figure 9.18. Flight path of helicopter during elliptical turn test.

One full rotation is sufficient to expose the full variation vehicle dynamics, and so the responses shown due to three full rotations demonstrates a high level of robustness.

Figure 9.19. Responses of (a) u_h and (b) v_h

9.7. Summary

This Chapter has assessed the application of ICAD to the design of a helicopter Translational Rate Command system. The system involved an inner system which controlled the attitude and outer system which controlled the translational velocities. Using the non-square methodology of Chapter 4 it was determined that the inner system did not cause the outer system to exhibit structural and/or phase sensitivity, except at approximately 5 rad/s where an unstable, very oscillatory, complex zero pair was found to exist. As the bandwidths of the velocity Channels were specified to be approximately 0.4 rad/s, this sensitivity was of no consequence as it was well above frequencies of interest.

ICA established that the desired velocity Channel bandwidths were attainable with high performance control.

The outer system was found to be robust within the context of ICA and as the inner system was robust and did not affect the sensitivity of the outer system, the complete system was regarded as possessing stability robustness.

To check the robustness of the system, a manoeuvre known as an Elliptical Turn was performed. This involved commanding a forward velocity and then yawing the helicopter and applying a sinusoidal cyclic input in an attempt to maintain the original speed and heading, whilst the helicopter rotated through three full circles. The TRC system enabled the helicopter to achieve this within tolerable limits and therefore showed that the system had a good degree of robustness.

The feedback controller had only six elements and 16 states. The prefilter had only 4 elements and 8 states, showing that high order, complex control is not a necessity to achieve robust TRC augmentation which meets Level 1 requirements.

In conclusion, ICAD has been found to be very well suited to the design of a helicopter Translational Rate Command system.

10.1. Conclusions

This thesis has assessed the applicability of Individual Channel Analysis and Design (ICAD) to the analysis and design of helicopter flight control laws. Particular attention has been made to the achievement of Level 1 Handling Qualities for both small-amplitude and moderate-amplitude manoeuvres. Two shortcomings in ICAD theory were identified during initial application of the technique. The first was the lack of an effective technique to calculate the various multivariable structure functions (MSFs) needed for analysis and design. The higher the number of inputs and outputs of a system, the less manageable the calculation of MSFs become, particularly if attempting to calculate determinants of transfer function matrices. Also, numerical errors associated with convoluting polynomials becomes more pronounced for systems with more than 2-inputs and 2-outputs, particularly if the order of the system is large. Because the systems under consideration in this work were exclusively state space, a state space technique was developed in Chapter 5 in order to calculate the MSFs. This technique is well suited to implementation in MATLAB[®] and has been found through experience to effectively and efficiently calculate MSFs with little numerical error. The largest order of model under consideration in this thesis in which an MSF was to be calculated was 4-input 4-output with 30 states. The state space algorithm was not troubled by a system of this size.

The second deficiency arose through a need to consider non-square systems. That is, a system with more outputs to be fed back than there are inputs. A particular example of such a system is a Translational Rate Command system which requires inner attitude

loop closure via the longitudinal and lateral cyclic and outer velocity closure via the longitudinal and lateral cyclic.

ICAD had no provision for the analysis of such a system before the work of this thesis and so a technique was required to be developed. Chapter 4 dealt with such a development. Care was taken to maintain the spirit of ICAD in the technique and the author feels that this has been achieved. The non-square technique was successfully applied to the design of a Translational Rate Command system.

Chapter 6 discussed the design issues concerned with systems with more than 2-inputs and 2-outputs. A design procedure using nested Channels was described and the design of stabilising controllers for both minimum phase and non minimum phase plants was presented. For non-minimum phase plants it was shown how one could trace the origin of the RHP transmission zero(s) and then determine design trade-offs from this information.

Chapters 7 through 9 presented the analysis and design of three different helicopter flight control laws. ICAD was found to be a highly visible technique for the designs and allowed explicit consideration of Handling Qualities issues during the design process. Although the models used for design were 19th order, the control laws were of lower order and highly effective. The robustness diagnostic that ICAD provides, via consideration of the Channel multivariable structure functions, showed that all the designs were expected to possess stability robustness except at very low frequencies. This lack of robustness at low frequencies was not considered as being a problem, as pilots are capable of controlling slow instabilities, which may arise, with a minimal increase in workload. For the ACAH and Rate Command designs of Chapters 7 and 8, the fixed control law designed for 30 knots forward flight was found to meet Level 1 requirements, not only at 30 knots, but over the range from hover to 80 knots for both linear and non-linear simulation. The Translational Rate Command design of Chapter 9 was found to meet Level 1 requirements and performed well in non-linear simulation for a manoeuvre known as an elliptical turn. This manoeuvre is designed to test the 'practical' robustness of a helicopter control law by forcing the helicopter to rotate through at least 360° while in forward flight.

It can be concluded that ICAD is an analysis and design technique which is extremely well suited to the analysis and design of high performance helicopter flight control systems. It enables explicit consideration of helicopter Handling Qualities requirements and results in simple, transparent and effective control laws, which are capable of operating at Level 1 over a large flight envelope. In addition, ICAD has been developed generically for effective use with non-square systems and systems described by state space models.

10.2. Future Work

There are various aspects of ICAD and helicopter flight control which are still to be investigated. These aspects are listed in no particular order.

The development of the non-square theory in Chapter 4 proposes conditions to assess the robustness of a non-square system. The conditions make sense from an engineering viewpoint, but proving the conditions will take a more rigorous mathematical approach than has been given in this thesis.

Chapter 6 mentioned that the nested design procedure could cater for guaranteeing closed-loop stability for systems with bounded errors. The guidelines for achieving this are relatively simple in concept. One would have to determine the bounds of the nested approximate MSFs and of the diagonal transfer function elements. Once this is done the design could proceed in a straightforward manner by ensuring that the bounded actual MSFs do not include the (1,0) point and that the gain and phase margins of the nested Channels remain positive. This is simple in concept but has the potential to be computationally extensive.

The low frequency sensitivity issue has left a couple of unanswered questions. First and foremost, what is the physical reason for the sensitivity? If this question can be answered then a general assessment of the sensitivity can be made. Second, for the rate command system it was found that three of the Channel MSFs go to *exactly* (1,0) at

zero frequency. This was due to three of the outputs essentially being the rate of change of heading angle at zero frequency. What is the significance of this in terms of robustness?

The designs in this thesis considered the flight range from hover to 80 knots. Extending the work to achieve a full flight-envelope design will require that speeds above 80 knots are considered.

There is current interest in the literature in the design of high bandwidth control systems which will either utilise rotor state feedback (Takahashi [72]) or will need to explicitly consider higher order dynamics which include rotor dynamics (Ingle and Celi [28]). Although the designs in this thesis used models which included rotor states, the rotor dynamics are fairly benign in that they model the rotor as a disc, as opposed to individual blades, and describe only flapping and coning modes. In addition, the bandwidths of the control laws, although Level 1, are not at high enough frequencies for the rotor dynamics to start coupling with the feedback control system. If higher bandwidths are to be achieved then models which include a more advanced representation of rotor dynamics is required. An individual blade element model has recently been developed at the University of Glasgow (Houston [26]) and a linear model derived from the non-linear model will have many more states due to the increased complexity of the dynamics. The only effective way to assess such a system will be to use the state space algorithms of Chapter 5. The ICAD techniques developed in this thesis are well tailored to the analysis of much more complex systems which more modern techniques will be unable to address satisfactorily due to the large number of states.

System integrity is a topic which was not dealt with in this thesis, e.g. what happens if a sensor fails? This aspect is important for fault tolerance analysis and safety issues.

Finally, automatic control laws implemented on helicopters do not operate autonomously, but in conjunction with the pilot. Operator-in-the-loop simulations is a natural extension to the work which will require real-time simulation. Work of this kind will give an indication of implementation issues arising from real-time considerations

and will also go one stage further in the assessment of the operating aspects of the control laws.

Bibliography

- [1] Adams, R.J., Sparks, A. and Banda, S.S., 'Full Envelope Multivariable Control Law Synthesis for a High-Performance test Aircraft', *Journal of Guidance, Control and Dynamics*, Vol. 16, No. 5, September-October, 1993.
- [2] Andry, A.N., Shapiro, E.Y. and Chung, J.C., 'Eigenstructure Assignment for Linear Systems', *IEEE Transactions on Aerospace and Electronic Systems*, Vol. 19, No. 5, 1983.
- [3] Anonymous, 'Aeronautical Design Standard - Handling Qualities Requirements for Military Rotorcraft (ADS-33D)', *United States Army Aviation and Troop Command, St. Louis, MO, Directorate for Engineering*, July 1994.
- [4] Apkarian, P.R., 'Structured Stability Robustness Improvement by Eigenspace Techniques: A Hybrid Methodology', *Journal of Guidance, Control and Dynamics*, Vol. 12, No. 2, pp 162-168, March-April 1989.
- [5] Athans, M., 'The Role and Use of the Stochastic Linear-Quadratic-Gaussian Problem in Control System Design', *IEEE Transactions on Automatic Control*, Vol. AC-16, No. 6, December, 1971.
- [6] Brinson, P.R., 'Towards Higher Bandwidth in Helicopter Flight Control Systems', *The Royal Aeronautical Society Helicopter Handling Qualities and Control International Conference - Conference Papers*, London, November 1988.
- [7] Catapang, D.R., Tischler, M.B. and Biezad, D.J., 'Robust Crossfeed Design for Hovering Rotorcraft', *International Journal of Robust and Nonlinear Control*, Vol. 4, 161-180, 1994.
- [8] Cooper, G.E. and Harper, R.P., 'The Use of Pilot Ratings in the Evaluation of Aircraft Handling Qualities', *NASA TM D-5133*, 1969.
- [9] Dudgeon, G.J.W., Gribble, J.J. and O'Reilly, J., 'The Use of Individual Channel Analysis and Design to Meet Helicopter Handling Qualities Requirements',

Proceedings of the 21st European Rotorcraft Forum, Vol. 3, Paper VII-3, 1995.

- [10] Dudgeon, G.J.W., Gribble, J.J. and O'Reilly, J., 'Individual Channel Analysis and Helicopter Flight Control in Moderate and Large Amplitude Manoeuvres', *Proceedings of The 13th IFAC World Congress*, Vol. P, Paper 8a-08 3, 207-212, 1996.
- [11] Dudgeon, G.J.W. and Gribble, J.J., 'Helicopter Translational Rate Command Using Individual Channel Analysis and Design', *Proceedings of UKACC Control'96*, Vol. 1, 632-637, 1996.
- [12] Fu, K-H. and Kaletka, J., 'Frequency-Domain Identification of BO105 Derivative Models with Rotor Degrees of Freedom', *Journal of the American Helicopter Society*, Vol. 38, No. 1, January 1993.
- [13] Garrard, W.L. and Liebst, B.S., 'Design of a Multivariable Helicopter Flight Control System for Handling Qualities Enhancement', *Journal of the American Helicopter Society*, Vol. 35, No. 4, October 1990.
- [14] Golten, J. and Verwer, A., 'Control System Design and Simulation', *McGraw-Hill Book Company*, 1991.
- [15] Gribble, J.J., 'Linear Quadratic Gaussian/Loop Transfer Recovery Design for a Helicopter in Low Speed Flight', *Journal of Guidance, Control and Dynamics*, Vol. 16, NO. 4, July-August 1993.
- [16] Gribble, J.J., and Murray-Smith, D.J., 'Command Following Control Law Design by Linear Quadratic Optimisation', *Proceedings of the 16th European Rotorcraft Forum*, Vol. 1, Paper III.5.3.1, 1990.
- [17] Ham, J.A., Gardner, C.K., and Tischler, M.B., 'Flight-Testing and Frequency-Domain Analysis for Rotorcraft Handling Qualities', *Journal of the American Helicopter Society*, 28-38, April 1995.
- [18] Harding, J.W., 'Frequency-Domain Identification of Coupled Rotor/Body Models of an Advanced Attack Helicopter', *Presented at the 48th Annual Forum of the American Helicopter Society*, Washington, D.C., June 3-5, 1992.

- [19] Hess, R.A. and Gorder, P.J., 'Quantitative Feedback Theory Applied to the Design of a Rotorcraft Flight Control System', *Journal of Guidance, Control and Dynamics*, Vol. 16, No. 4, July-August 1993.
- [20] Hess, R.A., 'Rotorcraft Control System Design for Uncertain Vehicle Dynamics Using Quantitative Feedback Theory', *Journal of the American Helicopter Society*. Vol. 39, No.2, 1994.
- [21] Hess, R.A., 'Rotorcraft Handling Qualities in Turbulence', *Journal of Guidance, Control and Dynamics*, Vol. 18, No. 1, January-February, 1995.
- [22] Hoh, R.G., 'Dynamic Requirements in the New Handling Qualities Specification for U.S. Military Rotorcraft', *The Royal Aeronautical Society Helicopter Handling Qualities and Control International Conference - Conference Papers*, London, November 1988.
- [23] Hoh, R.G., Transcript of discussion of 'Dynamic Requirements in the New Handling Qualities Specification for U.S. Military Rotorcraft', *The Royal Aeronautical Society Helicopter Handling Qualities and Control International Conference - Companion Volume: Post Conference Report & Late Papers*, London, November 1988.
- [24] Horowitz, I.M., 'Synthesis of feedback systems with large plant ignorance for prescribed time-domain tolerances', *International Journal of Control*, Vol. 16, No. 2, 1972.
- [25] Horowitz, I., 'Survey of quantitative feedback theory', *International Journal of Control*, Vol. 53, No. 2, 1991.
- [26] Houston, S.S., 'Validation of a non-linear individual blade rotorcraft flight dynamics model using a perturbation method', *The Aeronautical Journal of the Royal Aeronautical Society*, August-September, 1994.
- [27] Howitt, J., 'MATLAB Toolbox for Handling Qualities Assessment of Flight Control Laws', *Proceedings of the IEE International Conference on Control'91*, London, 1251-1256, 1991.

- [28] Ingle, S.J. and Celi, R., 'Effects of Higher Order Dynamics on Helicopter Flight Control Law Design', *Presented at the 48th Annual Forum of the American Helicopter Society*, Washington, D.C., June 1992.
- [29] Innocenti, M. and Schmidt, D.K., 'Quadratic Optimal Cooperative Control Synthesis with Flight Control Application', *Journal of Guidance, Control and Dynamics*, Vol. 7, No. 2, March-April 1984.
- [30] Innocenti, M. and Stanziola, C., 'Performance-robustness trade off of eigenstructure assignment applied to rotorcraft', *Aeronautical Journal*, Vol. 94, No. 934, 1990.
- [31] Kaletka, J. and Gimonet, B., 'Identification of Extended Models From BO 105 Flight Test Data for Hover Flight Condition', *Proceedings of the 21st European Rotorcraft Forum*, Paper No. VII-7, 1995.
- [32] Kim, F.D., Celi, R. and Tischler, M.B., 'High-Order State Space Simulation Models of helicopter Flight Mechanics', *Presented at the 46th Annual Forum of the American Helicopter Society*, Washington, D.C., May 1990.
- [33] Leithead, W.E. and O'Reilly, J., 'Investigation of the ICD structure of systems defined by state-space models', *International Journal of Control*, Vol. 60, No. 1, 1994.
- [34] Leithead, W.E. and O'Reilly, J., 'm-input m-output feedback-control by individual channel design Part 1. structural issues', *International Journal of Control*, Vol. 56, No. 6, 1992.
- [35] Leithead, W.E. and O'Reilly, J., 'New roles for feedforward in multivariable control by individual channel design', *International Journal of Control*, Vol. 57, No. 6, 1993.
- [36] Leithead, W.E. and O'Reilly, J., 'Performance issues in the individual channel design of 2-input 2-output systems Part 1. structural issues', *International Journal of Control*, Vol. 54, No. 1, 1991.

- [37] Leithead, W.E. and O'Reilly, J., 'Performance issues in the individual channel design of 2-input 2-output systems Part 2. robustness issues', *International Journal of Control*, Vol. 55, No. 1, 1992.
- [38] Leithead, W.E. and O'Reilly, J., 'Performance issues in the individual channel design of 2-input 2-output systems Part 3. nondiagonal control and related issues', *International Journal of Control*, Vol. 55, No. 2, 1992.
- [39] Leithead, W.E. and O'Reilly, J., 'The role of single-loop subsystems in multivariable control by individual channel design of 2-input 2-output systems', *International Journal of Control*, Vol. 57, No. 4, 1993.
- [40] Liceaga-Castro, J., Verde, C., O'Reilly, J. and Leithead, W.E., 'Helicopter flight control using individual channel design', *IEE Proc.-Control Theory Appl.*, Vol. 142, No. 1, January 1995.
- [41] Low, E. and Garrard, W.L., 'Design of Flight Control Systems to Meet Rotorcraft Handling Qualities Specifications', *Journal of Guidance, Control and Dynamics*, Vol. 16, No. 1, January-February, 1993.
- [42] MacFarlane, A.G.J. and Kouvaritakis, B., 'A design technique for linear multivariable feedback systems', *International Journal of Control*, Vol. 25, 1977.
- [43] Maciejowski, J.M., 'Multivariable feedback design', *Addison-Wesley Press*, 1989.
- [44] Manness, M.A., Gribble, J.J. and Murray-Smith, D.J., 'Multivariable Methods for Helicopter Flight Control Law Design: A Review', *Proceedings of the Sixteenth European Rotorcraft Forum*, Vol. 1, Paper III.5.2.1, 1990.
- [45] Manness, M.A., Gribble, J.J. and Murray-Smith, D.J., 'Helicopter Flight Control System Design Methodologies', September, 1991.
- [46] Manness, M.A. and Murray-Smith, D.J., 'Aspects of Multivariable Flight Control Law Design for Helicopters Using Eigenstructure Assignment', *Journal of the American Helicopter Society*, Vol. 37, No.3, 1992.

- [47] Mayne, D.Q., 'The design of linear multivariable systems', *Automatica*, Vol. 9, 1973.
- [48] McCormick, B.W., 'Aerodynamics, Aeronautics and Flight Mechanics', *John Wiley & Sons*, 1995.
- [49] McFarlane, D. and Glover, K., 'A Loop Shaping Design procedure Using H-inf Synthesis', *IEEE Transactions on Automatic Control*, Vol. 37, No. 6, June 1992.
- [50] McLean, D., 'Automatic Flight Control Systems', *Prentice Hall International*, 1990.
- [51] Mudge, S.K. and Patton, R.J., 'Analysis of the technique of robust eigenstructure assignment with application to aircraft control', *IEE proceedings*, Vol. 135, Pt. D, No. 4, July 1988.
- [52] Murray-Smith, D.J., 'Modelling limitations for helicopter flight control system design', *EUROSIM'95*, 1995.
- [53] O'Reilly, J. and Leithead, W.E., 'Multivariable control by 'individual channel design'', *International Journal of Control*, Vol. 54, No. 1, 1991.
- [54] Ockier, C.J. and Pausder, H.-J., 'Experiences with ADS-33 Helicopter Specification Testing and Contributions to Refinement Research', *Presented at the AGARD Flight Mechanics Panel Symposium on Active Control Technology: Applications & Lessons Learned*, Turin, Italy, May 9-12, 1994.
- [55] Ockier, C.J., 'Flight Evaluation of the New Handling Qualities Criteria Using the BO 105', *Journal of the American Helicopter Society*, January 1996.
- [56] Osborne, R.C., Adams, R.J., Hsu, C.S. and Banda, S.S., 'Reduced-Order H^∞ Compensator design for an Aircraft Control Problem', *Journal of Guidance, Control and Dynamics*, Vol. 17, No. 2, March-April 1994.
- [57] Osder, S. and Caldwell, D., 'Design and Robustness Issues for highly Augmented Helicopter Controls', *Journal of Guidance, Control and Dynamics*, Vol. 15, No. 6, November-December, 1992.

- [58] Osder, S., 'Practical robustness testing for helicopter flight control systems', *47th Annual Proceedings of the American Helicopter Society*, Phoenix, AZ, 1991.
- [59] Padfield, G.D., 'A Theoretical Model of Helicopter Flight Mechanics for Application to Piloted Simulation', *Royal Aircraft Establishment*, Technical Report 81048, 1981.
- [60] Padfield, G.D., 'Helicopter Flight Dynamics', *Blackwell Science Press*, 1996.
- [61] Padfield, G.D. and DuVal, R.W., 'Application Areas for Rotorcraft System Identification Simulation Model Validation', *Agard LS 178, Rotorcraft System Identification*, 1991.
- [62] Padfield, G.D., Jones, J.P., Charlton, M.T., Howell, S.E. and Bradley, R., 'Where Does the Workload go When Pilots Attack Manoeuvres? An Analysis of Results from Flying Qualities Theory and Experiment', *Proceedings of the 20th European Rotorcraft Forum*, October 4-7, 1994.
- [63] Prouty, R.W., 'Helicopter Aerodynamics', *PJS Publications Inc.*, 1985.
- [64] Prouty, R.W., 'More Helicopter Aerodynamics', *PJS Publications Inc.*, 1988.
- [65] Ray, L.R. and Stengel, R.F., 'A Monte Carlo Approach to the Analysis of Control System Robustness', *Automatica*, Vol. 29, No. 1, 1993.
- [66] Safonov, M.G., 'Stability margins of diagonally perturbed multivariable feedback systems', *IEE Proceedings*, Vol. 129, Pt. D, No. 6, November, 1982.
- [67] Saunders, G.H., 'Dynamics of Helicopter Flight', *Published by John Wiley and Sons, Inc.*, 1975.
- [68] Schroeder, J.A., Watson, D.C., Tischler, M.B. and Eshow, M.M., 'Identification and Simulation Evaluation of an AH-64 Helicopter Math Model', *AIAA Atmospheric Flight Mechanics Conference*, New Orleans, Louisiana, August 12-14, 1991.
- [69] Smerlas, A.J., Postlethwaite, I. and Walker D.J., 'Full Envelope Robust Control Law for the Bell-205 Helicopter', *Proceedings of the 22nd European Rotorcraft Forum*, 16-19 September, 1996.

- [70] Smith, J., 'An analysis of helicopter flight mechanics Part I - Users guide to the software package HELISTAB', *Royal Aircraft Establishment*, Technical Memorandum FS(B) 569, October 1984.
- [71] Stein, G. and Athans, M., 'The LQG/LTR Procedure for Multivariable Feedback Control Design', *IEEE Transactions on Automatic Control*, Vol. AC-32, No. 2, February, 1987.
- [72] Takahashi, M.D., 'H[∞] Helicopter Flight Control Law Design With and Without Rotor State Feedback', *Journal of Guidance, Control and Dynamics*, Vol. 17, No. 6, November-December, 1994.
- [73] Takahashi, M.D., 'Rotor-State Feedback in the Design of Flight Control Laws for a Hovering Helicopter', *Journal of the American Helicopter Society*, January 1994.
- [74] Tischler, M.B., 'Assessment of Digital Flight-Control Technology for Advanced Combat Rotorcraft', *Journal of the American Helicopter Society*, Vol. 34, No. 4, 1989.
- [75] Tischler, M.B., 'Digital Control of Highly Augmented Combat Rotorcraft', *NASA-Technical Memorandum 88346*, USAAVSCOM Technical Report 87-A-5, May 1987.
- [76] Tischler, M.B., 'System Identification Requirements for High-Bandwidth Rotorcraft Flight Control System Design', *Journal of Guidance, Control and Dynamics*, Vol. 13, No. 5, September-October 1990.
- [77] Tischler, M.B., Fletcher, J.W., Morris, P.M. and Tucker, G.E., 'Flying Quality Analysis and Flight Evaluation of a Highly Augmented Combat Rotorcraft', *Journal of Guidance, Control and Dynamics*, Vol. 14, No. 5, September-October 1991.
- [78] Walker, D.J. and Postlethwaite, I., 'Advanced Helicopter Flight Control Using Two-Degree-Of-Freedom H[∞] Optimization', *Journal of Guidance, Control and Dynamics*, Vol. 19, No. 2, March-April 1996.

- [79] Young, J-S. and Lin, C.E., 'Refined H^∞ -Optimal Approach to Rotorcraft Flight Control', *Journal of Guidance, Control and Dynamics*, Vol. 16, No. 2, March-April 1993.

This Appendix lists the configuration data, relevant to the equations listed in Section 2.2, which is used to configure the rationalised helicopter model (RHM) as a Lynx-like helicopter.

| | | |
|--|-----------|--------------------------|
| Helicopter mass | M_h | 4313.7 kg |
| Moments of Inertia | I_{xx} | 2767.1 kgm ² |
| | I_{yy} | 13904.5 kgm ² |
| | I_{zz} | 12208.8 kgm ² |
| Product of Inertia | I_{xz} | 2034.8 kgm ² |
| Rotor Stiffness | K_β | 166352 Nm/rad |
| Main rotor angular rate | Ω | 35.63 rad/s |
| Number of blades | N_b | 4 |
| | | |
| Main rotor collective actuator time constant | | 0.0795 sec |
| Longitudinal cyclic actuator time constant | | 0.0795 sec |
| Lateral cyclic actuator time constant | | 0.0795 sec |
| Tail rotor collective actuator time constant | | 0.04 sec |

The following state space matrices form the 19th order linear model of a typical combat rotorcraft in hover. The model was produced from HELISTAB (Smith [70]).

$$A = \begin{bmatrix} A_{\text{rigidbody}} & \vdots & A_{\text{body/rotor}} & \vdots & \\ \dots & \dots & \dots & \vdots & A_{\text{control}} \\ A_{\text{rotor/body}} & \vdots & A_{\text{rotor}} & \vdots & \\ \dots & \dots & \dots & \dots & \dots \\ & 0_A & & \vdots & A_{\text{actuators}} \end{bmatrix} \quad (\text{II.1})$$

where 0_A is a zero matrix of dimension (4,15) and,

$$A_{\text{rigidbody}} = \begin{bmatrix} -3.529e-3 & 2.271e-2 & 3.374e-3 & -3.209e+1 & 2.138e-4 & 1.308e-3 & 0.000e+0 & 0.000e+0 & 0.000e+0 \\ 2.382e-2 & -3.112e-1 & 4.464e-2 & -2.367e+0 & -2.891e-3 & -1.769e-2 & 1.709e+0 & 0.000e+0 & 0.000e+0 \\ 1.127e-4 & 6.864e-4 & -8.503e-4 & 0.000e+0 & 8.940e-6 & 5.467e-5 & 0.000e+0 & 0.000e+0 & 0.000e+0 \\ 0.000e+0 & 0.000e+0 & 9.986e-1 & 0.000e+0 & 0.000e+0 & 0.000e+0 & 0.000e+0 & 5.328e-2 & 0.000e+0 \\ 9.083e-5 & -1.182e-3 & 1.116e-4 & 1.237e-1 & -2.382e-2 & -7.506e-2 & 3.205e+1 & 4.487e-1 & 0.000e+0 \\ 2.402e-5 & -1.183e-4 & -1.388e-4 & 0.000e+0 & -1.396e-4 & 8.374e-5 & 0.000e+0 & -2.780e-2 & 0.000e+0 \\ 0.000e+0 & 0.000e+0 & -3.935e-3 & 0.000e+0 & 0.000e+0 & 1.000e+0 & 0.000e+0 & 7.374e-2 & 0.000e+0 \\ -7.583e-5 & 1.414e-3 & -4.901e-4 & 0.000e+0 & 1.479e-2 & 5.618e-2 & 0.000e+0 & -3.745e-1 & 0.000e+0 \\ 0.000e+0 & 0.000e+0 & -5.343e-2 & 0.000e+0 & 0.000e+0 & 0.000e+0 & 0.000e+0 & 1.001e+0 & 0.000e+0 \end{bmatrix} \quad (\text{II.2})$$

$$A_{\text{body/rotor}} = \begin{bmatrix} 0.000e+0 & 3.206e+1 & 0.000e+0 & 0.000e+0 & 0.000e+0 & 0.000e+0 \\ 0.000e+0 & 0.000e+0 & 0.000e+0 & 0.000e+0 & 0.000e+0 & 0.000e+0 \\ 0.000e+0 & -2.778e+1 & 0.000e+0 & 0.000e+0 & 0.000e+0 & 0.000e+0 \\ 0.000e+0 & 0.000e+0 & 0.000e+0 & 0.000e+0 & 0.000e+0 & 0.000e+0 \\ 0.000e+0 & 0.000e+0 & -3.206e+1 & 0.000e+0 & 0.000e+0 & 0.000e+0 \\ 0.000e+0 & 9.770e-5 & -1.609e+2 & 0.000e+0 & 0.000e+0 & 0.000e+0 \\ 0.000e+0 & 0.000e+0 & 0.000e+0 & 0.000e+0 & 0.000e+0 & 0.000e+0 \\ 0.000e+0 & 2.223e-4 & -2.903e+1 & 0.000e+0 & 0.000e+0 & 0.000e+0 \\ 0.000e+0 & 0.000e+0 & 0.000e+0 & 0.000e+0 & 0.000e+0 & 0.000e+0 \end{bmatrix} \quad (\text{II.3})$$

$$A_{\text{rotor/body}} = \begin{bmatrix} 0.000e+0 & 0.000e+0 \\ 0.000e+0 & 0.000e+0 \\ 0.000e+0 & 0.000e+0 \\ -4.912e-2 & 6.376e-1 & -6.195e-2 & 0.000e+0 & 6.018e-3 & 2.518e-2 & 0.000e+0 & 0.000e+0 & 0.000e+0 \\ -8.513e-1 & -5.951e-2 & 3.532e+1 & 0.000e+0 & 4.192e-1 & 7.301e+1 & 4.770e-6 & 0.000e+0 & 0.000e+0 \\ 4.182e-1 & 2.909e-2 & -7.302e+1 & 1.574e-4 & 8.533e-1 & 3.530e+1 & 3.815e-5 & -2.780e-2 & 0.000e+0 \end{bmatrix} \quad (\text{II.4})$$

$$A_{\text{rotor}} = \begin{bmatrix} 0.000e+0 & 0.000e+0 & 0.000e+0 & 1.000e+0 & 0.000e+0 & 0.000e+0 \\ 0.000e+0 & 0.000e+0 & 0.000e+0 & 0.000e+0 & 1.000e+0 & 0.000e+0 \\ 0.000e+0 & 0.000e+0 & 0.000e+0 & 0.000e+0 & 0.000e+0 & 1.000e+0 \\ -1.515e+3 & 0.000e+0 & 0.000e+0 & -3.173e+1 & 0.000e+0 & -2.110e-4 \\ -1.507e-2 & -2.731e+2 & -1.131e+3 & 0.000e+0 & -3.173e+1 & -7.126e+1 \\ 0.000e+0 & 1.131e+3 & -4.062e+2 & -4.221e-4 & 7.126e+1 & -3.173e+1 \end{bmatrix} \quad (\text{II.5})$$

$$A_{\text{actuators}} = \begin{bmatrix} -1.258e+1 & 0.000e+0 & 0.000e+0 & 0.000e+0 \\ 0.000e+0 & -1.258e+1 & 0.000e+0 & 0.000e+0 \\ 0.000e+0 & 0.000e+0 & -1.258e+1 & 0.000e+0 \\ 0.000e+0 & 0.000e+0 & 0.000e+0 & -2.500e+1 \end{bmatrix} \quad (\text{II.6})$$

$$A_{\text{control}} = \begin{bmatrix} 2.281e+1 & 5.166e-4 & 1.447e-4 & 0.000e+0 \\ -3.085e+2 & -7.274e-3 & -1.653e-3 & 0.000e+0 \\ 9.538e-1 & 2.476e-5 & 6.190e-6 & 0.000e+0 \\ 0.000e+0 & 0.000e+0 & 0.000e+0 & 0.000e+0 \\ -1.182e+0 & -2.067e-5 & 0.000e+0 & 1.845e+1 \\ 7.038e+1 & 1.545e-4 & 0.000e+0 & -1.125e+0 \\ 0.000e+0 & 0.000e+0 & 0.000e+0 & 0.000e+0 \\ 1.730e+1 & 3.278e-4 & 0.000e+0 & -1.515e+1 \\ 0.000e+0 & 0.000e+0 & 0.000e+0 & 0.000e+0 \\ 7.632e+2 & 9.155e-3 & 0.000e+0 & 0.000e+0 \\ 9.538e-1 & 0.000e+0 & 1.131e+3 & 0.000e+0 \\ 7.062e+0 & 1.131e+3 & 2.384e-5 & 0.000e+0 \end{bmatrix} \quad (\text{II.7})$$

$$B = \begin{bmatrix} \dots & \dots & 0_B & \dots & \dots \\ 1.258e+1 & 0.000e+0 & 0.000e+0 & 0.000e+0 \\ 0.000e+0 & 1.258e+1 & 0.000e+0 & 0.000e+0 \\ 0.000e+0 & 0.000e+0 & 1.258e+1 & 0.000e+0 \\ 0.000e+0 & 0.000e+0 & 0.000e+0 & 2.500e+1 \end{bmatrix} \quad (\text{II.8})$$

$$C_{\text{unc}} = \begin{bmatrix} 1.473e-2 & -1.992e-1 & 0.000e+0 & 0.000e+0 & 1.063e-2 & 0.000e+0 & 0.000e+0 & 0.000e+0 & \vdots \\ 0.000e+0 & 0.000e+0 & 1.146e+1 & 1.146e+1 & 0.000e+0 & 0.000e+0 & 0.000e+0 & 0.000e+0 & \vdots \\ 0.000e+0 & 0.000e+0 & 0.000e+0 & 0.000e+0 & 0.000e+0 & 1.146e+1 & 1.146e+1 & 0.000e+0 & \vdots \\ 0.000e+0 & 1.146e+1 & \vdots \\ 1.995e-1 & 1.471e-2 & 0.000e+0 & 0.000e+0 & -7.831e-4 & 0.000e+0 & 0.000e+0 & 0.000e+0 & \vdots \\ 0.000e+0 & 1.064e-2 & 0.000e+0 & 0.000e+0 & 1.997e-1 & 0.000e+0 & 0.000e+0 & 0.000e+0 & \vdots \end{bmatrix} \quad (\text{II.9})$$

where 0_B is a zero matrix of dimension (15,4) and 0_C is a zero matrix of dimension (6,11).

$$D = \begin{bmatrix} 0.000e+0 & 0.000e+0 & 0.000e+0 & 0.000e+0 \\ 0.000e+0 & 0.000e+0 & 0.000e+0 & 0.000e+0 \end{bmatrix} \quad (\text{II.10})$$

The state vector is,

$$x = [x_{\text{rigidbody}} \quad x_{\text{rotor}} \quad x_{\text{actuator}}] \quad (\text{II.11})$$

where,

$$x_{\text{rigidbody}} = [u \quad w \quad q \quad \theta \quad v \quad p \quad \phi \quad r \quad \psi] \quad (\text{II.12})$$

$$x_{\text{rotor}} = [\beta_0 \quad \beta_{1c} \quad \beta_{1s} \quad \dot{\beta}_0 \quad \dot{\beta}_{1c} \quad \dot{\beta}_{1s}] \quad (\text{II.13})$$

$$x_{\text{actuator}} = [\theta_{0_{\text{act}}} \quad \theta_{1s_{\text{act}}} \quad \theta_{1c_{\text{act}}} \quad \theta_{0T_{\text{act}}}] \quad (\text{II.14})$$

The translational rates are in ft/s and the angles and angular rates are in rad and rad/s respectively.

The values of the states which have non-zero trim values are,

$$\Theta_0 = 0.07371 \text{ rad}$$

$$\Phi_0 = -0.05412 \text{ rad}$$

The following state space matrices form the 19th order linear model of a typical combat rotorcraft trimmed at 30 knots forward flight. The model was produced from HELISTAB (Smith [70]).

$$A = \begin{bmatrix} A_{\text{rigidbody}} & \vdots & A_{\text{body/rotor}} & \vdots & \\ \dots & \dots & \dots & \vdots & A_{\text{control}} \\ A_{\text{rotor/body}} & \vdots & A_{\text{rotor}} & \vdots & \\ \dots & \dots & \dots & \dots & \dots \\ & 0_A & & \vdots & A_{\text{actuators}} \end{bmatrix} \tag{III.1}$$

where 0_A is a zero matrix of dimension (4,15) and,

$$A_{\text{rigidbody}} = \begin{bmatrix} 2.056e-3 & 3.855e-2 & -3.349e+0 & -3.212e+1 & 1.274e-3 & 3.664e-2 & 0.000e+0 & 0.000e+0 & 0.000e+0 \\ -1.632e-1 & -5.333e-1 & 5.122e+1 & -2.086e+0 & -1.718e-2 & -4.941e-1 & 1.303e+0 & 0.000e+0 & 0.000e+0 \\ 7.267e-4 & -1.137e-3 & -1.679e-1 & 0.000e+0 & 5.269e-5 & 1.516e-3 & 0.000e+0 & 0.000e+0 & 0.000e+0 \\ 0.000e+0 & 0.000e+0 & 9.992e-1 & 0.000e+0 & 0.000e+0 & 0.000e+0 & 0.000e+0 & 4.056e-2 & 0.000e+0 \\ 1.195e-2 & -6.676e-4 & 2.112e-2 & 8.467e-2 & -6.851e-2 & 3.191e+0 & 3.209e+1 & -4.975e+1 & 0.000e+0 \\ -1.785e-3 & -2.689e-3 & 3.039e-3 & 0.000e+0 & 1.707e-4 & 1.048e-2 & 0.000e+0 & -1.203e-1 & 0.000e+0 \\ 0.000e+0 & 0.000e+0 & -2.636e-3 & 0.000e+0 & 0.000e+0 & 1.000e+0 & 0.000e+0 & 6.494e-2 & 0.000e+0 \\ -1.122e-2 & -4.405e-3 & -9.598e-3 & 0.000e+0 & 2.256e-2 & 9.593e-2 & 0.000e+0 & -6.791e-1 & 0.000e+0 \\ 0.000e+0 & 0.000e+0 & -4.065e-2 & 0.000e+0 & 0.000e+0 & 0.000e+0 & 0.000e+0 & 1.001e+0 & 0.000e+0 \end{bmatrix} \tag{III.2}$$

$$A_{\text{body/rotor}} = \begin{bmatrix} 0.000e+0 & 3.202e+1 & 0.000e+0 & 0.000e+0 & 0.000e+0 & 0.000e+0 \\ 0.000e+0 & 0.000e+0 & 0.000e+0 & 0.000e+0 & 0.000e+0 & 0.000e+0 \\ 0.000e+0 & -2.778e+1 & 0.000e+0 & 0.000e+0 & 0.000e+0 & 0.000e+0 \\ 0.000e+0 & 0.000e+0 & 0.000e+0 & 0.000e+0 & 0.000e+0 & 0.000e+0 \\ 0.000e+0 & 0.000e+0 & -3.202e+1 & 0.000e+0 & 0.000e+0 & 0.000e+0 \\ 0.000e+0 & 7.275e-1 & -1.609e+2 & 0.000e+0 & 0.000e+0 & 0.000e+0 \\ 0.000e+0 & 0.000e+0 & 0.000e+0 & 0.000e+0 & 0.000e+0 & 0.000e+0 \\ 0.000e+0 & 1.615e+0 & -2.903e+1 & 0.000e+0 & 0.000e+0 & 0.000e+0 \\ 0.000e+0 & 0.000e+0 & 0.000e+0 & 0.000e+0 & 0.000e+0 & 0.000e+0 \end{bmatrix} \tag{III.3}$$

$$A_{\text{rotor/body}} = \begin{bmatrix} 0.000e+0 & 0.000e+0 \\ 0.000e+0 & 0.000e+0 \\ 0.000e+0 & 0.000e+0 \\ 3.193e-1 & 1.048e+0 & -1.770e+0 & 0.000e+0 & 3.550e-2 & 1.021e+0 & 0.000e+0 & 0.000e+0 & 0.000e+0 & 0.000e+0 \\ -1.536e-1 & -6.815e-1 & 3.264e+1 & 0.000e+0 & 3.644e-1 & 7.264e+1 & 0.000e+0 & 0.000e+0 & 0.000e+0 & 0.000e+0 \\ 3.988e-1 & 1.321e-1 & -7.298e+1 & 0.000e+0 & 5.602e-1 & 3.402e+1 & 0.000e+0 & 0.000e+0 & 0.000e+0 & 0.000e+0 \end{bmatrix} \quad (\text{III.4})$$

$$A_{\text{rotor}} = \begin{bmatrix} 0.000e+0 & 0.000e+0 & 0.000e+0 & 1.000e+0 & 0.000e+0 & 0.000e+0 \\ 0.000e+0 & 0.000e+0 & 0.000e+0 & 0.000e+0 & 1.000e+0 & 0.000e+0 \\ 0.000e+0 & 0.000e+0 & 0.000e+0 & 0.000e+0 & 0.000e+0 & 1.000e+0 \\ -1.515e+3 & 0.000e+0 & 0.000e+0 & -3.173e+1 & 0.000e+0 & -1.433e+0 \\ -1.021e+2 & -2.453e+2 & -1.131e+3 & 0.000e+0 & -3.173e+1 & -7.126e+1 \\ 0.000e+0 & 1.128e+3 & -2.453e+2 & -2.865e+0 & 7.126e+1 & -3.173e+1 \end{bmatrix} \quad (\text{III.5})$$

$$A_{\text{actuators}} = \begin{bmatrix} -1.258e+1 & 0.000e+0 & 0.000e+0 & 0.000e+0 \\ 0.000e+0 & -1.258e+1 & 0.000e+0 & 0.000e+0 \\ 0.000e+0 & 0.000e+0 & -1.258e+1 & 0.000e+0 \\ 0.000e+0 & 0.000e+0 & 0.000e+0 & -2.500e+1 \end{bmatrix} \quad (\text{III.6})$$

$$A_{\text{control}} = \begin{bmatrix} 2.212e+1 & 2.233e+0 & -1.653e-4 & 0.000e+0 \\ -2.983e+2 & -3.011e+1 & 2.315e-3 & 0.000e+0 \\ 9.150e-1 & 9.235e-2 & -6.100e-6 & 0.000e+0 \\ 0.000e+0 & 0.000e+0 & 0.000e+0 & 0.000e+0 \\ -8.572e-1 & -8.635e-2 & 1.033e-5 & 1.1592e+1 \\ 5.664e+0 & 5.715e-1 & 0.000e+0 & -9.705e-1 \\ 0.000e+0 & 0.000e+0 & 0.000e+0 & 0.000e+0 \\ 1.379e+1 & 1.391e+0 & -6.961e-5 & -1.307e+1 \\ 0.000e+0 & 0.000e+0 & 0.000e+0 & 0.000e+0 \\ 7.405e+2 & 6.221e+1 & 0.000e+0 & 0.000e+0 \\ -1.013e+2 & -1.021e+1 & 1.133e+3 & 0.000e+0 \\ 1.640e+2 & 1.134e+3 & 0.000e+0 & 0.000e+0 \end{bmatrix} \quad (\text{III.7})$$

$$B = \begin{bmatrix} \dots & \dots & 0_B & \dots & \dots \\ 1.258e+1 & 0.000e+0 & \dots & 0.000e+0 & 0.000e+0 \\ 0.000e+0 & 1.258e+1 & \dots & 0.000e+0 & 0.000e+0 \\ 0.000e+0 & 0.000e+0 & \dots & 1.258e+1 & 0.000e+0 \\ 0.000e+0 & 0.000e+0 & \dots & 0.000e+0 & 2.500e+1 \end{bmatrix} \quad (\text{III.8})$$

The C matrix for the ACAH design of Chapter 7 is given as,

$$C_{\text{acah}} = \begin{bmatrix} 1.297e-2 & -1.994e-1 & 0.000e+0 & 1.013e+1 & 8.095e-3 & 0.000e+0 & -2.662e-2 & 0.000e+0 & \vdots \\ 0.000e+0 & 0.000e+0 & 1.146e+1 & 1.146e+1 & 0.000e+0 & 0.000e+0 & 0.000e+0 & 0.000e+0 & \vdots \\ 0.000e+0 & 0.000e+0 & 0.000e+0 & 0.000e+0 & 0.000e+0 & 1.146e+1 & 1.146e+1 & 0.000e+0 & \vdots \\ 0.000e+0 & 1.146e+1 & \vdots \end{bmatrix} \quad (\text{III.9})$$

The C matrix for the Rate Command design of Chapter 9 is given as,

$$C_{\text{ratc}} = \begin{bmatrix} 1.297e-2 & -1.994e-1 & 0.000e+0 & 1.013e+1 & 8.095e-3 & 0.000e+0 & -2.662e-2 & 0.000e+0 & \vdots \\ 0.000e+0 & 0.000e+0 & 1.146e+1 & 0.000e+0 & 0.000e+0 & 0.000e+0 & 0.000e+0 & 0.000e+0 & \vdots \\ 0.000e+0 & 0.000e+0 & 0.000e+0 & 0.000e+0 & 0.000e+0 & 1.146e+1 & 0.000e+0 & 0.000e+0 & \vdots \\ 0.000e+0 & 1.146e+1 & \vdots \end{bmatrix} \quad (\text{III.10})$$

where 0_B is a zero matrix of dimension (15,4) and 0_C is a zero matrix of dimension (4,11).

$$D = \begin{bmatrix} 0.000e+0 & 0.000e+0 & 0.000e+0 & 0.000e+0 \\ 0.000e+0 & 0.000e+0 & 0.000e+0 & 0.000e+0 \\ 0.000e+0 & 0.000e+0 & 0.000e+0 & 0.000e+0 \\ 0.000e+0 & 0.000e+0 & 0.000e+0 & 0.000e+0 \end{bmatrix} \quad (\text{III.11})$$

The state vector is,

$$x = \begin{bmatrix} x_{\text{rigidbody}} & x_{\text{rotor}} & x_{\text{actuator}} \end{bmatrix} \quad (\text{III.12})$$

where,

$$x_{\text{rigidbody}} = [u \quad w \quad q \quad \theta \quad v \quad p \quad \phi \quad r \quad \psi] \quad (\text{III.13})$$

$$x_{\text{rotor}} = [\beta_0 \quad \beta_{1c} \quad \beta_{1s} \quad \dot{\beta}_0 \quad \dot{\beta}_{1c} \quad \dot{\beta}_{1s}] \quad (\text{III.14})$$

$$x_{\text{actuator}} = [\theta_{0_{\text{act}}} \quad \theta_{1s_{\text{act}}} \quad \theta_{1c_{\text{act}}} \quad \theta_{0T_{\text{act}}}] \quad (\text{III.15})$$

The translational rates are in ft/s and the angles and angular rates are in rad and rad/s respectively.

The non-zero trim values are given as,

$$U_0 = 50.53 \text{ ft/s}$$

$$W_0 = 3.304 \text{ ft/s}$$

$$\Theta_0 = 0.06525 \text{ rad}$$

$$\Phi_0 = -0.04093 \text{ rad}$$

The 8th order model used in Section 5.7 is given below,

$$A = \begin{bmatrix} -9.775e-3 & 3.054e-2 & -1.177e+0 & -3.212e+1 & -1.182e-2 & -4.597e-1 & 0.000e+0 & 0.000e+0 \\ -1.632e-1 & -5.333e-1 & 5.122e+1 & -2.086e+0 & -1.718e-2 & -4.941e-1 & 1.303e+0 & 0.000e+0 \\ 1.100e-2 & 5.800e-3 & -2.051e+0 & 0.000e+0 & 1.139e-2 & 4.320e-1 & 0.000e+0 & 0.000e+0 \\ 0.000e+0 & 0.000e+0 & 9.992e-1 & 0.000e+0 & 0.000e+0 & 0.000e+0 & 0.000e+0 & 4.056e-2 \\ 1.432e-2 & 1.892e-2 & -4.348e-1 & 8.467e-2 & -8.159e-2 & 1.033e+0 & 3.209e+1 & -4.975e+1 \\ 9.921e-3 & 9.528e-2 & -2.238e+0 & 0.000e+0 & -6.577e-2 & -1.085e+1 & 0.000e+0 & -1.203e-1 \\ 0.000e+0 & 0.000e+0 & -2.636e-3 & 0.000e+0 & 0.000e+0 & 1.000e+0 & 0.000e+0 & 6.494e-2 \\ -9.654e-3 & 1.290e-2 & -3.133e-1 & 0.000e+0 & 1.006e-2 & -1.886e+0 & 0.000e+0 & -6.791e-1 \end{bmatrix} \quad (\text{III.16})$$

$$B = \begin{bmatrix} 1.679e + 1 & -2.861e + 1 & 6.652e + 0 & 0.000e + 0 \\ -2.983e + 2 & -3.011e + 1 & 2.315e - 3 & 0.000e + 0 \\ 5.542e + 0 & 2.684e + 1 & -5.769e + 0 & 0.000e + 0 \\ 0.000e + 0 & 0.000e + 0 & 0.000e + 0 & 0.000e + 0 \\ 2.257e + 0 & -6.356e + 0 & -3.058e + 1 & 1.592e + 1 \\ 2.121e + 1 & -3.163e + 1 & -1.535e + 2 & -9.705e - 1 \\ 0.000e + 0 & 0.000e + 0 & 0.000e + 0 & 0.000e + 0 \\ 1.634e + 1 & -5.847e + 0 & -2.739e + 1 & -1.307e + 1 \end{bmatrix} \quad (\text{III.17})$$

$$C = \begin{bmatrix} 6.486e - 3 & -9.971e - 2 & 0.000e + 0 & 5.067e + 0 & 4.048e - 3 & 0.000e + 0 & -1.331e - 2 & 0.000e + 0 \\ 0.000e + 0 & 0.000e + 0 & 0.000e + 0 & 1.000e + 1 & 0.000e + 0 & 0.000e + 0 & 0.000e + 0 & 0.000e + 0 \\ 0.000e + 0 & 5.000e + 0 & 0.000e + 0 \\ 0.000e + 0 & 5.000e + 0 \end{bmatrix} \quad (\text{III.18})$$

$$D = \begin{bmatrix} 0.000e + 0 & 0.000e + 0 & 0.000e + 0 & 0.000e + 0 \\ 0.000e + 0 & 0.000e + 0 & 0.000e + 0 & 0.000e + 0 \\ 0.000e + 0 & 0.000e + 0 & 0.000e + 0 & 0.000e + 0 \\ 0.000e + 0 & 0.000e + 0 & 0.000e + 0 & 0.000e + 0 \end{bmatrix} \quad (\text{III.19})$$

The state vector is,

$$x = [u \quad w \quad q \quad \theta \quad v \quad p \quad \phi \quad r] \quad (\text{III.20})$$

The translational rates are in ft/s and the angles and angular rates are in rad and rad/s respectively.

The system matrix of the models used in Sections 3.5 and 6.9 is given as,

$$A = \begin{bmatrix} -3.2200e-2 & 4.0300e-2 & -2.2610e-1 & -9.8081e+0 & -2.1000e-3 & -1.0850e-1 & 0.0000e+0 & 0.0000e+0 \\ -9.5800e-3 & -8.0178e-1 & 4.1091e+1 & -2.1120e-1 & -1.9400e-2 & -4.5110e-1 & 3.2229e-1 & 0.0000e+0 \\ 2.7100e-2 & 2.8840e-2 & -2.3408e+0 & 0.0000e+0 & 1.0370e-2 & 4.1020e-1 & 0.0000e+0 & 0.0000e+0 \\ 0.0000e+0 & 0.0000e+0 & 9.9946e-1 & 0.0000e+0 & 0.0000e+0 & 0.0000e+0 & 0.0000e+0 & 3.2800e-2 \\ 4.3200e-3 & 1.4294e-2 & -1.2830e-1 & 6.9400e-3 & -1.6650e-1 & 1.9865e-1 & 9.8028e+0 & -4.0686e+1 \\ -3.7320e-2 & 2.3444e-1 & -1.9960e+0 & 0.0000e+0 & -1.6330e-1 & -1.0536e+1 & 0.0000e+0 & -2.8640e-1 \\ 0.0000e+0 & 0.0000e+0 & -7.0000e-4 & 0.0000e+0 & 0.0000e+0 & 1.0000e+0 & 0.0000e+0 & 2.1540e-2 \\ -2.5800e-2 & 2.3910e-3 & -8.8500e-2 & 0.0000e+0 & 1.0130e-1 & -1.7934e+0 & 0.0000e+0 & -1.3488e+0 \end{bmatrix} \tag{IV.1}$$

B is the control matrix of the model used in Section 3.5 Columns 1 and 2 of B is the (longitudinal) control matrix of the model used in Section 6.9.

$$B = \begin{bmatrix} 4.3447e+0 & -7.6327e+0 & 2.0578e+0 & 0.0000e+0 \\ -1.1779e+2 & -3.0891e+1 & 0.0000e+0 & 0.0000e+0 \\ 1.4078e+1 & 2.8540e+1 & -5.8552e+0 & 0.0000e+0 \\ 0.0000e+0 & 0.0000e+0 & 0.0000e+0 & 0.0000e+0 \\ 1.4985e+0 & -1.5282e+0 & -9.3201e+0 & 6.7038e+0 \\ 3.2071e+1 & -2.5031e+1 & -1.5323e+2 & -1.3426e+0 \\ 0.0000e+0 & 0.0000e+0 & 0.0000e+0 & 0.0000e+0 \\ 1.3947e+1 & -5.9564e+0 & -2.6807e+1 & -1.8096e+1 \end{bmatrix} \tag{IV.2}$$

C_1 is the observation matrix of the system used in Section 3.5. C_2 is the observation matrix of the system used in Section 6.9.

$$C_1 = \begin{bmatrix} 0.0000e+0 & 0.0000e+0 & 0.0000e+0 & 0.0000e+0 & 2.4283e-2 & 0.0000e+0 & 0.0000e+0 & 0.0000e+0 \\ 0.0000e+0 & 0.0000e+0 & -3.2867e-2 & 0.0000e+0 & 0.0000e+0 & 0.0000e+0 & 0.0000e+0 & 9.9969e-1 \\ 0.0000e+0 & 0.0000e+0 & 0.0000e+0 & 1.0000e+0 & 0.0000e+0 & 0.0000e+0 & 0.0000e+0 & 0.0000e+0 \\ 2.1547e-2 & -9.9923e-1 & 0.0000e+0 & 4.1182e+1 & 3.2852e-2 & 0.0000e+0 & -2.9167e-2 & 0.0000e+0 \end{bmatrix} \tag{IV.3}$$

$$C_2 = \begin{bmatrix} 2.1547e-2 & -9.9923e-1 & 0.0000e+0 & 4.1182e+1 & 3.2852e-2 & 0.0000e+0 & -2.9167e-2 & 0.0000e+0 \\ 0.0000e+0 & 0.0000e+0 & 0.0000e+0 & 1.0000e+0 & 0.0000e+0 & 0.0000e+0 & 0.0000e+0 & 0.0000e+0 \end{bmatrix} \tag{IV.4}$$

The D matrices are zero matrices.

The state vector is given as,

$$x = [u \ w \ q \ \theta \ v \ p \ \phi \ r] \quad (\text{IV.5})$$

The translational rates are in m/s and the angles and angular rates are in rad and rad/s respectively.

The state space model given below is the model used in Section 3.?

$$A = \begin{bmatrix} -1.4229e-2 & 2.3666e-2 & -3.9356e-1 & -5.9520e+1 & -1.0671e-2 & -6.7678e-1 & 0.0000e+0 & 0.0000e+0 \\ -1.4146e-1 & -3.0601e-1 & 6.2910e+1 & -1.2568e+0 & -1.8941e-2 & -3.1947e-1 & 9.4576e-1 & 0.0000e+0 \\ 1.9177e-2 & 9.5075e-3 & -2.5951e+0 & 0.0000e+0 & 1.0586e-2 & 4.1653e-1 & 0.0000e+0 & 0.0000e+0 \\ 0.0000e+0 & 0.0000e+0 & 1.0532e+0 & 0.0000e+0 & 0.0000e+0 & 0.0000e+0 & 0.0000e+0 & 5.6279e-2 \\ 1.3895e-2 & 1.1783e-2 & -2.3149e-1 & 6.2360e-2 & -3.7327e-2 & 2.9308e-1 & 4.5665e+0 & -3.2933e+1 \\ 9.5341e-3 & 3.7334e-2 & -1.8454e+0 & 0.0000e+0 & -9.3930e-2 & -1.7422e+1 & 0.0000e+0 & -1.2959e-1 \\ 0.0000e+0 & 0.0000e+0 & -1.6361e-3 & 0.0000e+0 & 0.0000e+0 & 1.6243e+0 & 0.0000e+0 & 3.5966e-2 \\ -7.6144e-3 & 5.9594e-3 & -2.2566e-1 & 0.0000e+0 & 1.1919e-2 & -3.1350e+0 & 0.0000e+0 & -8.1668e-1 \end{bmatrix} \quad (V.1)$$

$$B = \begin{bmatrix} 2.6423e+1 & -3.0533e+1 & 8.3154e+0 & 0.0000e+0 \\ -2.9679e+2 & -2.2245e+0 & 8.8782e-4 & 0.0000e+0 \\ 9.4358e+0 & 3.9950e+1 & -5.0338e+0 & 0.0000e+0 \\ 0.0000e+0 & 0.0000e+0 & 0.0000e+0 & 0.0000e+0 \\ 1.5649e+0 & -4.2099e+0 & -4.3112e+1 & 1.5031e+1 \\ 1.1011e+1 & -2.7939e+1 & -8.3885e+1 & -9.6235e-1 \\ 0.0000e+0 & 0.0000e+0 & 0.0000e+0 & 0.0000e+0 \\ 1.8961e+1 & -4.3511e+0 & -4.2808e+1 & -1.6529e+1 \end{bmatrix} \quad (V.2)$$

$$C = \begin{bmatrix} 6.4856e-3 & -9.9707e-2 & 0.0000e+0 & 5.0666e+0 & 4.0477e-3 & 0.0000e+0 & -1.3312e-2 & 0.0000e+0 \\ 0.0000e+0 & 0.0000e+0 & 0.0000e+0 & 1.0000e+1 & 0.0000e+0 & 0.0000e+0 & 0.0000e+0 & 0.0000e+0 \\ 0.0000e+0 & 0.0000e+0 & 0.0000e+0 & 0.0000e+0 & 0.0000e+0 & 0.0000e+0 & 5.0000e+0 & 0.0000e+0 \\ 0.0000e+0 & 5.0000e+0 \end{bmatrix} \quad (V.3)$$

$$D = \begin{bmatrix} 0 & 0 & 0 & 0 \\ 0 & 0 & 0 & 0 \\ 0 & 0 & 0 & 0 \\ 0 & 0 & 0 & 0 \end{bmatrix} \quad (V.4)$$

The state vector is given as,

$$x = [u \ w \ q \ \theta \ v \ p \ \phi \ r] \quad (V.5)$$

The translational rates are in ft/s and the angles and angular rates are in rad and rad/s respectively.

The .m file below calculates the approximate Channel MSF,

```
%  
% APPMSF.m  
% This function calculates the approximate MSF of a Channel  
%  
% [num,den]=appmsf(A,B,C,D,gam)  
%  
% (A,B,C,D) is the plant  
% gam is the desired approximate MSF.  
%  
function [num,den]=appmsf(A,B,C,D,gam)  
% form the state space system which is to be subtracted  
% from the full system to form the numerator system  
aa=A;ba=B;ca=C;da=D;  
ld=length(D);  
ba(:,[1:gam-1 gam+1:ld])=zeros(length(aa),ld-1);  
ca([1:gam-1 gam+1:ld],:)=zeros(ld-1,length(aa));  
% subtract the matrices  
[as,bs,cs,ds]=parallel(A,B,C,D,aa,ba,-ca,-da);  
% calculate the roots of the numerator  
zs=tzero(as,bs,cs,ds);  
% form the state space system which is to be subtracted  
% from the full system to form the denominator system  
aab=A;bab=B;cab=C;dab=D;  
ld=length(D);  
bab(:,[1:gam-1 gam+1:ld])=zeros(length(aab),ld-1);
```

```

cab(gam,:)=zeros(1,length(aab));
% subtract the matrices
[ab,bb,cb,db]=parallel(A,B,C,D,aab,bab,-cab,-dab);
% calculate the roots of the denominator
zb=tzero(ab,bb,cb,db);
% calculate the gain
w=logspace(-4,4,100);
for xx=1:length(w)
    ka(xx)=-det([j*w(xx)*eye(length(as))-as bs;-cs
ds])/det([j*w(xx)*eye(length(ab))-ab bb;-cb db]);
end
fkmax=find(ka==max(ka));
fkmax=fkmax(1);
num=poly(zs);
den=poly(zb);
[rkt,ikt]=nyquist(num,den,w(fkmax));
kt=rkt+ikt*j;
num=real(ka(fkmax)/kt)*num;

```

The .m file below calculates the actual Channel MSF,

```

%
% ACTMSF.m
% This function calculates the actual MSF of a Channel
%
% [num,den]=actmsf(ak,bk,ck,dk,A,B,C,D,ch)
%
% (ak,bk,ck,dk) is the controller
% (A,B,C,D) is the plant
% ch is the desired Channel
%
function [num,den]=actmsf(ak,bk,ck,dk,A,B,C,D,gam)
% form the system which is to be subtracted from the
% full system in order to create the numerator system

```

```

aa=A;ba=B;ca=C;da=D;
ld=length(D);
Im=eye(ld);Im(gam,gam)=0;
ba(:,[1:gam-1 gam+1:ld])=zeros(length(aa),ld-1);
ca([1:gam-1 gam+1:ld],:)=zeros(ld-1,length(aa));
% subtract the matrices
[as,bs,cs,ds]=parallel(A,B,C,D,aa,ba,-ca,-da);
% put the controller in series with (as,bs,cs,ds)
[ask,bsk,csk,dsk]=series(ak,bk,ck,dk,as,bs,cs,ds);
% calculate the roots of the numerator
zs=tzero(ask,bsk,csk,dsk+Im);
% form the system which is to be subtracted from the
% full system in order to create the denominator system
aab=A;bab=B;cab=C;dab=D;
ld=length(D);
bab(:,[1:gam-1 gam+1:ld])=zeros(length(aab),ld-1);
cab(gam,:)=zeros(1,length(aab));
% subtract the matrices
[ab,bb,cb,db]=parallel(A,B,C,D,aab,bab,-cab,-dab);
% put the controller in series with (ab,bb,cb,db)
[abk,bbk,cbk,dbk]=series(ak,bk,ck,dk,ab,bb,cb,db);
% calculate the roots of the denominator
zb=tzero(abk,bbk,cbk,dbk+Im);
% calculate gain
w=logspace(-4,4,99);
for xx=1:length(w)
    ka(xx)=-det([j*w(xx)*eye(length(ask))-ask bsk;-csk
dsk])/det([j*w(xx)*eye(length(abk))-abk bbk;-cbk dbk]);
end
fkmax=find(ka==max(ka));
fkmax=fkmax(1);
[numa,dena]=zp2tf(zs,zb,1);
[rkt,ikt]=nyquist(numa,dena,w(fkmax));

```

$kt=rkt+ikt*j;$

$numa=real((ka(fkmax)/kt))*numa;$

$num=numa;den=dena;$